INTERNATIONALER KONGRESS ÜBER KERNPHYSIK UND QUANTENELEKTRODYNAMIK

in Basel, vom 5. bis 9. September 1949

unter dem Patronat
der Internationalen Union der reinen und angewandten Physik
und der Schweizerischen Physikalischen Gesellschaft

Herausgegeben von der Redaktion der Helvetica Physica Acta

VERLAG BIRKHÄUSER BASEL

Printed in Switzerland by E. Birkhäuser & Co. Ltd., Basle.

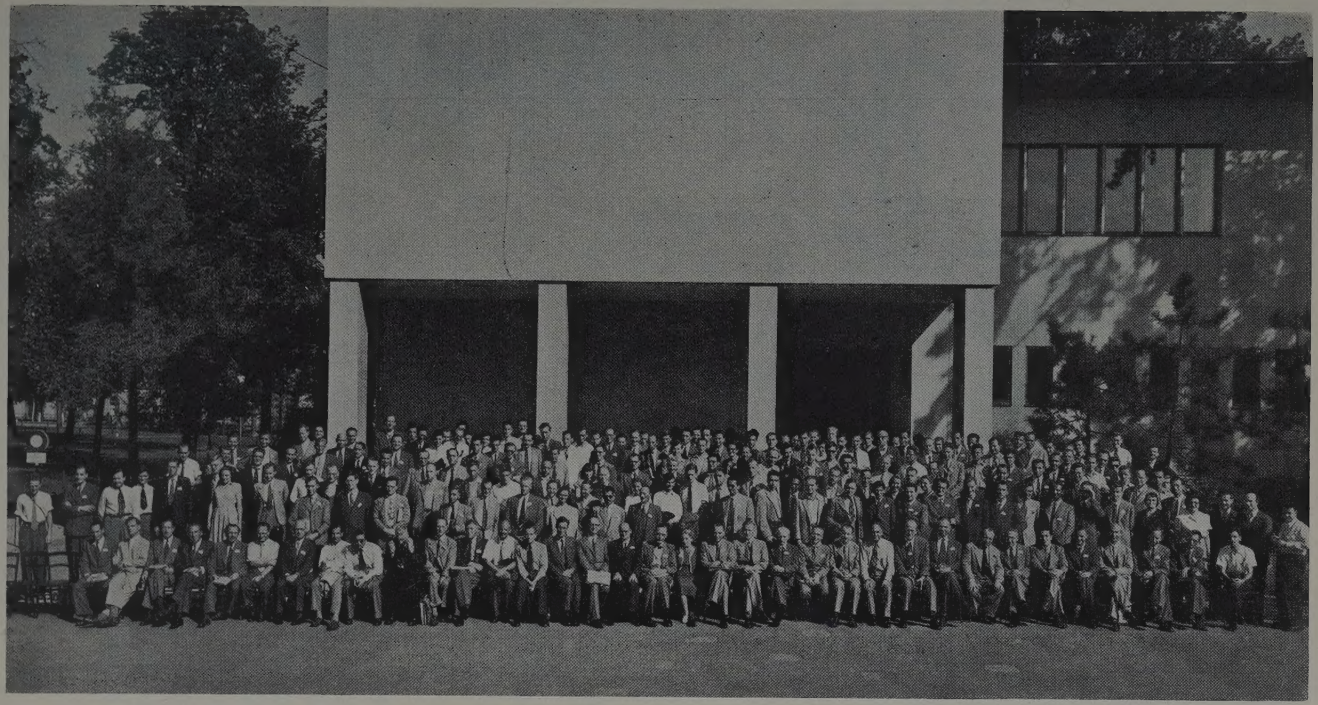

VORWORT.

Vom 5.—9. September 1949 wurde in Basel auf Anregung der „Union Internationale de Physique" von der Schweizerischen Physikalischen Gesellschaft ein internationaler Kongress über Kernphysik und Quantenelektrodynamik durchgeführt. Die Veranstaltung erhielt finanzielle Unterstützung durch die UNESCO (United Nations Educational, Scientific and Cultural Organization), den Kanton Basel-Stadt und verschiedene Industriefirmen. Das Organisationskomitee setzte sich wie folgt zusammen:

P. Huber, Präsident
K. Meyer, Sekretär
E. Baldinger
M. Fierz
E. Ganz
E. Miescher

Inhaltlich befasste sich der Kongress mit drei Gebieten aus der modernen Physik:

1. Apparate zur Erzeugung und zum Nachweis von Korpuskeln und Quanten.
2. Kernphysikalische Ergebnisse und Theorie der Kerne.
3. Neuere Entwicklung der Quantenelektrodynamik.

Die apparativen Fragen besitzen für die Beschaffung von zuverlässigem und umfassendem Beobachtungsmaterial, das als Grundlage zu einer theoretischen Bearbeitung dienlich ist, eine besondere Bedeutung. Aus dieser Erwägung wurde dem ersten Teilgebiet eine ziemliche Breite eingeräumt. Hauptvorträge wurden von den Herren E. Bretscher (Harwell), O. R. Frisch (Cambridge), H. den Hartog (Amsterdam), E. M. McMillan (Berkeley), B. Pontecorvo (Harwell), E. Segrè (Berkeley) und A. G. Ward (Harwell) gehalten. L. J. Haworth (Brookhaven) lieferte einen ausführlichen Bericht über das Protonensynchrotron.

Das zweite Gebiet umfasste als Hauptvorträge Referate von E. Segrè (Berkeley), E. M. McMillan (Berkeley) und L. Rosenfeld (Manchester). Der erste Bericht betraf experimentelle Resultate über die Neutron-Proton- und Proton-Proton-Streuung. E. M. McMillan besprach Versuche über die künstliche Erzeugung von π-Mesonen. Der Vortrag von Rosenfeld behandelte die bisherigen theoretischen Versuche zur Klärung des Kernbaus.

I. R. Rabi (Columbia University) trug über die experimentelle Bestimmung des zusätzlichen magnetischen Momentes des Elektrons vor. Diese Grösse kann mit Hilfe von höhern Näherungen der Quantenelektrodynamik berechnet werden. Andererseits ermöglicht ihre genaue Messung eine Prüfung der Theorie. J. Schwinger (Harvard University) skizzierte in seinem Vortrag die physikalisch-mathematischen Grundgedanken, die es ermöglichen, höhere Näherungen der Quantenelektrodynamik in eindeutiger Weise zu berechnen, trotz des divergenten Charakters dieser Theorie.

Um dem Leser den Überblick zu erleichtern, haben wir im vorliegenden Bericht die Beiträge der Kongressteilnehmer in 5 Gruppen geordnet. Wir hoffen, dass so der innere Zusammenhang der verschiedenen Vorträge und Mitteilungen auch äusserlich in Erscheinung tritt.

Allen, die uns durch die rasche Zustellung ihrer Manuskripte unterstützt haben, möchten wir auch an dieser Stelle danken.

P. Huber

M. Fierz.

INHALTSVERZEICHNIS.

I. Apparate zur Erzeugung energiereicher Teilchen und von Neutronen.

II. Apparate zum Nachweis von Kopuskeln und Quanten.

III. Experimentelle Ergebnisse der Kernphysik.

IV. Theorie der Atomkerne und ihre experimentellen Grundlagen.

V. Quantenelektrodynamik.

I.

Apparate zur Erzeugung energiereicher Teilchen und von Neutronen

High Energy Accelerators

by **Edwin M. McMillan**

Radiation Laboratory, Department of Physics. University of California.
Berkeley, California.

For the purpose of the following discussion we shall use a special definition of "high energy", since the nuclear physicist's idea of high energy may seem low to a cosmic ray investigator, making a numerical definition difficult. Accordingly, we shall call a "high energy accelerator" any device in which essential use is made of time-varying fields for the acceleration of particles. Energies up to a few million electron volts can be obtained by the use of constant electrostatic fields, and according to our present definition anything above this range is high. There are in use at present two general types of high energy machines, the resonance accelerator and the induction accelerator. In the resonance accelerator the particle passes through a series of electrodes (or repeatedly through a single set of electrodes) on which are applied oscillatory potentials so timed that the electric field seen by the particle while crossing the gaps between electrodes is always in the right direction to cause an increase in energy. The fact that a particular time relation is required between the motion of the particles and the variation of the electrode potentials leads to the use of the descriptive term "resonance". In the induction accelerator, on the other hand, the accelerating electric field is derived from a varying magnetic flux which is always changing in the same sense throughout the motion: therefore the force is always in the same direction, and the time relation is not important.

The general idea of resonance acceleration is best illustrated by the linear accelerator in its early form, resulting from the proposal of G. Ising and developed by R. Wideröe, E. O. Lawrence and D. Sloan, and others. In this device, the ions pass successively through a series of hollow cylindrical electrodes arranged in a straight line. The first, third, fifth, etc., electrodes are connected to one side of a source of high frequency voltage, while the even numbered electrodes are connected to the other side. Suppose that the ion is in the gap between electrodes 1 and 2 at a time

when the electric field in that gap is to the right, so that the ion is accelerated. At this time the field in the gap between 2 and 3 is in the opposite direction, but by the time the ion has traversed the length of the second electrode the field has reversed and the ion is again accelerated. Thus if the lengths of the electrodes are properly proportioned, the "resonance" between the high frequency oscillation and the times of crossing the gaps is maintained and the final energy is limited only by the gap voltage and the number of gaps. A practical limitation of the above design is given by the difficulty of obtaining high radio frequency potentials with that kind of circuit, making the number of gaps (and the overall length) very large if really high energies are to be produced. This situation has been changed by certain wartime radar developments, in particular the new high power high frequency oscillators and the experience in the use of wave guides and cavity resonators. These have led to a rebirth of interest in linear accelerators, and the recent development of the traveling wave accelerator for electrons and the standing wave accelerator for protons. The former (W. W. Hansen in the U.S.A. and the group at T.R.E. in England) uses a corrugated wave guide carrying a wave with its phase velocity adjusted to the electron velocity; the electrons go along the axis of the guide, "riding the crests" of the waves. The latter will be described in more detail later.

The best-known type of resonance accelerator is the cyclotron of E. O. Lawrence, which uses a magnetic field to make the ions move in circular paths, and a set of hollow half-cylindrical electrodes ("dees") as accelerating electrodes. The ions circulate with the angular velocity ω, which is related to the magnetic field H and the ion charge and mass e and m by the familiar equation:

$$\omega = \frac{eH}{mc} . \tag{1}$$

If the frequency ν applied to the dees is equal to $\omega/2\pi$, it is apparent that the ions will cross the gaps between the dees in step with the electric field oscillations, and will continue to be accelerated, describing larger and larger orbits up to a diameter limited by the dimensions of the magnet. This development has been of extremely great importance in the growth of nuclear physics, since it provided the first source of really high energy particles in large numbers.

The induction accelerator, althoug a rather old idea, was first brought to practical form by D. W. Kerst as an electron accelerator called the betatron. This device employs a magnetic field to guide the electrons in a circular path, and a changing flux through the

path to provide the tangential electric field which gives the acceleration. Since it is desirable to have the orbit radius r remain constant, the magnetic field H at the orbit must increase during the acceleration in a certain ratio to the increase in flux $\varnothing$. This "flux condition" is:

$$\frac{d\varnothing}{dt} = 2\pi r^2 \frac{dH}{dt}. \tag{2}$$

The machine usually operates with a sinusoidal variation of both H and $\varnothing$ at a frequency of the order of power line frequency; electrons are injected from an internal electron gun at a time near the zero point of the cycle, and reach their maximum energy at the peak of the cycle. The mechanism of injection, that is, the means by which the electrons fail to strike the electron gun in the first few turns after leaving it, is still a matter of controversy.

Before going any farther in the discussion of principles of operation, we might now stop to consider the necessary requirements for the practical operation of devices such as those described above at very high energies. One thing that is apparent is that long paths (or very many traversals of a circular path) will be necessary. Therefore the paths must be stable, or as is usually said, there must be focusing of the particles. In the linear accelerator focusing is provided by the electric field in the gaps. This has been discussed so many times that it will only be outlined here. The field lines are curved in such a way that there is a converging force as the particles enter the gap and a diverging force as they leave. Focusing is provided by an excess of the former effect over the latter. This can be obtained in three ways: (1) By the increase in velocity of the particles while crossing the gap, giving the diverging force less time in which to act. This accounts for the entire focusing effect in "steady potential" machines such as the Van de Graaff machine, but is probably not important in linear accelerators. (2) By the change in potential while the particle is crossing, which gives focusing if the particle goes through during a time of decreasing field, and defocusing if the opposite is true. (3) By putting grids or foils over the entrance to one of the electrodes, thus eliminating the diverging part of the field. Mechanisms (2) and (3) will be mentioned again later.

In machines with circular paths in a magnetic field, the chief focusing is provided by the curvature of the magnetic lines or force. In a uniform field, there is obviously no focusing at all; if the field H diminishes with radius r, the lines are curved in such a way that any orbit out of the median plane is pushed toward that plane, and

furthermore any orbit which is "off center" will tend to precess about the magnetic center. However, if the rate of decrease of field is too great, the circular orbit becomes a spiral and all stability is lost. The stable limits are most compactly given in terms of the "field index" n, defined by:

$$n = -\frac{r}{H}\frac{\partial H}{\partial r}; \tag{3}$$

the condition for stability is then that $0 < n < 1$.

In the above we have discussed stability in two coordinates only, but a third coordinate is necessary for a complete description of the motion, namely the distance measured along the path of the particle. This coordinate is not important in the case of induction acceleration where the particle is urged on by a steady push, but it is very important in resonance acceleration since it determines the timing of the arrival of the particle at the gaps. Therfore, if the number of gap crossings is to be large, stability in this coordinate is needed too. It was shown independently by V. Veksler in Russia and E. M. McMillan in the U.S.A. that this kind of stability does indeed exist, and the realization of this fact has made possible the recent extension of the energy range attainable by resonance accelerators. In order to illustrate the idea, let us express the position of the particle in terms of a phase angle, which may be the difference between the angular position in a circular orbit and the "electrical angle" of the high frequency oscillation. The value of this "phase" then determines at what time in the high frequency cycle the particle will cross the gap, and therefore the energy gained (or lost) in the crossing. If the resonance condition is exactly satisfied, the phase will remain constant, but if $\omega \neq 2\pi\nu$ it will change with each traversal of the orbit. This change will lead to either an increase or decrease in the energy gain per turn, depending on the initial value of the phase angle. We can now show that if ω depends on the energy E, and if the energy initially has a value which is not exactly right for resonance, the change can act in a direction to counteract the deviation of the energy from resonance, and therefore can lead to a stability in phase and energy. The angular velocity and the total relativistic energy E are related by:

$$\omega = \frac{eH}{mc} = \frac{ecH}{mc^2} = \frac{ecH}{E}. \tag{4}$$

Suppose that the energy is initially too small, so that ω is too high for resonance, and the phase will change in the sense that the particle arrives earlier and earlier at the gap. Suppose further that the

initial phase is at one of the two values where the particle crosses the gap at zero field. If it is at the particular one of these for which earlier arrival means a gain in energy, then the changing phase leads to an energy increase, tending to restore the initial energy deficiency. Then the condition for stability is satisfied, and further analysis shows that the phase will oscillate in a way exactly like the motion of a pendulum. If the initial energy error is too large, one has the case of a pendulum swinging over the top, so that true stability exists only within a certain range of energy and phase. For a linear accelerator the linear velocity v, given by:

$$\frac{v^2}{c^2} = 1 - \frac{m_0 c^2}{E^2}, \tag{5}$$

is the determining factor. This increases with E, so that phase stability exists about an initial phase where the energy gain is greater for later arrival at the gap. This condition for phase stability is incompatible with the requirement for focusing by mechanism (2) described above, leading to some difficulties in the design of high energy linear accelerators.

The discussion just given applies to a case of constant H and ν, as exemplified in the cyclotron. An ion, after leaving the source near the center, goes through a portion of one cycle of phase oscillation on its way to the outer edge. The rest of the cycle, if allowed to take place, would carry it to some maximum energy and then back to the center again, leading to the relativistic limit of cyclotron energy first pointed out by Rose and Bethe. However, if H or ν is made to change continuously during the acceleration, the situation is altered. So long as the change is not too rapid, the stability is not destroyed (in the pendulum model for phase oscillations, it is equivalent to applying a torque to the pendulum, which will not destroy the stable oscillations unless it is too large). The energy tends to oscillate about a "synchronous energy" E_s:

$$E_s = \frac{ecH}{2\pi\nu}, \tag{6}$$

while the mean phase shifts to a point where the energy gain in the gap is just enough to take care of the rate of change of E_s. This rate of change must of course be slow enough that the required energy gain does not exced the maximum available at the gap (or gaps). To complete the story, we should say that in the linear accelerator the parameter which changes with time is the spacing of the accelerating electrodes as seen by the moving particle.

Equation (6) leads to three technical modifications, which are especially suitable for different particles and have been given different names. That is, one can vary ν alone, H alone, or ν and H together. For accelerating electrons, the range to be covered by E, (from something near rest energy to several hundred MeV) is relatively so large that H-variation seems the only practical way. For heavy partcles up to a few hundred MeV, the range can be covered by ν-variation, and the difficulties of H-variation (laminated magnet, storage and transfer of energy of the magnetic field) can be avoided. Finally, for very high energy heavy particles, the combined variation is most suitable. The reason for the latter is best understood if one considers the orbit radius, determined by:

$$r = \frac{v}{\omega}. \tag{7}$$

For electrons of a few times the rest energy $v \sim c$, and r is approximately constant for fixed ω, so that a ring-shaped magnetic field can be used. For protons on the other hand r is still changing up to very high energies, so it is worth while to vary ν (and therefore ω) in such a way as to follow the variation in r, thus keeping the radius constant and allowing the great saving in both iron and magnetic energy consequent on the use of a narrow band of field.

The three modifications are then, in tabular form:

Name	Particles	H	ν	r
synchroton	electrons	varies	constant	$\sim$ constant
synchro-cyclotron or frequency-modulated cyclotron	protons or deuterons or helium ions	constant	varies	varies
bevatron (Berkeley) or cosmotron (Brookhaven) or proton-synchrotron (Birmingham)	protons or possibly other ions	varies	varies	constant

Finally, as illustrations of some of these devices, we shall use the machines at present operating at the Radiation Laboratory in Berkeley, the 60-inch cyclotron, the 184-inch synchro-cyclotron, the proton linear accelerator, and the synchrotron. The bevatron, now under construction, will be described in the following talk by Dr. Haworth.

Fig. 1.
The 60-inch cyclotron.

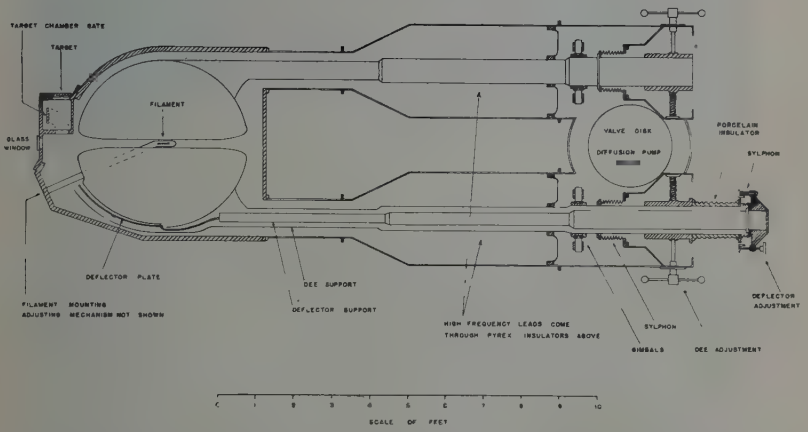

Fig. 2.
Plan view of 60-inch cyclotron vacuum chamber in cross section, showing the method of supporting the dees.

The *60-inch cyclotron* (i. e., diameter of magnet poles equals 60 inches) operates at a fixed frequency of 11.4 megacycles per second. The peak potential between dees is about 200 kilovolts, produced by about 60 kilowatts of high frequency power fed into a resonant dee system with a Q of 3500. The following energies and currents (deflected onto a target) are obtained: deuterons, 18.5 MeV, 50 to 100 microamperes; doubly charged helium ions, 37 MeV, 8 microamperes; hydrogen molecular ions, 9.25 MeV per proton, 25 microamperes. This machine is used chiefly for producing radio-

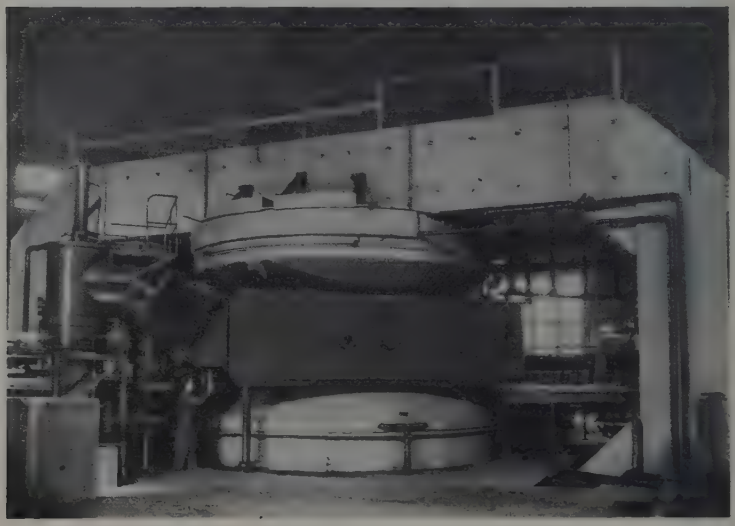

Fig. 3.
The 184-inch synchro-cyclotron without shield, showing magnet yoke and coils, vacuum chamber, and diffusion pumps.

active materials for biological and medical purposes, and in the study of nuclear reactions and their products among the heavy elements. Fig. 1 is a view of the 60-inch cyclotron without its present shield of water tanks. Fig. 2 shows the method of mounting the dees on resonant supports, which avoids the necessity of having the high dee voltage appear across insulators. The power is fed in at points near the grounded ends of the dee supports.

The *184-inch synchro-cyclotron* is shown in Figs. 3 and 4 with and without its concrete shield. Fig. 5 is a vertical section through the single dee and its associated resonant circuit, which consists essen-

tially of a coaxial transmission line with on eend grounded and containing a variable series capacitance. The rotating part of the variable condenser is shown in Fig. 6. The frequency is made to vary from 22.9 to 15.8 megacycles per second when accelerating protons, and from 11.5 to 9.8 megacycles when accelerating deuterons or helium ions, with a repetition rate of 60 per second. The peak dee potential is only 17 kilovolts, since the phase stability allows the ions to make many turns while being accelerated (37,000

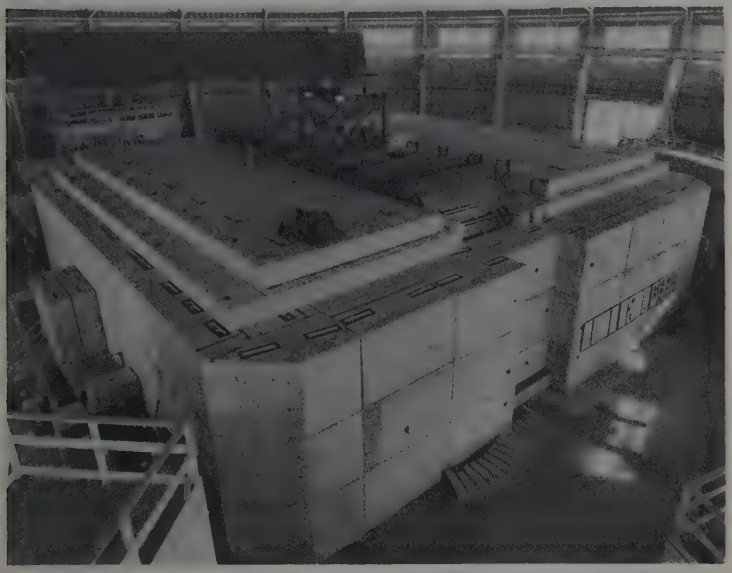

Fig. 4.
Same as Fig. 3 with 10 foot thick concrete shield in place.

in the case of protons). The magnetic field is 15,000 gauss at the center, 14,175 gauss at the final radius of 81 inches. The energies and currents (time average on an internal target) are: protons, 350 MeV, 0.75 microampere; deuterons, 195 MeV, 0.75 microampere; helium ions, 390 MeV, 0.1 microampere. These particles can be used directly to bombard internal targets, or a portion of the currents can be brought out by a deflecting system for experiments outside. Also, the neutrons produced by "stripping" of deuterons or exchange collisions of protons in the internal target can be allowed to emerge through a hole in the concrete shield, providing a

well-collimated beam of high energy neutrons. The experiments performed or in progress with this machine cover a wide range of high energy processes, which we shall not have time to describe here: probably the most striking are the studies of meson production, including the recent evidence for the production of neutral mesons of mass comparable to the π-meson.

The *linear accelerator* of Professor Alvarez uses standing waves inside a cylindrical resonant cavity to accelerate protons. Fig. 7 shows the general arrangement, and Fig. 8 is a photograph of the completed machine, looking toward the beam-exit end. The cavity,

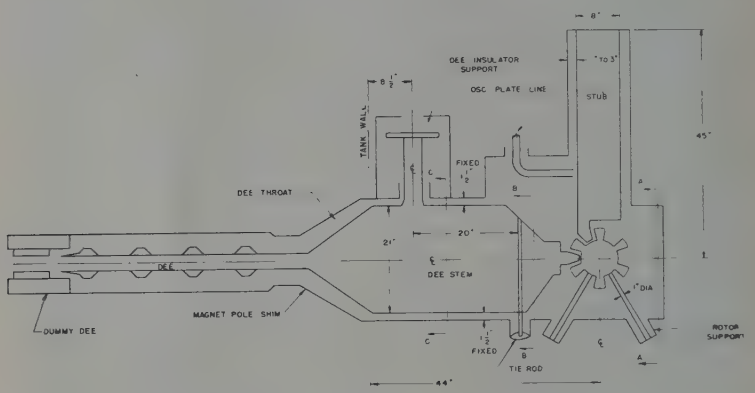

Fig. 5.

Vertical section through high-frequency resonant system of 184-inch synchrocyclotron. The rotary part of the condenser is in effect insulated from ground. The edge of the dee is at the center of the magnetic poles.

40 feet long and 3.2 feet in diameter and having a Q of 70,000, is excited at 202.6 megacycles per second in a mode for which the electric field is parallel to the axis, and uniform along the axis. It is driven by 28 converted radar sets operating in parallel, delivering pulsed high frequency power at an instantaneous rate of 2.5 megawatts, which provides a total potential drop along the cavity of 36 million volts. Protons are injected into the cavity at 4 MeV from a Van de Graaff machine. They are shielded from the effect of alternate half cycles by metal "drift tubes" arranged along the axis, as shown; these can be (and are) mounted on conducting radial supports, since the electric field is entirely longitudinal. The final proton energy is 32 MeV and the time average current is 0.1 microampere, delivered in 15 pulses of 400 microseconds length per se-

cond. The drift tubes are provided with grids in order to produce focusing by mechanism (3) discussed above, since mechanism (2) seems to be incompatible with phase stability. (Note added since giving the talk: Recently the machine has been operated successfully without the grids; apparently this possibility is allowed by its shortness compared to the period of a phase socillation.) The great advantage of the linear accelerator lies in the easy accessibility and good collimation of the beam; it has been used for measurements of *p-p* scattering and excitation curves of nuclear reactions, the discovery of some new light radioactive isotopes, etc.

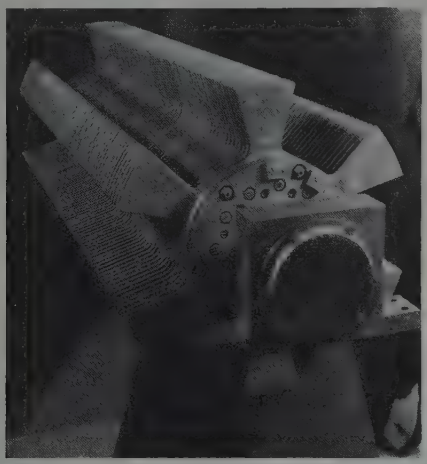

Fig. 6.
Rotating part of variable condenser indicated in Fig. 5.

The *synchrotron* accelerates electrons to 335 MeV. The magnet of this machine must be laminated because of the time-varying magnetic field, and therefore it is constructed entirely of transformer iron. It is excited by means of a condenser bank and an electronic switch consisting of four ignitrons. The condenser bank stores 124000 joules of energy at 17.8 kilovolts; this is discharged into the magnet coils when the switch is closed. The discharge is oscillatory with a frequency of 30 cycles per second, and after the completion of one cycle the switch is opened. This process is repeated at the rate of 6 times per second; the acceleration takes place during the first quarter cycle, and the only function of the second half cycle is to restore the condenser charge to its original polarity. A charging rec-

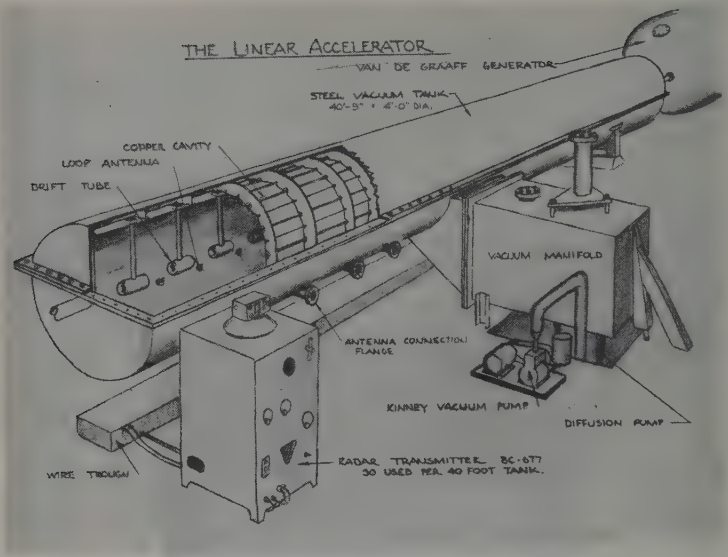

Fig. 7. Cutaway drawing of the linear accelerator.

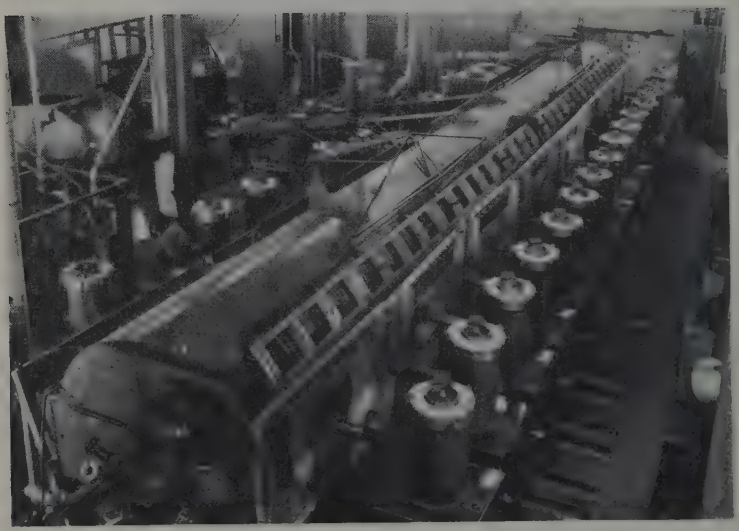

Fig. 8. The linear accelerator. The Van de Graaff machine used as an injector is out of the picture toward the observer.

tifier makes up for the losses in the discharge cycle. Fig. 9 is a drawing of the machine with a portion of the magnet cut away. It shows the rectangular yoke and the circular pole pieces, with the toroidal quartz vacuum chamber between them. Through the hollow center of the magnet pass laminated iron "flux bars" whose purpose is to provide flux for betatron-type acceleration during the early part of the operating cycle. To the right (not shown) is the electron gun that injects electrons into the orbit, and to the left the oscillator and resonant cavity that furnish the synchrotron-type acceleration. Fig. 10 shows the resonant cavity in more detail. A one-eighth segment of the quartz vacuum chamber is plated inside and out

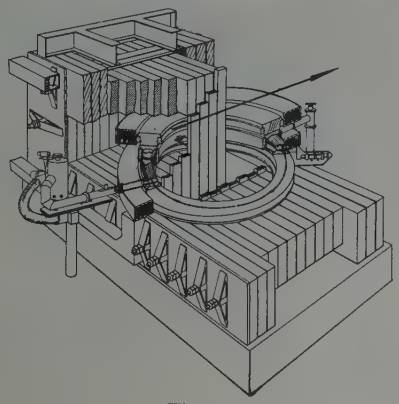

Fig. 9.
Cutaway drawing of the synchrotron.

with copper, and a gap is cut in the inside coating near one end, as shown. The conducting surfaces then form a quarter-wave resonant line, which is driven at 47.8 megacycles per second, corresponding to the circulation frequency of electrons at the velocity of light in an orbit of one meter radius. The peak voltage across the gap is 2 kilovolts.

The operating cycle is as follows: When H reaches 11 gauss, a pulse of 100 keV electrons is injected. The action of the changing flux accelerates these, bringing them to about 2 MeV by the time H has reached 80 gauss; at this time the oscillator is turned on, and most of the circulating electrons are caught into phase stable orbits. Shortly after this the flux bars become saturated, but their action is no longer needed. The electrons are then carried to their peak energy of 335 MeV at the peak field of 11,200 gauss, when the oscillator is turned off. Radiation losses cause the orbit to contract

rapidly until the electrons strike a platinum target 0.020 inch thick, producing a narrow beam of x-rays. No attempt has as yet been made to bring the electrons out. The time average x-ray intensity is around 100 roentgens per minute at one meter from the target, corresponding to about 10^8 electrons per pulse striking the target. The normal pulse length is 10 microseconds, but this can be extended to 3000 microseconds by turning off the oscillator slowly, which reduces the random coincidence problem in counter experiments. The most formidable operating problems are concerned with the errors in the field at the time of injection. These errors affect both

Fig. 10.

Copper-plated quartz section forming the accelerating unit of the synchrotron. The gap is visible just inside the end. Power is fed in through the far stub; the projections at the near end have no function. The longitudinal cuts reduce eddy currents caused by the changing magnetic field.

the radial and azimuthal field distributions, and are corrected by sets of coils (20 in all) carrying self-induced currents adjusted by variable series resistors. In our experience, the adjustments are best made empirically by observing the output during operation; since they are rather critical, the beam was first found by operating at low magnet excitation (200 volts) where the field errors are small. A view of the machine from the same aspect as in the drawing is shown in Fig. 11; the other side is shown in Fig. 12. The x-ray beam emerges normal to the flat side of the magnet, coming toward the observer in this view. Along the beam are arranged experimental equipment, collimators, and intensity monitors. A cloud chamber is placed 86 feet from the target. The experimental work with the

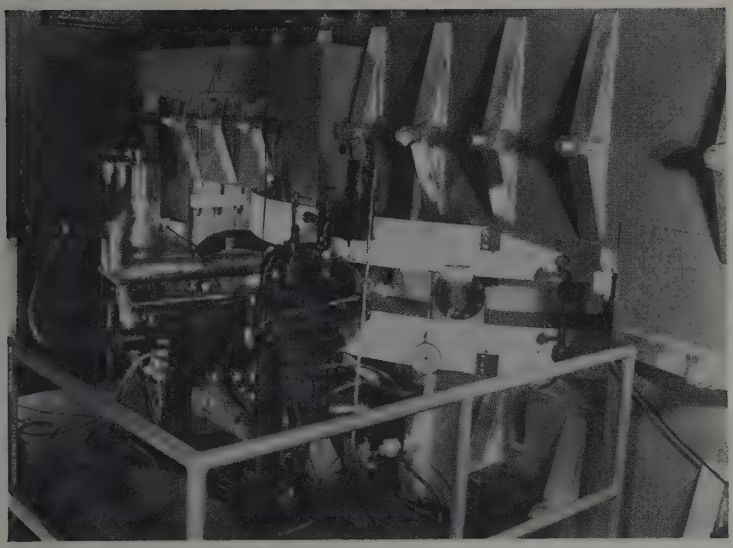

Fig. 11. View of synchrotron, showing at the left the oscillator (vertical brass cylinder) and the transmission line feeding power to the accelerating section.

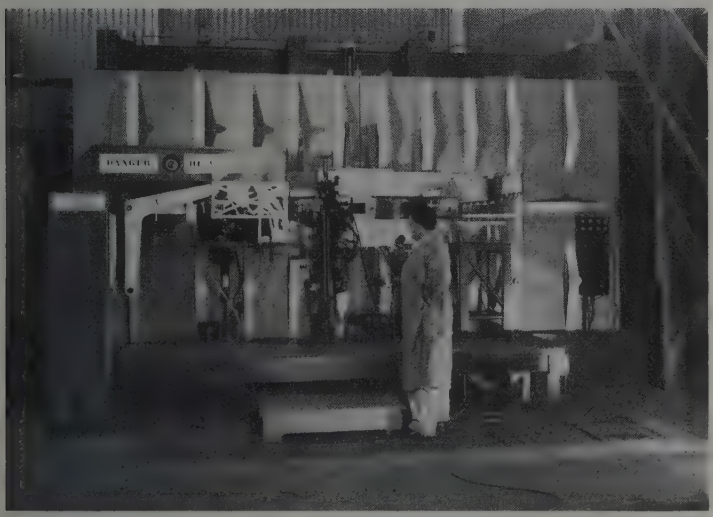

Fig. 12. Other side of synchrotron. The injector and its power supply are at the left, the x-ray beam emerges at the right, toward the observer.

machine has been concerned with measurements of the x-ray yield and spectrum, transition effects in ionization chambers, x-ray induced radioactivity, studies of the Compton effect at high energy, and observations of meson production.

As to the future of high energy accelerators, the next stage is represented by the bevatron, to be discussed by the following speaker. One should not forget, however, that this may not be the best machine for the purpose; it is the best that we know of, but our knowledge is finite, and it is always possible that some new combination of known principles, or some altogether new principle, may make possible the attainment of still higher energies.

Radiofrequency Ion Sources.

by **A. G. Ward.**
Atomic Energy Research Establishment, Harwell, Berks.

Summary. This paper reviews the published data on R. F. type ion sources. Various sources are compared, and factors influencing the design and performance of these sources are discussed.

Introduction.

Recently an article has appeared in Nucleonics[1]) reviewing the various types of positive ion sources developed for use with high voltage equipment. Radio-frequency ion sources (R. F. sources) are mentioned briefly in this article; I propose to review in this paper the data which has been published on this type of source and to consider the factors which influence its design and performance.

Desirable properties of positive-ion sources are well known; high proton percentage, low energy spread, large beam currents and low gas consumption, simplicity of construction and operation, long life and reliability of operation, low power consumption, are of varying importance depending on the particular requirements of the accelerating equipment. The R. F. source compares very favourably with earlier types on the basis of such requirements.

Historically, the first reported attempt to use radiofrequency excitation of a gas discharge for this purpose is mentioned by GETTING[2]) in 1941. His attempt was apparently not very successfull, and the first indication of the possibilities of this type of ion source was indicated by THONEMANN[3]), who described some preliminary work carried out at the University of Sidney, Australia.

Independently, D. ROAF, now at the Clarendon Laboratory, Oxford, started work on the use of an R. F. ion source at Chalk River Laboratory in Canada and I fell heir to his equipment when he returned to England. Four papers describing the successful development of R. F. ion sources have appeared in the literature and many such sources have been built and operated. There are for instance six such sources in use at the Clarendon Laboratory in Oxford, two at A.E.R.E., Harwell, one at Durham University, two or more in Cambridge, and many others.

Much of the material presented in this article is common knowledge amongst those who have used and operated these sources. A

detailed account of much careful work by THONEMANN[4]) on the development of a radiofrequency ion source is contained in his D. Ph. thesis, and I have had the benefit of several discussions with THONEMANN and his collaborators at the Clarendon Laboratory.

Description of Sources.

Figs. 1—8 have been taken from the published papers on radiofrequency ion sources. Fig. 1 shows the original source described by THONEMANN[3]). It consists of a two litre pyrex flask, two external electrodes for exciting an R. F. discharge in the flask, an extracting

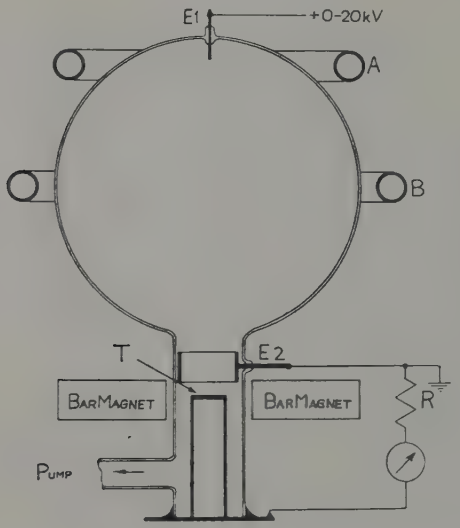

Fig. 1.

electrode and target located in the neck of the flask. THONEMANN described the formation of a concave boundary to the plasma, near the negative electrode, which moved away from the electrode as the extracting voltage was increased. Currents of the order of 10 ma with 10 k. v. applied voltage were obtained; the arrangement of electrodes produced a well focussed beam at the target but the beam was not brought out of the discharge tube.

Fig. 2 shows the source which Bayly and myself[5]) developed at Chalk River. It bears a close resemblance to the THONEMANN source. In this source the bottle used is smaller and some care has been

taken to reduce the metal area exposed to the discharge. The discharge is excited by a coil to obtain the more intense type of ring discharge, and electrodes 1, 2, and 3 (Fig. 2) are used for extracting. and initial focussing of the ion beam. Fig. 3 shows the electrode assembly in more detail. Beam currents of about 500 μamp. were obtained, containing $\sim$ 50% protons and the gas flow rate was $\sim$ 15 cc/hr. About 250 watts of R. F. power were used at 15 Mc/s frequency.

Fig. 4 shows the source developed at Glasgow University by Rutherglen and Cole[6]) at approximately the same time. In this

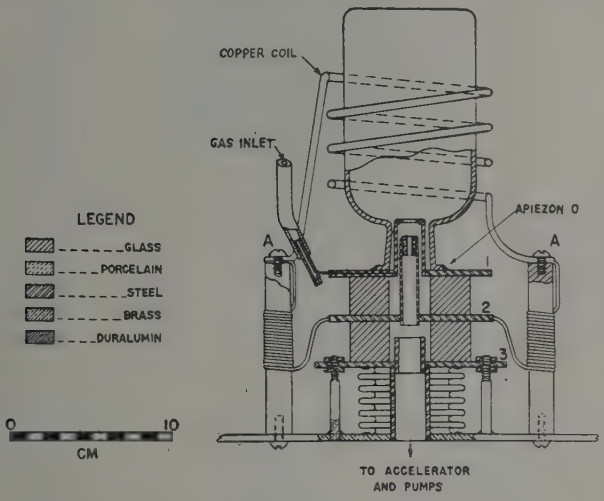

Fig. 2.
Improved model of the radio-frequency type ion source.

source electrostatic excitation of the discharge is used, with two external electrodes and the discharge vessel is smaller than in the previous figure. Great care has been taken to reduce the metal surface exposed to the discharge and an axial magnetic field is used to increase the intensity of the discharge. Only 30 watts of R. F. power at 180 Mc/sec. were used, and the performance data of the source are much the same as that of Fig. 2.

Fig. 5 shows the R. F. source developed by R. N. Hall[7]) working at the California Institute of Technology. This source uses a very small pyrex or quartz discharge chamber, but operates at a pressure of $\sim$ 5 times higher than that in the previous sources. A

high frequency, 450 Mc sec. is used to excite the discharge and the oscillator delivers ~ 60 watts output power. Again an axial magnetic field is used. The ions are allowed to diffuse out of the source before acceleration, and Fig. 6 shows an enlarged view of the discharge chamber and outlet hole. There is some difference of opinion

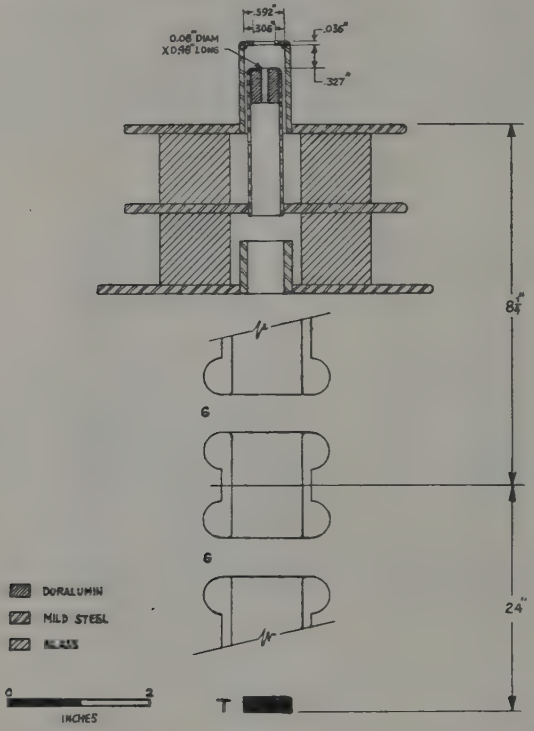

Fig. 3.
Arrangement of the ion source electrode assembly, the main accelerating gapi. *G*, *G*, and the target, *T*.

as to the merits of probe type extraction as compared with diffusion. the contention being that probe extraction increases the energy spread of the ions in the beam from the source. This point will be mentioned again. This source again gave ion currents ~ 400 μamp. containing $\sim 60\%$ protons and used 30 cc hydrogen per hour.

Fig. 7 shows the R. F. source developed by THONEMANN and his collaborators[8]) at the Clarendon laboratory. Proton currents of the

order of 500 μamp., with a gas consumption of 15 cc/hr. are obtained. Since this particular design of source has had widespread use, and its properties have been investigated carefully, it is considered in more detail. The pyrex discharge tube had been designed so that the metal exposed to the discharge is a minimum, and the extracting electrode projects into the centre of the discharge in the belief that the centre of the discharge, away from the walls, contains a higher percentage of atomic ions. Critical design points are the necessity

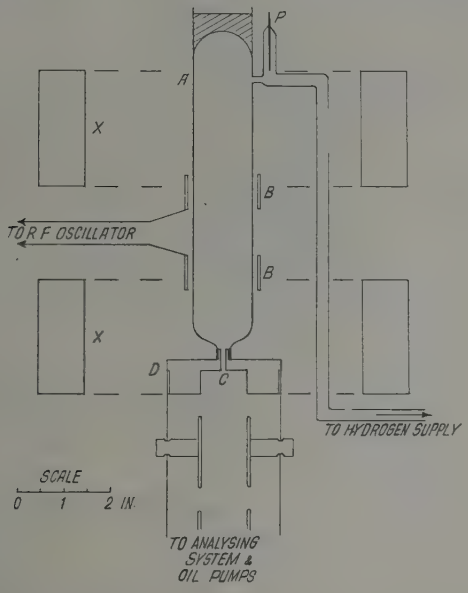

Fig. 4.

of having the glass sleeve surrounding the extracting electrode accurately concentric with it, and with its top surface carefully flattened.

Tables 1–3 gives the results of magnetic analysis of the beam from this source, using deuterium with about 7% hydrogen, and working under optimum conditions. These results are very good indeed. The variation of the atomic ion percentage with pressure in the discharge is also shown, and it can be seen that the pressure in the source is not a critical variable. THONEMANN[4]) has also investigated the effect of an axial magnetic field and has found that at a frequency of 20 Mc/sec. the magnetic field only improved the source performance

at very low power inputs. On the basis of the results given, there is of course little room for improvement of atomic ion percentage through the use of a magnetic field.

Fig. 8 shows the results of measurements of the energy spread of the ion beam from this source; the experimental curve is compared with that calculated from the constants of the analyser. These results, taken with probe type extraction, show that this method of extraction does not introduce an energy spread of the order of magnitude of the extracting voltage, and it is probable that there is

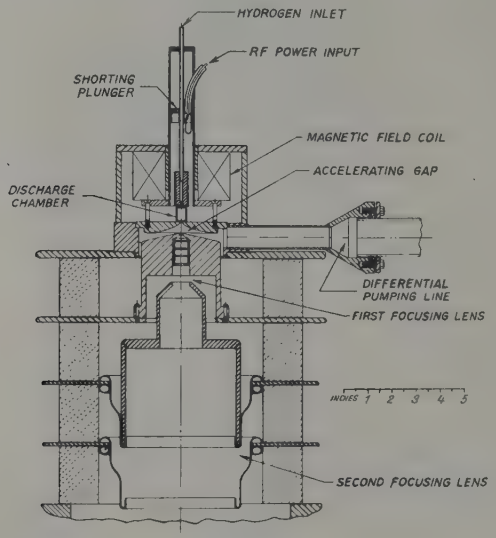

Fig. 5.

Radiofrequency ion source and accelerating electrode system.

little to choose between probe type of extraction and diffusion from the source as far as energy spread in the beam is concerned. On the other hand, probe type extraction should always improve the ratio of beam current to gas flow.

Production of Atomic Hydrogen.

Let us now consider in more detail some of the factors governing the production of beams containing a high percentage of protons. Conditions in the discharge tube must be favourable to the production of a high partial pressure of atomic hydrogen. The cross-section

for the production of protons by electron collision with a hydrogen molecule is not an important factor, since most of the ionizing collisions produce singly ionized molecules[9]). It seems reasonable to suppose that atomic hydrogen is produced as a primary reaction. The lifetime of atomic hydrogen in the discharge tube is such that the partial pressure of atomic hydrogen builds up and the protons are formed by ionization of this atomic hydrogen. Recombination of atomic hydrogen on the pyrex surface of the discharge vessel is sufficiently slow to allow this condition to be reached. Recombination of the atomic hydrogen by a three body collision in the gas is probably negligible at these pressures.

In a recent paper by G. I. Finch[10]), the following statement appears. "These experiments... show that dry hydrogen is not dis-

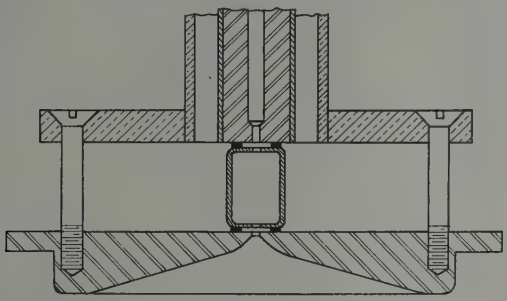

Fig. 6.
Details of ion source construction. The vacuum seal at each end of the discharge chamber is provided by two gaskets made of 0.018-in. fuse-wire.

sociated by the discharge, and that the minute amount of atomic hydrogen formed is attributable to that trace of moisture which can hardly be eliminated in an experiment of this kind carried out in an apparatus equipped with barometric mercury cut-offs." The experiments referred to deal with the excitation of an R. F. discharge using $\sim$ 150 watts at 26 Mc/s, at a pressure of about 30 microns. The glass discharge vessel was $\sim$ 10 cms. diameter and the hydrogen carefully purified. I mention this statement since it is apparently in direct contradiction to the results of experiments on R. F. discharges mentioned above. In the experiments at the Clarendon Laboratory, for instance, the hydrogen was introduced through a palladium leak and the spectrum of the discharge showed almost pure Balmer lines, with very little trace of the molecular spectra.

Extraction of Positive Ion Beam.

In most of the experimental arrangements discussed previously the ions are extracted from the discharge by a probe. The geometry is chosen so that a reasonable fraction of the ion current extracted from the discharge passes through the small hole in the extraction

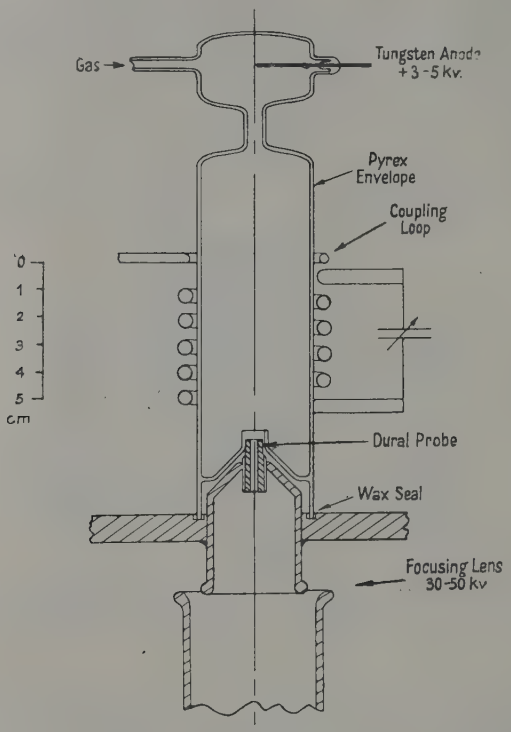

Fig. 7.
Assembly of the radio-frequency ion source.

electrode and emerges in a beam. The ratio of protons to emergent gas atoms or molecules is of the order of 1 or 2%, a value which is higher than that achieved in most of the earlier ion sources.

The optimum design of the extracting electrode arrangement is of major importance in the performance of the ion-source: further work on this problem would probably lead to marked improvement in the performance of this type of source. Qualitative arguments leading to the choice of canal dimensions are as follows: the beam

emerging from the ion source is usually subjected to further acceleration and focussing by an electrostatic lens system. For a voltage ratio on the first lens of the order of 10, the canal is usually located 2 or 3 lens diameters back from the centre of the first lens in order to form a real image. To avoid serious spherical aberration in the lens, the beam is allowed to fill about half the lens diameter. These

Table 1.

The mass spectrum of a deuterium ion beam.

Magnet current (ma.)	Species	Percentage abundance
29	D_1^+ from dissociation of D_3^+	0.9
32	H_1^+; D_1^+ from dissociation of D_2^+	6.0
54	D_1^+ and H_2^+	79.0
60	D_3^+ from dissociation of D_3^+	1.0
62	HD^+ and H_3^+	0.9
80	D_2^+ and H_2D^+	8.8
90	HD_2^+	1.4
99	D_3^+	2.1

Table 2.

Pressure (microns)		14	16	18	20	23	25	26	28
Percentage abundance	(H_1^+	84	85	88	89	90	90	92	91
	(H_2^+	14	11	10	8	7	8	5	6
	(H_3^+	2	4	2	3	3	2	3	3

Table 3.

Pressure (microns)		13	15	17	20	22	25	28	30
Percentage abundance	(D_1^+	72	73	85	85	84	89	87	87
	(D_2^+	23	20	13	11	12	8	8	8
	(D_3^+	5	7	2	4	4	3	5	5

considerations lead to a choice of the ratio of canal length to diameter of the order of 10. The actual canal diameter is then chosen to give either the required beam current or the maximum allowable gas consumption, depending on which limit is first reached. The sources described previously use canals of the order of $^1/_{10}''$ diameter, and deliver ion beams of the order of 500 μamps.

The following figures taken from an experimental arrangement in use at the Clarendon laboratory give a good example of what can be achieved by subsequent focussing of the extracted ion beam. A deuteron beam emerges from the ion source through a canal $^3{}_{32}''$

diameter and $^3{}_4{}''$ long at a voltage of 3,5 k.v. It is then accelerated to 40 k.v. by an electrostatic lens arrangement and focussed through a second canal $^1{}_8{}''$ diameter and 3″ long. A straight through type analyser (crossed electric and magnetic fields) is placed in front of the second canal. Emergent analysed deuteron beams of 180 μ a. have been obtained from the second canal. These represent preliminary results and may be improved by better alignment.

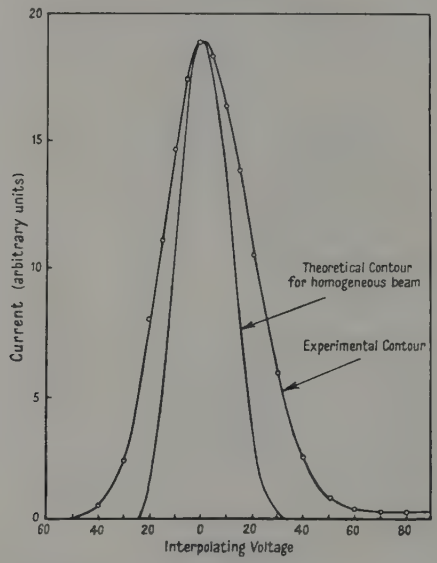

Fig. 8.
Comparison of the theoretical contour for a homogeneous beam with the D_1 ion contour.
$Vp = 3$ kv., $Va = 10$ kv., $p = 20\ \mu$; $s_1 = 0{\cdot}1$ mm; $s_2 = 0 \cdot 1$ mm.

The problem of arranging further focussing electrodes to deal with the emergent beam from an R. F. ion source can be calculated from the lens data available from the work on electron optics. The problem of designing the actual extracting electrode system is however complicated by two factors:

(1) The requirement that a minimum amount of metal surface be exposed to the R. F. discharge.

(2) The fact that the positive ion emitting surface is not well defined.

With the extracting electrode systems of the sources described previously the following behaviour is observed. The plasma potential remains close to that of the positive electrode, while near the

negative electrode a concave boundary is formed, relatively sharply defined, with a dark space in the region of the electrode. This boundary recedes from the negative electrode when the extracting voltage is increased, or the R. F. power is decreased. Apparently this boundary behaves as an emitter of positive ions, and adjusts its position so that space charge limited emission conditions prevail at the boundary. For any particular arrangement of the extracting electrodes, and a given value of the extracting potential, there is an optimum R. F. power, corresponding to best focussing of the positive ion beam through the canal.

The arrangement used with the Oxford type ion source has been investigated over a range of parameters such as the diameter of the extracting electrode, the diameter of the glass sleeve, and the location of the extracting electrode in the sleeve. The dimensions given in the published paper[8]) represent near optimum design for this particular arrangement. Calculations made by Bedford[11]) and Thonemann[4]) show that the current focussed through the canal at a given extracting voltage is only 10 to 15% of the maximum possible at this voltage, if this maximum is set by the space charge repulsion of the beam. It would seem likely that further work on the design of extracting electrodes would considerably improve the performance of the ion source.

Reliability of Operation.

The behaviour of R. F. sources and the more common types of failure under conditions of frequent use are of some interest. The R. F. sources are not trouble free. Fortunately, the performance of the source, as far as proton percentage is concerned, can be reliably estimated from the colour of the R. F. discharge. When operating with a high proton percentage ($> 50\%$) the discharge is bright red and deterioration of performance is associated with colour change of the discharge, a pale pink colour indicating a proton percentage of the order of 25%. Air leaks in the hydrogen supply line produce similar changes. It is also advisable to have ample R. F. power available, particularly in initial testing of a source, since the problem of properly coupling the power into the discharge is complicated by the changing impedance of the discharge as the power is increased.

Our experience in Canada showed that the source would operate for many days, giving reproducible results. When first switched on the source often took 1 to 2 hours to reach optimum conditions. Occasionally, however, it was necessary to remove the discharge vessel and clean it (with hydrofluoric acid) before proper perfor-

mance could be obtained. Accidents at the target end of the equipment, e. g. breaking counter windows, usually resulted in poor subsequent source performance until the bottle was cleaned. These changes may be associated with the entrance of pump oil vapour in relatively large quantities while the source is running, or the effect of oxygen on the surfaces inside the discharge vessel. Some thin deposits are usually visible on the surface of a discharge vessel which has operated for some time. These occur on the walls at the end of the tube where the discharge is least intense, and do not necessarily seriously affect the proton percentage. They probably arise from metal sputtered off the extracting electrode by the ion bombardment. The extracting electrode is usually made of aluminium to reduce sputtering.

At Oxford the failure of a source is usually indicated by a sudden change in colour of the discharge from red to white. Sometimes the discharge regains its red colour after running for a short time, persistent refusal to return to the red colour is rectified by careful cleaning of the discharge tube. Some of the Oxford sources have operated for several weeks without attention. Another fault which occurs in sources which have operated for some time is difficulty in starting the discharge. This is easily remedied by use of a Tesla coil or similar device, or momentarily increasing the pressure.

Conclusion.

Many of these sources are now being used as more or less standard equipment in high voltage accelerating apparatus. Work is being done at Cambridge and at Harwell to adapt this type of source for work in pressure insulated electrostatic generators. I believe they are sufficiently robust, trouble free, and efficient to find increasing favour for use in almost all applications where Ion Sources are required.

References.

[1]) M. Hoyaux and I. Dujardin, Nucleonics **4**, 7 (1949)
[2]) I. A. Getting, Phys. Rev. **59**, 467 (1941).
[3]) P. C. Thonemann, Nature, **158**, 61 (1946).
[4]) P. C. Thonemann, D. Ph. Thesis, Faculty of Physical Sciences, University of Oxford (1949).
[5]) A. J. Bayly and A. G. Ward, Can. J. Research, A. **26**, 69 (1948).
[6]) J. G. Rutherglen and J. F. I. Cole, Nature **160**, 545 (1947).
[7]) R. N. Hall, Rev. Sci. Inst. **19**, 905 (1948).
[8]) P. C. Thonemann, J. Moffatt, D. Roaf and J. H. Sanders, Proc. Phys. Soc. **61**, 483 (1948).
[9]) H. D. Smyth, Rev. Mod. Phys. **3**, 347 (1931).
[10]) G. I. Finch, Proc. Phys. Soc. **62**, 465 (1949).
[11]) L. H. Bedford, J. Sci. Inst. **13**, 177 (1936).

The development of a magnetic ion-source with high ionisation efficiency

by **P. C. Veenstra** and **J. M. W. Milatz.**
Physical Laboratory of the State University of Utrecht, Holland.

Introductory.

Though the magnetic ion-source offers several advantages compared with other types of sources, it is seldom used since the early work of A. Th. FINKELSTEIN[1]) and M. v. ARDENNE[2,3]). An exception is found by W. MAAS[4]).

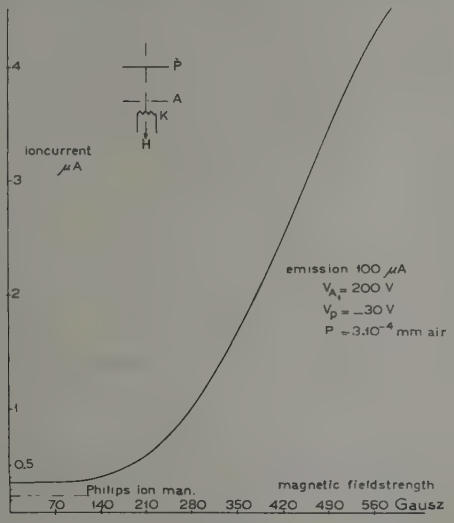

Fig. 1.

The principal advantages turn out to be:

1. the powerconsumption is low — power is obtained from storage-batteries. Consequently the source and its complete power supply can be put at a high potential;
2. gaspressure and hence gasconsumption are low;
3. high currents of monokinetic ions are obtained, with up to 50% atomic ions in the beam;
4. no artificial cooling is required.

Preliminary experiments.

In a magnetic ion-source the probability for an electron to ionize the gas is increased by a magnetic field which forces the electrons to describe a spiral. For this reason the first thing one is interested in is the relation between magnetic fieldstrength and ion current. This means to get some insight into the amount in which the spiralizing movement of the electrons increases the length of their orbits.

The result is to be found in fig. 1, showing that an increase in ion current up to a factor 15 easily can be produced.

Space-charge effects.

With higher cathode emission space-charge effects will occur. When repeating the former measurement a result as shown in Fig. 2 is obtained. In this graph both ion-current and emission have been

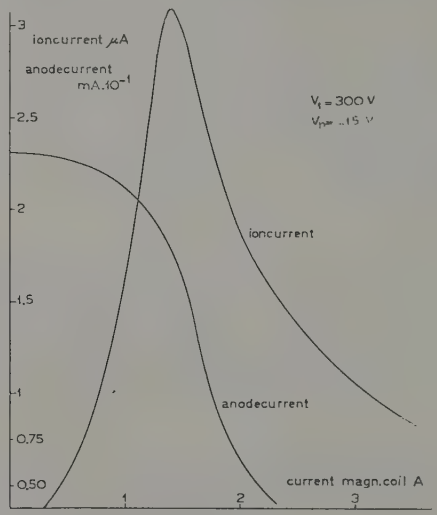

Fig. 2.

plotted against the magnetic field strength. The decrease of anode current is caused by a strong negative space charge introduced by the action of the magnetic field. Obviously the magnetic field narrows the electrons into a beam, representing a zone of high negative space charge. Owing to loss of speed the majority of the electrons in the beam loses for a certain pair of values of anode tension and the magnetic field strength the power to ionize the gas, so that the ion-current decreases.

We assume the electron space-charge density to be proportional to the magnetic field H and reciprocally proportional to the electron speed $\{V_A\}^{1/2}$, where V_A is the anode tension.

Assuming secondly the maximum ion-current in each case to occur as soon as a critical negative space-charge is reached, a straight line is to be expected if in each maximum of ion-current H is plotted against the corresponding value of $\{V\}^{1/2}$. Fig. 3 shows the results of a series of measurements.

In conclusion: the ion-current output of a magnetic source will be limited by negative space-charge introduced by the magnetic field. Compensation of the negative space-charge can readily be obtained by increasing the anode tension. It turns out to be

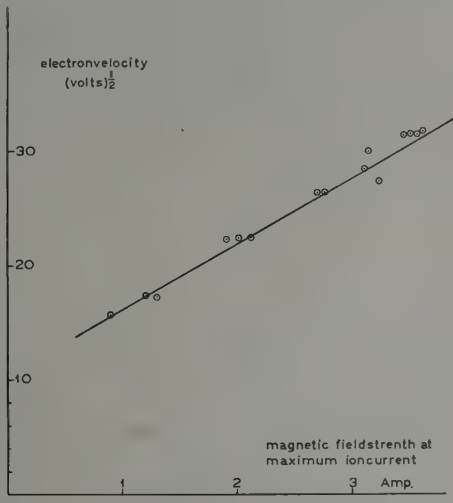

Fig. 3.

possible to build an ion-source operating at pressures down to $5 \cdot 10^{-5}$ mm. Hydrogen and giving an ion current up to 0·3 mA at a plate tension of 2 to 3 kV. It is however desirable to build a low-tension source and by this demand the source has to be operated at higher pressure.

Looking at Fig. 4, where once more the ion-current and the anode current are plotted against the magnetic field, this time for several pressures, it is clear that increase of pressure renders an automatic compensation of negative space-charge. At higher pressures the shape of the curves is changed: the ion current decreases less rapidly and finally there is a tendency to increase. Moreover the

maxima can be seen to shift to higher magnetic field strength when the pressure increases. Increasing pressure means growing ionisation density which implies introduction of positive space-charge. The result is that a stronger magnetic field can be used before the critical negative space-charge is reached. Bearing in mind that the ion-velocity is small compared with the electron-velocity, complete

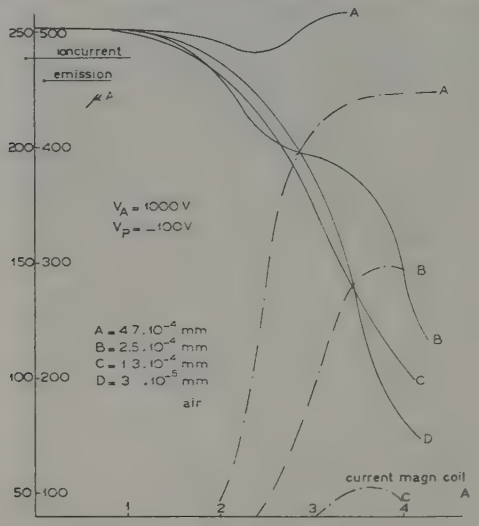

Fig. 4.

space-charge equilibrium may be obtained when the pressure is sufficiently increased and in this case strong ion-currents may be expected.

The oscillation of electrons.

The formation of space-charge equilibrium is greatly stimulated by the oscillation of secundary electrons, i. e. electrons generated by ionisation of the gas. It may be remarked that the primary electrons, i. e. electrons emitted by the cathode, will return into the cathode after performing one oscillation. The secondary electrons are formed at random in the ionisation space, hence they have a good upportunity to oscillate, so that they are far more effective for ionisation than the primary electrons. In a magnetic source the primary electrons only serve to start operation. As soon as a critical gas pressure has been reached the secondary electrons become far more essential as they have a much higher chance to oscillate. It is therefore necessary to stimulate the existence of electrons of

adequate average speed while, with an eye to space-charge balance, the ion-velocity must be kept as low as possible. Ion extraction therefore must be perfomed by diffusion.

When the critical ionisationdensity mentioned before is passed the ion-current increases to values up to 5 mA. The same is observed when, operating at the critical pressure the magnetic field is increased. The source operates quite stable in a higly efficient state which we have called "superstate". The most important property of this state is its irreversability, i. e. when operating in superstate obtained by increasing the magnetic field, it is possible to decrease the field without considerable loss of ions — untill the field reaches a definite value and the ion current drops to about 10% of its former value. This value corresponds to the normal ion-output of the source operating out of superstate.

The same can be observed by varying the pressure.

The larger the primary emission has been chosen the sooner the superstate will be observed and the larger the ion-output of the source will be. Recently we build a magnetic source equipped with water cooling. At a pressure of 0.5 micron of hydrogen ion currents up to 20 mA are obtained.

The percentage of atomic ions.

Magnetic analysis of the beam shows for hydrogen a proton percentage of about 50%, a figure which is surprising high for a source containing metallic surfaces. It however must be remarked that the tantalum anode system of the source runs red-hot during operation. Atomic recombination being a three-body phenomenon, recombination mainly occurs on surfaces covered with adsorbed atoms. A high temperature will prevent atoms sticking to these surfaces: the thermal equilibrium $H_2 \rightleftharpoons 2H$ is shifted to the right at high temperature, this being a reason for the satisfying proton-output of the source.

Technical development, drawing Fig. 5.

The ion source system housed in the lower end of the central copper tube A, consists of a tungsten cathode and a set of three anodes. The lower two represent a field-free space, the first anode has a slightly different potential for focussing purposes. The ion exit-canal and so the entire envelope of the source are kept at cathode potential. The anode system is insulated from the copper tube by means of a pyrex cylinder which also provides central adjustment.

The drawing shows that the dimensions of the ionisation space are very small and the space charge compensation makes it easy to get the ions out of the source. Measurement shows this to amount up to 50%.

The housing of the source consists of the copper tube *A*, welded to the iron plate *B*, centrally bearing the ion exit canal.

Concentrically with *A* is the iron tube *C*, closing via the iron upperplate *D* and the solid iron rod *E* the magnetic circuit of a

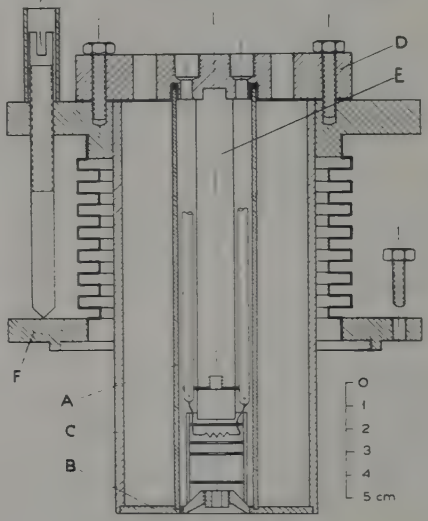

Fig. 5.

coil housed in the space between *A* and *C*. The entire magnetic field is between the iron rod *E* and the ion exit-canal.

The plate *D* is provided with a groove fitting the copper tube. A rubber ring assures vacuum thightness. Adjustment of the source is obtained by means of vacuum bellows and three screws.

Results.

When at high vacuum the cathode of the source is adjusted to give a primary emission of about 10 mA at a plate tension of 150 V. the current increases to 50 mA at a gas pressure of 0.6 micron hydrogen and the source is in "super state". The ion output passing an

exit canal of 3 mm diam. will amount to 1 mA. Summarizing we find:

gas pressure	0.6 micron hydrogen
normal emission	10 mA
total emission	50 mA
anode tension	100—300 V
magnetic field	1000 Gauss

On increasing the input power the ion current rapidly increases.

emission	300 mA
ion current	3 mA

When the pressure is increased up to 0.8 micron, the ion current will increase to 5 mA.

Cold emission sources.

The principal drawback of the magnetic source is the presence of a hot cathode having a limited lifetime.

When the acceleration equipment posesses sufficient pumping speed, the cathode may be omitted and after slight alterations the source will operate with cold emission as described by PENNING[5], and recently by R. KELLER[5]), showing superstate like the hot cathode type. The presence of a field-free space in the anodesystem as described before is strictly required to get stable operation.

Operating data are:

gaspressure	10 micron H_2
plate current	20 mA
plate tension	800 V
magnetic field	1000 Gauss
ion current	2 mA
diam. ion exit canal	3 mm

The proton percentage has not been measured so far, but after 10 minutes operation the discharge in the source becomes bright red, so that we may expect the proton output is high.

Bibliography.

[1]) A. TH. FINKELSTEIN, R. S. I., vol. II, No. 3, 94 (1940).
[2]) M. v. ARDENNE, Ph. Z. **43**, 90 (1942).
[3]) M. v. ARDENNE, Zs. f. Ph. **121**, 236 (1943).
[4]) W. MAAS, Thesis Utrecht 1948.
[5]) F. M. PENNING and J. H. A. MOUBIS, Physica **4**, 1190 (1937).
[6]) R. KELLER, Helv. Ph. A., vol. XXII, fasc. prim. 1949.

Physical problems in high-intensity ion sources

by **C. J. Bakker** and **J. Kistemaker**

Stichting voor Fundamenteel Onderzoek der Materie, Afd. Massaspectrografie, Zeeman-laboratorium, Amsterdam.

Three criteria are of great importance for high intensity ion sources:

1. the production of the ions in the discharge;
2. the transportation of the positive ions to the edge of the plasma, or out of the discharge in the direction of the exit opening;
3. the extraction of the ions from the source without disturbing the discharge.

We give a short discussion of these three points.

1. The gas in ion sources is usually ionized by electron impact. Call P_i the number of ions created per electron per unit path length and per unit of pressure at 0° C. Then the total number N_i of ions created per second is

$$N_i = i_e P_i p \bar{x}/e$$

where i_e is the electron current, p the pressure and $\bar{x}$ the mean path length of an electron in the source. P_i shows a maximum at about 100 eV[1]). It is favourable to increase i_e and $(p\bar{x})$ as much as possible. The factor $(p\bar{x})$ is most interesting as, in order to avoid the use of big pumps, the pressure in the source must be reduced as much as possible to enable the extraction and acceleration of the ions. A theoretical expression for $(p\bar{x})$ results from the following considerations.

Let us denote by P the probability for the disappearance of an electron from the discharge per unit path length. P will depend strongly on the type of ion source. In a first approximation it may be supposed however that in capillary arc sources (Lamar) and in magnetic sources (Finkelstein, Heil).

$$P = P_a + P_c p$$

where P_a represents the loss of electrons to the anode and the walls independent of the pressure; $P_c p$ represents the loss of electrons at pressure p, due to collisions with gasmolecules. Both P_a and P_c

are very sensitive to the velocity of the electrons and an applied magnetic field H. If H is parallel to the electric field, both P_a and P_c tend to decrease with increasing H. The same expression for P may hold approximately in high tension ion sources if $\bar{x}$ is taken along the electron path. According to our definition of P we have:

$$i_e = i_{e,o}\, e^{-Px}$$

and

$$(p\bar{x}) = p \int_0^\infty P e^{-Px}\, x\, dx$$

or

$$(p\,\bar{x}) = \frac{p}{P} = \frac{p}{P_a + P_c\, p}\,.$$

As the recombination coefficient is certainly smaller than 10^{-10} it can be easily shown that in our case the number of electrons lost by recombination is much smaller than the number of electrons present.

We distinguish between:

a) Capillary-arc ion sources and to some extent also high tension ion sources. Usually $p \leqslant 10^{-1}$ mm Hg. As the loss of almost all electrons is due to the electrode configuration $P_a \gg P_c\, p$ and $(p\bar{x}) \sim p/P_a$. This means that N_i is linearly proportional with p.

b) Magnetic sources, with oscillating electrons. The pressure range p is 10^{-5}—10^{-2} mm Hg. If anode dimensions and p are chosen well $P_a \ll P_c\, p$ and consequently $(p\bar{x}) \sim 1/P_c$. This means that N_i is pressure independent.

c) High frequency ion sources differ from the preceding types in several respects. The value of $\bar{x}$ is always several times the size of the source if diffusion losses are reduced. The electron current i_e depends on the pressure, as all electrons originate from the gas by ionisation; i_e is maximum if the electron collision frequency in the gas equals about the frequency ν of the field. Consequently the optimum in p increases with ν. A frequency of 100 M.C. corresponds with about $p = 3 \cdot 10^{-2}$ mm Hg.

The sources of type *b* seem to be very convenient to obtain high values of N_i at low pressures. The electron current i_e can be made high and $(p\bar{x})$ can be raised considerably by increasing H.

2. The maximum current which can be drawn from a source depends on the potential distribution and degree of ionisation in the plasma or discharge as well as on the extraction conditions. The ion

currents obtain their maximum value if they are so called "space charge limited". The minimum ion density $n^*_{\min}$ at the emitting aequipotential surface, which we will call the "virtual cathode" of the ion source, giving rise to space charge limited currents, follows according to LANGMUIR[2]) from

$$\alpha\, n^*_{\min}\, \bar{v}^*\, eO = 5{,}4 \cdot 10^{-8}\, \frac{O}{d^2} \left(\frac{V^3}{M}\right)^{1/2}$$

where $\bar{v}^*$ is the mean velocity of the ions at the virtual cathode; this is the aequipotential surface at which the electrons are reflected back into the discharge. This surface is situated approximately at B in Fig. 1. The factor α is about 0.25 for thermal ions and 1 for

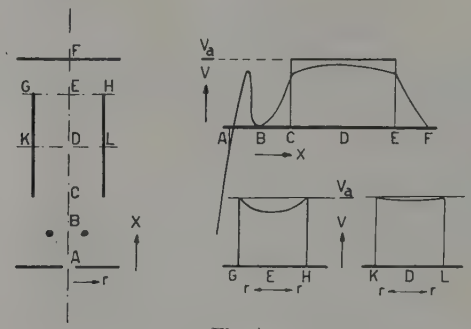

Fig. 1.

Scheme of the potential distribution in a magnetic ion source with coaxial magnetic field. Direction of ion extraction and magnetic field coincide.

a) The source with electrodes;
b) axial potential distribution for space charge limited ion currents;
c) radial potential distributions.

perfect unidirectional ions. O is the area of the virtual cathode, d its distance from the extraction electrode, V the extraction voltage in Volts and M the mass number of the ions.

In order to obtain space charge limited ion currents with an ion density $n^*_{\min}$ as small as possible, one must realize:

a) $\bar{v}^*$ as large as possible; increase from thermal velocity (0,1 eV) to 100 eV increases $\bar{v}^*$ already with a factor thirty.

b) $\alpha = 1$, which means unidirectional ions.

c) the depth of the source, from which the unidirectional ions are transported to the virtual cathode as large as possible. To a certain extent the number of ions is proportional with this depth.

The ion density $n_{\min}$ in the ion production region (CD in Fig. 1) of the plasma is related with $n^*_{\min}$ by

$$n_{\min}\,\bar{v} = n^*_{\min}\,\bar{v}^*$$

if $\bar{v}$ is the mean velocity of the ions in the plasma.

We touch here one of the most fundamental problems, *viz.* how to transport the ions from the production zone in the source to the emitting aequipotential surface, without loosing them to all directions. A good source is self focussing. The potential distribution forces the positive ions to the emitting surface. In this case there

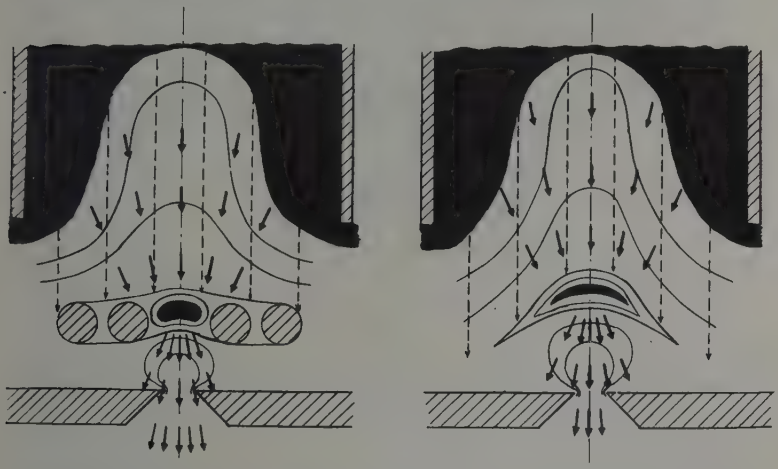

Fig. 2.

Comparison between the extraction mechanism for space charge limited ion currents in a magnetic ion source with a filament at the extraction side (grid functioning) and the usual FINKELSTEIN type. The drawn lines indicate the electric aequipotential surfaces; the block lines indicate the electron oscillation paths. The arrows give the paths of the positive ions. Black regions are regions with a potential which is relatively high, approx. anode potential.

will be a potential trough, as there is *e. g.* in the magnetic ion source of the FINKELSTEIN type, Fig. 1, and also in the high tension sources. A bad source has a potential mountain in the production zone, which gives a diverging ion beam in the plasma itself. This can happen in a capillary arc source.

3. The space charge limited current indicated in 2. holds for a plane emitter. However the "penetrating" field of the strongly negative extraction potential displaces and curves the ion emitting surface, which induces a resemblance with Langmuir's external

emitter. It also results in an increase of d. In this way an increasing high tension field partially eliminates its favourable action ([1] [2]) by the increase of d, but especially by a deformation of the ion emitting surface. The latter effect can easily reduce the maximum ion currents with a factor 4.

These facts are of great influence in high tension type ion sources, and also in some high frequency types, if the discharge is not intense. No doubt also in the Lamar-type capillary-arc ion source and in the Heil-type magnetic source some influence remains, but there

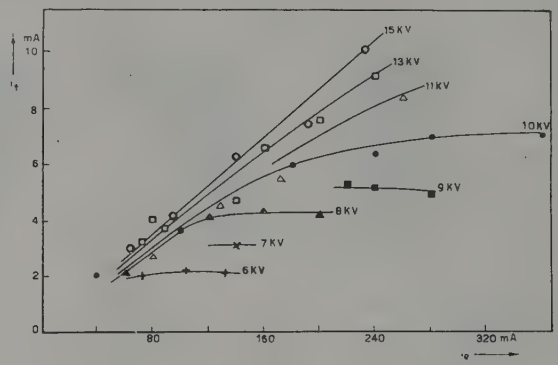

Fig. 3.

The ion current on the target (i_t) as a function of the emission current of the filament i_e, for helium gas. The accelerating tensions vary from 6 to 15 kV.

it must be kept small in order to prevent extinguishing the discharge. From these points of view it follows that for the latter two types the presence of a grid over the extraction opening might be favourable. The influence one can observe in Fig. 2.

As a consequence of the facts mentioned sub 1, 2 and 3 we constructed a magnetic ion source in Amsterdam[3]) producing typically sp. ch. lim. ion currents of the order of 5 mA, at a gas pressure in the source of $4 \cdot 10^{-4}$ mm Hg. The number of accelerated ions leaving the source, was about 80% of the total number of gasmolecules consumed. We used H_2, He and N_2 gas. The beam was not yet analyzed. The typical space charge limited ion currents are shown in Fig. 3.

Bibliography.

[1]) A. v. Engel and M. Steenbeck, Elektrische Gasentladungen I, 35 (1932).

[2]) I. Langmuir and K. T. Compton, Rev. Mod. Phys. **3**, 237 (1931).

[3]) J. Kistemaker and H. L. Douwes Dekker (to be published shortly in Physica).

Atomic Piles and their Use in Nuclear Physics

by **E. Bretscher** (Harwell).

The use of the atomic pile as an instrument for the nuclear physicist falls under two headings. Firstly, there are methods which use the chain reacting mechanism of the pile to perform a measurement. Secondly, one can use the pile simply as a source of neutrons.

In order to be able to explain the methods using the pile mechanism, it is useful to summarise the simplest ideas about piles:

1. Physics of a Multiplicative System based on Slow Neutron Fission (Homogeneous System).

(A) *Slowing Down and Diffusion Processes (in the absence of fissile materials).*

When we introduce a fast neutron source into an infinite block of graphite or a large volume of water, we find that the neutrons lose energy by inelastic collisions till they have become thermal. If the moderator used has a low absorption cross section, the thermal neutrons thus produced diffuse through the medium until either they escape or are captured by the moderating medium. We can characterise the first of the two processes, namely, the slowing down process, by a slowing down length, L_s, up to which the neutrons on the average travel till they have reached a specified energy. This length L_s depends on the scattering mean free path, the average cosine of scattering b and the number of collisions N necessary to reach from an initial energy E_i to the final energy E_f. L_s can be obtained from the following relations provided the scattering cross-section is energy independent:

$$L_s^2 = \frac{2\,l_s}{3\,(1-b)}\,N \qquad (1)$$

$$l_s = \frac{1}{\Sigma n_i\,\sigma_i} \qquad (2)$$

where n_i and σ_i are number and cross section of the i_{th} atom per cm^3. If it is assumed that the collisions are symmetrical in the centre of mass system, b depends in a simple manner on the mass

of the atoms making up the medium, N is obtained from the average logarithmic energy loss:

$$N = \frac{1}{a} \log \left(\frac{E_i}{E_f} \right) \tag{3}$$

$$\text{where } a = \left(\log \frac{E_i}{E} \right)_{\text{av.}} \tag{4}$$

and has the value:

$$a = 1 - \frac{(M-1)^2}{2M} \log \left(\frac{M+1}{M-1} \right) \tag{5}$$

To give an example: about 100 collisions are required to reduce the energy of a neutron from 2 MV to 1 eV in graphite, in the course of which it travels about 18 cm from its origin.

It ought to be noted that such elementary considerations are only roughly true since it is assumed that the l_s is energy independent.

After the neutrons have just reached thermal velocity, they will migrate until they are captured. This situation can be described by a diffusion equation, which in the stationary case simply states that the production S of thermal neutrons in a unit volume is just balanced by the absorption of neutrons in the volume (n/τ) and the outflow of neutron current j

$$S = \frac{n}{\tau} + \operatorname{div} j \tag{6}$$

where n is the thermal neutron density at the point, τ the mean life of the neutron, j the neutron current, and S the number of neutrons becoming thermal per cm^3 and sec. If we make the simplest assumption, we can say that $j = -D \operatorname{grad} n$, where D is a diffusion coefficient which can be shown to be equal to

$$D = \frac{l_s v}{3} = \frac{l_s \cdot l_c}{3\tau} \equiv \frac{L^2}{\tau} \tag{7}$$

If we note that $l_c = \bar{v}\tau$ (l_c capture mean free path) and define a quantity $L^2 = D\tau$, we can write the diffusion equation as follows:

$$\nabla^2 n - \frac{n}{L^2} = -\frac{S}{L^2} \tag{8}$$

(B) *Multiplying Homogeneous Medium.*

We will now apply the above equation to the case of a moderator containing fissile material: in this case the source strength S is proportional to the thermal neutron density. Let us indicate with k the number of secondary neutrons produced when one thermal

neutron is captured. Then we have a source of neutrons $S = kn$ and the above equation becomes:

$$\nabla^2 n + \frac{(k-1)}{L^2} n = 0 \tag{9}$$

Equation (9) is in actual fact incorrect, because we tacitly assumed that the source S emits neutrons which are thermal, but in fact the fission neutrons are fast. It can be shown by a combination of the slowing down mechanism and diffusion theory that L^2 in the above equation has to be replaced by a quantity M^2, the migration length, obtained in the following manner:

$$M^2 = L^2 + L_s^2 \tag{10}$$

The *pile equation* in its simplest form is therefore:

$$\nabla^2 n + \frac{k-1}{M^2} n = 0 \tag{11}$$

where $\frac{k-1}{M^2}$ is often called the Laplacian $\varkappa^2$.

As a solution for a cubical homogeneous pile of length a we obtain

$$n(x, y, z) = N_0 \cos \frac{\pi}{a} x \cos \frac{\pi}{a} y \cos \frac{\pi}{a} z \tag{12}$$

fulfilling the boundary condition that n must vanish at the face of the cube. The critical size a of the pile would result, when the solution (12) is inserted into pile equation (11):

$$\frac{3\pi^2}{a^2} = \frac{k-1}{M^2} \tag{13}$$

N_0, the number of neutrons at the centre of the cube is arbitrary and determined by the power at which the pile is being run. That (12) is indeed the correct solution and (13) the critical size can be shown by considering the time dependent equation. The general solution then shows that the higher harmonics of the solution die out and only the fundamental remains for stationary piles. We note that the critical size a of a pile increases with the migration length M: a graphite pile has to be larger as the C atoms are poor in slowing down compared to water or D_2O. In addition the neutron balance is more favourable in the D_2O pile as $k - 1$ is larger in this case than for a graphite pile; the critical dimension a becomes smaller, therefore, for D_2O than C. These simple considerations are quite important for the experimental physicist who wishes to use a pile as a source of neutrons.

(C) *Time Variation of Neutron Level in a Pile as a Whole.*

If at any moment we have N neutrons in a pile which is not stationary, we have a rate of change dN/dt which is determined by the multiplication and absorption plus loss such that

$$\frac{dN}{dt} = \frac{N(k_e - 1)}{\tau} = \frac{N}{T} \tag{14}$$

$$T = \frac{\tau}{k_e - 1} \tag{15}$$

(T is often called the pile relaxation time, k_e is the effective multiplication constant), so that N increases exponentially if $k_e \quad 1 > 0$ or decreases for $k_e - 1 < 0$. To give a numerical value let us assume $k_e = 1 \cdot 01$ and $\tau = 1.5 \cdot 10^{-3}$ sec., this being assumed as the neutron

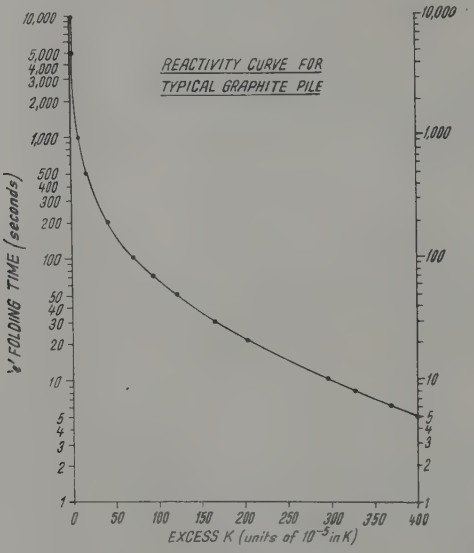

Fig. 1.

Relexation time of a pile as a function of reactivity $\delta = k_e - 1$.

mean life holding for a graphite pile. With these data, T becomes 0.15 seconds. The pile power will therefore rise with alarming speed. This situation, fortunately, does not occur in practice, because about 1% of the neutrons from fission are delayed and it is in fact they which control for small values of $k_e \quad 1$ the speed with which the neutron level rises (the longest delayed period is 85 se-

conds). A calculation taking the effects of the delayed neutrons into account gives, instead of (14) (δ = reactivity):

$$\delta \equiv k_e - 1 = \frac{\tau}{T} + C\sum \frac{\mu_i \tau_i}{T+\tau_i} \approx \frac{\tau + C\Sigma\mu_i\tau_i}{T} \quad \text{(for } T > \tau_i \text{ maximum)} \quad (16)$$

where C signifies the fraction of all delayed neutrons, μ_i the relative contribution of neutron period τ_i. Obviously, for relaxation times T large to this period the reactivity δ is again inversely proportional to T and this fact makes it very convenient to use the rise time T as a measure of k_e. For this case, with the correct numerical constant, δ becomes $\delta = 2.5 \cdot 10^{-5}/T$ (with T measured in hours) (Fig. 1).

(D) *Actual Piles.*

A pile of the type described but spherical (the water boiler) is at present in operation in Los Alamos. It consists of a solution of U^{235} dissolved in water, the container being surrounded by a re-

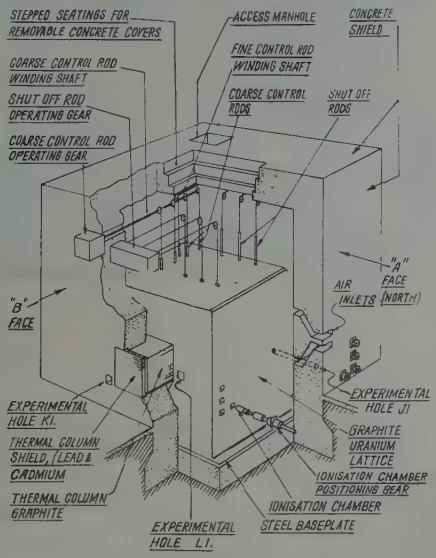

Fig. 2.
Schematic view of Gleep.

flector. Most piles in operation, however, are *inhomogeneous* such as *graphite* or *heavy water* piles. This is done to prevent neutrons in the epithermal energy region from being captured by the U^{238}

since it absorbs strongly above thermal energies and therefore has an unfavourable effect on the neutron balance. I will restrict my remarks to an example, namely, the small experimental pile in Harwell, called Gleep (Graphite Low Energy Experimental Pile). It is an assembly of pure graphite through which channels are provided which contain the uranium. This arrangement of a lattice of channels modifies the simple neutron distribution through the pile: the simple cosine-distribution as found in the homogeneous pile is now modulated with periodicity of the lattice. The reacting core is surrounded by a reflector which diminishes the quantities of

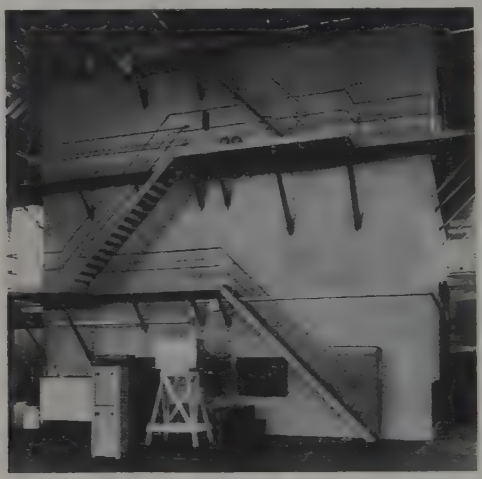

Fig. 3.
Gleep: Pile Face. Experimental hole under stairs with „beam catcher" in front of it and health monitor in foreground.

metal necessary and increases the average output of power per ton of material. The *control* is obtained by a set of control rods made of heavily absorbing material, and the *neutron level* is measured with the help of boron trifluoride ionization chambers placed at various spots inside the graphite. The *cooling* is achieved by blowing air through the uranium carrying channels. This simple arrangement allows us to go up to 100 kW. design power. The second and larger Harwell pile, Bepo, has a more effective cooling system which permits the design power to run up to 6000 kW. The Chalk River *heavy water* pile consists of a large tank filled with D_2O into which uranium rods penetrate. The rods are cooled with ordinary water,

a measure which has allowed the design power to reach 10,000 kW. Since the pile dimensions are smaller and the power rather high, it is at present the best pile in existence insofar as neutron flux is concerned.

2. The Use of the Pile as a Measuring Instrument.

Two applications of the pile will be discussed below: (A) the determination of the absorption of a specimen. (B) the absolute calibration of a neutron source with the pile.

(A) *Absorption Measurements.*

In the past, the pile has often been used to measure the absorption cross section of nuclei for thermal neutrons. The method was first described in a paper by Anderson. Fermi. Wattenberg. Weil and Zinn. and is often referred to as the "danger coefficient" method. It is based on the fact that the introduction of an absorber into the pile diminishes the reactivity of the chain reacting system. This change can be observed by measuring the relaxation period of the pile (equation (16)). The method serves only to compare absorption. since a calibrating substance. such as boron. has to be used for calibration. The influence on $\delta = k_r - 1$ is proportional to the total absorption of the specimen and proportional to the square of the neutron density. as will be seen in the next section. The sample is therefore placed in the centre of the pile. For the actual performance of the measurement. there are several possible modifications. One way of doing it is the following: the pile power, as indicated by the B-ionization chamber current. is allowed to increase slowly by adjusting the control rod. Next a specimen is introduced, so that the power diminishes. The difference of the reciprocal T-values is a measure of Δk_r. The procedure is now repeated with the calibrating substance placed at the same positions in the lattice. Boron is generally preferred. since its cross section varies with 1 v and has been measured with great precision (Fermi and Marshall: $\sigma = 704$ barns for Borax at 2200 m s neutron velocity).

The method is most reliable with elements of large absorption cross sections. If the specimen scatters strongly. or slows down appreciably. the reactivity is affected even in the absence of absorption (in the opposite sense). For this reason the absorber must be placed in a region of low neutron density gradient. so that the general neutron distribution is not appreciably changed by the insertion of the absorber. Fermi and collaborators have been able to take scattering

and slowing down into account and determined the absorption of beryllium (loc. cit).

One may ask what is the accuracy of such a method? A limit is set by the stability of a pile, namely, the variation of the reactivity of the pile through temperature effects and through the change of barometric pressure: since the X-ray density of graphite is 2.25, the bulk density only 1.6, it is evident that about one quarter of the pile volume is filled with air, disregarding channels. Since molecular nitrogen has a thermal absorption cross section of about 3.4 barns, any change of air pressure will affect the pile reactivity. A change of 10^{-3} atmospheres has the same effect as the introduction of about 1 cm^2 absorber into the centre of the pile.

To improve the pile method of absorption cross section measurements, the *pile oscillator* was invented[2]). Let us suppose that the

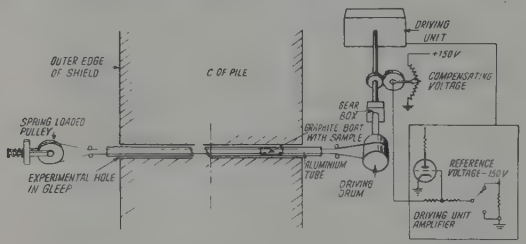

Fig. 4.

Pile oscillator: schematic view.

pile power in the absence of the absorber is slowly rising ($k_e - 1 > 0$) and that the insertion of the absorber has the effect of making the pile power diminish with time ($k_e - 1 < 0$). If we move the absorbing specimen periodically in and out of the pile, a periodic change of the pile power will be brought about, the amplitude being proportional to the total absorption of the specimen. It is obvious that this method avoids, to a great extent, effects due to irregular changes in pile reactivity. They only produce a slow drift of the pile power as read from the ionization chamber current of a recording instrument. This method has the further advantage that the periodic part of the ionization current, which is due to the effect of the absorber, can be amplified by A.C. methods, which introduce considerable simplification of design. Such pile oscillators have been used in the Argonne and Clinton Laboratories in the U.S.A., in N.R.C. Laboratories in Chalk River in Canada, and at A.E.R.E. There are many modifications and considerable refinements of this beautiful method

which, however, are too detailed to be discussed in this review. With the improvements, it is possible with our instrument in Harwell to measure a total absorption cross section of 1 cm^2 with an accuracy of 1% (example: 5 mgr. gadolnium).

(B) *Determination of the Number of Neutrons emitted by a Source.*

Mr. Littler[3]) has recently made experiments to determine with a pile the *absolute number of neutrons* emitted by a *radium-beryllium source*. The method is based on the following considerations: let us consider the case that a pile is just critical, i. e. that the neutron level does not increase or diminish with time. In this case as many neutrons are created per second as are absorbed or escape. Most of the created ones are due to the chain reaction, but a finite number

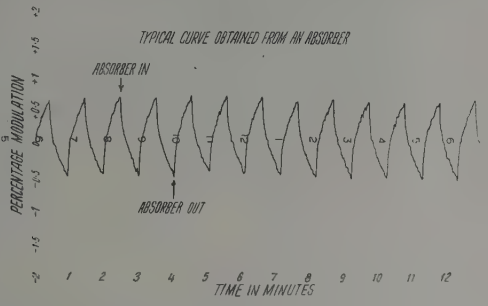

Fig. 5.
Experimental record of periodic part of ionisation current variation due to absorber.

are always produced in the pile through spontaneous fission, α-n processes and cosmic ray effects. The effective reproduction factor k_e is in the stationary state therefore just a trifle below 1. If these neutrons could be cut out somehow, the neutron loss would be greater than production and the neutron level would diminish since $k_e - 1 < 0$. Conversely, if we introduce a neutron source into a steadily going pile, by similar arguments, the neutron level would be expected to increase as a function of time. The situation is, however, a little complicated by the fact that the radium contained in the usual neutron sources has a large neutron absorption cross section which affects the reactivity in the opposite manner. However, the positive contribution of neutron emission is power-independent, whilst the number of neutrons absorbed increases with the neutron level. To eliminate the absorption effect, we make ob-

servations of the change of reactivity for various pile powers and can, in this way, eliminate the absorption effect fairly satisfactorily.

In order to obtain a quantitative result, the following procedure is carried through: a pile, in the steady state, is considered which has a cavity at first empty. Next the source to be calibrated is introduced into the cavity and the balance of the pile disturbed. To obtain equilibrium again, k_e has to be changed by δk_e. A calculation with the two group theory shows how this δk_e depends on the various factors:

$$\delta k_e = \frac{\tau \cdot n^2}{W / n^2 \, dV} \left(\alpha - \frac{SW}{n} \right) \tag{17}$$

$$\text{where } W = \frac{(\varkappa^2 L_g^2 + 1)\, p}{k_1} \tag{18}$$

where W consists only of known pile constants.

If δk_e as a function of $1/n \sim \frac{1}{\text{power}}$ is determined, the slope of the line thus obtained would give S except for a constant of proportionality. As a rule, n or the power is obtained from the ionization current I in an ion chamber: we therefore write

$$n = BI \tag{19}$$

(17) now becomes:

$$\delta k_e = A \left(\alpha - \frac{SW}{B} \times \frac{1}{I} \right) \tag{20}$$

where A stands for the expression in front of the brackets of (17).

In order to eliminate the constants we make an additional experiment: we determine the effect on k of an absorber which becomes radioactive (δk_A), such as Na or P, when it is brought into the cavity (without source). Next we determine absolutely the number N_0 of active Na or P atoms formed per second at one definite pile power (or ionization current I_0) by standard beta ray coincidence counting methods. Now the effect of the absorber Na or P on k will be:

$$\delta k_A = A \beta \tag{21}$$

and the radioactivity produced is:

$$N_0 = \beta \cdot n = \beta B I_0 \tag{22}$$

where β is the total effective absorbing surface of the Na or P.

Inserting (21) and (22) into (20) one obtains:

$$\frac{\delta k_e}{\delta k_A} = \frac{\alpha}{\beta} - \frac{S \cdot W}{N_0} \frac{I_0}{I} \tag{23}$$

Since W is known, N_0 and I_0 are measured, S the source strength

is obtained from the slope of the straight line, where the left-hand side of equation (23) is plotted against $1/I$.

A consideration of the errors leads one to assess an accuracy of about 6% for this method in the present stage of development.

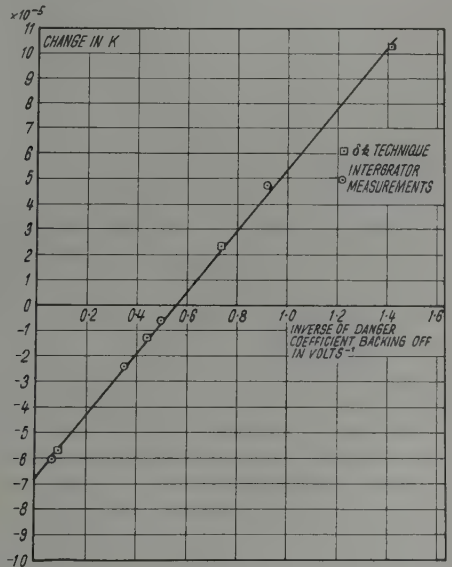

Fig. 6.

Change in k produced by Ra-Be Source as Function of Pile Power.

3. The Pile as a Source of Neutrons.

For many slow neutron experiments, the intensity of the slow neutron beam available is decisive. It may therefore be useful to review the various neutron sources available to the physicist. Let us calculate the neutron flux in the centre of an imaginary pile running at 100 kW.: the number of fissions is roughly $3 \cdot 10^{15}$ per second and the number of neutrons say 10^{16} sec^{-1}. For a pile of say 10 m length, and a neutron life-time $1.5 \cdot 10^{-3}$ sec., the neutron density becomes: $10^{16} \cdot 1.5 \cdot 10^{-3} / 10^{9} = 1.5 \cdot 10^{4}$ on the average over the pile. In the centre, however, the neutron density is larger by about a factor 4 over the average. Assuming a velocity of the neutrons of about $2 \cdot 10^{5}$ cm/sec., the neutron flux becomes: $1.5 \cdot 10^{4} \times 4 \times 2 \cdot 10^{5} = 1.2 \cdot 10^{10}$ n/cm^2 sec. In piles running at higher powers it is easy to achieve a thermal neutron flux of say 10^{12} n/cm^2 sec. If

one then allows a canalization factor of $10^{-6} - 10^{-7}$, the beam intensity becomes 10^6—10^5 neutrons/cm^2 sec., enough for use with crystal spectrometers or velocity selectors.

It should be borne in mind, in this connection, that the experimentally available neutron flux out of a pile does not increase indefinitely with the power of the pile because high power piles have generally cooling mechanisms which absorb reactivity, and this loss of reactivity has to be compensated by making the pile bigger. A considerable factor, however, can be gained by using a heavy water pile instead of a graphite pile as a neutron source, because for a given pile power the volume of the heavy water pile is smaller. I shall return to this matter again at the end of the discussion.

For comparison we may note the fast neutron yields of other frequently used neutron sources: the cyclotron will at best produce a total yield of 10^{12}—10^{13} neutrons from its target; the high voltage set in Cambridge running with 200 μ amps. deuterons on a lithium target with a bombarding energy of 1 MeV provided approximately 3×10^{10} neutrons, whilst ordinary radium-beryllium sources emit 10^7 particles per gram. Though the total number of neutrons is fairly high in a cyclotron, the necessity to slow them down in a moderator leads to a great dilution in neutrons which reduces the fluxes available in the thermal energy region. For thermal neutron beams, the pile remains the superior instrument.

I would next like to survey very briefly the main groups of experiments which have been carried out with the help of piles, without being able to go into the details of these researches.

A. *Experiments requiring Slow Neutron Beams.*

(a) *Neutron spectroscopy.*

The high intensity of slow neutron beams has made it possible to develop a proper neutron spectroscopy[4]). This work, mainly initiated by Zinn at the Argonne Laboratory, has led to a very large amount of information about the variation of the cross section of various nuclear processes of many elements. The set-up at A.E.R.E. is very similar to that published in the Physical Review by Zinn. As a deflecting crystal we use lithium fluoride (100) or calcium fluoride (110) and as a detector a boron trifluoride chamber. It lends itself satisfactorily for the measuring of the total collision area, activation cross section, fission cross sections as a function of neutron energy up to several volts. Though the neutrons are roughly distributed according to a Maxwellian distribution for lower ener-

gies, the higher energy neutron density falls off about as $E^{-3/2}$. This and other factors set a limit to the resolving power $E/\delta E$ which becomes one at about 50 eV in our case.

Equally important is the high intensity of the neutron beam from a pile for velocity selector experiments[5]), as initiated by FERMI and MARSHALL several years ago, and used to determine the all important boron absorption cross section. At higher neutron energies, the modulated cyclotron is at present superior to the pile. The situation, however, may be changed with the development of better mechanical velocity selectors.

I would like to refer to some other experiments which have been done with the slow neutron beams in Chalk River and which were made possible only through the high intensity obtainable there.

(b) *Neutron capture experiments.*

Dr. ELLIOTT[6]) of Chalk River has been able to determine the binding energy of the neutron in heavy hydrogen by measuring the gamma ray emitted when a neutron is captured by a proton. To this end a slab of paraffin wax $25'' \times 25'' \times 5''$ was placed in the thermal column of the pile. The gamma rays emitted were collimated by a conical lead shell and allowed to fall on to a uranium radiator. The electrons ejected were energetically analyzed in a beta ray spectrograph and thus permitted to obtain the energy of the gamma ray. The analysis of the spectrometer curve yielded a value of 2.236 ± 0.005 MeV for the gamma ray, a result which is 50 kV higher than the usually accepted one derived from the photodisintegration of the deuteron. At present Dr. KINSEY, in the same laboratory, is engaged in measuring, with the help of an electron pair spectrograph, the gamma rays emitted when a thermal neutron is captured by carbon and other elements. Clearly, a very large field is thrown open in this case through the high thermal neutron intensity of the pile. Another experiment where the high neutron flux was useful was recently carried out at A.E.R.E. by Mr. FLOWERS[7]), who disintegrated with slow neutrons the He^3 contained in a dilution of 10^6 in ordinary helium. The reaction process is $He^3 + n = T + H$. The reaction is remarkable for its high cross section of 3700 barns.

(c) *Neutron lifetime experiments.*

The decay of the neutron into a proton and an electron with an energy release of about 800 kV is obviously of the greatest importance and many physicists have thought of means to observe this

phenomenon. At the moment Dr. Snell at the Clinton Laboratory and Mr. Robson of the Chalk River Laboratory are pursuing this problem with great ingenuity. The method is based on the simultaneous observation of the disintegration proton, which is being recorded by an electron multiplier, and the disintegration electron. I believe that at present disintegration protons have been observed which vanish when the slow neutron beam is cut off with a thin boron layer. Experiments of this type seem quite impossible without a high flux pile.

B. *Fast Neutron Experiments.*

Slow-Fast Converter.

The neutrons in a pile consist of a mixture of slow and fast neutrons whose proportion varies according to the position in the pile. For some experiments it is desirable to have as many fast neutrons available as possible. This can be achieved by a converter consisting of a cylinder of uranium metal. About half of the slow neutrons are absorbed by U^{235} which gives rise to fission neutron emission. This inhomogeneous neutron source can be used to study the nuclear properties averaged over a large energy region with the centre of its energy at about 1 MeV. Such experiments were recently carried out by Dr. Hughes[7]) at the Argonne National Laboratory, and have yielded interesting information about the density and width of levels for a large number of nuclei.

Another, though not very efficient conversion mechanism, is based on irradiating LiD, which leads to the process $Li^6 + n = T + He^4$. The recoiling tritium will occasionally interact with the deuterium because of the large cross section of this reaction according to $T - D = He^4 - n$. Such a mixture placed in a thermal beam of neutrons therefore provides neutrons of energy of about $14^1/_2$ MeV.

The uranium converter for fast neutrons in a pile has become a most important tool for the study of the changes which occur in the solid body when it is exposed to a fast neutron flux[7]). Under these conditions nuclei are, by collision with the fast neutrons, displaced from their customary positions in the crystal lattice. They may come to rest between crystal planes, a process which leads to changes of practically all the properties of the crystal. Dimensional changes have been observed, changes of the electrical and thermal conductivity, the internal energy of the crystal is altered; some of the electrical properties such as rectifying power and Hall effect are changed in a very spectacular manner by relatively small neutron energy doses. These problems are investigated on both sides of the

Atlantic with great interest partly because of their great practical importance. As an example, Fig. 7 shows how the characteristics of a germanium rectifier are changed by irradiation with the comparatively small dose of 10^{15} neutrons.

C. *Production of Radioactive Elements.*

I have up till now not referred to the immense amount of information which has come about through the large number of radioactive isotopes which a pile produces. I only wish to summarize

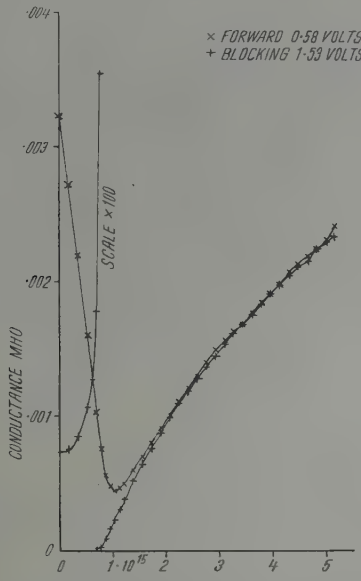

Fig. 7.
Effect of fast neutron irradiation of Germanium Rectifier.
(T. M. Fry – A.E.R.E.)

briefly some of the features which are important to the physicist, especially those working in the field of radioactivity. We have essentially three different ways in which a pile yields material for the physicist:

(a) *Fission products.*

Here the activities available are, for practical purposes, unlimited. However, the extraction and purification requires the chemical processing of pile uranium, which can, because of its enormous activity,

only be done in specially equipped laboratories. Many operations have to be performed by distant control mechanisms and extensive shielding for the protection of the workers has to be provided. In this manner thousands of curies of activity can be handled. It is in the nature of the processes leading to their production that the fission products are free from stable isotopes, therefore of very high specific activity and suitable for beta ray work.

(b) *Carrier free isotopes.*

These products are produced, as a rule, by n-p and n-α reactions or by n-γ reactions with a successive beta decay. The substance mostly in demand from A.E.R.E. is I^{131} produced from tellurium, from which it can be isolated chemically. The amounts available are usually determined by the effort required to process the large amounts of tellurium and are not by restrictions through the pile. The specific activity is high and it is at present being marketed in a solution containing 10 m. curies/cm^3. The total production at present is 700 mc. per week. The other radio-element which is very much in demand is P^{32}, obtained by extraction of irradiated sulphur. About 0.5 curie is being despatched per week at present, but much more could be made if necessary. This source can be made practically carrier free. In some cases the Szilard-Chalmers method has been successful, such as the preparation of Fe^{55} and Fe^{59}, by extracting irradiated ferrocyanic acid.

(c) *Isotopes produced by neutron capture.*

The activities obtainable depend on the cross section for neutron absorption and the neutron flux. The activity per gramme of material is naturally very much smaller than in the cases (a) and (b), since the material consists mostly of inactive isotopes, but the total activity of specimens can easily go into 1—10000 curies as in the case of sodium and cobalt. One example is *radio sodium*, which interests the physicists as a source of gamma rays for nuclear photo-disintegration experiments, is made with specific activity of 0.4 curies per gramme in the bigger Harwell pile. Obviously much higher specific activity could be obtained in Chalk River. One of the acute problems of such sources is caused by the safety regulations which allow, at present, only 20 millicuries to be transported on the plane.

I would like to add finally a few words about production of one of the most desirable pile products, namely *tritium*, and its decay product He^3. In order to use the neutrons in a pile economically,

materials with large absorption cross sections have to be placed into the reflector where the neutrons, many of which anyway escape from the reacting core, can still be used up. The reduced flux in the reflector, however, necessitates the processing of larger amounts of materials than if the material had been put into the centre of the pile. In order to produce one litre of tritium per year we would have to process eventually about 80 kilos of lithium salt, a problem which the members of the Isotope Division of HARWELL do not consider very favourable. For this reason, tritium and its decay product He^3 will not, in our Establishment, be very abundant in the near future.

D. *Production of Transuranium Elements.*

The production of the transuranium element plutonium on an industrial scale is perhaps the most spectacular result of the pile development. It has received so much publicity that a few words will suffice. To appreciate the size of the task I have only to mention that one megawatt-year pile power produces about 400 gr plutonium. The amount of energy to be disposed of, is therefore enormous. To this has to be added the effort to process chemically the exposed uranium: to extract the plutonium under radiation intensities which run into $10^5 - 10^6$ curies.

E. *Higher Order Reactions.*

For the physicist great interest attaches to the possibility to produce by successive incorporation of several neutrons new radioactive bodies. Such processes have been observed in many cases, but I will refer only to the example of I^{131}

$$\underset{8\,\mathrm{d}}{I^{131}} + n \rightarrow \underset{2.7\ \mathrm{hrs.}}{I^{132}}$$

for which at Chalk River a cross section of 420 barns has been found.

The transuranium elements curium and americium furnish further interesting cases. Since the formation of these elements depends on $(nvt)^m$, where nvt is the neutron dose, and m the number of neutrons incorporated, the high neutron density becomes a pre-requisite for its formation.

F. *Neutrino Experiments.*

The high rate of β-processes occurring at any time in a going pile gives rise to the emission of a large number of neutrinos. If we take our example of a cubic pile of 10 m length and a pile power of

10^4 kW, one obtains about $7 \times 3 \cdot 10^{17} - 2{,}1 \cdot 10^{18}$ neutrinos per second (7 β processes per fission). Per cm^2 of pile surface, this represents a flux of $3.5 \cdot 10^{11}$ neutrinos per second. Since this flux extends over a large area, there is a chance to observe inverse beta- processes in large volumes of matter. Dr. Pontecorvo is at present planning such an experiment.

4. Future Possibilities.

It may be asked in which direction future development may be expected from the physicist's point of view. In the first instance, the research worker wants higher neutron fluxes and more powerful neutron beams. To achieve this the number of fissions per second in the uranium slugs has to be increased, or technically the number of megawatts per ton of metal raised. It is obvious that with present constructions there is a limit, as the traditional cooling mechanism becomes too inefficient. Reactors are in the design stage in various places which will be more powerful. On the whole this matter rests in the hands of the engineers and metallurgists. Great uncertainty in all such planning lies in the fact that little is known about the behaviour of constructional materials under neutron bombardment. This is one of the cardinal problems which has to be solved with the help of high flux experimental reactors.

One attractive suggestion of a physics tool, the so-called *Dragon*, has been made by Professor Frisch. It is based on a fast reactor which can be made supercritical for prompt neutrons for a short period only. One might have a cylinder of pure plutonium with a hole through it. It would be of such size that it would be subcritical and a plug could be shot at great speed through the hole, making the system for a short period supercritical. Since the neutron lifetime in such an assembly may be of the order of 10^{-8} seconds, a very large multiplication would take place during the passage of the slug through the hole. This burst of neutrons could serve for time-of-flight experiments, extending over a large distance, say 100 m. The burst could last 10^{-4} sec. and yield 10^{15} neutrons, producing at a distance of 100 m still a neutron flux of 10^7. This method would permit the study of neutron properties up to several times 10^4 eV, a region which is still rather inaccessible.

Bibliography.

[1]) *Absorption Measurements.* H. L. Anderson, E. Fermi, A. Wattenberg, G. L. Weil, W. H. Zinn, Phys. Rev. **72**, 16 (1947).

[2]) *Pile Oscillator. Theory:* A. M. Weinberg and H. C. Schweidler, Phys. Rev.

74, 851 (1948). *Experimental:* J. I. Hoover, W. H. Jordan, C. D. Moak, L. Pardue, H. Pomerance, J. D. Strong, E. O. Wollan, Phys. Rev. **74**, 864 (1948).

[3]) *Neutron Source Calibration:* D. J. Littler. In course of preparation for publication.

[4]) *Neutron Spectroscopy. Crystal Spectrometer:* W. H. Zinn, Phys. Rev. **71**, 752 (1947); W. J. Sturm, Phys. Rev. **71**, 757 (1947).

[5]) *Velocity Selector:* E. Fermi, J. Marshall, L. Marshall, Phys. Rev. **72**, 193 (1947); T. Brill, H. V. Lichtenberger, Phys. Rev. **72**, 585 (1947).

[6]) *Neutron Capture by Protons:* R. E. Bell, L. G. Elliott, Phys. Rev. **74**, 1552 (1948); *Neutron Life Time:* A. H. Snell, L. C. Miller, Phys. Rev. **74**, 1217 (1948).

[7]) *Fast Neutron Experiments. Nuclear Physics:* D. J. Hughes, W. D. Spatz, N. Goldstein, Phys. Rev. **75**, 1781 (1949); *Effects on Solid Body:* "Effect on neutron bombardment on order in the alloy Cu_3Au". Sidney Siegel. AECD-2465 (1949); Also Phys. Rev. **75**, 1823 (1949); "Nucleon bombarded germanium semiconductors" Lark-Horovitz and others, AECD-2054; "Neutron irradiated semiconductors" W. E. Johnson and K. Lark-Horovitz, Phys. Rev. **76**, 442 (1949).

Quelques caractéristiques de la pile de Châtillon en tant que source de neutrons thermiques

par **L. Kowarski** (Paris).

Ce bref exposé suppose connues aussi bien les généralités sur la nature des piles atomiques (voir par exemple[1]) que les propriétés particulières de la pile de Châtillon pour autant qu'elles ont été rendues publiques (voir[2]). Nous admettons notamment que le lecteur a présents à l'esprit: la symétrie essentiellement cylindrique du système; la division en trois zones concentriques (cuve à réaction, réflecteur en graphite, protection en béton); la répartition des ingrédients réagissants (barreaux verticaux en UO_2 gaîné d'aluminium, plongeant dans l'eau lourde); et les dispositifs expérimentaux tels que:

canaux horizontaux traversant le béton et le graphite, radialement ou tangentiellement par rapport à la cuve, et habituellement obturés;

tube creux vertical suivant l'axe de la cuve;

colonne diffusante en graphite («thermal column») encastrée dans le béton sur l'un des côtés de la pile.

A partir du 1er mai 1949 la pile a été soumise à un régime de marche en principe continu, les nuits et les fins de semaine étant utilisées pour la marche à puissance maxima afin d'accumuler les produits de fission et le plutonium dans les barres uranifères, ainsi que d'irradier au maximum les spécimens introduits dans les canaux. La puissance maxima admissible a été trouvée par tâtonnements: comme la chaleur produite est supérieure à la chaleur évacuée (par les parois, surtout directement au-dessus et au-dessous de la cuve à réaction, et par un courant d'air entretenu entre la cuve et le réflecteur, à l'aide de deux ventilateurs), la marche provoque un échauffement du milieu réagissant. En se donnant comme condition de ne jamais dépasser une certaine température (indiquée par un thermocouple plongé dans le ralentisseur non loin du centre de la pile), on arrive à un maximum de 6 à 8 kW pour marches de fin de semaine au milieu d'été, et près de 10 kW pour une marche de nuit ordinaire.

Compte tenu de la nécessité de marcher à faible puissance pour des expériences de physique durant la journée normale de travail, et des arrêts dus à de menus incidents, la conduite de la pile a effectivement réalisé, entre le 1er mai et le 1er septembre 1949, une moyenne journalière de 121 kWh, soit l'équivalent d'une *marche continue à 5 kW*. Il est raisonnable de considérer ce dernier chiffre comme un minimum prudent pour le calcul des longues irradiations futures. Pour les expériences de physique d'une durée de quelques heures ou de quelques jours au maximum, on peut baser les prévisions sur une puissance sensiblement plus élevée.

Les chiffres ci-dessus résultent de l'intégration de la densité neutronique. La distribution de cette densité, à l'intérieur du milieu réagissant et dans le réflecteur, a été calculée théoriquement et nos mesures d'intensité, en unités relatives, au moyen de détecteurs de Mn ont confirmé ces calculs d'une manière satisfaisante. Nous avons étalonné nos mesures relatives par rapport à la densité mesurée dans l'eau à 10 cm d'une source de Raα + Be d'intensité absolue connue. Pour cette dernière donnée, nous ne disposons pour le moment que d'une valeur provisoire, comportant une possible erreur de 10 à 15%, qui se retrouve proportionnellement dans notre évaluation de la puissance de la pile.

En exprimant, selon l'usage, les densités neutroniques sous forme de «flux» (nombre de neutrons par cm^3, multiplié par la vitesse moyenne conventionnelle de 2200 m/sec), nous trouvons pour un régime normal de marche à grande puissance:

1. Flux à la mi-hauteur du tube creux formant l'axe vertical central de la pile: $3 \cdot 10^{10}$ neutrons par $cm^2 \cdot sec$.

2. A la mi-hauteur d'une génératrice de la paroi extérieure du milieu réagissant: $1{,}1 \cdot 10^{10}$.

3. Au fond du canal radial à la mi-hauteur de la pile, le plus près possible de la cuve: $1{,}0 \cdot 10^{10}$.

4. Dans le canal tangentiel, le plus près de la cuve: $0{,}84 \cdot 10^{10}$.

5. Dans le canal radial, à la frontière réflecteur/béton: $6 \cdot 10^{8}$.

6. En dehors de la pile, à 1 mètre de la face du béton, dans l'axe du canal radial vidé de son bouchon: $0{,}9 \cdot 10^{6}$.

7. Sur la face extérieure de la colonne diffusante: $2{,}2 \cdot 10^{4}$.

Pour les expériences qui demandent une puissance constante, il est facile d'obtenir celle-ci, c'est-à-dire la réactivité zéro, en manœuvrant les contrôles chaque fois que la puissance observée montre une tendance à s'écarter du niveau choisi. Si, au contraire, l'expérience demande que l'on ajoute à la réactivité, ou en retranche, une

fraction $\triangle k$ réglable à volonté, il est intéressant de signaler quelle est la vitesse et la reproductibilité des moyens dont l'opérateur dispose à son gré:

1. Les plaques de contrôle en métal cadmié:
Position reproductible à 0.5 mm près, correspondant à
$\triangle k = 0{,}25 \cdot 10^{-5}$ ou «un quart pour cent mille».

2. Le niveau de l'eau lourde dans la cuve à réaction:
Position reproductible à 1 mm près, correspondant à
$\triangle k = 5 \cdot 10^{-5}$ ou «cinq pour cent mille».

3. Température de l'eau lourde. Nous mentionnons ce facteur surtout pour mémoire, car il ne dépend pas entièrement de l'opérateur. Si la puissance est suffisante pour faire varier la température de 10^0 ou 20^0 au cours d'une expérience, la réactivité décroît d'une quantité nettement supérieure à ce qui serait admissible en tant qu'une petite correction. Il est donc essentiel d'exécuter les expériences de quelque durée à faible puissance si l'on veut éviter tout déplacement appréciable des contrôles. L'inertie thermique du système contribue heureusement à amortir les variations normales de la température ambiante.

La valeur de l'«unité pour cent mille» employée ci-dessus résulte de son nom; c'est ainsi que, par exemple, une réactivité de 100 p.c.m. correspond à k effectif 1,001. D'après les définitions expérimentales de l'«inheure» américaine, 1 ih = 2,5 p.c.m.

L'étalonnage des contrôles en fractions de k (inheures ou p.c.m.) exige l'observation de la montée exponentielle de la puissance à réactivité constante et son interprétation d'après les formules cinétiques bien connues (voir par exemple[3]). Dans les piles à eau lourde, le comportement cinétique dépend non seulement (comme c'est le cas des piles au graphite) des neutrons différés de fission, mais aussi des photoneutrons produits dans l'eau lourde par les rayons gamma émanant des produits de fission accumulés dans les barreaux uranifères. L'évaluation de cette influence dépend à la fois des propriétés connues des produits de fission (voir [4]), et des caractéristiques de la pile (dimensions et distribution spatiale des ingrédients). Notre étude théorique de ces facteurs n'est pas encore terminée; par conséquent, la traduction des temps de montée en p.c.m. (ou inheures) suivant la formule bien connue

$$k - 1 \approx \sum \frac{\beta_i \tau_i}{T + \tau_i}$$

(avec $\beta_0 \tau_0 \approx$ vie moyenne du neutron thermique dans le système, et les autres valeurs de l'indice i couvrant tous les neutrons différés

de fission et gamma-n) n'a pas encore acquis toute la précision désirable.

Le cas où la réactivité est périodiquement déprimée et rétablie, au moyen d'une introduction oscillatoire d'un corps qui absorbe les neutrons thermiques a été étudié théoriquement[5]) et expérimentalement[6])[7]) et l'application de ce procédé à la mesure des propriétés absorbantes de diverses substances est désormais bien connue. Dans des expériences préliminaires réalisées à Châtillon, l'absorbant oscille à l'intérieur du tube creux axial, entre la région centrale de la pile et la région au-dessus du niveau de l'eau lourde. La période totale de l'oscillation est actuellement de 28 secondes (10 sec pour le séjour en haut ou en bas et 4 sec pour le déplacement) et la puissance oscillante de la pile est suivie par un galvanomètre accordé sur cette période. Le seuil de sensibilité atteint jusqu'ici est de l'ordre de 0.5 mm^2, c'est-à-dire: il est possible de distinguer entre deux corps absorbants dont les produits $\Sigma n_i \sigma_i$ (n nombre de noyaux absorbants d'espèce i présents, σ_i section de capture de chacun de ces noyaux pour les neutrons thermiques) diffèrent d'au moins $5 \cdot 10^{21}$ barns.

La plupart des expériences et mesures citées ci-dessus ont été exécutées en collaboration avec MM. Ertaud, Baugé, Fauquez, Vautrey et Cohen; nous avons l'intention de les décrire dans des publications plus détaillées.

Bibliographie.

[1]) "The Science and Engineering of Nuclear Power" (séminaires M.I.T.), en particulier chap. 9, 5 et 8.

[2]) «Atomes», numéro spécial de février 1949.

[3]) Comme [1]), p. 168, vol. I.

[4]) Bernstein, Preston, Wolfe, Slattery, Phys. Rev. **71**, 573 (1947).

[5]) Weinberg et Schweinler, Phys. Rev. **74**, 851 (1948).

[6]) Langsdorf, Phys. Rev. **74**, 1217 (1948).

[7]) Hoover, Jordan, Moak, Pardue, Pomerance, Strong, Wollan, Phys. Rev. **74**, 864 (1948).

Sur l'étude des neutrons des piles atomiques par la méthode photographique

par **P. Cüer***).

Les émulsions nucléaires chargées au Bore et au Lithium permettent de déceler de faibles flux instantanés de neutrons lents (Flux intégré Φ de 10^7 à 10^9 neutrons cm $^{-2}$). Les émulsions nucléaires normales permettent, grâce à l'azote de la gélatine de doser jusqu'à $\Phi \sim 10^{11}\, n.\,(\mathrm{cm}^{-2}$. Dans des mesures quantitatives précises, la méthode à l'azote est préférable en raison de la répartition parfois inhomogène des sels, nécessitant des statistiques plus longues, et de l'incertitude de leur concentration.

La méthode fournit d'intéressants renseignements sur:

La mesure directe des flux de neutrons lents.

Le pouvoir filtrant de diverses substances envers les neutrons rapides.

La valeur expérimentale précise du pouvoir d'arrêt des émulsions nucléaires pour des particules chargées de faible énergie.

La distribution des zones de sensibilité variable dans l'émulsion étudiée.

A) Dosage.

La fidélité de la méthode a été éprouvée au cours de nombreux tests au cours desquels un même observateur avait plusieurs densités différentes à reconnaître et la même plaque remesurée par une équipe d'observateurs. Pour une même série d'émulsions, aux fluctuations statistiques près les résultats sont reproductibles pour un nombre de traces de B au N inférieur à ~ 100 par champ ($D \sim 80\ \mu$).

La constance du flux neutronique issu du tube à haute tension de Strasbourg a été contrôlée à cette occasion à 1% près.

Dans les expositions aux piles (réflecteur ou colonne thermique) on opère généralement en flux isotrope $\Phi = vnt$, n, densité spatiale. A partir d'une statistique normale de 600 champs, l'erreur sur la moyenne du nombre de traces devient négligeable par rapport aux autres causes d'incertitude:

*) Les mesures afférentes aux résultats ci-dessous ont été effectuées par R. Locqueneux, laboratoire Morand (Paris) et une équipe dirigée par J. P. Lonchamp, laboratoire Gorodetzley (Strasbourg).

Etalonnage absolu. A l'aide d'échelles étalons gravées et de nombreuses mesures soignées, on peut atteindre $\sim 0{,}3\%$.

Concentration de l'élément. Celle de l'azote est la plus constante $\sim 2\%$ près.

Mesure de l'épaisseur vierge de l'émulsion. Elle est très délicate à préciser, soit par la tranche au microscope, soit au comparateur de précision. Elle varie de quelques pour cent avec l'humidité relative. Des améliorations de cette mesure sont encore en cours.

Valeur de σ_N. Une certaine difficulté existait entre les anciennes mesures approximatives de Lapointe et Rasetti (H_2O) et Cüer (paraffine) d'une part ($\sim 1{,}3$ b) et les mesures récentes des Américains au compteur proportionnel (Coon, Nobles, P. R. *75*, 1358 (1949) ($\sigma_N = 1{,}76 \pm 0{,}05$ b).

En raison de l'incertitude des concentrations de nitrure de sodium et de citrate de Lithium, des épaisseurs vierges et des statistiques différentes de Li et N dans les émulsions utilisées par Cüer (Journ. Phys., Mars 1947), la mesure a été reprise très soigneusement à l'aide du générateur de Strasbourg en comparant une émulsion nucléaire à grains fins (Ilford E_1) et une émulsion au Bore (Ilford $C_2 + B$) situées à 30 cm de la cible entourée de 5 cm de Pb, cible de Be + D (1 MeV; 300 μ A; 60 m) dans un bloc de paraffine de 70 cm d'arête. Les résultats actuels portant sur 600 champs de chaque sorte indiquent $\sigma_N \sim 1{,}75$ b*) avec une incertitude actuellement encore élevée ($\sim 5\%$). Une bonne calibration absolue à l'aide d'une autre technique nous permettra d'atteindre $\sim 3\%$.

Résultats. Une émulsion d'essai exposée au sein de la colonne thermique de la G.L.E.E.P. (Harwell) a donné $\Phi \quad 1{,}27 \cdot 10^{10}\, n.\,\mathrm{cm}^{-2}$ (c'est l'ordre de grandeur du flux le plus favorable aux mesures).

B) Filtrage.

C'est la seule méthode directe pouvant fournir cette caractéristique en un point donné au cours d'une exposition unique.

Le nombre (nb) de protons de recul issus des neutrons rapides résiduels permet le calcul approximatif du coefficient de pureté, $Cp = nb$ de neutrons rapides sur nb de neutrons lents. On ne peut discriminer les protons rapides de ceux de la réaction qu'au-delà de 0,7 MeV. La distribution des neutrons étant quasi-isotrope, le spectre des protons est la dégradation de celui des neutrons de E_0 à 0 ($E = E_0 \cos^2 \alpha$). La forme du spectre et le domaine d'énergie permettent de fixer d'après la littérature $\sigma_H \sim 10$ b.

*) Par référence a $\sigma_B = 703$ b.

Après évaluation convenable du *nb* de protons s'échappant dans l'air et le verre (les traces de contamination affaiblies de l'air sont la limite pratique de la méthode), on trouve le nombre de neutrons rapides connaissant la proportion d'H_2.

L'allure exacte du spectre de neutrons n'est donc pas abordable par cette technique de géométrie quelconque, les limites et l'abcisse du maximum sont seules conservées ici. Des expériences en «bonne géométrie» sont en cours pour l'étude du spectre de la fission et de celui provoqué par quelques ralentisseurs.

Modérateurs absorbants (paraffine). Un spectre de Be (cible épaisse) *D* (1 MeV) après 30 cm de paraffine a un $Cp \sim 10^{-1}$ à 10^{-2} selon l'étendue du spectre de neutrons rapides considéré.

Modérateurs élastiques (graphite). L'émulsion exposée dans la colonne de graphite de la pile à graphite (Harwell) indique un $Cp \sim 2 \cdot 10^{-6}$. Le spectre des protons émis par les neutrons résiduels de la colonne thermique a commencé à être étudié sur 120 traces (~ 65 mm^2). Un maximum semble situé vers 2,5 MeV, l'extrémité du spectre étant vers 6 MeV.

C) Pouvoir d'arrêt.

Le grand nombre de traces disponibles pour les mesures a permis de fixer avec précision la courbe parcours-énergie pour les faibles énergies jusqu'ici très incertaine dans les émulsions nucléaires (1 cm d'air pour les protons de l'azote, 2 cm d'air pour les protons équivalents aux tritons du Lithium) avec une incertitude inférieure à celle existant actuellement dans l'air. (Voir Comm. Gorodetzky, Cüer.)

D) Zones de sensibilité.

L'étude détaillée de la courbe *nb* de champs en fonction de nombre de traces par champ permet de déterminer des zones de sensibilité anormalement élevées ou faibles en dehors des fluctuations statistiques dans une émulsion non imprégnée. Par exemple l'étude complète d'une C_2 a montré l'existence d'une région de 2 mm de diamètre contenant une traînée de Bore augmentant sensiblement la moyenne locale. Les régions de densité moindre sont plus diverses. A part quelques zones accidentelles de densité très faible (parfois nulle) et le pourtour de l'émulsion où l'action plus prolongée du fixateur rend la discrimination difficile (perte fréquente de 30 à 50% des traces), la distribution des zones rentre dans le cadre d'un schéma photographique où ces «trous de sensibilité» sont explicables par les variations locales des conditions physico-chimiques de sensibilisation des grains (on a vérifié que la densité du voile et celle des traces sont en corrélation directe).

II.

Apparate zum Nachweis von Korpuskeln und Quanten

Recent progress in ionization chambers technique

by **Emilio Segrè**

Department of Physics, University of California Berkeley, California.

The ionization chamber as an instrument of nuclear research is one of the earliest and most used but although over 50 years old, significant advances in its technique have been made during the last few years. The improvement of the electric systems for measuring potentials with fast amplifiers, has made it possible to study the time dependent details of ionization pulses and not only their integral effect.

In order to take advantage of these possibilities offered by the electrical part of the apparatus it is necessary to use electron collection which is much faster than heavy ion collection. The motion of electrons in a gas is discussed and measurements of the drift velocity of electrons in several pure gases (Argon, Hydrogen, CO_2, BF_3) are presented. The motion of electrons in mixtures of Argon and Carbon dioxide is then also discussed, with special reference to the increase in drift velocity obtainable by the use of mixtures. Data on the attachment of electrons to impurities, notably O_2 and water are also presented.

In the case of electron collection special designs of the ionization chamber are necessary to obtain proportionality between voltage pulse and ionization. This problem has been solved either by the use of additional grid electrodes in the chamber or by special geometrical construction of the same.

Finally several types of ionization chambers for special purposes are illustrated. Among them:

1. a high precision differential chamber for half life measurements;
2. a differential chamber to detect fission pulses, while the beam of a cyclotron goes through the chamber;
3. high energy neutron monitor chamber, using fission of bismuth;
4. a special spiral chamber to monitor slow neutrons by fission;
5. a chamber suitable for a precise analysis of alpha pulses;
6. medical chambers for the protection of workers.

The greatest part of the subject of this report is taken from

B. Rossi and H. Staub — Ionization chambers and counters-Experimental Techniques — McGraw-Hill 1949.

This book was published after the report was given and for this reason reference is made to it and more detailed report on the subject is not presented here.

Discussion following the report of E. Segrè on „Recent developments of ionisation chambers"

W. Bothe, Heidelberg: An ionisation pulse chamber of special design for studying (n, α)- and (n, p)-reactions in gases after the Wilhelmy method is in use in our laboratory since some time (Fig.). The main chamber consists of the collecting grid E_1, connected to a linear amplifier (1), and the voltage grids E_2. The main chamber is surrounded by an auxiliary chamber, the second collecting electrode E_3 being connected to a second amplifier (2). The two collect-

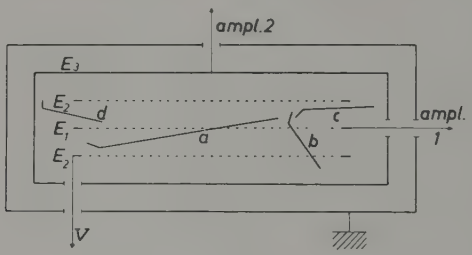

ing systems are connected in anticoincidence. When a particle released by a neutron in the gas filling hits the "wall" of the main chamber from either side (b, c, d) it will not be recorded, because amplifier 1 is blocked by amplifier 2, so "wall effects" are suppressed. Moreover, since the main chamber is rather flat, it is possible, by adjusting the gas pressure, to select only particles running in a direction nearly normal to the electric field (track a).

In this way the background of resonance energy spectra is greatly reduced, so Dipl. Phys. W. Stetter could observe a number of new evels of the N^{15}-nucleus.

Theory of Grid ionisation Chambers

by **O. Buneman** (Harwell).

The efficiency is calculated with which a grid can shield the collector plate of an ionisation chamber from fields induced by the positive charge in the ionisation tracks. Further, conditions are calculated for all electrons from the tracks to be collected on the plate rather than being intercepted by the grid. Formulae are given which enable the designer to choose geometries and potentials such that both complete collection and high efficiency are achieved. The theory is developed for both planar and cylindrical chamber geometries and for all practical grid mesh dimensions. There is good agreement with experiments.

A full account of the theory is published in the Canadian Journal of Research, vol. **27,** p. 191 (1949) in a paper entitled: "Design of Grid Ionisation Chambers" by O. Buneman, R. E. Cranshaw and J. A. Harvey.

High pressure ionization Chambers used in Oxford

by **L. Beghian, C. H. Collie, H. Halban** and **R. Wilson.**

High pressure, hydrogen, deuterium and methane filled ionization chamber counters have been used in this Laboratory. In each case there has been electron collection. This has been achieved by using a pure gas, and thoroughly cleaning and outgassing the counters before filling.

In order to take full advantage of the electron collection, it is

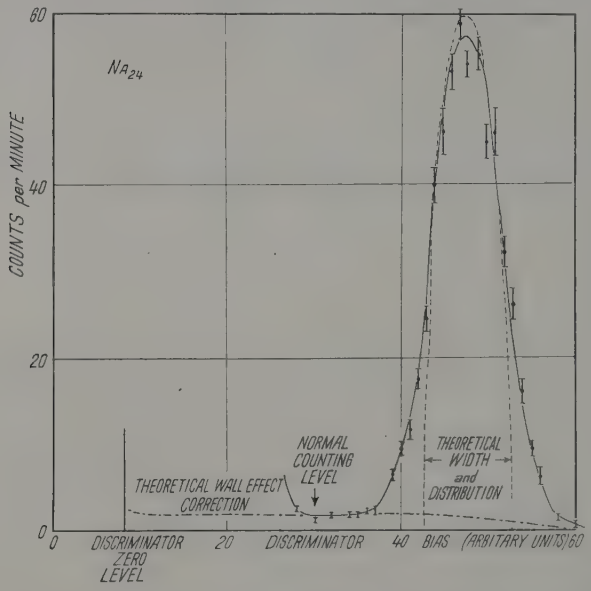

Fig. 1.

Pulse Height Distribution Photoprotons from Disintegration by Radiosodium

important to minimize the contribution of the positive ions. This is achieved by suitable choice of counter geometry. We have employed cylindrical counters, 20 cms. long and 4 cms. diameter with an axial 1 mm. rod as collector, and spherical counters, 4 cms. diameter, with a 1 mm. rod with rounded end as collector. The latter

type of counter lends itself particularly well to good definition (0.1 %) of the counting volume. With pure hydrogen and deuterium the positive ion mobility is also high, so that at no part of the counter does the pulse height vary by more than 15% from the maximum with amplifier time constants of 1 μs. The electron mobility is not so high for hydrogen and deuterium as it is for methane; the maximum time taken for an electron to create a pulse (pulse delay time) is about 1 μs for methane at 35 atmospheres pressure, and 5 μs for hydrogen or deuterium at the same pressure. This is in rough agreement with the results of STAFFORD[4]).

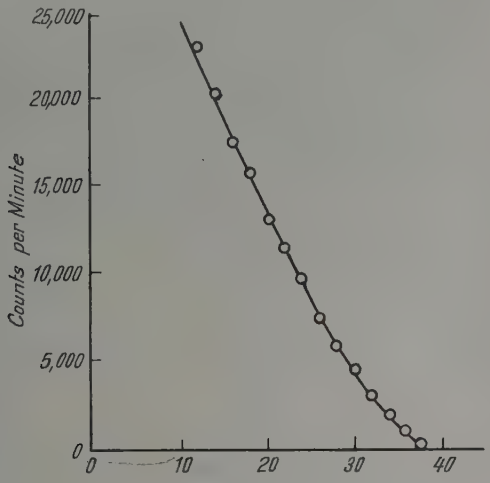

Fig. 2.
Pulse height distribution for methane chamber filled to 35 atmospheres using D+D neutrons.

The counters have been made with brass, copper, stainless steel and aluminium alloy with similar results; the high voltage and collector leads are brought through the pressure containing vessel by Kovar to glass seals. In some cases the pressure containing vessel acts as a guard ring and there is a high voltage cylinder or sphere inside, in other cases, two coaxial seals are used, with the join between them as a guard ring, and the pressure vessel is connected to the high voltage.

After assembly the counters are sealed by screwing together, and sealing the thread with soft solder (or in the case of the aluminium alloy counters, Cenco Sealstix); they are outgassed by pumping with

a mercury diffusion pump for several hours, preferably with slight heating till the pressure does not rise when the pump is disconnected.

The filling gas is obtained in different ways. The pure hydrogen is obtained from a hydrogen liquefier, immediately after a charcoal cleaning stage (Jones, Simon and Larson, 1948); the deuterium is obtained by electrolysis of heavy water, and after recombination of any oxygen of a palladium catalyst and liquid air trap, is condensed onto charcoal immersed in liquid air. There is then a single stage of fractionation on charcoal at liquid air temperature, and the pure deuterium is obtained at pressure after removal of the liquid air. The methane is supplied to us from a multi-stage fractionating column by Messrs. Kronberger and London of A.E.R.E. Harwell (Beghian and Halban, 1949). In each case the gas is sufficiently pure to give electron collection up to 35 atmospheres — the highest pressure yet tried. At this pressure there is about 10% loss of pulse height due to recombination.

Fig. (1) shows the differential distribution of pulses from 280 kV protons, in a counters with well defined counting volume, filled with deuterium at 8 atmospheres pressure.

Fig. (2) shows the integral distribution of pulses from a larger neutron detector (filled to 35 atmospheres of methane) irradiated with 2.5 MeV neutrons.

The counters are used as hydrogen recoil neutron detectors, and as direct detectors of the photodisintegration of deuterium (Wilson, Collie and Halban, 1948, 1949).

References.

[1]) Beghian and Halban, 1949, Proc. Phys. Soc. A, vol. LXII, p. 395.

[2]) Jones, Simon and Larsen, 1948, Research, vol. 1, p. 420.

[3]) Wilson, Collie and Halban, 1949, Nature, vol. 163, p. 245, 1948. Nature, vol. 162, p. 185.

[4]) Stafford, 1948, Nature, vol. 162, 771.

Arbeit pro Ionenpaar in N_2-Ar-Mischungen für α-Teilchen

von **P. Huber, E. Baldinger** und **W. Häberli** (Basel).

Um bei Messungen mit Ionisationskammern aus der Ladung auf die Energie der ionisierenden Teilchen schliessen zu können, muss der Energieaufwand zur Bildung eines Ionenpaares (Arbeit pro Ionenpaar) bekannt sein. Die experimentelle Bestimmung dieser Arbeit kann erfolgen, indem die von α-Teilchen bekannter Energie erzeugte Ladung mit Hilfe eines Verstärkers und eines Impulsspektrographen gemessen wird. Aus der Sättigungsladung und der Eichung der Verstärkeranordnung bestimmt sich die Zahl der Ionenpaare. Zusammen mit der bekannten Energie des α-Teilchens lässt sich hieraus der Energieaufwand pro Ionenpaar ausrechnen.

Erfährt ein α-Teilchen in einer Gasmischung mit den Komponenten 1 und 2 den Energieverlust ΔE und werden dabei Δn Ionenpaare erzeugt, so ist die Arbeit J_M pro Ionenpaar

$$J_M = \frac{\Delta E}{\Delta n}.$$

Der Energieverlust ΔE des α-Teilchens setzt sich aus den Energieverlusten zur Erzeugung der primären Ionen in den beiden Gassorten zusammen:

$$\Delta E = \Delta E_1 + \Delta E_2.$$

Die Zahl der Ionen Δn ist die Summe aus den vom α-Teilchen direkt erzeugten und den indirekt durch δ-Elektronen und Lichtquanten in der Gasmischung gebildeten Ionen.

Es fragt sich nun, wie die Arbeit J_M der Mischung sich aus den Arbeiten J_1 und J_2 der reinen Gase berechnen lässt. J_M kann in erster Näherung durch folgende Annahme ermittelt werden: Die Zahl Δn_1 bzw. Δn_2 der Ionen der beiden Gaskomponenten sei einzig bestimmt durch die Grössen

$$\Delta n_1 = \frac{\Delta E_1}{J_1} \quad \text{und} \quad \Delta n_2 = \frac{\Delta E_2}{J_2}.$$

Bei diesem Ansätze ist also die ionisierende Wirkung der δ-Elektro-

nen und der Lichtquanten der einen Gassorte auf die andere vollständig vernachlässigt. In Wirklichkeit werden sich die Ionisierungen, erzeugt durch δ-Elektronen und Lichtquanten gegenseitig in der Mischung etwas kompensieren, so dass diese, auf den ersten Blick sehr unwahrscheinliche Annahme nicht ganz schlecht zu sein braucht. Damit wird

$$\Delta n = \Delta n_1 + \Delta n_2 = \frac{\Delta E_1}{J_1} + \frac{\Delta E_2}{J_2} \quad \text{und}$$

$$\frac{1}{J_M} = \frac{\Delta E_1}{\Delta E_1 + \Delta E_2} \cdot \frac{1}{J_1} + \frac{\Delta E_2}{\Delta E_1 + \Delta E_2} \cdot \frac{1}{J_2} .$$

ΔE_1 und ΔE_2 sind proportional dem Produkt aus atomarem Brems-

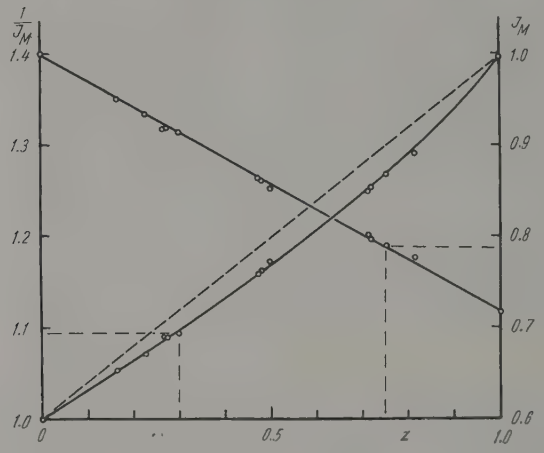

$\frac{1}{J_M}$ und J_M in Abhängigkeit von $z = \frac{s_{Ar} p_{Ar}}{s_{Ar} p_{Ar} + s_{N_2} p_{N_2}}$ – für N_2-Ar-Mischungen.
Die Messungen wurden mit U-α-Teilchen ausgeführt.

vermögen s und Partialdruck p der Gaskomponenten. Es ergibt sich daher

$$\frac{1}{J_M} = \frac{s_1 p_1}{s_1 p_1 + s_2 p_2} \cdot \frac{1}{J_1} + \frac{s_2 p_2}{s_1 p_1 + s_2 p_2} \cdot \frac{1}{J_2} .$$

Dieser Ausdruck lässt sich umformen in

$$\frac{1}{J_M} = \frac{s_1 p_1}{s_1 p_1 + s_2 p_2} \left(\frac{1}{J_1} - \frac{1}{J_2} \right) + \frac{1}{J_2} .$$

$\frac{1}{J_M}$ ist in dieser Näherung linear abhängig von der Grösse $z = \frac{s_1 p_1}{s_1 p_1 + s_2 p_2}$. Zum Vergleich ist es daher angezeigt, die experi-

mentellen Werte von $\frac{1}{J_M}$ in Funktion von z aufzutragen. Für die atomaren Bremsvermögen von Argon und N_2 relativ zu Luft benutzten wir die Werte[1]) $s_1(\mathrm{Ar}) = 0{,}95$ und $s_2(\mathrm{N_2}) = 0{,}99$. Die Werte für $\frac{1}{J_M}$ sind relativ zum reinen N_2 eingezeichnet.

Wie Figur zeigt, ergeben sich Abweichungen bis zu 3% zwischen Experiment und Näherung. Die Abweichungen sind derart, dass die Arbeit J_M in der Mischung grösser ist als nach dieser Näherung berechnet wird. J_M in Abhängigkeit von z aufgetragen, ergibt für N_2-Ar-Mischungen eine Gerade.

---

[1]) K. Schmieder, Ann. d. Phys. **35**, 445 (1939).

An electrometer with mechanical conversion

by **F. A. Muller**

Laboratory of Physics, Amsterdam University.

A short description is given of a type of converting vacuum-tube electrometer developed in Amsterdam during recent years. The principal part of such an electrometer is a vibrating condensor which converts DC charges into AC voltages. The vibrating element in this condensor is a square steel plate of 0.5 mm thickness and 30 mm sides. This plate vibrates with the corners alternately in phase thus leaving the center stationary and flat to a high degree of approximation. Here the plate is tightly fixed on a quartz insulator.

Opposite the corners of the plate there are eight soft iron pole pieces, rods with coils around them, of which four drive the plate at two corners in its natural vibration frequence, while the remaining four provide the feedback voltage for the oscillator. In order to make electromagnetic driving possible the whole instrument is magnetized by a direct current. If the driving current magnetizes two poles opposite one corner, with the same polarity, this corner is magnetized too and drawn to one side by the constant magnetic field. The feedback voltage originates from the same mechanism in the opposite direction. The eight poles are also acting as the grounded (or feedback)-electrode of the vibrating condensor.

Thus the capacitance varies in the second harmonic of the vibration. Around the plate an electrostatic shielding is provided, while the coil-forms are made from brass and grounded.

This condensor is of a comparatively simple construction and has the following properties:

It is extremely rugged, it has a high conversion frequency (4600 Cps) and as the conversion frequency is the second harmonic of the driving frequency the latter is not apt to give much trouble.

The conversion is not very high, the effective capacitance variation is about 1 pF (2.5 pF top to top), the total capacitance being 16 pF. Due to the high conversion frequency it allows to measure quite easily with a RMS error of 10^{-16} C in 1 second corresponding with a RMS error of $3 \cdot 10^{-16}$ A measuring a current during 1 second and of $1 \cdot 10^{-16}$ A measuring during 2 seconds. The utmost performance seems to give an accuracy which is twice as good.

The crystal counter

by **J. M. W. Milatz** and **H. A. van der Velden**
Physical Laboratory of the State University of Utrecht, Holland.

Introduction.

As is well known it is possible to detect α-rays with the help of an ionisation chamber backed by a linear amplifier and an oscillograph. Each α-particle gives rise to slight ionisation in the gas of the chamber. The electrodes of the instrument between which a high voltage is applied, are charged with 10^5 elementary charges, when an α-particle of 4 MeV enters the chamber. The corresponding voltage-pulse is amplified and detected on the screen of an oscillograph. The pulse-size on the screen is proportional to the charge-pulse on the electrode of the ionisation chamber and the ratio between signal and noise is optimal when the electrical behaviour of the amplifier and oscillograph is equivalent to an ideal differential circuit backed by a ballistical oscillograph of an indication time of 0,03 à 0,001 sec.[1]).

The ordinary combination of gasfilled ionisation chamber and linear amplifier is not sensitive for β- and γ-rays because their differential ionisation is too small. The range of a α-particle of 4 MeV f. i. is 2,5 cm in air of 1 atm, so that by using an ionisation chamber with a cross-section of a few cm, we can catch the total range within the chamber. The range of a β-particle of the same energy is however many meters. This means that an adequate ionisation-chamber would require impractically large dimensions and capacity.

Increasing the pressure of the gas or using a liquid generally gives difficulties, caused by the small mobility and the high rate of recombination of the ion pairs produced. There is one interesting exception: the solid and liquid argon-counter developed in England by Davidson and Larsh and by Hutchinson[2]).

In 1942 Mr. van Heerden proposed in our laboratory the use of a crystal instead of a gas in the ionisation-chamber. The electrons of the ion pairs formed in the crystal under the influence of α-, β- of γ-particles would move through the conductionband of the

crystal and a charge would be induced on the electrode of the ionisation chamber exactly as in the case of a gas filled chamber. Indeed he succeeded in detecting α-, β- and γ-particles using an ionisation chamber consisting of a small parallel plate condenser with an AgCl crystal as dielectricum[3]).

The so-called crystal counter was cooled to the temperature of liquid air in order to eliminate the electrolytic conductivity in the AgCl.

During the congress we demonstrated a crystal counter working with a crystal of diamond, which was bombarded with α-particles.

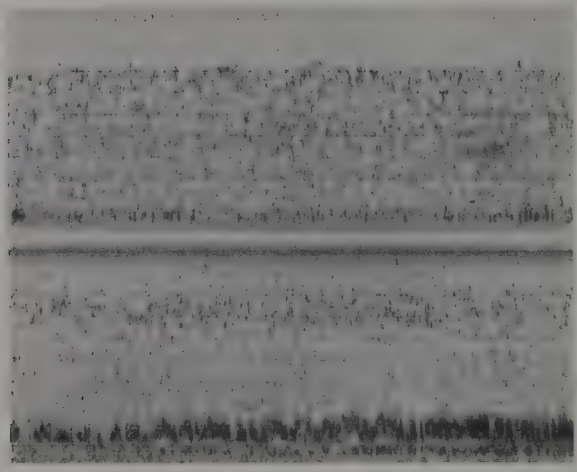

Fig. 1.

In Fig. 1 a record is reproduced obtained with the crystal counter of VAN HEERDEN. The lower part shows a number of practically equal pulses produced by mono-energetic β-particles which appear indeed to be of about the same sizes. The upper part shows a number of pulses produced by α-particles. In this case an AgCl-plate of a cross section of 1,5 cm and a thickness of 1,7 mm was used.

One of the great advantages of the crystal counter is the possibility of measuring the energy of a α-, β- or γ-ray. This is possible because under certain circumstances the number of ion pairs produced is proportional to the energy of the particle. Other advantages of the crystal counter are: high counting efficiency (~ 1) owing to the higher density and better conversion of energy into ion-pairs than in a gas and a short resolving time ($< 10^{-7}$ sec.).

Certain disadvantages may appear, when strains are present in the crystal, when polarisation effects occur or when a low temperature is necessary for the good performance of the crystal.

Determination of the energy of a α- or β-particle.

One of the advantages of the counter mentioned is the possibility of measuring the energy of a particle detected. In order to investigate this possibility in the case of β-rays VAN HEERDEN and one of the authors performed an experiment in which a mono-energetic beam of β-particles was projected on an AgCl-crystal[5]). To this purpose a RaE preparation and the crystal counter were placed in a magnetic β-ray spectrograph. The AgCl-crystal used was grown, selected and tempered with great care in order to obtain a single crystal without strain.

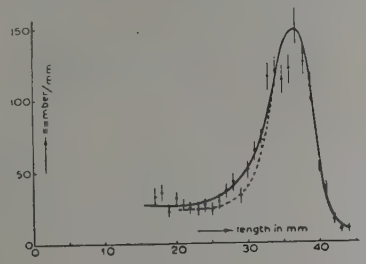

Fig. 2.

The distribution curve of the deflections caused by homogeneous β-rays. $H\varrho = 2500$; $E = 0.4$ MeV. $V = 200$ volt; 1 mm = 1200 e. c. Dotted: curve expected theoretically.

The distribution curve of the pulse-sizes obtained when the crystal was bombarded with mono-energetic electrons of 3.4 MeV is shown in Fig. 2. Most pulses have a size of 35 mm. There is, however, a spread in this size, which could be expected. The main causes are the noise of the amplifier and the reflection of the β-particles by the crystal. These effects being known, one can predict the result that would have been obtained with an ideal crystal and an ideal amplifier. It is shown by the dotted curve in Fig. 2. The conclusion is that the AgCl-crystal used behaves like an ideal crystal within the measuring-errors: β-particles of the same energy produce the same charge-pulses in the crystal, so that a crystal counter can be used for the measurement of the energy of β-particles.

Fig. 3 gives the relation between the size of the charge-pulses and the energy of the β-particles. For energies between 0 and 1.0 MeV

the relation is linear. The crystal counter completely fulfills the requirements. The mean energy necessary to produce one pair of ions is remarkably low: 7.6 eV (in nitrogen gas of 1 atm. 36 eV).

Fig. 4 gives the distribution of pulse-sizes obtained with the same AgCl-crystal when it is bombarded with mono-energetic α-particles of Polonium. Contrary to the expectation the size of the pulses is

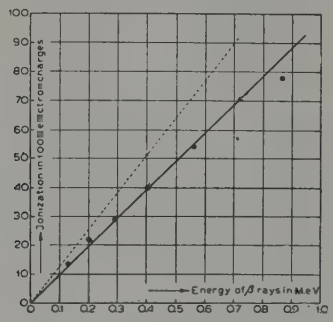

Fig. 3

The relation between the ionization and the energy of β-rays.
Dotted: the extrapolated saturation curve.

not the same. Also the mean energy for the production of an ion-pair is much higher (5.6 times) than in the case of β-particles. These two discrepances can be explained by assuming the existence

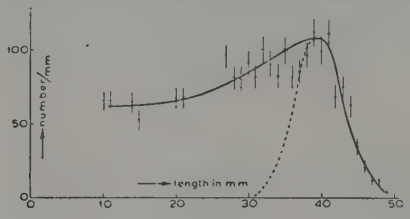

Fig. 4.

Distribution curve of α-ray reflections of Polonium.
1 mm = 2100e.c.
Dotted: curve expected theoretically.

of a surface-layer of bad quality. In this connection the recent experiments of Yamakawa[6]) on α-particles produced *within the body* of a mixed crystal by slow neutron capture (LiBr-AgBr) are of interest. They indicate that under these circumstances the energy per ion-pair appears indeed to be not substantially different from the value obtained for β-particles.

Elimination of polarization phenomena.

A rather troublesome disadvantage of the crystal counter is its polarization. This polarization becomes detectable as an appreciable decrease of the pulse size and the number of pulses, when the crystal is irradiated for a long time.

The explanation is slow accumulation of trapped charges, which give an electric field opposite in sign to the applied one. For diamond f. e. irradiated by α-particles an appreciable decrease occurs after about 10^7 α-particles have been counted.

We have carried*) out experiments on the way in which this polarization effect can be avoided. Various methods are in use.

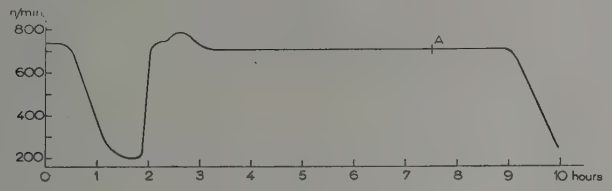

Fig. 5.

Counts per min. as a function of the duration of irradiation with α-particles. During the first two hours no red light is used. At that time the irradiation with red light begins and the counts per min. is rising to the original level. At A the red light is turned of.

In the first place one can periodically reverse the applied field, each time the same number of pulses have been counted. This method can only be applied however, when the charges captured are evenly distributed throughout the crystal, which is the case for high energy particles, for instance when measuring the output of a pulsed accelerator.

When measuring low energy particles, this method can not be applied, as in this case the trapped charges are not evenly distributed. This is due to the fact that the depth of penetration of the particles is only a fraction of the crystal thickness.

According to a second method the crystals are heated after a certain amount of irradiation. A disadvantage of this method is the decrease of the sensitivity during the irradiation.

We applied a third method by irradiating the crystal, in this case a diamond, with infrared and red light, during the counting. It turned out that the intensity of the red light can be increased to such an extent, that no charge is trapped at all, the trapped charges

*) These experiments were carried out by FREEMAN and VAN DER VELDEN.

being immediately removed by the red light. Fig. 5 shows the influence of the red light.

This methods can be applied to all sorts of particles, because there is no restriction regarding the place where the charge is trapped.

For diamonds at least the minimum wave length of the red light can be chosen in such in way, that there is no photoconductivity. After such an irradiation with red light, the crystal behaves like an entirely new one and polarisation becomes appreciable again after an impingement of about to 10^7 α-particles per mm^2.

It is clear that one of the serious disadvantages of the crystal counter can be overcome, so that the applicability of the crystal counter is increased.

Bibliography.

[1]) Milatz and Keller, Physica **9**, 97 (1942); Keller, Thesis Utrecht, 1945; Keller, Physica **13**, 326 (1947).

[2]) Davidson and Larsh, Ph. Rev. **74**, 200 (1948); Hutchinson, Nature **162**, 610 (1948).

[3]) Van Heerden, Thesis Utrecht, 1945; Van Heerden, Physica, in preparation.

[4]) Compare also the work of Kosmata, Huber and Jentschke: Stetter, Verh. deutsch. Phys. Ges. **22**, 13 (1941).

[5]) Van Heerden and Milatz, Physica, in preparation.

[6]) Yamakawa, Thesis, Princeton 1949; Hofstadter, Nucleonics, April and May 1949.

The Crystal Counter Method for the Measurement of γ-Ray Energies

by **D. Maeder** (ETH, Zürich).

The experiments described in the lecture by Prof. MILATZ[1]) have established under certain geometrical conditions exact proportionality between the energy of β-particles (< 1 MeV) entering an AgCl-crystal and the charge pulses induced in the crystal. For an electron source outside the crystal, the pulse amplitude measurement should therefore yield a good determination of electron energy. In the case of γ-ray counting, however, secondary electrons will be produced mainly inside the crystal and their energies will be spread over a wide range even for monochromatic γ-radiation. Only for energies higher than ~ 2 MeV does the fraction of secondaries emitted in forward direction become so preponderant that most of the pulses should involve either nearly the full quantum energy or (for pair production) 1 MeV less. On the other hand we must reduce the collecting field in order to provide favourable geometrical conditions for the energy measurement, because the secondaries are distributed at random between anode and cathode of the crystal. If most of the tertiary electrons are trapped in the crystal, then we may expect the same pulse amplitude-energy relationship to hold for nearly all secondary electrons; but also the pulse amplitudes will be at least one order of magnitude below the saturation values, so that amplifier noise becomes a serious limitation for this type of measurement. This is particularly true if we wish to make use of the short rise time offered by the crystal counter with conventional pulse shaping techniques; however, the influence of amplifier noise can be kept near the natural limit without sacrifice in time resolution by a new pulse measuring circuit which we shall describe below.

In connection with ionization chamber and crystal counter amplifiers, MILATZ and coworkers[2]) have introduced the concept of "natural precision": The behaviour of the amplifier input stage is described by two characteristic data $\overline{q_0^2}$ and τ_0[3]), with the meaning that the difference between the averaged output potentials before and after the pulse should be taken as a measure of the charge Q of the pulse, in order to find Q with the smallest possible uncertainty q_0^2. The averaging process should be carried out with exponential

weight functions (time constants $\pm \tau_0$); any different pulse treatment will lead to an uncertainty $\overline{q^2} > \overline{q_0^2}$.

For the measurement of pulses at a finite counting rate, this definition of $\overline{q_0^2}$ should be modified because of the possibility of overlapping pulses. To define the natural precision ${}^{N}\overline{q_0^2}$ at a given counting rate N/sec, we extend the averaging procedure only over time intervals free from pulses, so that no other pulse can contribute to the measurement of the pulse under consideration. According to the formulae derived from this definition[4]), ${}^{N}\overline{q_0^2}$ increases with counting rate N much more slowly than the $\overline{q^2}$-value of the more conventional pulse measuring systems, which suffer from the superposition of pulses. In order to attain experimentally the natural precision at all counting rates, we need 2 time-dependent averaging circuits, the first one being switched on and off by the preceeding and the considered pulses respectively, and the second one by the considered and the following pulses, respectively. Such a device offers, as compared with conventional circuits, (1) the advantage of much higher permissible counting rates for a given uncertainty in charge measurement, and (2) the possibility of combining direct energy measurements with coincidence counting. The appropriate circuits are being incorporated in a fast pulse spectrograph in course of construction.

Our investigations on crystal counters have so far been carried out with a less refined apparatus. AgCl-crystals prepared by M. Sempert[5]) were exposed to the Th(B + C)- and Li(p, γ)-radiations. With the latter radiation the pulse amplitude distribution showed a pronounced peak at about 6 times the maximum amplitude of the 2.6 MeV-measurements. Apart from demonstrating the possibility of estimating unknown γ-ray energies, this result confirms the proportionality between electron energy and pulse amplitude over a wide energy range. The accuracy was limited by the relatively high noise level of the apparatus used for these preliminary experiments. The pulse amplitude analyser was the same as described in a note on proportional counter measurements[6]).

References.

[1]) Milatz, van der Velden and Veenstra, Remarks on the Crystal Counter (this report, p. 89).

[2]) Milatz and Keller, Physica **9**, 97 (1942); van Heerden, Dissertation, Utrecht (1945).

[3]) This case is covered in a more general discussion of the noise problem by den Hartog and Muller, Physica **13**, 571 (1947).

[4]) Maeder, Helv. Phys. Acta **21**, 174 (1948).

[5]) Sempert, Diplomarbeit ETH., Zürich 1948.

[6]) Maeder and Medicus, Measurement of Converted γ-Radiation by the Proportional Counter Technique (this report, p. 175).

Recent Developments in Proportional Counter Technique

by **B. Pontecorvo**, A.E.R.E., Harwell, Berks, England.

Introduction.

Proportional counters have been used in nuclear physics research for a long time, both in detecting ionizing particles and in measuring their energy. Here it will be sufficient to quote the excellent work of Rossi and Staub[1]) and of Corson and Wilson[2]) as a general introduction on the properties of proportional counters. Constructional details can be found in the book of Korff[3]).

In most of the investigations performed in the past, the particles detected were of the strongly ionizing type, such as protons, alphas, etc., and consequently the energy spent by the particles inside the counter was high, let us say $\gtrsim$ 100 kV (i. e. the input ionization $\gtrsim$ 4,000 ion pairs). In the accounts of these investigations it had been often stated that, for the proper behaviour of proportional counters, the gas amplification factor M must be below a maximum value of about 100. As we shall see below, this statement is certainly incorrect, in its generality, although it may be correct when the input ionization is large. Probably because of this erroneous idea, the potentiality of the proportional counters was not fully made use of until recently; this is remarkable because the outstanding advantage of a proportional counter is just its ability to measure very low energy radiations, which in a non-multiplying ionization chamber would be masked by the amplifier noise. As a matter of fact a considerable fraction of the researches which used proportional counters in the past could have been performed with non-multiplying ionization chambers, although the gas amplification may have been proved useful.

In this paper we discuss mainly problems which could not be solved by a non-multiplying chamber, i. e. problems where it is the gas amplification of the proportional counter which makes it possible to detect and measure a small ionization.

The *detection* of relativistic electrons in a proportional counter at a high multiplication factor has been described in detail by Benson[4]).

In certain applications, such as coincidence work, where fast counting rate is essential, the counter in the proportional region has advantages over the GEIGER counter, because of its small dead-time. In addition its working life is much longer. Nowadays, proportional counters with flowing gas, in which it is possible to introduce a radioactive sample internally (no windows), are frequently used for detecting soft beta particles such as those from C^{14} and H^3 [5].

Among the pioneer work in *measuring* a small input ionization, by means of a proportional counter, we wish to mention first the unpublished experiments of Bernardini, who more than ten years ago went as far as recognising an intermediate component in the cosmic radiation, but was unable to draw definite conclusions for lack of quantitative information on the proportional counter technique and for lack of a good energy calibration. Again, the fairly recent work of NIKITIN[6]) who obtained a differential spectrum of ionizations brought about by individual cosmic ray particles passing through a proportional counter, is to be mentioned.

In the field of nuclear physics, initial ionizations as low as 1000 ion pairs were masured in a proportional counter by MADSEN[7]), who investigated the energy required to produce an ion pair by recoil atoms from Po, ThC, ThC'.

In the experiments just mentioned, as well as in others, not much attention was given to the ion calibration of the counter, i. e. to the accuracy of the energy determination, and to the resolving power, or energy resolution, of the method. It is our impression that the technique was not pressed forward until recently because of unjustified lack of confidence in the proportional counter as an accurate instrument. The development of a quantitative proportional counter technique for accurate measurements of energies in the range 100 e. v. to 50 k. e. v. (or more) was made independently in the last two years at the University of Glasgow[8]) and at the Chalk-River Laboratory[9]). As we shall see, the technique is extremely simple when considering the amount of information it yields, and may be applied to the study of beta spectra in the low energy region. With respect to the conventional β spectrometry techniques, the proportional counter technique not only brings down to about 100 e. v. the region which is possible to investigate, but also avoids windows and, in many cases, material supports, inasmuch as the radioactive substance under investigation may be placed in a gaseous form inside the counter.

Experimental Apparatus.

The apparatus, briefly, consists of a proportional counter placed in a shielded box, connected to a linear amplifier the output of which is fed into a multi-channel pulse analyser (Chalk River), or an oscilloscope provided with a camera (Glasgow) to photograph the pulses. Another possibility would be to feed the output of the linear amplifier into a single amplitude discriminator, in order to obtain an integral curve of the pulse distribution (a so-called "bias curve", giving the number of pulses as a function of the discriminator bias setting).

The Method for Sorting Pulse Amplitudes.

The single discriminator technique is extremely simple and is sufficient to recognise, for example, a mono-energetic line of electrons produced inside the counter gas[10]). However, since to cover the entire pulse distribution a great number of readings may be needed, an integral curve (as well as a differential one taken with only few channels) obviously requires much more time than the multichannel or the photographic methods. This means that, quite apart from the actual loss of time, various counter, amplifier, and discriminator instabilities will make it impossible, in practice, to use the technique for very accurate or difficult work.

As far as the two techniques used at Chalk River and Glasgow are concerned, the main advantages of the photographic method are its low cost and the fact that a permanent record of the pulse distribution is available. The main disadvantage of the photographic technique is the very long time which is required to sort out from the film, by visual measurements, the pulse size. Again a considerable advantage of the pulse analyser is the possibility of getting the results during the measurements, rather than afterwards. This permits changes of conditions (amplifier and counter gains, etc.) to be made according to the problem under investigation, without serious loss of time. Further, a not negligible advantage of the pulse analyser over the photographic method is its objectivity: while sorting pulse sizes visually from a film, it is very difficult to avoid psychological errors. As emphasised by D. West, this difficulty tends to yield pulse distribution which are pointed in appearance, i. e. tends to underestimate the width of a "peak".

Because of the longer time involved in sorting pulses in the photographic method, work with the pulse analyser having a sufficient

number of channels will give, in practice, a better statistical accuracy. The pulse analyser used at Chalk River was described by WESTCOTT and HANNA[11]). Fig. 1 and Fig. 2 illustrate some differential pulse distributions obtained at Chalk River and Glasgow, respectively with a pulse analyser and photographic method.

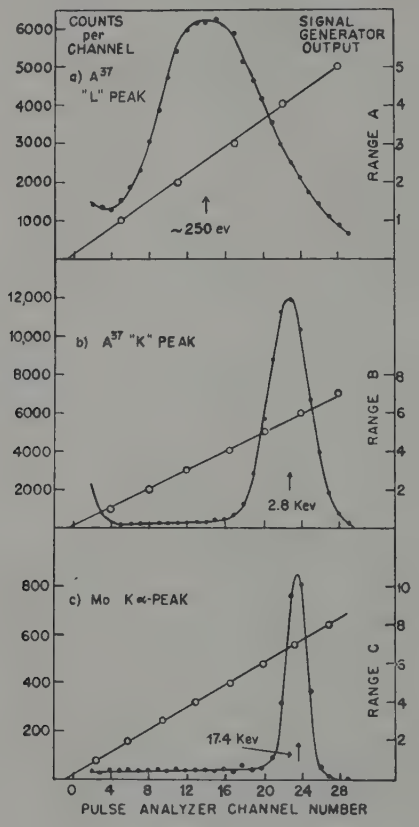

Fig. 1.

Peaks produced by ~ 250 eV, 2.8 KeV, and 17.4 KeV radiations, obtained with an electronic pulse analyser according to ref. 9. A decrease in percent width of the peaks with increasing energy is apparent. The straight lines refer to the signal generator calibration. Precise measurements of widths, however, were made using a biased amplifier to spread the 2.8 KeV and 17.4 KeV peaks over many channels of the pulse analyser. The 17.4 KeV (MoKα) radiation is obtained from a crystal spectrometer. The ~ 250 eV and 2.8 KeV are obtained from orbital nuclear capture A^{37}.

Counters.

Because constructional details are available in the literature[3]), we limit ourselves to few remarks and mention points concerning only the recently developed method of studying β-spectra by introducing a radioactive gas inside the counter.

The design of a proportional counter is usually less critical than the design of a GEIGER-MÜLLER counter. The homogeneity of the wire, however, is important in a proportional counter, because

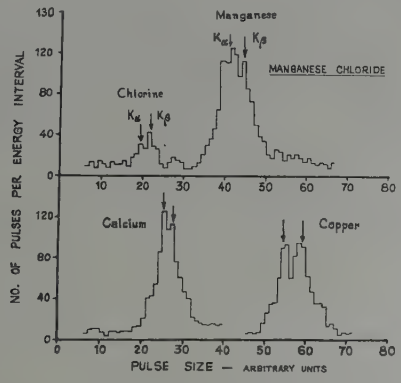

Fig. 2.

Histograms of fluorescence K X-rays obtained with the photographic methods according to ref. 8. It will be noticed that while the K_α and K_β are resolved, at least in certain cases, for calibration purposes it would be better if only one of the two lines were allowed to enter the counter.

spread in pulse size is introduced by irregularity in the wire. At HARWELL the degree of inhomogeneity of the wire is studied by examining the wire with a microscope, and in addition, by using it in a "test counter" containing A^{37}: if the distribution of pulses from the A^{37} K capture line is wider than it should be, the wire is rejected.

The counter filling, again, is not critical: in most of our experiments we have filled the counters with a noble gas (A or Xe) and CH_4, at various pressures, the proportion of CH_4 being in general not far from 20%. The presence of CH_4, as it is well known, increases the voltage for a given multiplication factor but decreases the steepness of the curve multiplication factor v. voltage; it provides, in other words, a stabilising influence. Purity of the gas is important. In Chalk River the argon and methane used were obtained from a normal tank. In HARWELL, however, the purity of the gases from

normal tanks is not sufficient, and apparently purification is needed. The problem of the "purity and nature of counting gas" in chambers with and without multiplication, has been discussed in ref[2]) and in the lecture of SEGRÉ given at this congress.

As for the dimensions, counters from 2 mm. to 5 cm. in diameter and tungsten wire 0.1 mm. in diameter were used in Chalk River. In Glasgow, for the study of the spectrum of C^{14}, a counter at a pressure of 5 atmospheres of A and 0.5 atmosphere of N_2 was used, with a diameter of 14 cm.

When the proportional counter is used for measuring energies of beta particles by placing a radioactive gas inside the counter there

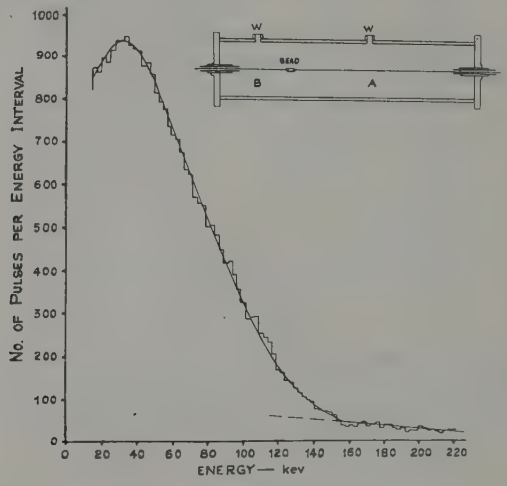

Fig. 3.

Diagram of the "split counter" according to ref. 8. The two windows W are for calibration of the two independent sections A and B. The curve gives a histogram of the C^{14} pulse distribution obtained in the section A of the counter. The correct distribution, free from end effect, is obtained by subtracting from the distribution obtained in section A that obtained in section B.

is an important source of error (end effect): at the end of the counter the weakening of the field reduces the multiplication factor, so that a fraction of the volume of the counter is associated with a "wrong multiplication factor". The counter length associated with the "wrong multiplication factor" is of the order of one counter radius, at each end, as it may be determined directly by firing a beam of α particles or X-rays in a direction perpendicular to the counter axis, at various distances from the end [1) 7) 8) 9)]. The end effect on

a "peak", produced by a mono-energetic radiation emitted by a gas introduced inside the counter, produces a low energy "tail" rather than a spread. When dealing with electron lines (for example, in the investigation of the nuclear L capture in A^{37} [9]). this effect may not be serious, provided the ratio of the length to the radius of the counter is sufficiently high, let us say 20. However, in dealing with continuous beta spectra, the effects are usually far from negligible, especially at low energies, even with the highest length to diameter ratio which can conveniently be made. An ingenious way of solving the problem has been devised by Angus and collaborators[8]), who have applied it to the investigation of the beta spectrum of C^{14}. In their research the counter consisted of a cylinder of copper 75 cms. long and 14 cms. internal diameter and is shown diagrammatically in Fig. 3. The central wire consisted of two portions of different lengths held together by a little glass rod 1.5 cm. long and 1 mm. in diameter. In this way the counter is effectively divided into two independent sections, *A* and *B*, of identical "end effects", but with different wire length. If the pulse distribution is measured at each end (i. e. in each counter section) the distribution obtained by subtracting the differential curve characteristic of the short section from that characteristic of the long section, represents the distribution which would be obtained by a hypothetical counter, of length equal to the difference in length of the two sections, free from end effects. The distribution from the section *A* for the C^{14} spectrum is also illustrated in Fig. 3.

Electronic Problems.

We limit ourselves to some general considerations, since linear amplifiers of conventional design can usually be used. The most desirable properties of the amplifier are: (1) stability, (2) low noise, (3) lack of paralysis. Points (1) and (2) are common to most problems of nuclear physics where a linear amplifier is used. As far as noise is concerned, requirements are usually less severe than in problems where a non-amplifying ionization chamber technique is used, for example in measurements of alpha particles or proton energies*). In fact, with the large multiplication factors which it is permissible to use, the effect of the amplifier noise on the width of a line is frequently negligible. To give an example, one of our amplifiers had a peak noise equivalent to 10^4 ion pairs. At a multiplica-

*) The following discussion will be more easily understood after the section on statistical spread and on range of usable multiplication factors has been read.

tion factor of 10^4, the 2.8 kV ($\sim$ 100 initial ion pairs) K capture line in A^{37} gives a signal at the counter output of 10^6 ions, in comparison of which the noise is negligible. As for the 280 eV L_I capture line in A^{37} ($\sim$ 10 initial ion pairs), its statistical inherent width is much greater than the amplifier noise, so that the modulation by noise is very small, and one starts to count noise peaks directly even before the statistical width is appreciably increased. This is illustrated in Fig. 4.

This does not mean that one should neglect to reduce the noise: in fact, if a beta spectrum is to be investigated, the highest multipli-

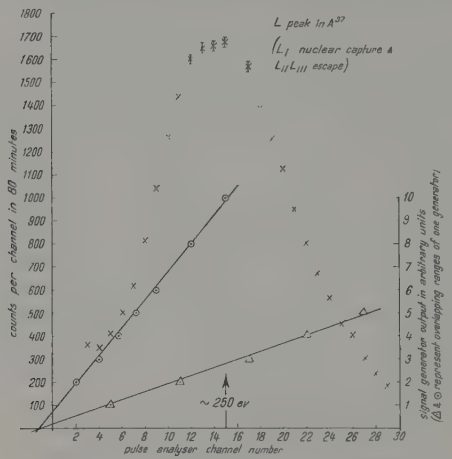

Fig. 4.

L peak from A^{37} according to ref. 9. The peak arises from the nuclear capture of L_I electrons (280 eV) and from the escape of *K* X-ray photons from the counter, with release of the Cl $L_{II} - L_{III}$ ionisation potential energy (200 eV). Pure nuclear capture can be observed in a counter having high stopping power for X-rays. The figure shows the direct counting of noise peaks at very low energy.

cation factor which can be used under conditions of proportionality is determined by the maximum beta ray energy, and may be well below one thousand. In this case, the investigation of the low energy part of the spectrum may present difficulties, unless the amplifier noise is kept sufficiently low.

The main emphasis on our Chalk River work was placed on the possibility of using high multiplication factors, since we had spent considerable time in studying the conditions under which such high multiplication factors can be used in the proportional region, and

had experimentally shown the existence of a simple "good behaviour" criterion. (See section on range of multiplication factors.) In Glasgow the main emphasis was placed on the use of low amplifier noise (an amplifier having a peak noise as low as 1500 ion pairs was used).

The problem of avoiding paralysis is very typical of proportional counter research in beta spectroscopy. While in alpha particle work, or similar work done with non-multiplying chambers, the range of energy to be covered is usually small, investigation of beta spectra requires an enormous energy range to be investigated. This is true even in simple cases[8] [9]) such as the investigation of the beta spectrum of H^3 and the investigation of the L capture in A^{37}. The general procedure is to use amplifier attenuation, when investigating the high energy particles. When studying the low energy part of an extended spectrum, with little or no attenuation, a large number of necessarily saturating pulses is present due to the high energy particles. Avoiding paralysis so that the distribution of small pulses is not disturbed by the presence of the saturating pulses, is the main amplifier problem. This was satisfactorily solved by G. C. Hanna, and the amplifier used will be described in a forthcoming publication[12]).

Amplifier and Pulse Analyser Calibration.

A signal generator feeds pulses of knwon size into the counter through a small capacity. In this way the "history" of the artificial pulses is the same as that of the (gas amplified) counter pulses. This is essential in accurate work, as the following information can be obtained:

(1) The amplifier noise can be measured directly, if necessary, by measuring the spread of the artificial pulses out of the amplifier.

(2) The multiplication factor can be determined in this way, since feeding artificial pulses of known size through a known capacity provides directly a "charge" calibration. This enables one to measure the charge at the output of the proportional counter (i. e. after gas amplification) and consequently the multiplication factor, since the input charge is also known provided the energy of the radiation is known. The described method would be very accurate if the artificial pulse and the counter pulse had identical shapes, or, if this is not the case, if the amplifier time constant is sufficiently long. Because differences in the rising time of artificial and counter pulses, the differentiation chops counter pulses and artificial pulses a different height, pro-

ducing uncertainties in the absolute value of the multiplication factor. However, this is not of much importance because what is of interest mainly is an approximate value of the multiplication factor, and corrections can be made when necessary.

(3) By feeding an artificial pulse before and after an experiment, it is possible to verify whether the amplifier and pulse analyser have drifted. Incidentally, similar information referring also to the counter can be obtained by making pulse analyser runs with a calibrated ionization, produced by X-rays, before and after any experiment.

(4) Usually a series of artificial pulses, of relative size accurately known, is fed into the counter, as in Figs 1 and 4.*). In this way, one can express all energy peaks in terms of signal generator output: this avoids the effects of any amplifier nonlinearity, and avoids the errors in the energy determination which would be produced by lack of accurate knowledge of bias.

(5) Expression of energy peaks in terms of signal generator, further, facilitates the use of a biased amplifier[12]) to obtain an expanded view of any part of an electron spectrum.

Ion Calibration.

The method usually adopted in the past for calibration, a polonium source, is obviously inadequate in proportional counter work at low energies.

Two calibration methods have been used at Chalk River (see also Fig. 1). First, A^{37}, a radio-isotope decaying by K capture with a period of 34.1 days, is introduced inside the counter. This provides[9]) a "calibration line" at 2800 eV, from the decay of A^{37} by K capture, and also a line at 280 eV, from the decay by capture of L_I electrons. The advantage of these calibration lines in beta ray spectroscopy is that they are truly representative of the properties of the counter as a whole, since A^{37} disintegrations are produced uniformly throughout the counter volume. For many researches A^{37} is ideal for calibration purposes: in a pile it can be obtained easily and in quantities sufficient for many calibrations ($A^{36}(n, \gamma)A^{37}$). It can be obtained in other nuclear reactions with the cyclotron[13]). Secondly, the X-ray method of calibration (extensively used by the Glasgow Group[8]) was used. This method has the advantage of providing a practically unlimited number of calibration lines. In addition, and

*) This is usually done with the counter voltage on and with the X radiation on, in order to avoid changing conditions because of bias produced by steady currents.

contrary to A^{37}, an X-ray calibration line can be turned off and on at pleasure. The main disadvantage is that an X-ray calibration line does not give the property of the counter as a whole, being fired into a small volume in the counter. This may not be serious in applications where only a small part of the counter is used. There are several ways of using X-ray lines for calibration*) in proportional counter work:

(i) Using fluorescent radiations. This method which has been used systematically by the Glasgow Group is simple and permits to have the K_α and K_β lines fired at the same time inside the counter. It is illustrated in Fig. 2. Although we have used this method at Chalk River, for accurate calibration we have selected the following technique.

(ii) A mono-energetic beam (mainly the K_α X-radiation) from a crystal spectrometer is "fired" into the counter: although this is slightly more complicated than the fluorescence method, it gives unquestionably a better energy calibration, at least in the energy region below 30 kV. This is so because due to the unavoidable statistical widths of a line, the K_α and K_β radiations, which enter the counter in the fluorescence method, are not sufficiently well resolved for good energy calibrations. Within a small energy interval only one energy mark, the molybdenum K_α from a crystal spectrometer in most of our work, provides a better energy calibration in our opinion. In addition, the fluorescence method, in practice, gives a more intense background of white radiation.

(iii) Characteristic radiation excited at the target of the X-ray tube, in combination with filters, may give a sufficiently monoenergetic calibration.

A very ingenious idea for calibrating a proportional counter by X-rays has been proposed by T. E. Cranshaw of the Cavendish Laboratory. A pulsed X-ray tube gives a strong beam of monoenergetic radiation (let us say, photons of 17.4 kV — the molybdenum K_α). The intensity of the beam is arranged so that the probability that several photons (produced during one X-ray pulse) produce photo-electrons in the counter gas is not negligible (the amplifier time constant is fairly long). Under such conditions an analysis of the counter pulse sizes will reveal events in which one

*) It is a pleasure to thank Drs. Hurst, Knowles and Walker for their extremely useful help in the X-ray work.

photon has interacted with the gas (17.4 kV peak), 2 photons have interacted with the gas (34.8 kV peak) etc.

When technical considerations preclude the use of an X-ray tube (for example, lack of space, or work in high mountains) a simple way of getting a calibration line is being used by D. West at Harwell: a radio-element decaying by K capture is prepared in the pile and K X-ray radiation excited under K capture provides the source. A useful source is Zn^{65} (250 days).

A supplementary remark may be useful, in connection with low energy work.

When a gas like argon or xenon is used in the counter, the number of photo-electrons liberated from the wall or window of the counter, and penetrating into the counter, is much smaller than the number of these liberated in the gas. This state of affairs is entirely different from that arising with gamma ray work, where most of the counting rate is due to the counter wall rather than to the gas. It follows that the number of spurious low energy pulses due to photo-electrons liberated from the wall is usually negligible in X-ray calibration work.

The Mean Energy necessary to produce an ion pair.

The method described for β spectroscopy requires that the mean number of ion pairs n produced by a radiation is accurately proportional to the initial energy E_i of the radiation, i. e. that the mean energy W necessary to produce an ion pair is a constant, independent of the energy. The variation of W with energy is discussed below.

A considerable amount of work has been done, mainly by measuring the ionisation current in air. Here it will be sufficient to quote the papers of Eisl[14]), Gerbes[15]) and Gray[16]), which review the results of several investigations on the energy expended per ion pair in air. The results may be summarised as follows: in air W is approximately constant for electron energies greater than 10 kV and increases for energies below 10 kV. Since energies well below 10 kV are of interest in connection with the subject of this paper, it is important to investigate further the problem. The proportional counter technique is eminently suitable for this investigation. This was done independently at Chalk River and Glasgow. The results of Curran and others[8]) on nitrogen and methane counters in the region 3 kV—25 kV show that the variation of the curve ionisation versus energy is remarkably linear in nitrogen, whereas in methane some increase in energy expenditure with decreasing energy is

found*). This indicates that the increase in W for air at low energy, mentioned above, must be due to oxygen. The Glasgow Group, in addition, has investigated a mixture of argon (60 cm. Hg) plus methane (15 cm. Hg) in the electron energy range 3 kV—40 kV. Their results provide "strong evidence in favouring the view that the energy expenditure per ion pair by an electron is, for argon, very nearly constant".

We have reached the same conclusion for an A + CH_4 mixture and for a Xe + CH_4 mixture (methane represents 20—25%) in the electron range 2.8 kV—17.4 kV. More precisely we have found, for example, that the ratio of the most probable output pulse sizes produced by radiations totalling energy of 17.4 kV and 2.8 kV is $\frac{17.4}{2.8}$ within our experimental accuracy of 1.5%. In addition, our direct observation of the nuclear capture of L electrons in A^{37} permits us to draw conclusions on the behaviour of W down to initial energy of about 250 eV for A + CH_4 and Xe + CH_4 mixtures. The experiment is done by measuring the ratio of the most probable output pulse size produced by radiations totalling 2800 eV (K ionization potential of Cl) and $\sim$ 250 eV (the L ionization potential of Cl). In this case the accuracy is not as good because (1) the L peak is in fact a mixture[9]) of radiations of energy corresponding to the ionization potentials of the L_{I} shell and of the L_{II} and L_{III} shell, and (2) the large statistical width of the L peak prevents an accurate determination of the most probable pulse size. It can be concluded, taking the errors into account, that electrons of 280 eV produce a mean number of ion pairs greater or equal to 80% of one tenth of the mean number of ion pairs produced by 2800 eV electrons. In other words W for electrons of 200—300 V is *at most* 20% greater than W for high energy electrons. It is believed that this result on W at very low energy is the most accurate known until now. Our upper limit for W in a mixture of A + CH_4, combined with the statement of Curran and others on the increase of W in methane, proves that, at least in A or Xe, W is constant down to the lowest energies**).

In conclusion it may be stated that the fundamental requirements for the validity of the proportional counter technique in measuring energies is met, and at least in a number of gases and

*) Curran and collaborators[8]) state 'for methane alone an increase in energy expenditure with increasing energy was found", but in the opinion of the writer this is a misprint.

**) As pointed out by J. D. Cockcroft, this may have application in biological problems involving radiation tolerance dosage.

over wide electron energy ranges, the number of ion pairs produced by an electron is accurately proportional to its energy. This statement should not be extended to particles different from electrons (i. e. particles of low velocity): in particular[7]) for single recoil atoms from Po, ThC, ThC[1], W in argon was found to be as high as 67 v. per ion pair in an energy interval of the recoils 100—170 kV.

Extension of the Technique to Beta Spectra of High Energy End Point.

We have assumed until now that the range of the electrons liberated inside the gas is small in comparison with the dimensions of the counter. In fact some particles will escape from the counter (wall effect). It may be easily shown that the fraction of spuriously low pulses (corresponding to the particles hitting the counter walls) is $R/2b$, where R is the range of particles which are supposed to be generated uniformly throughout the counter, and b is the radius of the counter. When a considerable fraction of electrons do not spend all their energy inside the counter, difficulties arise in studying beta spectra. In such a case the method is obviously unsuitable to study the energy of particles escaping from the counter, and, further, the particles escaping from the counter produce spuriously low size pulses, preventing even the low energy part of the extended spectrum to be studied. The first step in reducing the electron escape is fairly obvious: increase the dimension of the counter and or gas pressure. Rossi and Staub[1]) have used (for purposes which are different from the one discussed here, however) proportional counters at a pressure of several atmospheres. In the study of the beta spectrum of C^{14}, as mentioned above, Angus and collaborators[8]) have used a large counter filled at more than 5 atmospheres. It should be noticed that with a counter with a high ratio of diameter to length the device of the "split counter" (Fig. 3) is essential.

Another step in reducing the escape is being studied at Harwell at present. The idea is to curve the particles in a strong magnetic field in order to prevent their escape, more precisely, in order to increase their path in the gas. In a homogeneous magnetic field a particle with velocity parallel to the field is not affected by the field. However, if one is interested in studying the low energy part of an extended spectrum, what is required is that the number of spuriously low energy pulses, which are due to escape, is small compared with the number of genuine low energy pulses due to low energy electrons. A homogeneous field parallel to the counter axis can serve the purpose. For this, however, it is essential that the counter behaviour is not disturbed by the field. Rothwell and

West have studied this problem by measuring the pulse size distributions in a proportional counter placed in a strong magnetic field, in conditions such that a magnetic field does not change at all the escape probability. This condition is verified when alpha particles are fired into the counter, and also when A^{37} is introduced inside the counter (in the last case the range of the electron is completely negligible in comparison with the counter dimensions and consequently the average escape probability is practically zero, i. e. unaffected by the field). Fig. 5 shows results obtained with a counter

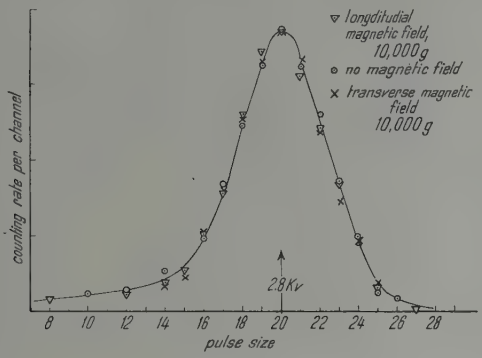

Fig. 5.

Behaviour of proportional counter containing A^{37} in strong magnetic field according to P. Rothwell and D. West. Clearly the counter characteristic is not adversely affected by strong magnetic fields.

with $A + CH_4$ plus traces of A^{37} filling, with and without a 10,000 gauss homogeneous field parallel or normal to the counter wire. The identity of the differential pulse size distributions in the three cases proves conclusively that the counter is completely unaffected by the field, i. e. that from an instrumental point of view the method suggested is operative. Although this might have been expected, on account of the small free path of electrons drifting to the wire, the results are gratifying in view of possible applications of the technique. When a radioactive gas, emitting high energy electrons, is introduced in the counter, on the other hand, a considerable increase of the number of large size pulses was observed, as expected.

Another possibility for studying the low energy part of an extended spectrum is the (anti-coincidence) technique of rejecting pulses corresponding to particles having escaped from the proportional counter. This is being considered at present at Harwell.

Spread in Pulse Size (Trivial Causes).

Even if a mono-energetic radiation is absorbed in the counter, there would be some spread in the counter pulse amplitudes. Trivial causes of spread are:—

1. Instability of the multiplication factor during an experiment. Generally, the drift of the multiplication factor M was found to be quite small even in runs lasting more than one hour. M varies approximately exponentially with the voltage, and modern stabilised H. T. supplies are sufficiently stable: by this we mean that the drift due to change in voltage can be made smaller*) than the spread due to fundamental causes. In one of our typical counters M varied by a factor 2 for a change of voltage of 80 volts.
2. Drift in amplifier and pulse analyser. It would be out of place to discuss here the general problem of stability. The drift in the counter *and* electronic equipment, as a whole, can be measured by a calibrating X-ray line.
3. Spread due to imperfect electron collection and in general to gas impurities. Although this may be very serious, the problem, wich has been discussed in reference (2), is soluble.
4. Inhomogeneities in the wire counter. Careful selection of the wire is recommended.
5. Amplifier noise. It has already been stated that in a proportional counter this cause of spread is frequently negligible.

When careful attention is paid to the above-mentioned causes it may be stated that, when the energy is below 40 kV, the spread produced by them can be kept definitely below the spread produced by the fluctuations in the initial number of ionizations and fluctuations introduced by the statistics of the multiplication process in the counter, which are discussed below.

Statistical Spread.

The first point we have investigated at Chalk River was the dependence of the spread upon the multiplication factor. We have found that the width of a peak expressed in percent of the energy is in fact independent of the gas multiplication factor over an enormous range. More precisely, the "constant width" range extends from the low values of M, at which the peak under investigation still

*) This is only true, however, provided that the radiation being investigated has a fairly small energy, let us say, less than 40 kV.

stands well above the amplifier noise, to values of M where lack of gas proportionality, due to space charge effects, is measurable. We will discuss in the next section the practical and theoretical significance of this critical value of the multiplication factor, function of the initial ionization, at which both increase in width and lack of linearity start to appear. Here, when referring to the width and shape of a peak, it is intended to refer to these in the region of "constant width". In a typical counter, for example, the width of the 2.8 KeV A^{37} line was found to be constant for voltages ranging from 2100 to 2900 volts.

Correcting for the low energy tail, the shape of the peaks produced by the 17.4 and 2.8 kV radiations was found to be Gaussian, at least

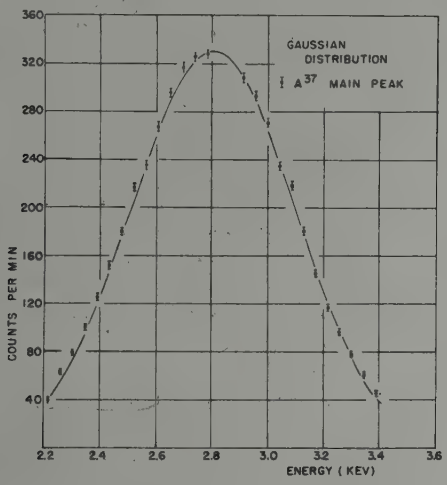

Fig. 6.
Gaussian distribution of the A^{37} K capture peak.

over the energy range ($\pm$ 3 standard deviations) where background fluctuations do not disturb the measurements. Fig. 6, for example, indicates the Gaussian character of the A^{37} peak, which in this run was spread over all the channels.

Since the spread is due not only to statistical fluctuations but also to trivial causes, it cannot be concluded that the "ideal" peaks (i. e. peaks with the spread due to statistical causes only) would be Gaussian. However, for the counter of which we give data — one of our counters giving the least spread — we have reasons to believe that the "trivial" spread is fairly small in comparison with the

statistical spread*). Anyway the observed values of the standard deviation of the pulse size obtained by fitting the experimental points to a Gauss distribution will give an upper limit to the standard deviation of the corresponding "ideal peak". Table I summarises the results.

Table I.

Radiation energy (ev) E_i	Estimated mean number of ion pairs released by radiation, n	Observed standard deviation (% of pulse size)
17,400	700	$(4.0 \pm 0.2)\%$
2,800	110	$\left(8.8 \begin{cases} + 0.3 \\ - 0.1 \end{cases}\right)\%$
~ 250	~ 10	$(36 \pm 4)\%$

It is seen that the observed standard deviation, measured in percent of pulse size (a convenient quantity to express the spread of a peak) for radiations of 17,400, 2800, ~ 250 eV is not very different from $\pm \sqrt{n}/n$, n being the mean initial number of ion pairs released by these radiations. It is interesting to compare these results with published theories. A theoretical analysis of the fluctuations of the initial number of ionisations produced when a radiation is completely absorbed in the gas was given by Fano[17]). This author estimates that the mean square deviation of the number of ionisations is substantially smaller than that governed by a Poisson distribution (which would be n) and may be of the order of $n\,K$ with K between 2 and 3. To this variance one has to add the variance introduced by the statistics of the multiplication process in the counter, which was discussed by Snyder and by Frisch[18]), and found to be equal to n. Consequently the theory predicts a mean square deviation at the output of the proportional counter, referred back to the initial number of ions, n, equal to $n/K + n$.

This value is considerably higher than the observed value, even if K were to be higher than the value predicted by Fano. Since K is unlikely to be very great, and in any case the observed values are upper limits for the mean square deviation, our results show definitely that the gas amplification introduces less spread than the theory would predict. As emphasised by G. C. Hanna, the reason of the discrepancy between our experiments and the theory

*) The fact that the standard deviation is approximately proportional to the square root of the input energy is best indication of the validity of the statement.

is probably the over-simplification of the starting assumptions of the theory.

To evaluate the variance introduced in the counter multiplication process, in fact, FRISCH[18]) assumes that the probability for an electron, drifting to the wire, to produce an ion pair in the gas is solely a function of the electric field, i. e. solely a function of its distance from the wire. Actually the probability must depend upon the previous history of the electron, because an electron having just produced an ion pair must be accelerated again, no matter what its distance from the wire is. This produces a compensating effect probably responsible for the discrepancy between theory and experiment.

From a practical point of view, the discrepancy is gratifying, in as much the energy resolution of the method, observed experimentally, is better than had been expected.

The useful range of gas multiplication.

The range of useful multiplication factors was studied carefully by

(1) measuring the widths of the 2.8 KeV and of the 17.4 KeV peaks as a function of the voltage;

(2) measuring the ratio of the most probable outpout pulse sizes produced by the 2.8 KeV and the 17.4 KeV radiations, as a function of the voltage.

The linearity of the gas multiplication was established within the experimental accuracy of 1.5%, over a range extending from the lowest value at which careful width measurements could be made ($M \approx 300$) to a fairly critical value, M_c, where lack of linearity is easily detected. The critical value M_c is a function of the radiation energy E_i being greater the smaller E_i. As mentioned above, when the multiplication factor is close to $M_c(E_i)$, the width of the peak corresponding to the energy E_i increases in an easily detectable way. All these facts strongly suggest that proportionality and correct peak width are maintained up to that multiplication factor which produces a certain total output pulse, that is $E_i \times M_c(E_i) =$ constant. In a typical counter the constant was about 3×10^8 eV. It follows that for low energy measurements correspondingly large multiplication factors may be used. In practice a quick criterion to verify that the range of voltage is satisfactory is to inspect on an oscilloscope the spread of the peak produced by the most energetic radiation under investigation: the maximum voltage which can be used

must be, let us say, 50 volts below the voltage at which an increase in percentage width is plainly observable.

We want to discuss now the observed "good behaviour criterion", i. e. $E_i \times M$ must be smaller than about 10^8 e. v.*). The existence of a fairly critical output pulse must correspond to a total charge which is not negligible in comparison with the pre-existing charge at the wire — which is of the order of 10^9 electron charges per cm. Now the relation $E_i \times M < 10^8$ e. v. means that the charge after gas amplification must be less than $10^8/25 = 4 \times 10^6$ electron charges. If the electron of an avalanche diffuse over about 1 mm, it is seen that the "critical pulse" corresponds to about 4% of the pre-existing charge.

Conclusions.

In conclusion it may be useful to list here the problems for the investigation of which the described technique of the proportional counter, used at high multiplication with careful ion calibration, is eminently suitable.

(1) Investigations of beta spectra of radio-elements, of low end point energy, which may be introduced in gaseous form into the counter (e. g. H^3, C^{14})[8][9]).

(2) Investigation of the low energy part of the beta spectrum extending to energies of about 1 MeV. This is being done at the present at Harwell, by Rothwell and West (magnetic fields).

(3) Investigation of beta spectra of very weak intensity. The high solid angle of a counter makes possible this application.

(4) Investigation of orbital electron capture. Nuclear capture of L_I electrons was first observed by this technique[9]).

(5) Isomeric transitions and low energy gamma rays. Study of X-ray emission in nuclear problems. As an example we quote the study of the Ra-D radiations[8]).

(6) X-ray applications. In every problem of X-ray research where the intensity is weak and a Geiger counter was used until now as a detector, it is clear that the use of a proportional counter will reduce background by giving supplementary information on another parameter, the energy of the X-ray quantum.

(7) Fluorescence X-ray analysis. This was initiated by Knowles and Walker at Chalk River.

*) The condition is certainly less stringent than this when the original ionisation is spread over a large distance.

(8) Cosmic Ray work. Measurements of the specific ionisation in a proportional counter can be used in the investigation of mass spectra of intermediate particles, when the magnetic rigidity is measured at the same time.

(9) Study of the specific ionisation as a function of the energy of a particle. According to a kind communication of Professor Dee, this problem is being investigated in his laboratory.

(10) Study of fluctuation of ionisation[9]).

(11) Study of the change of the mean energy W spent in producing an ion pair as a function of the energy[8])[9]). An absolute determination of W in various gases can also be made.

(12) In some cases the proportional counter technique can reduce the effective background when counting extremely weak intensities of a radio-element. For example, in an attempt to detect free neutrinos, it was proposed[19]) to irradiate a large mass of Chlorine, and to measure A^{37} produced in the reaction Cl^{37} + neutrino $\rightarrow$ A^{37} + electron. Clearly, if one measure the pulse size distribution in a proportional counter, the effective background of the counter is greatly reduced due to the narrow width of the A^{37} peak. In this way a counter having an effective background as low as one count in several hours has been obtained.

(13) In some problems such as the exploration of the neutron density in a pile, it may be useful to detect neutrons at considerable distances from electronic equipment. For this purpose proportional counters (BF_4, CH_4 filled, B or U coated counters) have been used at Chalk River and Harwell: in these counters the (positive) H. T. voltage was connected to the wire by a cable, having a length of the order of 100 ft. The counter case was grounded and the first tube of the amplifier (about 100 ft. from the counter) was insulated from the wire by a condenser.

Acknowledgments.

The Chalk River investigations were performed in the Nuclear Physics Division of W. B. Sergent, by G. C. Hanna, D. H. Kirkwood, in collaboration with the writer: this paper does not carry their names merely due to the nature of this review lecture. It is a pleasure to thank T. E. Cranshaw, O. R. Frisch, G. C. Hanna, D. Hurst, W. B. Lewis, A.G. Ward, D. West and D. H. Wilkinson for illuminating discussions.

Bibliography.

[1]) B. Rossi and H. Staub, A series of Los Alamos reports to be issued in the form of a book.

[2]) D. R. Corson and R. R. Wilson, Rev. Sci. Inst. **19**, 207 (1948).

[3]) S. A. Korff, Electron and Nuclear Counters, D. van Nostrand Co., Inc., New York, 1946.

[4]) B. B. Benson, Rev Sci. Inst. **17**, 533 (1946); see also S. Werner, Z. S. f. Phys. **90**, 384 (1934).

[5]) J. A. Simpson, Jr., Rev. Sci. Inst. **18**, 884 (1947); C. J. Borkowski and E. Fairstein, Phys. Rev. **74**, 1243 (1948).

[6]) S. Nikitin, Journ. of Phys. XI, 196 (1947).

[7]) B. S. Madsen, Det. Kgl. Danske Videnskabernes Selskab. Mat-Fys. Meddelelser, XXIII, No. 8.

[8]) S. C. Curran, J. Angus, A. L. Cockroft, Nature, 162, 302, 1948; Phil. Mag. **40**, 53 (1949); Phil. Mag. **40**, 36 (1949); J. Angus, A. L. Cockroft, S. C. Curran, Phil. Mag. **40**, 522 (1949).

[9]) D. H. Kirkwood, B. Pontecorvo, G. C. Hanna, Phys. Rev. **74**, 497 (1948); G. C. Hanna, D. H. Kirkwood, B. Pontecorvo, Phys. Rev. **75**, 985 (1949); G. C. Hanna, B. Pontecorvo, Phys. Rev. **75**, 983 (1949); B. Pontecorvo, G. C. Hanna, D. H. Kirkwood, Phys. Rev. **75**, 982 (1949).

[10]) G. A. Renard, C. R. **228**, 310 (1949).

[11]) C. H. Westcott and G. C. Hanna, Rev. Sci. Inst. **20**, 181 (1949).

[12]) G. C. Hanna, D. Kirkwood, B. Pontecorvo, to be submitted for publication in the Can. Journ. Res.

[13]) P. K. Weimer, J. D. Kurbatov and M. L. Pool, Phys. Rev. **66**, 209 (1944).

[14]) A. Eisl, Ann. Phys. Leipzig **3**, 277 (1929).

[15]) W. Gerbes, Ann. d. Phys. **23**, 648 (1935).

[16]) L. H. Gray, Proc. Camb. Phil. Soc. **40**, 72 (1944).

[17]) U. Fano, Phys. Rev. **72**, 26 (1947).

[18]) H. S. Snyder, Phys. Rev. **72**, 181 (1947); O. R. Frisch, The Statistics of Multiplicative Processes, as yet unpublished.

[19]) B. Pontecorvo, Nuclear Physics Conference, Montreal 1946; L. W. Alvarez, Private Communication, 1948.

The precise use of proportional Counters over long periods of Time

von **D. H. Wilkinson,** Cavendish Laboratory, Cambridge, England.

Introduction.

It is not necessary to labour the merits of a proportional counter in determining particle energy when that energy is small. If the energy dissipation is a few MeV the variance in the pulse height distribution due to intrinsic straggling in the ionisation yield is becoming comparable with that due to amplifier noise and so there is little point in using a proportional counter. But for energies below about 1 MeV gas amplification is essential if a precise estimate of particle energy is to be made.

The chief objection to the use of a proportional counter is its lack of stability. The gas amplification A is a more-or-less rapidly increasing function of the voltage V applied to the counter. Under good conditions when A is not too high it may require V to be increased by 200 volts or so in order to double it: but if A is to be pushed to its limit it may double in 20 volts or less. Now the straggle in ionisation produced by particles up to 1 MeV is a few tenths of a percent, so for work of the highest precision A should be held constant to this order. If we take as typical a doubling of A for a 70 volt increase in V, then a variation of V by $^1/_{10}$ volt (perhaps in 1000 volts) will give a $^1/_{10}\%$ change in A. Such voltage stabilisation is impossible to achieve over a period of hours and even if it were achieved the problem would not be solved: unless a proportional counter has been violently outgassed absorption and emission of gas by the walls causes A to drift quite considerably over long periods. Such behaviour is most strongly marked in counters containing pure noble gases, but even in the presence of polyatomic molecules the trouble remains to a lesser degree.

One cannot then attain the highest precision over long periods of time by using proportional counters in the conventional way.

It is the object of this paper to show how the desired precision may be attained by deriving control of the counter from within itself, and then to discuss the operation of the machine which has

been developed to analyse the pulse distribution coming from the counter.

The principle of the method is to include permanently within the counter a group of α-particles such as that of polonium. It is then arranged by a feed-back mechanism between a discriminator and the voltage V that the voltage group emerging from the amplifier should always register in the same channel of the pulse amplitude analyser. In this way an over-all stabilisation of gas and electronic amplification is achieved: leaks in the counter and drifts in the amplifier are automatically compensated for, the stability of the whole arrangement remaining better than 1%. It will be seen that this stability depends essentially on the ratio of two resistances in the stabiliser proper and a resistance-capacity time constant in the pulse amplitude analyser: no voltages need to be highly stabilised anywhere in the system.

The stabiliser.

The stabiliser operates in the following way. The output from the amplifier is fed through two discriminators. One fires at x_1 and the other, which is not so important, fires at x_2 ($x_1 > x_2$ and it is only necessary that $x_1 - x_2$ should be bigger than the width of the α-particle group used for stabilisation). The discriminators are coupled so that the one firing at x_1 passes a pulse down channel A whenever it fires, and that firing at x_2 passes a pulse down channel B only when no pulse goes down channel A. Channels A and B feed into opposite sides of a flip-flop: one of the anodes of this flip-flop is directly coupled through a large resistance to the grid of a tetrode. The tetrode derives its anode voltage through a high resistance from an unstabilised high voltage line somewhat higher in voltage than the maximum which must be applied to the counter. The counter itself receives its voltage V from the anode of the tetrode. When a pulse passes down channel A the anode potential of the flip-flop rises and with it the grid potential of the tetrode. The current through the tetrode increases and so its anode voltage — the counter voltage V — falls. Similarly a pulse down channel B causes V to rise. A large condenser is connected from anode to grid of the tetrode and this exerts a damping effect on the changes of anode potential of the tetrode and makes them linear with time. So the voltage V applied to the counter is always either rising or falling at a constant rate. If the counter leaks, the gas amplification falls, more pulses pass down channel B instructing the counter volts to rise in compensation. Similarly an increase in electronic amplifica-

tion or a hardening of the counter by the absorption of gas on the walls will cause an increase in pulse height, an excess of pulses in channel A and the counter volts will fall, rectifying the situation.

It is obviously of importance to know how efficient this stabiliser is going to be. It is clear that, if the whole set-up is perfect, then the use of the stabiliser is going to make the situation worse, introducing an extra variance into the pulse height distribution. One must know how great this variance is and how the situation is affected by a non-perfect set-up. We will follow through the argument assuming that the electronic amplifier is perfect — the generalisation to a non-perfect amplifier is immediate.

Suppose the differential relation

$$\delta A = k A \, \delta V$$

between A and V; suppose also that when the volts are instructed to change they do so at the rate c volts/sec. The variation of gas amplification due to leaks or something against which stabilisation is provided is given by the relation, for constant V

$$\delta A = -b A \, \delta t$$

We assume, to perform an approximate calculation, that the stabilising group of α-particles has width an amount ω either side of a mean centred at unity corresponding to a gas amplification A_0. Now in operation A will distribute itself about some mean value which will not be A_0 because c is finite. We assume a Gaussian distribution for the probability $p(A)\delta A$ that A should lie at any instant between A and $A + \delta A$.
Thus

$$p(A) = \frac{1}{\sigma \sqrt{2\pi}} e^{-\frac{(A-(A_0-\delta))^2}{2\sigma^2}}$$

and if the operation of the device is to be satisfactory we must have

$$\left(\frac{\sigma}{A_0}\right)^2 \ll \omega^2$$

the extra variance introduced by the device being small compared with that intrinsically present.

If now the stabilising particles arrive at the random rate N/sec. we find

$$\delta = \frac{A_0 b \omega}{k c}$$

$$\sigma^2 = \frac{A_0^2 \omega}{N k c} (k^2 c^2 - b^2)$$

The biggest extra variance comes when $b = 0$ when the above condition for satisfactory operation becomes

$$kc \ll \omega N$$

so with typical values $k = 1/100$, $\omega = 1/100$ and with $c = 1$ we have satisfactory operation with a counting rate from the stabilising particles of a few per second. If now, for example, the counter leaks so that, without the use of the stabiliser, A would halve itself every hour, $b \sim 10^{-4}$ and the group shifts by a fraction of its width given by

$$\frac{\delta}{A_0 \omega} = \frac{b}{kc} = 2 \times 10^{-2}$$

a negligible effect. With $N = 10$/sec. the intrinsic variance is increased by 10%, again a negligible effect.

The particles in which we are really interested give pulses lying below x_2 and so do not disturb the action of the stabiliser. Their number may be as great or as small as is desired.

The pulse amplitude analyser.

The stabiliser described above may, of course, be used in conjunction with any form of pulse amplitude analyser, but in general will demand the stabilisation of a high voltage line: x_1 is defined through the junction of resistances, R_1 and R_2 feeding from a positive line of voltage V_1 to ground. Thus

$$x_1 = \frac{R_2}{R_1 + R_2} V_1$$

and the stability of the stabiliser itself is determined by V_1 as well as R_1/R_2. This is undesirable and is not necessary.

The analyser to be described is particularly suitable for use in conjunction with the stabiliser as it has itself a high degree of stability over long periods. It has ninety-nine channels and is simple to make, the number of valves being much less than the number of channels.

The principle is to convert the incoming pulse of a certain height in volts into a pulse of standard height whose length in time is proportional to the height of the input pulse. This time pulse then gates a continuously-running oscillator and so produces a number of pulses proportional to the height of the input pulse. These pulses are passed into two rings of ten in series. Thus if thirty-eight pulses are generated, the eighth valve of the "units" ring will be left in an extraordinary state and the third of the "tens" ring also. These

valves cause two relays to close and the relays in turn operate the appropriate telephone message register. (The fact that the registration is made directly on message registers means that the analyser is slow. A blocking circuit is, however, incorporated in the input stage so that a high input pulse rate may be tolerated). It will be realised that the only portions of the machine which require a high degree of stabilisation are the oscillator and the unit which converts the input pulse into the time pulse. Now the oscillator frequency may easily be stabilised to better than 1% so occasions no worry. The converter unit operates by charging a condenser C to the peak value of the input pulse through a diode. When the input pulse has passed away the diode is cut off and the condenser C becomes the grid-to-anode condenser of an ordinary MILLER time-base pentode. The running down of this pentode is controlled by a high resistance R connected from the positive line at voltage V_2 to the grid side of C. Thus the anode runs down at the rate V_2/RC volts/sec. The stability of the height-time conversion is then seen to reside in the stability of V_2 and RC. It is found in practice that this stability is very good, being better than 1% over a period of some months. But now if the analyser and the stabiliser are working together the height of the stabilising group is $x_1 = \frac{R_2}{R_1 + R_2} V_1$ and so the corresponding time pulse is of duration $RC \frac{R_2}{R_1 + R_2} V_1/V_2$. If now the stabiliser and analyser share the same positive line $V_1 = V_2$ and the time pulse has a duration $RC \frac{R_2}{R_1 + R_2}$ dependent only on the time constant RC and the ratio R_1/R_2 as remarked earlier. So the stabilising group always registers in the same channel though no high degree of voltage stabilisation is provided anywhere in the apparatus.

In this way a proportional counter may be used as a precision instrument even at high gas amplification and over periods of weeks if necessary.

Speed Limitations of Geiger-Müller Counters

by **Hendrik den Hartog.**

Laboratory of Physics University of Amsterdam.

Summary. This paper summarizes the three main speed limitations imposed on the use of GEIGER-MÜLLER counters, viz. the electron transit time, the development of the discharge and the finite rise time of the pulse associated with it, and finally the deadtime. This deadtime is analysed more fully for low and high counting rates. Finally a technique is described for eliminating most of the complications connected with very high counting rates.

Migration of the Secondary Electrons.

GEIGER-MÜLLER counters consist of a small active and a large passive region, in the latter of which the ionization by the radiation under observation takes place.

A considerable time is required for the electrons liberated to migrate through the comparatively low field in the neighbourhood of the wall to the active region of the wire, where multiplication is initiated.

In contrast to newly developed secondary-emission devices, GEIGER-MÜLLER counters show an initial time lag caused by this effect. Measurements by SHERWIN[1]) and by MULLER, VAN ROODEN, VERSTER, and the author[2])[3]) have yielded a fairly complete, although not yet entirely consistent picture. In a typical counter of 30 mm cathode diameter and filled with 90 mm of argon and 10 mm of ethyl alcohol the maximum time lag is 0.35 microseconds. This time lag is roughly proportional to the alcohol pressure and to the square of the diameter but for the very smallest pressures and diameters, when the mobility might no longer be constant, and the additional time necessary for the first avalanches to develop to a detectable extent becomes relatively appreciable.

In Fig. 1, data are collected of electron transit times in the mixture just mentioned. Sherwin quotes a transit time of 0.1 microsecond for a radius travelled of 1 cm, in a filling of 92 mm Hg of argon and 8 mm of amyl-acetate. The measurements of Sherwin cover the high field-strength region of the counter, and do not seem to con-

form to a constant mobility. SHERWIN's findings can be described by the formula

$$v = 4.5 \left(\frac{F}{p}\right)^{\frac{1}{2}} \text{cm}/\mu\,\text{sec.},$$

where F is the field-strength in volt per cm, and p the total pressure in mm of Hg.

Data on the mobility k derived from the radii r travelled in times t by means of the formula $k = r^2/4tCV$ as published by the Dutch authors are shown in Fig. 2. Here C is the capacitance $1/2 \ln(r_c/r_a)$ per unit length of counter, and V is the voltage across it.

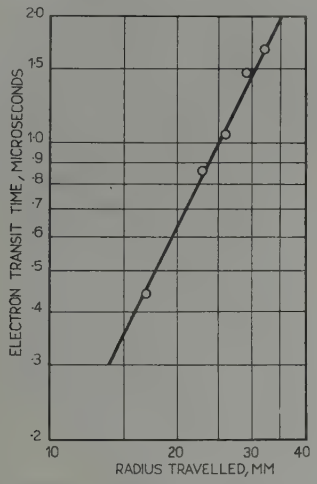

Fig. 1.

Electron transit times observed in a counter filling of 90 mm Hg of argon and 10 mm Hg of alcohol vapour. (Wire diameter 0.1 mm, cathode diameter 68 mm, operating voltage 1300 volts.)

From the experimental work of SHERWIN[1]) and the theoretical investigations of WILKINSON[10]) it appears that a second delay must be taken into account during which the avalanche activity develops to a detectable level. In consequence of the exponential nature of the development of the discharge, this delay cannot appreciably be reduced by increasing the amplification. In one specific instance, WILKINSON calculates an extra delay of 0.015 microseconds at 100 volts overvoltage, and of 0.06 at 30 volts overvoltage, but it must be remembered that this second delay depends critically on the photon free path, varying approximately as the square of this

quantity (counter data: cathode diameter 20 mm, wire diameter 0.2 mm; 65 mm Hg of argon and 5 mm of alcohol vapour).

Much shorter time lags can be obtained by using parallel-plate counters, but most investigators have found it necessary to use quenching circuits keeping the counter inoperative for a long time.

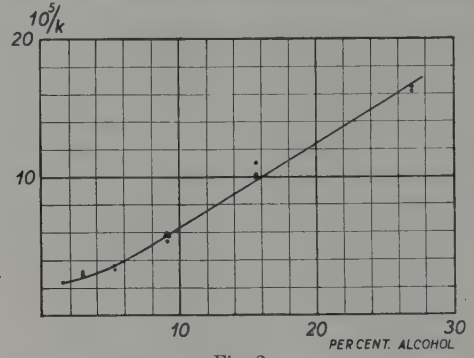

Fig. 2.

Reciprocal plot of electron mobility k versus alcohol content. Data reduced to a total pressure of 100 mm Hg.

sometimes as long as 0.01 seconds. Muller has shown that parallel-plate counter characteristics can be much improved by introducing a liquid cathode. Counters with an alcohol cathode operate satisfactorily with a 100-megohm quenching resistor (Fig. 3). But even so, Geiger-Müller counters are much more stable and reliable and will be preferred when they can be at all used.

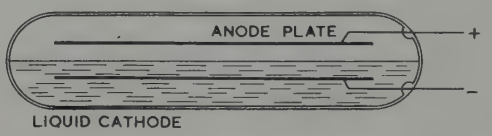

Fig. 3.

Parallel-plate liquid-cathode type of counter developed by F. A. Muller. Spacing between anode and alcohol cathode 8 mm, argon pressure 100 mm, operating voltage 3500 volts.

Propagation of the Discharge along the Counter Anode.

In the Geiger region of operating, the additional gas amplification offered by the spreading of the discharge along the counter wire is also used, but in most high-speed coincidence work, the pulse is shortened and normalized in such a way that actually only a very

small part of the extension of the discharge is used. In such applications, there ultimately seems to be little gained and much lost by operating the counter above the GEIGER threshold, thus introducing the ill effects of the deadtime.

Experimental and theoretical work by VAN GEMERT, MULLER, and the author[4]), by ALDER, BALDINGER, HUBER and METZGER[5–8]), by LIEBSON[9]) and recently by WILKINSON[10]) has yielded much material for an adequate description of the mechanism of the discharge, although here again the picture is not quite consistent. The speeds

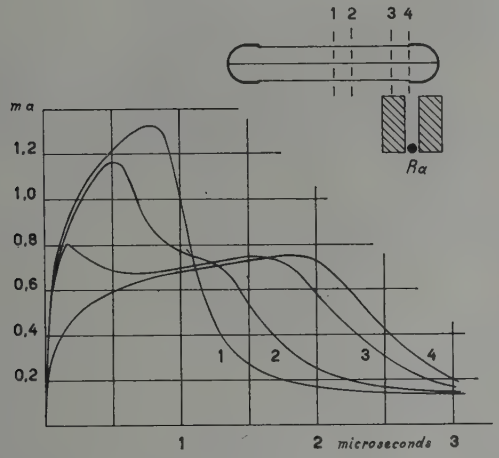

Fig. 4.

Family of current characteristics observed in counter irradiated as indicated in sketch. Counter data: length 200 mm, wire diameter 0.1 mm, cathode diameter 70 mm; counter gas: 45 mm Hg of argon, 45 mm of neon, 10 mm of ethyl-alcohol vapour; operating voltage 1500 volts, overvoltage 215 volts.

of propagation observed average around 10 cm per microsecond, and the rate of current increase is of the order of a few mA per microsecond.

Fig. 4 is the first figure published by VAN GEMERT c. s. showing the dependence of the shape of the counter current pulse on the point of irradiation. It is seen how the propagation in both directions causes the pulse 1 initiated at the centre to have double the rate of increase and half the duration of pulse 4 initiated at the end.

Much more accurate measurements were taken a few years later by ALDER, BALDINGER, HUBER and METZGER[5-8]).

A rise time of 8 mA per μsec was found for a pulse started away from the end of a counter described as follows:
cathode radius r_c = 9 mm, wire radius r_a = 0.075 mm, alcohol pressure 16 mm of Hg, argon pressure 64 mm of Hg, voltage 1150 volts.

The slowness of propagation along the wire, though usually a nuisance, can sometimes be utilized for determining the point of incidence of the radiation. MULLER's focussing device for WILSON cloud chambers shown in Fig. 5 is based on this principle. Rays

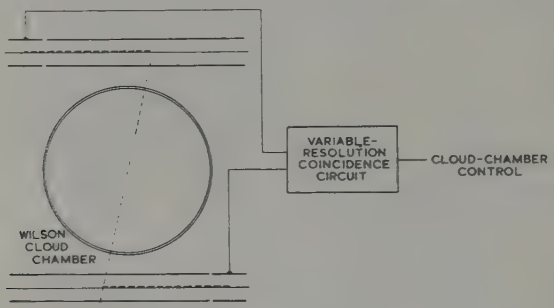

Fig. 5.

F. A. MULLER's system of cloud-chamber control focussing. Width of useful beam can be adjusted by means of the coincidence-circuit resolving time.

passing not too far from the centre of the cloud chamber will be observed only, provided the diameters of the counters are small, so that the extra delays due to the electron transit time are sufficiently small also, and provided the velocities of propagation in the counters are equal. At equal operating voltages, this calls for accurately equal gas mixtures. It is possible but not necessary to let the counter gas volumes communicate so as to keep the mixtures identical during the full useful life of the counters.

The deadtime.

Although most of the counters in current use are of the self-quenching type, self-quenching characteristics are sometimes dispensed with, and non-quenching counters used instead. In these counters, a certain time is lost during which the discharge burns before it is quenched by some external means. But also selfquenching counters involve a time loss after each discharge, the deadtime, during which the counter is inoperative.

Deionization phenomena.

After the fundamental work of C. G. and D. D. Montgomery[11] it was realized that many phenomena in a Geiger counter could be quantitatively accounted for by simple calculations on the motion of the ion sheath in the counter subsequent to the active period of the discharge. In 1942, Stever in the U. S.[12] and van Gemert. Muller and the author in Holland[13] published very similar theoretical and experimental work on the dead time. In a recent paper.

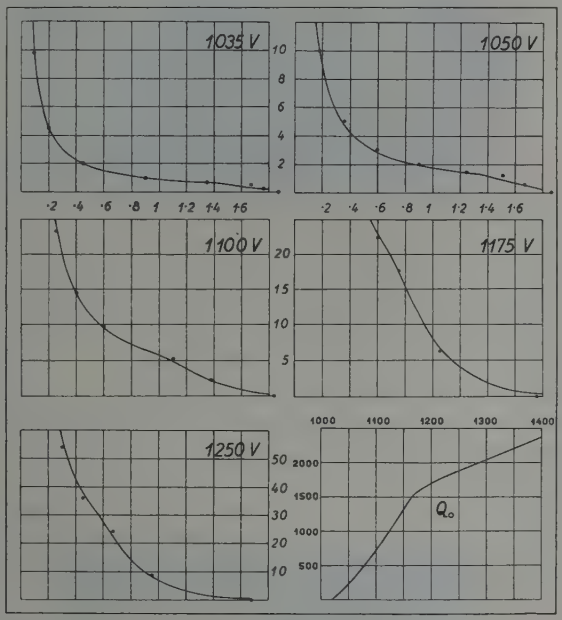

Fig. 6.

Currents observed in a counter with a cathode diameter of 38 mm and a wire diameter of 0.1 mm, filled with 94 mm Hg of argon and 12 mm Hg of alcohol vapour. Horizontal time scales: milliseconds; vertical time scales: 10^{-9} amp per cm counter length. Curves measured, dots calculated from theory on the basis of a uniform ion mobility $k = 5.6$ cm/sec per volt/cm. (Ordinates in the charge characteristic: equivalent calibrating pulses on the counter cathodes, volts.)

Muller and the author [14-15] pointed out how very accurate the agreement between theory and experiment is if a number of corrections are introduced and if precise measurements are taken of both the charge Q developed per unit length of counter wire and the mobility k of the ions in the ion sheath.

Fig. 6 shows a plot of pulse size versus counter voltage, and five experimental curves of deionization currents in a counter of 38 mm cathode diameter and 0.1 mm wire diameter, filled with 12 mm Hg. of ethyl-alcohol and 94 mm of argon. Dots are added indicating current values calculated from the charges measured on the basis of a mobility $k = 5.6$ cm/sec per volt/cm. It will be seen that the agreement is good enough to allow of an accurate determination of k. For further details the reader is referred to the original paper.

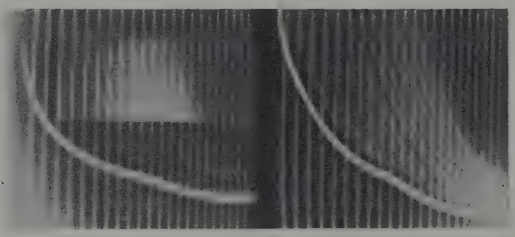

Fig. 7.
After-discharges observed in a counter operating at a high overvoltage. These after-discharges occur within a sharply defined interval of time not coinciding with the arrival of the alcohol ions on the cathode cylinder.

As alcohol ions fall onto the cathode from the break until the termination of the current, it can be seen from an oscillogram of a counter showing afterdischarges (Fig. 7) that these are caused by ions faster than alcohol ions, possibly by argon or decomposition products.

Once k and Q are known, the recovery characteristic can be cal-

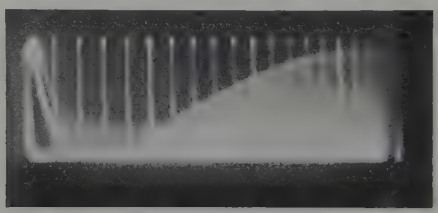

Fig. 8.
Recovery characteristic of the counter described in the caption to Fig. 6, operating at 1125 volts. Time scale: 0.1 millisecond divisions.

culated, that is the way the field strength at the counter wire is restored after the formation and subsequent migration of an ion sheath. Fig. 8 shows the well-known way in which this recovery can

be visualized on a C.-R. oscilloscope with a time base triggered by the pulses themselves. Translating pulse size into effective voltage V_{eff}, i. e. the voltage to be applied to a deionized counter to get the same pulse size, the recovery characteristics of Fig. 9 are obtained. The dots added are calculated for a space-charge sheath with the mobility k and the charge Q determined before, moving from wire to cathode while a constant potential difference V_s is being applied to the electrodes. Here again, the agreement is quite satisfactory. When V_{eff} passes the starting voltage V_s, the deadtime during which the counter is inoperative is completed. The time for any effective voltage to be reached can be shown to be

$$t = r_c r_a \ln \frac{r_c}{r_a} \frac{e^{-V/Q}}{2 k Q} \overline{Ei}\left(\frac{V_{\text{eff}}}{Q} + \ln \frac{r_c}{r_a}\right),$$

where

$$\overline{Ei}(x) = \int_0^x \frac{e^y \, dy}{y} .$$

The deadtime τ_0 can be found by substituting $V_{\text{eff}} = V_s$. In Fig. 10, the theoretical curve is compared with experiment (dots and circles).

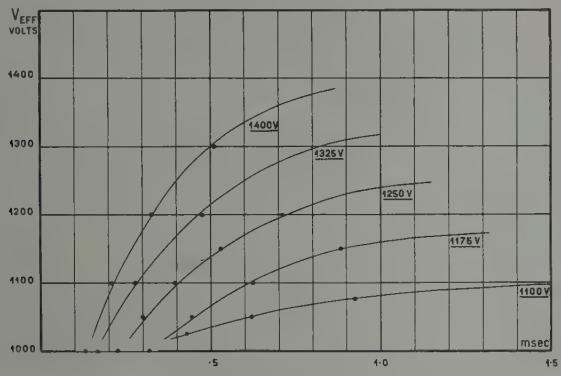

Fig. 9.

Recovery characteristics of the counter described in the caption to fig. 6. Dots are calculated from theory, using the same value for the mobility k.

Corrections for the deadtime.

When n discharges per second are actually produced by the counter, it will be inoperative for the fraction of time $n\tau_0$ so that of the incident counting rate n_0 only the rate $n = (1 - n\tau_0) n_0$ is actually observed, and the counting loss is

$$\frac{n - n_0}{n_0} = \frac{\tau_0}{\tau_0 + 1/n_0} . \qquad (1)$$

This formula will only apply if after all pulses the dead time is τ_0. When, however, pulses occur shortly after a preceding pulse, they are not only smaller than normal according to a recovery characteristic, but also give rise to a smaller than normal deadtime, so that there is a recovery as to deadtime as well. When only the probability for two ion sheaths to be present in a counter has to be taken into account, and the probability of three ion sheaths is negligible, this effect can be accounted for by assuming that for a time $(\psi - 1)\,\tau_0$ after the deadtime has elapsed, new pulses occur but do not produce a new dead period. This factor ψ can be found by calculating the deadtime with two ion sheaths present in the counter, and is of the order of 2. With this correction

$$\frac{n-n_0}{n_0} = \frac{\tau_0}{\psi\,\tau_0 + 1/n_0}\,. \qquad (2)$$

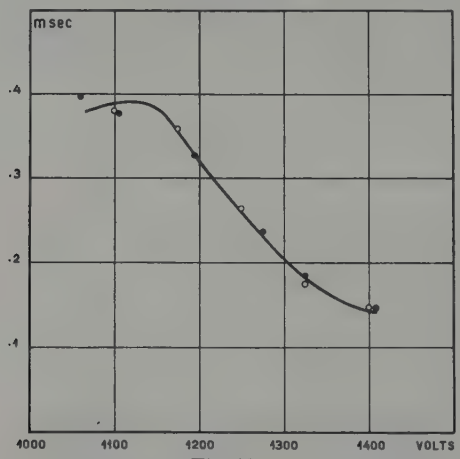

Fig. 10.

Dead times measured (dots and circles) and calculated (curve). Counter data and mobility as in Figg. 6 and 9.

For apparent reasons, this formula gives to low a value for the counting loss at very high counting rates, when reduced pulses are normal rather than exceptional.

From the experimental work of Muelhause and Friedman[16] and of Baldinger and Huber[17]), it is known that with this type of operation, the counting loss becomes nearly constant independent of the counting rate. With a few suitable approximations, this other extreme of a great many ion sheaths present in the counter at the same time becomes very simple, as will be shown in the next section[21]).

Operation at very high counting rates.

The rapid succession of ion sheaths can be approximated by a continuous current I flowing in unit length of counter. When the average effective voltage is V_1, the average field strength at the wire is $2\,CV_1/r_a$, and at any point at radius r reached by the ions after a time t

$$F(r) = \frac{2}{r}\,2\,(CV_1 + It) = \frac{1}{k}\,\frac{dr}{dt}\,.$$

From this, the motion of the ions is found to be

$$r^2 - r_a^2 = 2\,k\,(2\,CV_1\,t + It^2)$$

and the field strength

$$F(r) = \frac{2}{r}\,(C^2\,V_1^2 + (r^2 - r_a^2)\;I/2\,k)^{\frac{1}{2}}.$$

Putting

$$V = \int_{r_a}^{r_c} F\,dr$$

we have

$$V = 2\,(C^2\,V_1^2 + r_c^2\;\mathrm{I}/2\,k)^{\frac{1}{2}} - 2\,CV_1 + V_1$$
$$- 2\,CV_1 \ln\left\{1 + \frac{(C^2V_1^2 + r_c^2\;\mathrm{I}/2\,k)^{\frac{1}{2}} - CV_1}{2\,CV_1}\right\}.$$

For overvoltages not exceeding 200 volts, we may use the approximation $\ln(1 + x) = 2\,x/(x + 2)$, so that we finally obtain the formula

$$\frac{V - V_1}{2\,CV_1} = \frac{r_c^2\;\mathrm{I}/2\,k\,C^2\,V_1^2}{3 + (1 + r_c^2\;\mathrm{I}/2\,k\,C^2\,V_1^2)^{\frac{1}{2}}}\,, \qquad (3)$$

indicating the difference between voltage V and average effective voltage V_1 at which a current I will flow.

The recovery characteristics at very high counting rates.

The recovery characteristic must be known so that the average effective voltage V_1 can be calculated as well as the mean time τ elapsing between two discharges.

Now space-charge sheaths not too near to the wire can be averaged on the basis of a time average to a very good approximation as far as their induction on the wire is concerned.

Taking for instance the induction $i = l/t$, for $1 < t < 2$, caused by a space charge moving between one and two units of time after

it has left the wire, this charge can also be represented by a continuous succession of space charges leaving from $1 - \Delta$ earlier to Δ later:

$$i' = \int_{\Delta-1}^{\Delta} \frac{1}{t+\tau}\, d\tau .$$

Putting

$$\int_1^2 i\, dt = \int_1^2 i'\, dt ,$$

we find $\Delta = 0.56$, and the following set of values

$t = 1$	1.2	1.5	2
$i = 1$	0.833	0.667	0.500
$i' = 1.027$	0.839	0.665	0.495

When an ion sheath leaves the wire, it is preceded by a number of ion sheaths of different charges according to a statistical distribution, and showing different time intervals. As we shall see presently, these quantities are proportional within wide limits, and can be represented by the same average current I.

This approximation does however not hold for the space-charge sheath nearest to the wire, so that we shall treat that sheath separately. We shall suppose this sheath to be preceded by a succession of space charges that will be represented by a continuous ion current I interrupted at the anode a time t_0 before.

Neglecting the small variation of effective voltage about the average value V_1, we have for the current induced by the sheath treated separately

$$i_1 = CQ/(t + r_a^2/4\,k\,CV_1),$$

and for the current induced by the continuous current:

$$i_2 = IC \ln (r_e^2/4\,k\,CV_1\,(t + t_0)).$$

With $Q = I\tau$, the counter will after a time τ be able to produce another pulse of charge Q, or

$$\int_0^{\tau} (i_1 - i_2)\, dt = Q.$$

This integration yields

$$t_0 = 0.5425\ \tau.$$

Putting ΔV_{eff} for the difference of the instantaneous effective vol-

tage and the effective voltage V_{eff} at the time of discharge, we have

$$\int_0^t (i_1 + i_2)\, dt - Q = \Delta V_{\text{eff}}/C$$

so that we obtain on integrating

$$\frac{\Delta V_{\text{eff}}}{Q} = \frac{t}{\tau} + \frac{t}{\tau} \ln \frac{r_c^2}{4\, k\, C V_1 (t+t_0)} - \frac{t_0}{\tau} \ln \frac{t+t_0}{t_0} - \ln \frac{r_c^2}{4\, k\, C_1 V t + r_a^2} \cdot \qquad (4)$$

For $t = 0$, $\Delta V_{\text{eff}}/Q = -1/C$. r_a can be neglected for $t/\tau > 0.1$, and the counter recovery can be described in terms of one variable t/τ and of one parameter $r_c^2/4\, k\, CV_1\, \tau = \vartheta^+/\tau$, where ϑ^+ is the ion transit time at the calculated voltage V_1. For the counter mentioned before, recovery characteristics are collected in Fig. 11.

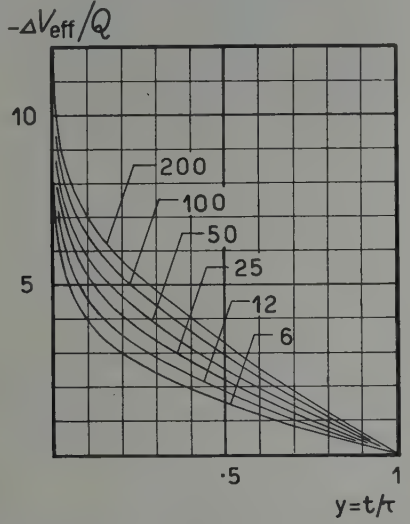

Fig. 11.

Family of calculated recovery characteristics indicating values of $-\Delta V_{\text{eff}}/C$ as a function of t/τ. Values of ϑ^+/τ are indicated on curves. Counter data as for Fig. 6.

For one value of Q, the effective voltage V_{eff} is found from the experimental pulse-size characteristic. The counter overshoots by a factor of $Q/C\ (V_{\text{eff}} - V_s)$, and will not be able to produce another pulse until the initial drop in effective voltage is reduced by a reciprocal factor. The initial drop in $-\Delta V_{\text{eff}}/Q$ being $1/C$, this means that the ordinate in Fig. 11 must have dropped to $(V_{\text{eff}} - V_s)/Q$.

Fig. 12 shows the dependence of $(V_{\text{eff}} - V_s)\ Q$ on Q/C as computed from the pulse-size characteristic included in Fig. 6. Thus, assuming values for Q and $\vartheta^+ \tau$, Fig. 11 gives the fraction of τ after which the counter is operative again, which is apparently the fractional counting loss f. Also, from the surface under the recovery characteristic, the mean effective voltage V_1 is found. After this, the

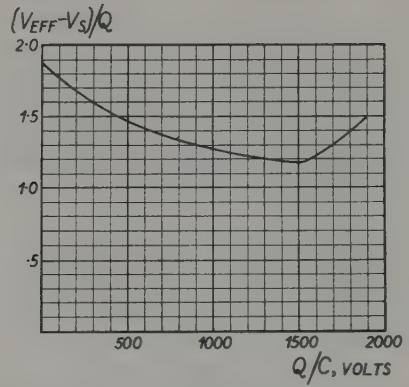

Fig. 12.

Pulse size versus voltage characteristic of fig. 6 rearranged for application of the present theory. For counter data see caption to fig. 6.

expression (3) found for $(V - V_1)\ 2\,CV_1$ can be used to find the voltage V across the counter, as

$$\frac{r^2\,\mathrm{I}}{2\,k\,C^2 V_1^2} = 2\left(\frac{\vartheta^+}{\tau}\right) \cdot \frac{Q}{CV_1} \cdot$$

Finally, the corrected counting rate is found to be

$$n_0 = \frac{4\,k\,CV_1 \cdot (\vartheta^+/\tau)}{r_c^2 \cdot (1-f)} \cdot$$

Results are collected in Fig. 13, and Fig. 14 shows values of R $(V - V_s)\ I$ for four overvoltages and starting voltage. The Nawijn limit $R = \vartheta^+$ for starting voltage and infinite counting rate is also indicated.

Further corrections.

It is seen from Fig. 11 that the recovery after the deadtime is approximately linear. Within wide limits, the current is constant at constant overvoltage independent of counting rate (Fig. 14) as is the counting loss, so that the slope of the recovery characteristic is

constant and equal to $I/(1-f)$. In the preceding section, the loss was calculated after a pulse preceded by an equal pulse started a time τ before, or a continuous current interrupted a time of about $^1/_2\tau$ before, and it was shown that these two cases could be interchanged. Therefore, our approximation is extremely good at counting losses of about $^1/_2$. At higher counting losses, large pulses are preceded

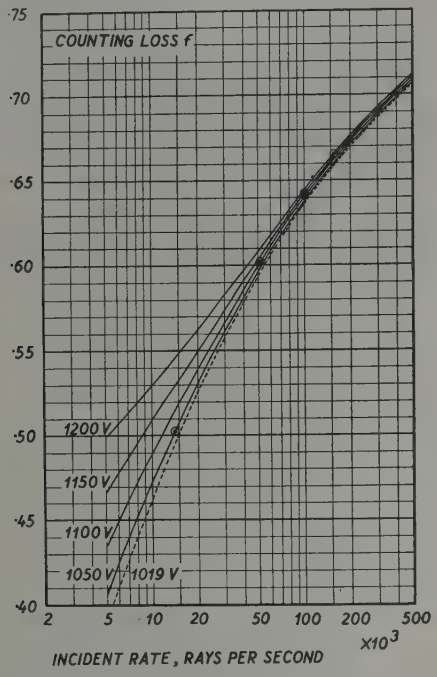

Fig. 13.

Theoretic values for the counting loss at the voltages indicated on left curves. Counter data as described in the caption to Fig. 6. Circles indicate operating conditions giving rise to pulses occurring at a low counting rate at 5 volts overvoltage. Further data are shown in Fig. 15.

more closely by smaller pulses and more remotely by larger ones, so that the average calculation given becomes less representative of the entire range.

The counting rate $n=n_0(1-f)$ is further diminished by two effects.

Firstly, the average effective overvoltage at which the counter discharges becomes very low. Fig. 15 gives the counter voltage necessary at various counting rates so that the average effective over-

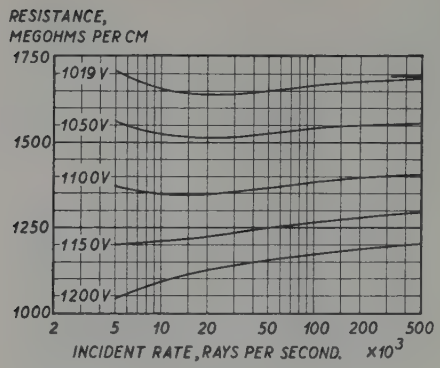

Fig. 14.

Resistance in megohms. cm of the same counter.

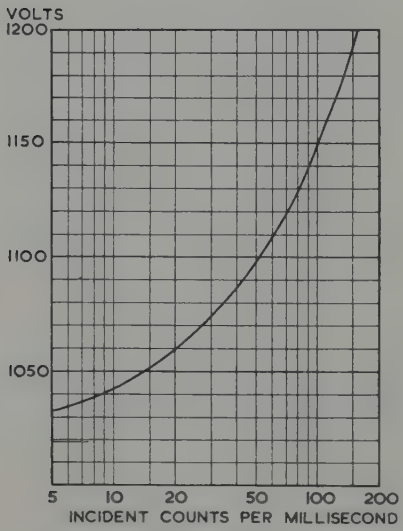

Fig. 15.

Increase of operating voltage necessary for keeping the avarage pulse height equivalent to an overvoltage of 5 volts and low counting rate. Data for other equivalent overvoltages can be derived from Figg. 13 and 14.

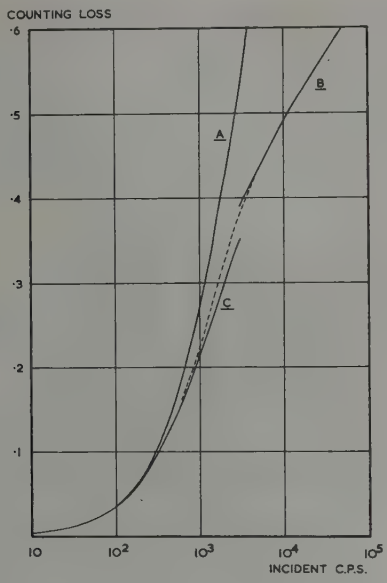

Fig. 16.

Comparison of various correction formulae, as explained in text.

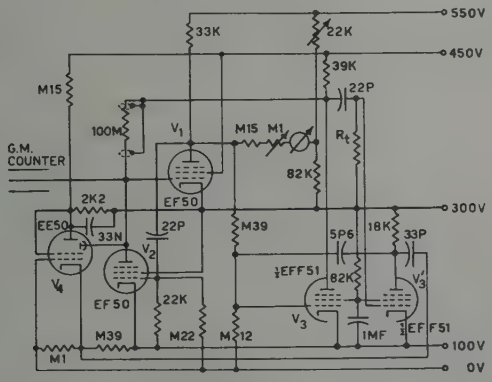

Fig. 17.

Input circuit for dead-time correction indication. The milliameter indicates the fraction of time during which the counter is sensitive to the incident radiation. Satisfactory operation is obtained with any type of counter, either selfquenching or non-selfquenching.

voltage at the time of discharge is 5 volts. Other values may be derived from Figg. 13 and 14. Consequently, part of the counts will be lost because of poor counter efficiency. Assuming that the radiation under observation produces minimum pulses Q_0, below which the efficiency is zero, and above which it becomes unity, the average pulse size will no longer be $I/n_0(1 - f)$, but now become $Q_0 + I/n_0 (1 - f)$, so that the counting rate will be

$$n = \frac{n_0}{n_0 Q_0/I + 1/(1-f)}.$$

Secondly, when the recording circuit records only pulses $> Q'$, the fraction

$$\exp\left(\frac{(1-f)\, n_0}{I}(Q_0 - Q')\right)$$

will be recorded only.

Comparison of correction formulae.

In Fig. 16 the various corrections for deadtime losses at 1100 volts are collected for comparison. Curve A is based on Equ.(1) and gives far to large corrections at intermediate and high counting rates. Curve C is Equ. (2) for $\psi = 2$, and is added as a possible approximation for intermediate counting rates. Curve B has been taken from Fig. 13. For practical purposes, Equ. (2) with $\psi = 1.77$ fits curve A for the lowest rates, and curve B up to 12,000 incident rays per second, and will not be much in error for the intermediate counting rates. It is indicated by the dashed line.

Circuit-controlled insensitive time.

Competing with this way of dealing with high counting rates, three other methods operating at constant counter efficiency and pulse size have been introduced, reducing the deadtime by voltage reversal (DuToit[18]), Hodson[19]), artificially lengthening the deadtime to an accurately known value determined by a number of circuit constants (Cooke-Yarborough, Florida and Davey[20])), or determining the fraction of time during which the counter is made inoperative by the circuit and thus automatically correcting for deadtime losses (Muller and the author[14])[21])).

The latter system is shown in Fig. 17. The correction is read from a miliammeter, and should be averaged during the complete run. This complication is avoided in the modified system of Fig. 18,

where the total sensitive time during the run is measured by counting at the same time coincidences between circuit sensitivity and pulses from a standard pulse generator. This system can also be applied to coincidence counting. In that case, the sensitive period must be determined by counting coincidences of oscillator pulses and sensitive periods of all counting channels.

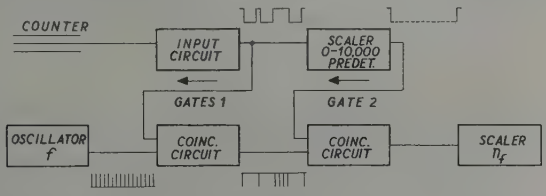

Fig. 18.

Counting system using the input system of Fig. 17, and two scalers counting the counter pulses and the oscillator pulses occurring in the same time intervals, respectively. The counting rate is found by comparing the scaler readings.

Bibliography.

[1]) C. W. Sherwin, Rev. Sci. Inst. **19**, 111 (1948).

[2]) H. den Hartog, F. A. Muller and N. F. Verster, Physica **13**, 251 (1947).

[3]) H. den Hartog, F. A. Muller and C. S. W. van Rooden, Physica **15**, 581 (1949).

[4]) A.G.M. van Gemert, H. den Hartog and F. A. Muller, Physica **9**, 556 (1942).

[5]) P. Huber and F. Alder, Helv. Phys. Acta **18**, 232 (1945).

[6]) P. Huber, F. Alder and E. Baldinger, Helv. Phys. Acta **19**, 204 (1946).

[7]) P. Huber, F. Alder, E. Baldinger and F. Metzger, Helv. Phys. Acta **19**, 207 (1946).

[8]) F. Alder, E. Baldinger, P. Huber and F. Metzger, Helv. Phys. Acta **20**, 73 (1947).

[9]) S. H. Liebson, Phys. Rev. **72**, 602 (1947).

[10]) D. H. Wilkinson, Phys. Rev. **74**, 1417 (1948).

[11]) C. G. and D. D. Montgomery, Phys. Rev. **57**, 1030 (1940).

[12]) H. G. Stever, Phys. Rev. **61**, 38 (1942).

[13]) A.G.M. van Gemert, H. den Hartog and F. A. Muller, Physica **9**, 658 (1942).

[14]) H. den Hartog, Counters with Argon and Alcohol, Thesis, Amsterdam 1948 (in Dutch).

[15]) H. den Hartog and F. A. Muller, Physica **15**, 789 (1949).

[16]) C. O. Muelhause and H. Friedman, Rev. Sci. Instr. **17**, 506 (1946).

[17]) E. Baldinger and P. Huber, Helv. Phys. Acta **20**, 470 (1947).

[18]) S. J. du Toit, Rev. Sci. Instr. **18**, 31 (1947).

[19]) A. L. Hodson, J. Sci. Instr. **25**, 11 (1948).

[20]) E. H. Cooke-Yarborough, C. D. Florida and C. N. Davey, J. Sci. Instr. **26**, 124 (1949).

[21]) H. den Hartog and F. A. Muller, Physica **15**, November 1950.

Experimentelle Untersuchungen über das Verhalten von Zählrohren mit reiner Dampf-Füllung

von **Ewald Fünfer** und **Hugo Neuert.**
(Weil am Rhein.)

Unsere Versuche haben gezeigt, dass ausser den Zählrohren mit reiner Gas-Füllung und den Zählern mit Gas- und Dampf-Füllung auch Zählrohre mit reiner Dampf-Füllung Zähleigenschaften besitzen, die für manche Anwendungen vorteilhaft sind. Aus den Versuchen geht hervor:

1. Die Impulsgrössen bei den reinen Dampfzählern sind für bestimmte Dämpfe im Mittel von der gleichen Grösse wie bei normalen Auslösezählern unter gleichen Bedingungen. Im einzelnen sind die Impulse aber stark verschieden, je nach der Grösse der primären Ionisation.

2. Die Entladung im Zählrohr löscht von selbst ohne Anwendung äusserer Schaltmittel. Infolgedessen konnten die Versuche mit kleinen Ableitwiderständen (z. B. 1 kΩ) durchgeführt werden.

3. Für die obere Grenze der Impulsdauer ergab sich aus oszillographischen Beobachtungen ein Wert von einigen 10^{-7} sec.

4. Eine Dead-Time, wie sie bei normalen Zählrohren auftritt, scheint bei diesen Zählern nicht vorhanden zu sein. Demnach hat man es vermutlich nicht mit einer Entladung mit Ionenschlauchausbreitung, sondern mit lokalisierten Lawinen zu tun.

Nach diesen Ergebnissen handelt es sich hier offensichtlich um Proportionalzähler mit besonders hohem Verstärkungsgrad. Es wird noch gezeigt werden, dass die genannten Resultate speziell für den beschränkten Proportionalbereich gelten. In den hier gefundenen günstigsten Fällen liegt der Verstärkungsfaktor im beschränkten Proportionalbereich ebenso hoch oder höher wie bei normalen Zählrohren im ersten Teil des Auslösebereichs. Die Versuche wurden mit Zählrohren von 20 cm Länge, 2 cm Durchmesser und 0,15 mm Drahtdurchmesser ausgeführt.

Die besten Ergebnisse wurden bei Verwendung von Methylal, d. h. Methylen-Dimethyläther erzielt, das infolge seines hohen Dampfdruckes von 90 mm bei -10^{0} C und mehr als 200 mm bei Zimmertemperatur als Zählrohrfüllung recht geeignet ist.

Zum näheren Studium der Verhältnisse bei solchen Zählern wurde die Abhängigkeit der Impulsgrösse von der Zählrohrspannung über einen möglichst weiten Spannungsbereich gemessen[1]). Die Messungen wurden mit Linearverstärker und Diskriminatorstufe durchgeführt. Die folgenden Figuren zeigen einige charakteristische Messresultate. Dabei wurden die Amplitudenkurven für

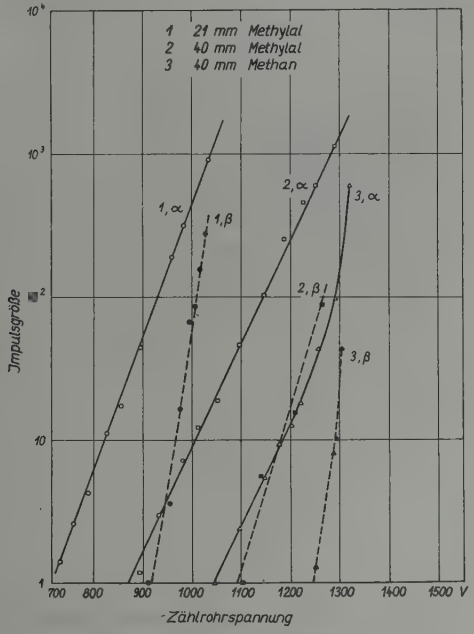

Fig. 1.

α- und β-Strahlen getrennt aufgenommen. Fig. 1 zeigt die Verhältnisse bei Methylal für 2 verschiedene Drucke (21 mm und 40 mm) und für Methan. Wie es für den beschränkten Proportionalbereich zu erwarten ist, erhält man bei logarithmischer Auftragung hier einen flacheren Anstieg für die α- als für die β-Kurven, infolge des grösseren Einflusses der Raumladung bei der stärkeren Primärionisation. Der Einfluss des Druckes besteht, wie zu erwarten, in einem Abflachen der Kurven mit zunehmendem Druck. Ausserdem beginnt die α-Kurve bei hohen Verstärkungsgraden abzubiegen,

[1]) Es handelt sich also um Messungen der Impulsspitzen und nicht der Gesamtladung.

wenn der Dampfdruck erhöht oder der Zählrohrdurchmesser wesentlich vergrössert wird. Das Zusammenlaufen der α- und β-Kurve bezeichnet man üblicherweise als den Beginn des Auslösebereichs. Man sieht, dass im Falle des Methans dieser Punkt mindestens eine Grössenordnung früher als beim Methylal erreicht wird. In Figur 2 werden die Amplitudenkurven von reinem Methylal mit denen der üblichen Argon-Alkohol-Mischung verglichen. Hier sieht man besonders deutlich den Beginn des Auslösebereichs. Es ist ferner eine

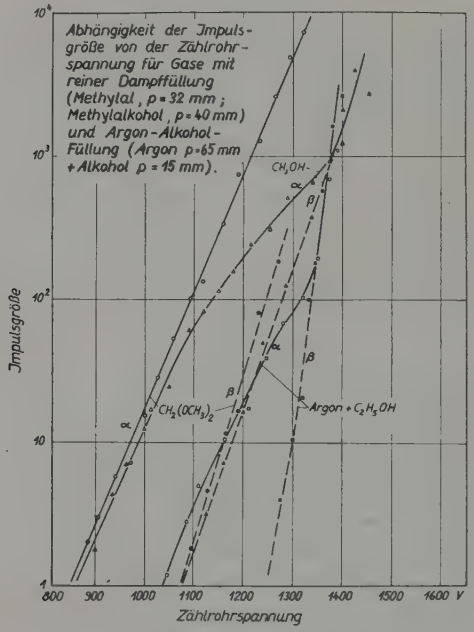

Fig. 2.

Kurve für Methylalkohol aufgetragen. Man erkennt, dass bei den kleinen Amplituden die α- und die β-Kurve fast parallel laufen, man befindet sich hier offenbar gerade noch im eigentlichen Proportionalbereich. Der sich anschliessende beschränkte Proportionalbereich ist hier verhältnismässig klein, verglichen mit dem Fall des Methylals[1]).

[1]) Sämtliche hier wiedergegebenen Amplitudenkurven für α-Strahlen beziehen sich auf radiale Einstrahlung mit grossem Öffnungswinkel. Spätere Messungen haben gezeigt, dass bei axialer Einstrahlung auch bei Methylal ein Abbiegen der α-Kurve auftritt ähnlich wie bei Methylalkohol.

In Fig. 3 wird nun gezeigt, wie sich die Verhältnisse ändern, wenn man dem Methylal Gase wie z. B. Argon zusetzt. Eine Mischung von 20 mm Methylal und 20 mm Argon ergibt einen weiten geraden Anstieg für die α-Kurve, dagegen schliesslich einen rascher als geraden Anstieg für die β-Kurve. Fügt man noch mehr Argon zu (70 mm Argon und 10 mm Methylal), so erhält man einen typischen Auslösezähler. Die Vereinigung der beiden Kurven wird hier

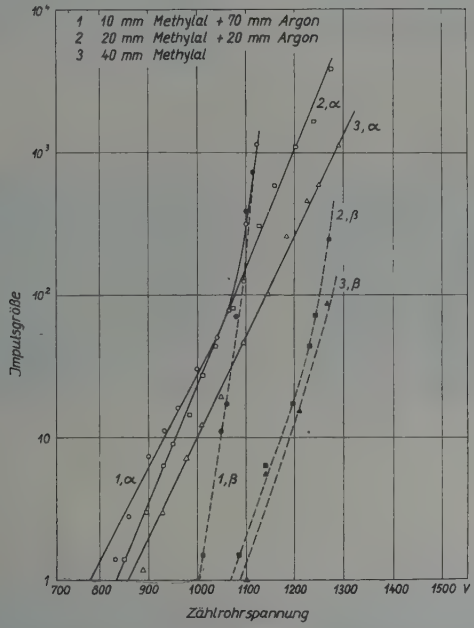

Vergleich zwischen reinem Methylal und Methylal-Argon-Gemischen

Fig. 3.

schon bei verhältnismässig niedrigen Verstärkungsfaktoren erreicht, ähnlich dem Falle des Argon-Alkohol-Zählers. Eine Abschätzung des Verstärkungsfaktors für α-Strahlen bei radialer Einstrahlung bei einigen Gas-Füllungen zeigt die Fig. 4. Man sieht, dass man bei geeigneten Dämpfen Verstärkungsfaktoren grösser als 10^6 im beschränkten Proportionalbereich erhalten kann. Bei Argon-Alkohol-Zählern liegt für eine Verstärkung von 10^5 bereits der Beginn des Auslösebereichs vor, ebenso für Methan.

Ausser den schon genannten Gasen wurde noch Äthylalkohol, Tetrachlorkohlenstoff, Chloroform, Amylacetat und Aceton unter-

sucht. Als Zusatzgase wurden Wasserstoff, Argon und Luft verwendet. Die Ergebnisse zeigen ein recht unterschiedliches Verhalten der verschiedenen Dämpfe.

Eine Zwischenstellung zwischen den reinen Dämpfen und dem normalen Argon-Alkohol-Zähler nimmt als einziges untersuchtes Gas das Methan ein.

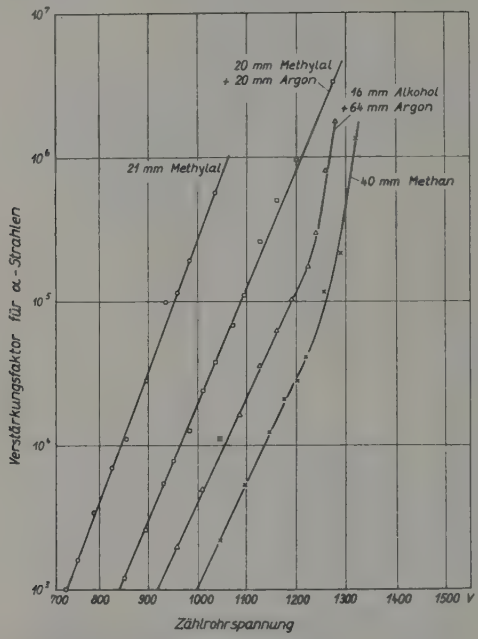

Abhängigkeit des Verstärkungsfaktors für α-Strahlen von der Gasfüllung.

Fig. 4.

Aus dem Kurvenverlauf lassen sich die besonders geeigneten Dampf-Füllungen für α-Zählung bei starkem β-Untergrund oder für β-Zählung allein entnehmen. Man wünscht, dass im ersten Fall die α-Kurve im beschränkten Proportionalbereich möglichst flach verläuft im Vergleich zur β-Kurve. Für den Fall der β-Zählung sollte die β-Kurve möglichst weit gerade und parallel zur α-Kurve verlaufen. Für α-Zähler wird man z. B. Methan oder Methylal, für β-Zähler Methylal oder Methylalkohol verwenden.

Wir wollen uns nun noch einer Betrachtung der Impulsformen zuwenden. Einige Versuche mit Doppelzählern mit gemeinsamem

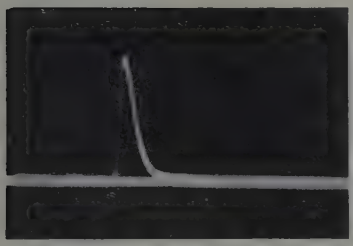

22 mm Methylal

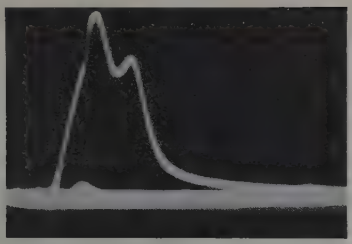

40 mm Methan. Ende

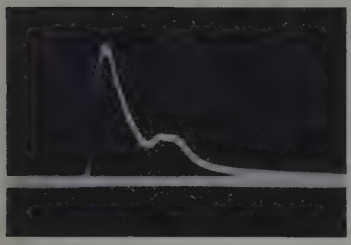

10 mm Methylal + 100 mm H_2. Ende

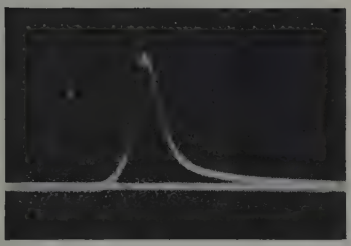

10 mm Methylal + 100 mm H_2. Mitte

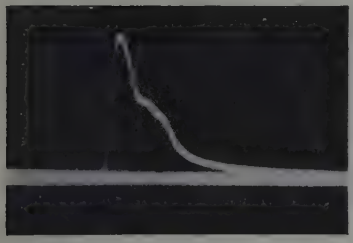

10 mm Methylal + 100 mm H_2 $l = 1/3$

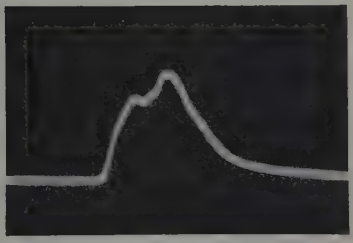

3 mm Methylal + 90 mm H_2 $l = 1/3$

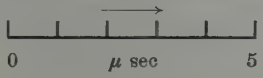

Fig. 5.

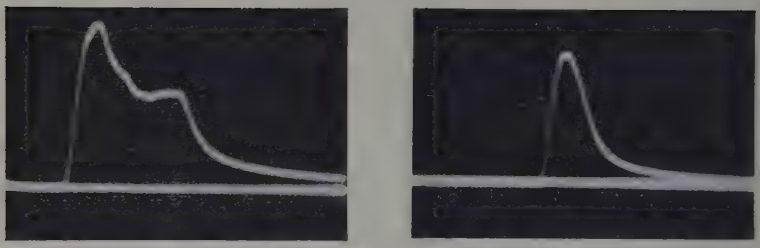

Ende Mitte

15 mm Methylal + 50 mm Argon

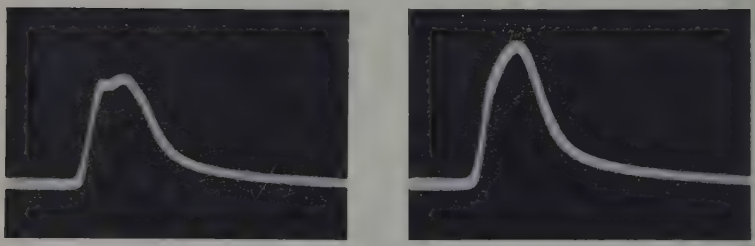

= 1/3 Mitte

10 mm Alkohol + 50 mm Argon

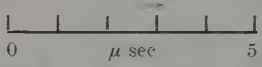

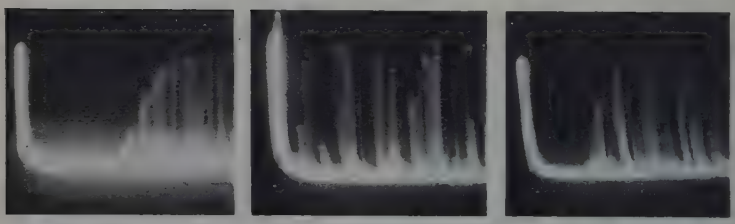

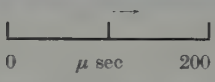

Messung der Dead-time bei

Argon + Alkohol Auslösebereich | Methylal Proportionalbereich | Methylal Auslösebereich

Fig. 6.

Draht ergaben zunächst, dass im Falle des Methylals nur lokalisierte Lawinen auftreten. Koinzidenzen in beiden Zählern, d. h. das Auftreten eines Ionenschlauchs wurde erst bei Spannungen merklich, die erheblich über der Spannung des Zusammentreffens von α- und β-Kurve liegen. Im Falle des Methans wurden Koinzidenzen schon etwas unterhalb des Vereinigungspunktes festgestellt. Dies erklärt auch das Aussehen der Impulse, wie sie mit Breitbandverstärker und Oszillograph aufgenommen wurden. Fig. 5 bringt einige typische Beispiele. Zunächst den reinen Methylal-Impuls, der einen vollkommen glatten Verlauf zeigt und besonders kurz ist. Die Halbwertsdauer liegt unterhalb einiger 10^{-7} sec. Diese Impulsform ist unabhängig vom Einstrahlungsort. Man hat es hier mit einem reinen Lawinenimpuls zu tun, wie man ihn bei Proportionalzählern erwarten muss. Mischt man dem Methylal andere Gase bei, so erhält man Impulsformen, die allen Übergängen bis zum reinen Ionenschlauchzähler entsprechen. So zeigen die folgenden Impulse das allmähliche Auftreten eines 2. Maximums und die Abhängigkeit vom Einstrahlungsort bei Zumischung verschiedener Anteile von Wasserstoff. Charakteristisch sind die Impulse für 10 mm Methylal und für 3 mm Methylal bei Einstrahlung auf $^1/_3$ der Länge des Zählrohrs. Bei 10 mm Methylal tritt sehr deutlich noch der reine, sehr schnell ansteigende Lawinenimpuls hervor, während bei 3 mm Methylal die Ionenschlauchentladung überwiegt. Methan nimmt auch hier eine Zwischenstellung ein.

Ähnliche Verhältnisse treten bei Zumischung von Argon zu Methylal auf. Fig. 6 zeigt die Mischung von 15 mm Methylal und 50 mm Argon. Bei Einstrahlung am Ende ist die Trennung des schnellen Lawinenimpulses und des Ionenschlauchimpulses deutlich sichtbar, bei Einstrahlung in Mitte fallen beide Impulse zusammen. Zum Vergleich sind hier noch einige Impulskurven des normalen Argon-Alkohol-Zählers mit Ionenschlauchentladung wiedergegeben.

Schliesslich seien noch 3 Aufnahmen der Messung der Dead-time gezeigt, die gemäss der Steverschen Anordnung aufgenommen worden sind. Das erste Bild zeigt die typische Ausbildung einer Dead-time für den Argon-Alkohol-Zähler. Die Dead-time beträgt hier grössenordnungsmässig 10^{-4} sec. Das zweite Bild bringt den gleichen Versuch für den Methylalzähler und zeigt, dass eine Dead-time im üblichen Sinne hier nicht vorhanden ist. Bei sehr hohen Spannungen tritt auch beim Methylalzähler eine Dead-time auf, was in Bild 3 zu sehen ist.

Scintillation Counters

O. R. Frisch, Cavendish Laboratory, Cambridge. England.

Zinc sulphide and diamond produce scintillations (light flashes) on bombardment with α-rays; that property was discovered early in this century and for about two decades it remained the only means of detecting individual α-particles. Much of the classical work in radioactivity and nuclear physics was done with its help. Scintillations were counted in those scattering experiments (by GEIGER and MARSDEN) which led to RUTHERFORD's nuclear atom; in RUTHERFORD's discovery that nitrogen nuclei could be disintegrated (transformed) by impact of an alpha particle, and in all the early work on nuclear transformation which followed. It was even used (1932) in COCKCROFT and WALTON's first successful disintegration of lithium nuclei by artificially accelerated protons.

Yet the method had severe short-comings. It was laborious, unreliable, and slow; not much more than twenty scintillations per minute could be counted, or the observer was likely to miss a good many. Conversely at low counting rates the observer was likely to "see" scintillations which were not there.

When electronic valve amplifiers were developed which could detect the small ionisation currents due to single alpha-particles and protons the scintillation method went out of use. Now, after about 20 years, it has come back, owing to the development of a new electronic tool, the photo-multiplier.

An electron multiplier contains, in a high vacuum, a number of "dynodes", suitably shaped electrodes made from a material with high secondary electron emission. An electron falling on one of the dynodes will liberate, say, three secondary electrons which, owing to the shape of the dynodes, will be attracted to the next dynode where each of them will again produce three secondary electrons, and so on. In this way, with ten dynodes, a single electron falling on the first dynode will cause about 10^5 electrons to be ejected from the last dynode, representing a current pulse which can be easily recorded by a moderately sensitive amplifier.

In a photo-multiplier a photo-sensitive cathode (usually a cesium layer on a suitable substratum of Ag or Ag—Sb) is so arranged that the electrons emitted from it are directed towards the first dynode

of an electro-multiplier. Cathodes can be arranged to emit electrons on the same side from which the light falls on them, or on the other side. The latter type is very convenient, because the light source can be placed very close to the photo-cathode, on the outside of the glass envelope, while the first dynode can also be close to the cathode, on the other side. Both these features make for compactness and high efficiency.

Even in the complete absence of light, electrons are emitted from the cathode because of its low work function: this thermal current is the greater in general the more sensitive the cathode. It causes background pulses to appear at the output of the multiplier, which under unfavourable conditions can be numerous enough to completely obscure the scintillation pulses.

To reduce the importance of that thermal background, several methods are available. In the first place, one can cool the multiplier. Cooling with solid carbon dioxide is usually sufficient to reduce the background pulses to a negligible amount. Secondly, if the background is not too large, one can employ two photo-multipliers in coincidence, both looking at the same piece of phosphor: it is very unlikely that two thermal pulses should happen to occur simultaneously and thus simulate a scintillation.

Both these methods entail additional trouble and expense. The best way is to use a good phosphor which produces large scintillation pulses each of which ejects many electrons from the photo-cathode and thereby produces a pulse much larger than the pulses due to thermal emission.

Of phosphors there is now a considerable variety. In addition to zinc sulphide a number of new inorganic scintillating phosphors have been found, such as zinc oxide, fluorite (CaF_2), thallium-activated sodium (or potassium) iodide, Scheelite ($CaWO_4$) and others. In addition, organic crystals containing co-ordinated double bonds have been found suitable, such as solid benzene, naphtalene, anthracene, stilbene, and suitable mixtures thereof: naphtalene containing 0.1% of anthracene is getting very popular. The effect of such small admixtures indicates the need for high purity.

The behaviour of inorganic and organic phosphors differs in several respects. In the first place, it has been stated that alpha particles give bigger pulses in inorganic phosphors than electrons of the same energy, while in organic phosphors the relation is reverse. However, recent measurements have thrown doubt upon this observation.

An important difference exists in the time behaviour, and this is connected with the different mechanism of luminescence. In the

inorganic phosphors a fast particle which passes through the crystal throws electrons out of their positions into the lattice, creating a number of vacancies at the same time; light is emitted when the electrons return to the vacancies. However, as the number of the electrons diminishes so does the number of vacancies, and the remaining electrons find it increasingly difficult to find a vacancy into which to drop. As a result the light emission does not fall off exponentially, but with a gradually increasing time constant, roughly as 1/t. Empirically, the time constants found for various inorganic phosphors are usually greater than a microsecond.

In an organic phosphor the particle which passes through it excites individual molecules on its way, and the light emission is due simply to the de-excitation of those molecules. Hence the emission decays exponentially, and usually with a very short time constant. Decay times down to .02 microsecond have been reported, and it is not clear whether that lower limit is not imposed by the present measuring instruments.

The fact that organic phosphors give such very brief scintillations makes it possible to use them in connection with coincidence circuits of high resolution. In measurements of that kind, it is also a great advantage that scintillation counters have a very high sensitivity for gamma rays. That is due simply to the fact that fairly large blocks of phosphor can be prepared in a sufficiently transparent or translucent form to allow most of the light to escape, while absorbing a substantial fraction of the gamma quanta.

The high sensitivity for gamma rays and the short time constant of scintillation counters make them particularly suitable for the study of correlations between two gamma quanta emitted from a nucleus (or one gamma quantum and one other particle). Let us consider a specimen in which N nuclei decay per second, each decay giving rise to the practically simultaneous emission of two gamma quanta. Two counters may be placed near that source in such a way that their efficiencies are ε_1 and ε_2 respectively (the efficiency here is defined as the probability that any given quantum should be recorded by that counter; it therefore includes the solid angle subtended by the counter). The counting rates recorded by the two counters separately will then be

$$A = N\varepsilon_1, \quad B = N\varepsilon_2$$

while the number of genuine coincidences is $C = N\varepsilon_1\,\varepsilon_2$ (neglecting angular correlation between the two quanta). In addition we have always a certain rate of accidental coincidences when the two coun-

ters are independently triggered within the resolving time τ. The number of these accidental coincidences is $D = 2\,\tau\,N^2\varepsilon_1\varepsilon_2$ and should obviously be kept below the number of genuine coincidences so that it can be easily allowed for. This imposes the condition $2\,\tau\,N < 1$ on the strength of the source, and the rate at which true coincidences can be recorded is thus limited to about $C_{\max} \approx \varepsilon_1\,\varepsilon_2/2\,\tau$.

Scintillation counters have approximately ten times shorter τ, and more than ten times higher gamma sensitivity than GEIGER counters. Hence their use allows one to record gamma coincidences at about a thousand times the rate possible with GEIGER counters. The recent great advance in our knowledge of angular correlation between successive gamma quanta would have been impossible with GEIGER counters.

The high gamma sensitivity of scintillation counters is also an advantage in the measurement of very weak gamma activities; this may have important applications in biology (use of gamma-active tracers). In that connection it should be welcome that the life of a scintillation phosphor and a photo-multiplier is probably nearly unlimited.

Scintillation counters for counting alpha particles and protons do not offer such fundamental advantages. But the arrangement is simpler, more robust, and more long-lived than the traditional ionisation chamber or proportional counter with its attending amplifier. The phosphor must be covered with a very thin metal foil which must be light-tight but need not be air-tight and is not liable to burst when the counter is introduced into a vacuum.

The light from a phosphor can be conveyed to the photo-cell either by lenses or mirrors, or more simply by internal total reflection in a rod of glass or transparent plastic. In this way the phosphor can be inserted into confined places or strong magnetic fields, while the photo-multiplier can be in a more convenient position.

Information on the energies of the particles entering the phosphor can be obtained from studying the intensity of the light flashes. In the case of monokinetic alpha particles falling on single crystals of suitable sulphides, the light flashes were found to be all equal to within a few percent. In the analysis of gamma rays by large crystals of organic phosphors the loss of light in the crystal may be substantial and may vary from point to point; it is not yet known to what extent this source of error can be reduced.

Ultimately the accuracy of energy measurements will be limited by purely statistical factors. The number of light quanta produced

by a particle of given energy is similar to the number of ions produced by the same particle in an ionisation chamber. However, only a fraction of these light quanta can be made to strike the photo-cathode, and of them only a fraction will eject a photo-electron. Hence the relative statistical fluctuation of pulse size is bound to be larger than in an ionisation chamber. The fluctuations will be raised by a further small factor (probably about 2 or less) owing to the statistical features of the electron multiplication process. However, the resulting accuracy may still be good enough to be very valuable in certain nuclear physics experiments.

Current research on the improvement of the method is concerned partly with the development of better multipliers. Unfortunately, the demands for highly efficient photo-cathodes and low thermal emission are somewhat contradictory; yet it might be possible to develop a photo-cathode which is very sensitive in the blue or near ultra-violet, while having sufficiently high work function to make thermal emission negligible. To achieve high resolution in coincidence work the multipliers should have enough stages to produce an output pulse big enough to be fed to a coincidence circuit without further amplification.

More immediate progress is to be expected from the improvement of phosphors both in the direction of brighter pulses and shorter time constants. The development of uniform and transparent crystals will be important for the measurement of particle energies.

References

W. H. Jordan and P. R. Bell. Nucleonics 5, No. 4, 30 (1949) and references therein.
G. Cowper, "Scintillation Counting", Lecture given at Chalk River, June 1949. NRCC LE–22.
Conference on Scintillation and Crystal Counters, Univ. of Rochester, July 22–23, 1948.
Conference on Scintillation Counters, Oak Ridge, June 3–4, 1949.
G. T. Reynolds and F. B. Harrison, Phys. Rev. **76**, 169 (1949).
P. R. Bell and J. M. Cassidy, Phys. Rev. **76**, p. 183.
W. S. Koski and C. O. Thomas, Phys. Rev. **76**, p. 308.
E. C. Farmer, H. B. Moore and C. Goodman, Phys. Rev. **76**, p. 454.
J. Pine and R. Sherr, Phys. Rev. **76**, p. 455.
P. R. Bell, B. H. Ketelle and J. M. Cassidy, Phys. Rev. **76**, p. 574.
L. B. Robinson and J. R. Arnold, Rev. Sci. Inst. **20**, 549 (1949).
J. D. Graves and J. P. Dyson, Rev. Sci. Inst. **20**, 560 (1949).
M. A. Grace, R. A. Allen and H. Halban, Nature **164**, 538 (1949).
E. J. Bowen and P. D. Lawley, Nature **164**, 572 (1949).
O. Huber, F. Humbel, H. Schneider and R. Steffen, Helv. Phys. Acta **22**, 418.
K. P. Meyer, E. Baldinger, B. Hahn and P. Huber, Helv. Phys. Acta **22**, 420.
A. Lallemand, Journ. de Physique **10**, 235 (1949).

The Detection of Alpha Rays by Single Crystals of Thallium Activated Sodium Iodide

by **E. G. Michaelis**, Birkbeck College, University of London.

§ 1. Introduction.

The work described below has been carried out in an attempt to find phosphors for scintillation-counting which respond efficiently to alpha-rays or heavier particles and which are available in large transparent crystals.

Neither the widely used organic materials nor the various activated zinc sulphides fulfill both these conditions. Broser and Kallmann[1]) first pointed out that in the former the light production per unit energy loss in the crystal is much more efficient for electrons than for heavy particles. The zinc sulphides, on the other hand, are almost opaque to their fluorescent radiations[2]), whence the practical light yield falls of very rapidly with grain size. It appears, moreover, that artificially activated zinc sulphides are difficult to obtain in grains larger than a tenth of a millimetre.

Other inorganic materials such as cadmium sulphide, Scheelite, or the activated alkali halides suggest themselves, and a few results obtained with single crystals of thallium activated sodium iodide will here be reported.

Hofstaedter[3])[4]), stated that sodium iodide powder containing one percent thallium iodide appeared to respond to alpha rays with great efficiency, but that its usefulness was limited by the extreme hygroscopicity of the substance. We have attempted to find conditions in which this phosphor yields reliable results and to compare its response with that of silver activated zinc sulphide.

§ 2. Experimental Details.

For the purpose of the investigation single crystals of sodium iodide activated with one percent thallium iodide were used. These were grown by Dr. Ehrenberg and Mr. Franks of this College by a method which they have recently developed[5])[6]). The crystals were cleaved to obtain specimens of one to two millimetres thickness, which were then bombarded with alpha-rays from a polonium source giving about a thousand disintegrations per second.

Source and crystal were enclosed in a tubular holder through which a slow stream of air was passed containing water vapour at the vapour pressure of a saturated solution of sodium iodide in water. This was achieved by allowing air previously dried to pass over such a solution and then filtering it through a bed of sodium iodide powder. By this means condensation of water on the crystal as well as excessive drying-out were avoided. The crystals were attached to a window at one end of the holder; a micrometer screw carrying the source was mounted at the other end.

The silver activated zinc sulfide used for comparison was powder No. 256 manufactured by the Brimsdown Chemical Company, Brimsdown, Middlesex, which was mounted in form of a small screen in place of the sodium iodide scintillator.

The scintillations were recorded by means of a Mazda 27M1 nine-stage photo-multiplier followed by an amplifier giving a gain of 2000 and by discriminating, pulse-shaping and scaling units. The photo-cathode potential of — 1000 volts was provided by a stabilized Power Supply Unit, Type 1007.

In the experiments the crystals were allowed to attain equilibrium with their surroundings, indicated by a constant counting rate for given source distance and discriminator bias. Counts were then taken for various distances of the source from the phosphor and for a series of discriminator-settings in each case. After each count the source was removed, and a background count was taken. The source was then brought to a standard distance and with standard amplifier and discriminator-settings a fixed number of counts were timed to provide a check of the stability of the entire recording system.

§ 3. Results.

Let $N(v)$ represent the counting rate for pulses exceeding v volts after subtraction of the background rate. The variation of $N(v)$ with v for various alpha-ray energies is illustrated by the integral bias curves shown in figures 1 and 2 for sodium iodide and zinc sulphide respectively.

From the results indicated we have calculated the mean size of the output pulse by the formula

$$\bar{v} = \frac{\int_0^\infty N(v)\,dv}{N(o)}$$

where $N(o)$ is the total number of counts of all sizes. We have also

estimated the standard deviation of the mean using the expression

$$\sigma_m = \frac{\sqrt{\left(\frac{\Sigma N(v_i)\,\sigma_0}{N(o)}\right)^2 + \Sigma\sigma_i^2}}{N(o)}\,\Delta V$$

where the $N_1(v_i)$ are the individual integral counting rates, σ_i the standard deviations of $N_1(v_i)$ and ΔV the equal intervals between the values of discriminator bias at which counts were taken.

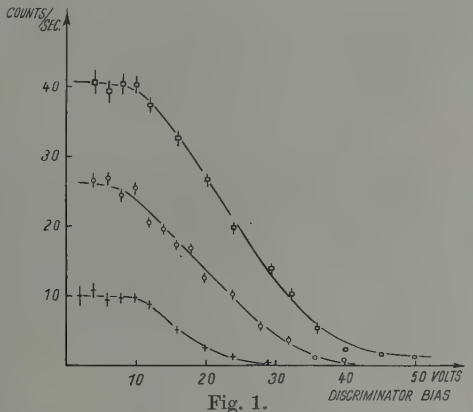

Fig. 1.

Sodium iodide Activator: 1% Tl

□ Source at 0.85 cms ○ Source at 1.35 cms + Source at 1.85 cms

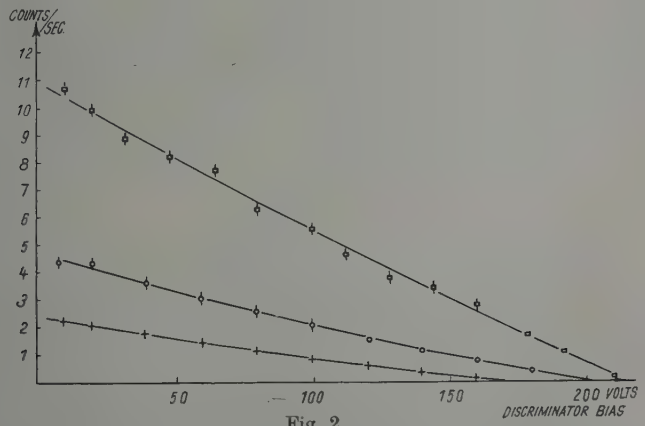

Fig. 2.

Zinc Sulfide Activator: Ag

□ Source at 0.85 cms ○ Source at 1.35 cms + Source at 1.85 cms

The calculated values of $\bar{v}$ and σ_m are shown in table I together with the fraction E/E_0 of the alpha-ray energy $E_0 = 5.4$ MeV absorbed in the phosphor.

Table I.

E/E_0	Mean Pulse Size $\bar{v}$	
	NaI	ZnS
0.575	15.8 ± 0.9	89.1 ± 3.2
0.695	18.8 ± 0.5	105.8 ± 3.5
0.825	23.5 ± 0.6	116.9 ± 1.8

The results are shown graphically in Fig. 3.

§ 4. Discussion.

The pulse size distribution is obtained from $N(v)$ by differentiation. This yields for zinc sulphide the approximately uniform distribution often associated with micro-crystalline phosphors and for sodium iodide an approximately Gaussian distribution characteristic for single crystal scintillators and similar to those found for other materials by Broser and Kallmann[7]), Garlick and Fatehally[8]) and Harding, Flowers and Epstein[9]).

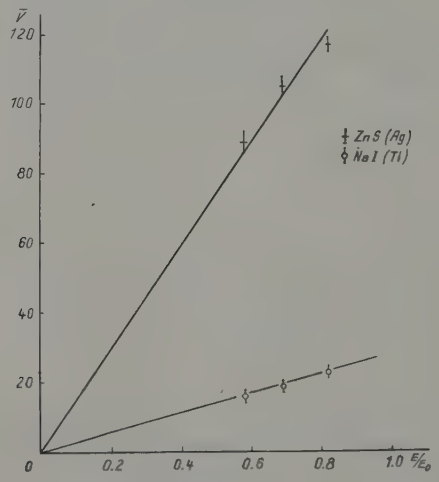

Fig. 3.
Mean Pulse Size as function of alpha-ray energy.

The reasons for the spread in pulse size have been discussed by Hoyt[10]). It is thought major causes of the wide spread in the case

of the sodium iodide scintillators may have been the finite size of the alpha-ray source and certain imperfections in the crystal specimens, resulting in a considerable fluctuation of the number of photons arriving at the photo-cathode.

Fig. 3 indicates that the response is a linear function of the energy for both phosphors.

The values of the mean pulse size $\bar{v}$ for a given alpha-ray energy enable us to compare directly the efficiencies of the two phosphors when used in conjunction with a 27M1 photo-multiplier. Let this efficiency be η_1 for sodium iodide and η_2 for zinc sulphide. Then we have for excitation by alpha-rays

$$\frac{\eta_1}{\eta_2} = 0.19$$

The centre of the band of light emitted by thallium activated sodium iodide is quoted as 4100 A.U. by Milton and Hofstaedter[11]), the corresponding value for silver activated zinc sulphide is, according to Kallmann[12]), 4500 A.U. In view of the variation with wavelength of the sensitivity of the photo-multiplier we arrive at a corrected ratio of 0.23 for the intensities of the recorded light flashes.

Accepting Kallmann's value of 28% for the efficiency of light production by silver activated zinc sulphide under alpha-ray bombardment[12])[13]) we find a figure of about 6% for sodium iodide. This value does not confirm Hofstaedter's estimate[3]), according to which the alpha-ray response of sodium iodide is about the same as that of zinc sulphide. Comparison with the data for other phosphors given by Kallmann[12]) shows nevertheless that the material under investigation is a more efficient phosphor for alpha-ray counting than any of the substances listed except the zinc and cadmium sulphides. It may further be concluded that thallium activated sodium iodide is capable of yielding reproducible results if suitable precautions are taken.

§ 5. Acknowledgements.

The writer's thanks are primarily due to Dr. E. P. George for continued help and encouragement. Valuable assistance was also received from Dr. W. Ehrenberg and Mr. J. Franks of this College and from Dr. H. Meyer of the Brimsdown Chemical Company. Dr. W. Rigby and Dr. R. W. Pittman gave advice on chemical problems, and Mr. M. Wise on statistics.

The work was partly supported by the University of London Central Research Fund.

References.

[1]) Broser and Kallmann, Zeit. f. Naturf., **2**a, 642 (1947).
[2]) Kallmann, Phys. Rev., **75**, 623 (1949).
[3]) Hofstaedter, Phys. Rev., **74**, 100 (1948).
[4]) Hofstaedter, Phys. Rev., **75**, 796 (1949 .
[5]) Ehrenberg and Franks, Crystal Growth (Discussions of the Faraday Society, No. 5), p. 358 (1949).
[6]) Franks, Study of the growth of single alkali halide crystals from the melt, Thesis, London (1949).
[7]) Broser and Kallmann, Nature, **163**, 21 (1949).
[8]) Garlick and Fatehally, Phys. Rev. **75**, 1446 (1949).
[9]) Harding, Flowers and Epstein, Nature, **163**, 990 (1949).
[10]) Hoyt, Rev. Sci. Inst., **20**, 178 (1949).
[11]) Milton and Hofstaedter, Bull. Am. Phys. Soc., 24, No. 1, E. 10 (1949).
[12]) Kallmann, Reserach, **2**, 64 (1949).
[13]) Broser, Kallmann and Martaius, Z. f. Naturf., **4**a, 204 (1949).

Koinzidenz-Anordnung mit einem Auflösungsvermögen bis zu $2 \cdot 10^{-9}$ sec unter Verwendung von Multipliern als Zähler*)

von **K. P. Meyer, E. Baldinger** und **P. Huber**, Basel.

Zweck der Anordnung ist es, die Eigenschaften der Multiplier zu benützen, um das Verfahren der verzögerten Koinzidenzen auf die Messung noch kürzerer Lebensdauern als bisher anwenden zu können.

Als Zähler werden Multiplier mit 16 Vervielfachungsstufen verwendet (gebaut von N. Schaetti, Institut für technische Physik an der E.T.H., Zürich). Bei der vorliegenden, lediglich die Methodik betreffenden Untersuchung, wurde mit γ-Quanten gearbeitet, welche an den aus Goldblech bestehenden Kathoden der Multiplier direkt Photo- bzw. Compton-Elektronen auslösen. Trägt man die Zahl der an der Multiplier-Anode entstehenden Impulse, deren Amplituden einen vorgegebenen Wert (A) überschreiten, als Funktion von A auf, so erhält man ein „Plateau". Innerhalb dieses „Plateaus" ist die gemessene Impulszahl, wie beim Geiger-Müller-Zählrohr, von den Betriebsbedingungen des Multipliers unabhängig und lediglich durch Quellenstärke, Ansprechwahrscheinlichkeit und Geometrie bedingt. Es wird jedes an der Au-Kathode ausgelöste und auf die 1. Vervielfachungselektrode fokussierte Elektron gezählt (der Nulleffekt beträgt ca. 0.5 Impulse/sec). Der Lage des „Plateau"-Endes entspricht eine Ladung von ca. $2 \cdot 10^{-10}$ Coulomb Impuls bzw. eine Vervielfachung von $1{,}2 \cdot 10^{9}$. Kleinere Impulse treten mit messbarer Häufigkeit (ca. 2%) nicht auf. Die beiden letzten Elektroden jedes Multipliers sind separat ausgeführt und über konzentrische Kabel direkt mit den Steuergittern der Koinzidenz-Mischstufe verbunden. Am Eingang zur Mischstufe sind die Kabel mit ihrem Wellenwiderstand (52 Ohm), d. h. reflexionsfrei abgeschlossen.

Die Koinzidenzmischung erfolgt in 2 Trioden (6J4) mit gemeinsamem Kathodenwiderstand. Die Zeitkonstante dieser Stufe beträgt $3 \cdot 10^{-8}$ sec für Koinzidenz- und $5 \cdot 10^{-9}$ sec für Einzel-Impulse. Arbeitet man mit Impulsen, die kürzer als $3 \cdot 10^{-8}$ sec sind, so wird das Amplitudenverhältnis von Koinzidenz- zu Einzelimpulsen am Ausgang der Mischstufe kleiner und strebt dem Grenzwert 2 zu.

*) Eine ausführliche Veröffentlichung erfolgt in den Helv. Phys. Acta. **23**, Heft 1/2, 1950.

Die Ausgangsimpulse müssen daher noch mit einer passend vorgespannten Germanium Diode (1N34) diskriminiert werden, bevor sie über 10^{-6} sec integriert und in üblicher Weise registriert werden (Scale mit 10^{6} sec Auflösungsvermögen und $3{,}3 \cdot 10^{4}$facher Untersetzung). Die Messung des Auflösungsvermögens dieser Anordnung erfolgte mit Test-Impulsen, die durch Entladung eines konzentrischen Kabels erzeugt und durch Zwischenschaltung von Laufzeit-Kabeln gegeneinander verzögert werden. Es ergibt sich, dass Koinzidenzen zweier Impulse von $2 \cdot 10^{-9}$ sec Breite bereits aufgelöst werden, wenn man sie um $1 \cdot 10^{-9}$ sec gegeneinander verzögert.

Um das Auflösungsvermögen in bezug auf koinzidierende Multiplier-Impulse, d. h. im wesentlichen deren mittlere Breite zu messen, wurde wie folgt vorgegangen: Mit den Impulsen eines Multipliers wurden beide Eingänge der Koinzidenzstufe gespiesen. Dann entspricht jedem Impuls eine Koinzidenz. Durch einseitige Einschaltung von Laufzeit-Kabeln lassen sich diese künstlichen Koinzidenzen auflösen. Wie zu erwarten, hängt das Auflösungsvermögen von der Lage des Arbeitspunktes in bezug auf das oben beschriebene Plateau ab. Am Ende des Plateaus entspricht eine Verzögerung von $1 \cdot 10^{-8}$ sec einer Reduktion der Koinzidenzrate auf 50%, und eine Verzögerung von $3{,}5 \cdot 10^{-8}$ sec löst 99,99% aller Koinzidenzen auf. Wählt man den Arbeitspunkt weit ausserhalb des Plateaus, so benützt man nur die Spitzen der grössten Impulse. An einem Arbeitspunkt, in dem z. B. die Ausbeute im Vergleich zum Plateau auf etwa $^{1}{}_{8}$ gesunken ist, löst eine Verzögerung von $2 \cdot 10^{-9}$ sec bereits 50% aller Koinzidenzen auf. Um sicherzustellen, dass die Streuung der mittleren Laufzeit eines Elektronenpaketes im Multiplier keine Rolle spielt, wurde auch eine Messung mit Hilfe von wahren Koinzidenzen und zwei *verschiedenen* Multipliern durchgeführt. Als Quelle diente die Annihilationsstrahlung der Positronen von Zn^{63}. Koinzidenzverluste wurden dabei nicht festgestellt und die oben angegebenen Werte für das Auflösungsvermögen bestätigt.

Für die Anwendungsmöglichkeiten der vorliegenden Anordnung spielt natürlich die Ansprechwahrscheinlichkeit der Zähler eine entscheidende Rolle. Diese ist für γ-Quanten an einer Au-Kathode nur etwa 10^{-3}. Sehr viel günstiger liegen bekanntlich die Verhältnisse bei direkter Einstrahlung von schweren oder β-Teilchen und für alle Partikel bei Anwendung der Scintillationsmethode. Da bei unseren Multipliern nur die Auslösung eines einzigen Photoelektrons erforderlich ist, wird man bei Benützung der Scintillationsmethode eine wesentlich grössere Freiheit in der Auswahl geeigneter Scintillations-Materialien haben als bisher.

Prinzip eines Zweilinsen-β-Spektrographen

von **W. Bothe,** Heidelberg.

Bei den bisherigen Linsenspektrographen wurden meist sehr dicke magnetische Linsen verwendet, um den schädlichen Einfluss der sphärischen Aberration herabzudrücken. Solche Geräte sind ziemlich kostspielig im Bau und Betrieb. Eine andere Lösung des Problems besteht in der Verwendung *zweier dünner* Linsen mit dem in der Figur schematisch dargestellten Strahlengang. L_1 L_2 sind die

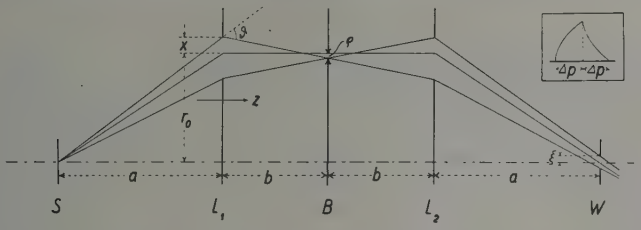

beiden gleichartigen Linsen, welche breite Ringblenden enthalten. In der Mitte dazwischen ist eine enge Ringblende B angebracht. Alle drei Blenden haben denselben mittleren Radius r_0. Die von der Quelle S ausgehenden Elektronen bilden bei B einen Ringfokus und werden in dem Achsenpunkt W (Zählerfenster) wieder zu einem Punktfokus vereinigt. Beide Fokuse sind scharf, und der Strahlengang ist vollkommen symmetrisch, wenn 1. alle Ablenkungen ϑ klein sind, und 2. ϑ linear von dem Einfallsradius $r = r_0 + x$ abhängt, nämlich

$$\vartheta = \frac{r_0}{a} + \frac{x}{f}; \quad \frac{1}{f} = \frac{1}{a} + \frac{1}{b}.$$

Hierdurch ist bei gegebener Form des Magnetfeldes ein bestimmtes Verhältnis a/b festgelegt:

$$\frac{a}{b} = \left(\frac{r}{Q}\frac{dQ}{dr}\right)_{r_0} - 1; \; Q(r) \approx \int_{-\infty}^{\infty} \frac{\partial (A^2)}{\partial r} \, dz,$$

wo A der Betrag des Vektorpotentials des Magnetfeldes ist.

In nächster Näherung sei nun

$$\vartheta = \frac{r_0}{a} + \frac{x}{f} + \gamma x^2.$$

Das quadratische Glied bewirkt, dass der Ringfokus bei B eine endliche Breite ϱ und der Punktfokus bei W einen endlichen Radius ξ bekommt:

$$\varrho = \gamma\, b\, x^2;\ \xi \approx 4\,\gamma^2\, a\, b\, x^3,$$

wo jetzt $2x$ die Breite der Linsenblenden bedeutet. Der Ausdruck für ξ ($\sim \gamma^2 x^3$) besagt, dass der Punktfokus zunächst noch *sehr scharf bleibt*. Der Zähler kann also sehr klein sein, was im Hinblick auf den Nulleffekt sehr günstig ist. Durch ϱ ist die Breite der Zwischenblende B bestimmt, und damit die Auflösung. Die theoretische Auflösekurve ist in der Nebenfigur dargestellt, und zwar wird

$$\frac{\Delta p}{p} \approx \frac{1}{2}\frac{\varrho}{r_0}\frac{a}{b} = \frac{1}{2}\gamma\,\frac{a}{r_0}\,x^2.$$

Die hier gerechnete Näherung wird vielleicht praktisch noch nicht ganz ausreichen, sie lässt aber die wesentlichen Eigenschaften eines solchen Systems erkennen. Die Untersuchung zweier in unserem Institut gebauter Linsen lässt erwarten, dass sich damit eine Auflösung von rund 1% bei ansehnlicher Lichtstärke wird erreichen lassen, das ist um etwa eine Grössenordnung besser als für die Einzellinse. Die grössere Entfernung zwischen Quelle und Zähler ist ein weiterer Vorteil (γ-Störstrahlung von der Quelle!).

In einer mir gerade bekannt gewordenen Notiz von Slätis und Siegbahn[1]) wird ein Spektrometerprinzip mit einem ähnlichen Strahlengang, jedoch mit einer dicken Linse beschrieben. Die Wirkungsweise ist weniger durchsichtig.

[1]) H. Slätis und K. Siegbahn, Phys. Rev. **75**, 1955 (1949).

III.

Experimentelle Ergebnisse der Kernphysik

Magnetic analysis of Disintegration products

by **W. W. Buechner** (M. I. T. Cambridge, Mass.).

An annular magnet, in which use is made of 180-degree focusing, has been employed to study the charged particles from several nuclear reactions. The region of uniform field, in which the particles are deflected, is approximately 70 centimeters in mean diameter and 5 centimeters wide with a spacing of 1.5 centimeters between the pole faces. The magnetic field strength is measured with a sensitive null-type flux meter calibrated in terms of deflection of polonium alpha-particles. The energy of the incident particles is also determined in terms of this standard by measuring their deflection after they have been elastically scattered from various thin targets. Nuclear track plates have been used to detect the analysed particle groups. As the apparatus is normally employed, each plate is exposed at a different magnetic field strength, the incident bombarding voltage being held constant. Thus, each plate covers a certain interval in the energy spectrum of the particles resulting from the reaction, the width of the interval for a particular plate depending upon the field strength at which it was exposed. The high resolution of apparatus when used in conjunction with an electrostatic accelerator makes it particularly suitable for measuring reaction energies and for searching for particle groups that provide information regarding nuclear energy levels[1]).

Thus far, attention has been given mainly to proton groups from reactions produced by deuterons having energies in the range of 1.5 MeV. The energies of the first energy levels in Li^7, Be^{10}, C^{13}, and O^{17}, expected when these nuclei are produced in such reactions, have been found to be 0.483 ± 0.003; 3.375 ± 0.015; 3.098 ± 0.008; and 0.876 ± 0.009 MeV, respectively. A particular search has been made for particle groups that would indicate additional lower energy levels in Be^{10} and C^{13} to see whether any exist that might be correlated with known levels in the mirror nuclei B^{10} and N^{13}. While such correspondence would be expected for equal neutron-neutron and proton-proton forces, no such evidence for additional levels has been found. This lack of correlation between the energy levels of mirror nuclei appears also to be the case for Li^7 and Be^7. Studies of the

various reactions in which Be^7 is produced[2)3)4)] show no indications of an excited state in Be^7 that would correspond to the well-known level in Li^7 at 480 MeV[5)].

The energy levels in N^{13} have been studied by the $C^{12}(p, \gamma)N^{13}$ reaction. A resonance has been found for both gamma-ray emission and for positron activity at a proton energy of 1.697 ± 0.012 MeV, the half-width of the resonance being 74 ± 9 KeV. This indicates that, in addition to the one at 2.383 ± 0.018 MeV[6)], there is an energy level in N^{13} at 3.523 ± 0.019 MeV. These measurements show that, in the range of proton energies from 0.6 to 2.1 MeV, there are no additional resonances with a peak intensity so large as 0.12 that of the one at 1.70 MeV. The existence of these levels has been confirmed by the recent work of Grosskreutz on the energy of the neutron groups from the $C^{12}(d, n)N^{13}$ reaction[7)].

The energies evolved in a number of reactions have been measured. The following values are for the reactions that lead to the formation of the residual nuclei in their ground states, the values being in MeV:

$Li^6(d, p)Li^7$:	5.006 ± 0.014	$Li^7(d, p)Li^8$:	-0.193 ± 0.008
$Be^9(d, \alpha)Li^7$:	7.145 ± 0.024	$Be^9(d, p)Be^{10}$:	4.576 ± 0.012
$C^{12}(d, p)C^{13}$:	2.729 ± 0.009	$O^{16}(d, p)O^{17}$:	1.925 ± 0.008

This work has been assisted by the joint program of the Office of Naval Research and the Atomic Energy Commission.

Bibliography.

[1)] The apparatus is described in more detail in an article to appear in the December 1, 1949 issue of The Physical Review.

[2)] Freier, Lampi and Williams, Phys. Rev. **75**, 901 (1949).

[3)] Burcham and Freeman, Nature **163**, 167 (1949).

[4)] Mandeville, Swann and Snowden, Phys. Rev. **76**, 980 (1949).

[5)] Note added in proof: Recent work has indicated the existence of excited states in Be^7 at 0.205, 0.470, and 0.745 MeV. (W. A. Fowler, private communication; Grosskreutz and Mather, Bul. Amer. Phys. Soc., **24**, November 25, 1949.)

[6)] Fowler and Lauritsen, Phys. Rev. **76**, 314 (1949).

[7)] J. C. Grosskreutz, Phys. Rev. **76**, 482 (1949).

Filter methods in neutronspectroscopy

by **Hl. de Vries**, Groningen, Holland.

In the last ten years several direct methods of neutronspectroscopy have been developed. (Mechanical and electrical velocityselectors, crystalspectrometers.) In some cases, however, the older indirect methods of filtering are still of interest. Indeed, optical spectroscopy with coloured glasses would be impossible, but it should be mentioned that the absorption bands for slow neutrons are relatively much broader than spectral lines of free atoms and this enables a study of resonance levels without "neutron spectroscopes". Some recent measurements will be described of the width and the positions of resonance levels which were made in Groningen*). To explain the essential features of the method used, we confine ourselves first to the measurement of the shape of the resonance level of Ag. By an Ag absorber a "hole" is made in the energyspectrum of a beam of neutrons. After that this beam is reflected by a scattering substance. The energy loss in the elastic collisions is

$$\Delta E = \frac{2E(1-\cos\varphi)}{A}.$$

In this way the hole in the spectrum is shifted to a lower energy and if ΔE is large enough the intensity of resonance neutrons as detected by a silverfoil may be just as large as if no hole had been made in the spectrum; this depends on the value of ΔE relative to the levelwidth. With decreasing ΔE (increasing A) the activity of the Ag detector decreases and from its dependance on ΔE the shape of the resonance level can be determined. It is essential for the method (which will be called the *displacement method*) that the values of ΔE, given above, happened to be of the order of magnitude of the width of the resonance levels, if we confine ourselves to values of E below 100 eV. The same technique was also used in studies of the overlapping of levels. In that case the detecter and the absorber which made the "hole" were different elements.

*) See Physica **8**, 825 (1941); **10**, 281 (1943); **10**, 299 (1943); **10**, 312 (1943); **10**, 381 (1943); **11**, 345 (1943); **11**, 396 (1946); **11**, 481 (1946); Nature **159**, 569 (1947).

It can be said that at present the resolving power of this method is at least as good as the resolving power of velocity selectors.

Some results are summarised in the tables I, II and in Fig. 1.

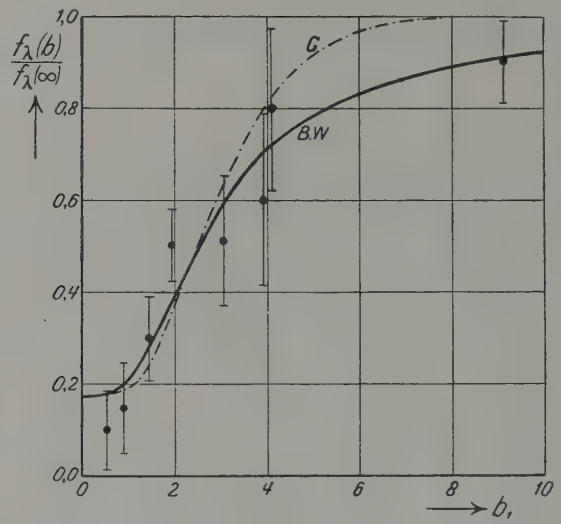

Fig. 1.

Activity of Ag detector as a function of the energy-loss ΔE by the reflecting collision with nuclei of various elements. (b is a parameter proportional to ΔE, containing also Γ. The activity caused by scattered neutrons ($f_\lambda(b)$) is devided by $f_\lambda(\infty)$, the activity which was found when no hole had been made in the spectrum in order to account for the different reflecting powers of the various reflectors. G = curve predicted by a Gaussian form of the resonance level. BW = predicted by the BREIT-WIGNER formula. The value of the level with Γ has already been adjusted to give the best fit.

Table I.

Resonance energies (eV).
Second row: our results (BORON method).
Third row: our results (overlapping).
Fourth row: american reports.

Element	Ag^{108}	Au^{198}	$Ag^{110}_{(a)}$	Sb	$Ag^{110}_{(b)}$	Cd^{117}	Cu^{66}	Cu^{64}	Zn^{69}	Al^{28}
Reson. energy .	23	4.6	5.6		90	110	100	140	500	60
Energy difference		0.31	0.7							
Time of flight .	16	4.8	5.1	5.8						

Table II.

Results of various measurements of the level width Γ.
σ_0 = absorption coefficient for resonance neutrons.
(Time of flight method from american reports.)

Method	Direct experimental result	Results for Ag^{110} (5.1 eV)	Results for Au^{198} (4.8 eV)
1. Displacement method	Γ	0.18	
2. Time of flight . . .	$\sigma_0 \Gamma^2$	0.18	0.15[5]
3. One level formula (BREIT-WIGNER)	$\sigma_0 \Gamma^2$		0.16
4. Activability	$\sigma_0 \Gamma$		0.16[5]
5. Overlapping	$\Gamma, \frac{K_{12}}{K_{11}} \frac{K_{21}}{K_{22}}$	0.18	0.17

Disintegration of nitrogen by fast neutrons

by **C. P. Sikkema** (Groningen).

I. Introduction.

Nuclear energy levels can be studied by measuring the yield of nuclear reactions as a function of the energy of the incident particle. At certain energies maxima may appear. These so-called resonances occur when the incident particle has an energy which, after the particle has been captured by the initial nucleus, leads to a stationary state of the compound nucleus, thus formed. For these experiments particles of homogeneous and variable energy must be available. In the case of charged particles, this offers no difficulty, as they are produced by various types of accelerators. Monochromatic neutrons can only be obtained by a few reactions, the most important of which are

$$^{7}_{3}\mathrm{Li} + {}^{1}_{1}\mathrm{p} \rightarrow {}^{7}_{4}\mathrm{Be} + {}^{1}_{0}\mathrm{n}$$
$$^{2}_{1}\mathrm{D} + {}^{2}_{1}\mathrm{D} \rightarrow {}^{3}_{2}\mathrm{He} + {}^{1}_{0}\mathrm{n}$$

Barschall and Battat[1]) studied the $(n\alpha)$ and (np) reactions in nitrogen, using the first process as a neutron source. The neutron energy was varied between 0.2 and 1.7 MeV, by varying the accelerating potential of the protons above the threshold value of 1.8 MeV. We studied the same reactions, using the D + D neutrons[6]). They can be produced by deuterons of low energy. In this case the large variation of the neutron energy with the angle between the neutron path and the beam of deuterons can be used. With a deuteron energy of 475 keV, neutrons with energies between 2.1 and 3.4 MeV were obtained when the angle is varied between 30° and 132°. This follows from the laws of conservation of energy and momentum, and the value $Q = 3.31$ MeV for the D + D reaction.

Wilhelmy[2]), who first studied resonance effects with fast neutrons, followed a different method. He used a neutron source giving neutrons of continuous energy distribution. The total kinetic energy of the reaction products (α-particle resp. proton plus recoil nucleus) is measured in an ionisation chamber, and the distribution of the pulse heights is determined. In this distribution certain maxima appear. They represent reaction-products which are caused by neu-

trons with resonance energy. These energies can be calculated with the help of the value of the reaction energy. The most recent measurements of this type with nitrogen were carried out by STEBLER and HUBER[3]).

II. Method.

Deuterons were accelerated to a mean energy of 475 keV, and after magnetical separation from other ions, fell on the heavy ice target. The thin D_2O target was made by depositing a volume of

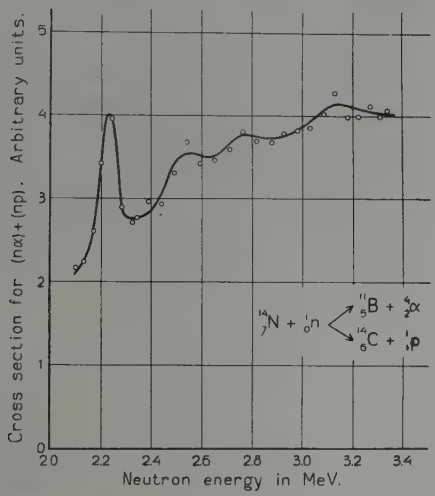

30 cm³ saturated D_2O vapour upon a copper surface, cooled by liquid oxygen. The target thickness was about 45 keV. It was measured by comparing the neutron yield with the thick target yield.

A proportional counter served as a detector for the reactions

$$^{14}_{7}N + ^{1}_{0}n \rightarrow ^{11}_{5}B + ^{4}_{2}\alpha$$

and

$$^{14}_{7}N + ^{1}_{0}n \rightarrow ^{14}_{6}C + ^{1}_{1}p$$

The counter is filled with 2 at. of nitrogen.

The diameter of the wire is 0.05 mm, of the cylinder 6 cm. The operating voltage is about 5000 V. The counter was exposed to neutrons of various energies by placing it in various positions with respect to the target. The intensity of the neutron source is, of course, not constant. Therefore the number of neutrons emitted during the

time of measurement, is determined by a BF_3 proportional counter, which is kept in a fixed position. The number of neutrons getting into the nitrogen counter is then calculated with the aid of the function $1 - A \cos^2 \vartheta$ which gives the angular dependence of the neutron intensity in the centre of gravity co-ordinate system. In our case $A = 1.7$.

III. Result.

The combined cross section for the $(n\alpha)$ and (np) reactions is obtained as a function of neutron energy in the interval between 2.1 and 3.4 MeV. A sharp maximum appears at 2.23 MeV, which indicates a resonance level in the intermediate ${}^{15}_{7}N$ nucleus. The width may be estimated to be 50 -100 keV. In the higher energy region no large variation in cross section is observed. Stebler and Huber[3] from their measurements also concluded, that at 2.20 MeV neutron energy a resonance occurs. The results of Wilhelmy suggested the presence of more pronounced peaks. It is, however, possible that the groups found by Wilhelmy and others[4][5] are caused by neutrons of much higher energy, and therefore cannot be found in our experiment.

Bibliography.

[1] H. H. Barschall and M. E. Battat, Phys. Rev. **70**, 245 (1946).
[2] E. Wilhelmy, Z. Phys. **107**, 769 (1937).
[3] A. Stebler and P. Huber, Helv. Phys. Acta **21**, 59 (1948).
[4] G. Ortner and G. Protiwinsky, Phys. Z. **44**, 116 (1943).
[5] H. I. Zagor and F. A. Valente, Phys. Rev. **67**, 133 (1945).
[6] C. P. Sikkema, Nature **162**, 698 (1948).
A later measurement is presented here.

Measurement of Converted γ-Radiation by the Proportional Counter Technique

D. Maeder and **H. Medicus**, ETH. Zürich.

Corrections for internal conversion with a solid source.

Of late the use of proportional counters has been extended to very high multiplication factors, enabling the determination of unusually low γ- and β-ray energies from pulse amplitude measurements[1)2)]. Whereas for true γ-rays this method always yields the full γ-ray energy, for converted radiation the full energy is observed only in case the source forms part of a counter filling which absorbs practically all the x-ray quanta following the emission of a conversion electron. As there are only relatively few substances available in gaseous form, we will discuss in the following the complications arising from a source deposited on the counter wall. If the counter filling absorbs most of the x-ray quanta involved, then for geometrical reasons the following 4 cases have about the same probability:

case	conversion electron	x-quantum	pulse amplitude corresponds to
1	counted	counted	$< \gamma$ (= transition energy)
2	counted	not counted	$< \gamma - x$
3	not counted	counted	x
4	not counted	not counted	(no pulse)

Owing to the finite source thickness, the pulse amplitudes observed in cases 1 and 2 will be spread over a considerable range. If the Auger-effect is negligible, case 3 produces a sharp peak in the amplitude distribution, regardless of source thickness. The intensity of these lines corresponding to the different shells gives us valuable information about the conversion coefficients.

Application to measurements of Tc^{99*}.

These considerations, when applied to the results of a recent investigation[3)] of the highly converted isomeric transition of Tc^{99},

lead us to a transition energy of 1.8 keV. As neither K- nor L-quanta were found, the conversion must take place either in the M- (additional lines to be expected at 0.5 and 1.3 keV) or in the N-shell (0.06 and 1.7 keV). The experimental evidence for a considerable number of very small pulses indicates that the conversion coefficient α_N exceeds α_M.

In experiments with proportional counters the energy determination depends on the comparison with a calibrating radiation of known energy. We used Fe^{55} for this purpose, produced from Mn by a (p, n)-process [4], which decays by K-capture followed by emission of x-rays from Mn. With the K-quanta the calibration can easily

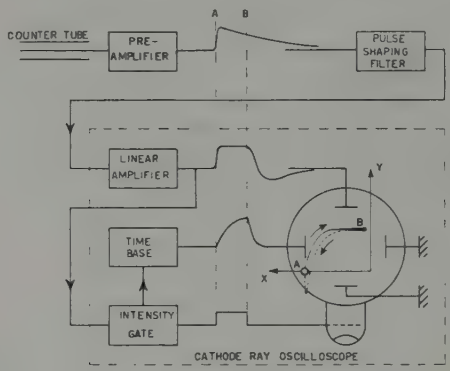

Fig. 1.

Block diagram of a simple pulse spectograph.

be effected from outside the counter through a relatively thick Al window. The long half-life and the nearly complete absence of other radiations make Fe^{55} an excellent calibrating substance.

Photographic pulse analysing system.

In view of the 6 h-period of Tc^{99*}, it was important to have the analysis of the pulse height distribution ready within a rather short time after each run. As there was no elaborate pulse analysing apparatus available, we recorded the pulses by a conventional cathode ray oscilloscope modified in such a way that the exposure of some 10^4 pulses on a single photographic plate produced automatically an amplitude distribution curve, in a manner similar to the one described previously [5] in this journal. As is evident from Fig. 1, any commercial cathode ray oscilloscope, if equipped with a single sweep

time base and a spot suppressor circuit, can easily be converted into a simplified pulse spectrograph by means of a pulse shaping filter which consists mainly of a short-circuited delay line.

This method of producing rectangular pulses calls for a larger bandwidth than theoretically required for the measurement of pulse heights. The corresponding increase of the noise level is however of no consequence for proportional counter measurements and did not even prevent the use of the same apparatus in crystal counter experiments.

The usual linearising tube in the time base circuit is replaced by an ohmic resistance, so that the sweep voltage follows an exponential law. Hence the exposure at a point (x,y) on the plate is inversely proportional to the deflection x along the time axis, and directly proportional to the number of pulses at an energy corresponding to y. This means that on the photographic plate the curves of constant blackening represent the relative numbers of pulses with an essentially linear intensity scale. Since such a curve can easily be produced by a simple photographic printing process, our recording method saves much time in determining the pulse height distribution curve with good statistics, without the need of a complicated multichannel counting arrangement.

Bibliography.

[1]) Curran, Angus and Cockcroft, Phil. Mag. **40**, 36 and 53 (1949).

[2]) Pontecorvo, Recent Developments of the Proportional Counter Technique (this report, p. 97).

[3]) Medicus, Maeder and Schneider, Helv. Phys. Acta **22**, 603 (1949).

[4]) Bradt, Gugelot, Huber, Medicus, Preiswerk, Scherrer and Steffen, Helv. Phys. Acta **19**, 222 (1946).

[5]) Maeder, Helv. Phys. Acta **20**, 139 (1947); Maeder, Huber and Stebler, Helv. Phys. Acta **20**, 230 (1947).

Radioactive X-Ray Emitters

by **M. L. Pool.**

The Ohio State University, Columbus, Ohio.

Some 725 different species of radioactive nuclei[1]) are now available for useful applications or for additional detailed study. Of these some 200 are distinguished by their ability to decay in such a way that the emission of characteristic x-rays result. This decay, leading to x-rays, is accomplished by either a K-electron capture process or by an internal conversion gamma-ray process. A nucleus of atomic number Z when experiencing the former process emits an x-ray characteristic of element Z-1, and when experiencing the latter process emits an x-ray characteristic of element Z. Table I shows a listing of x-ray emitting nuclei. The element of which the x-ray is characteristic is also shown. In addition it is evident that most of the x-ray emitting nuclear species also emit beta-rays and gamma-rays as well. There are only a few species which emit x-rays only and of these only a fraction can be made in great strength in a nuclear reactor (pile) or by a cyclotron.

A^{37}: One of the first recorded x-ray only emitting nuclei was A^{37}. It can be strongly and best produced by a cyclotron bombardment of KCl with deuterons[2]). Both reactions $K(d, \alpha)$ and $Cl(d, 2n)$ contribute to a high specific argon activity. This 34.1-day active gas is very useful in the calibration of proportional counters.

Ge^{71}: An 11.4-day x-ray activity can be obtained by the reactions Ga^{71} $(d, 2n)$, Ge^{70} (d, p) and Ge^{70} (n, γ). The former reaction with a cyclotron yields a high specific activity while the latter reaction with a pile yields a high total activity[3]). The decay is entirely by K-electron capture; no gamma- or beta-radiation is emitted. Since the x-rays are of 1.34 Angstrom wave-length, excellent contrast on x-ray films can be obtained when thin tissues or substances which have a surface density that varies from 0 to 0.15 gm cm^2 are photographed with these "soft" x-rays.

Pd^{103}: A deuteron bombardment of Rh yields a very strong Pd activity of 17-day half-life[4]). X-rays only result in the decay. A Cauchois spectrograph shows that the x-rays are characteristic of Rh. A Rh fraction taken from the 17-day Pd activity decays with a 56-minute half-life. However, only about $^1/_{10}$ of the total Pd acti-

vity is obtained in the Rh fraction. Two internal conversion lines of energies 39.9 and 42.7 KeV are obtained with a magnetic spectrograph. *L*-conversion seems to be absent, which is unusual. The *K*-conversion seems to be complete since no gamma-rays of 63.1 or 65.9 KeV are present. The x-rays, two per disintegration, observed from Pd^{103} thus result from the processes of *K*-electron capture and of internal conversion[5]).

The above data can be interpreted by postulating two excited states of Rh^{103}, one of which has a half-life of 56 minutes and the other of much shorter duration. The *K*-electron capture process leading to the 56-minute level is about $^1/_{10}$ as frequent as capture leading to the short lived level.

Cb: When two species of long lived nuclei are present in the same element, the Cauchois spectrograph[6]) is very useful in clarifying the decay process. Cb^{92} has a half-life of 10.1 days, decays by *K*-electron capture and emits Zr x-rays. Cb^{95} has a half life of 3.75 days, decays by internal conversion and emits Cb x-rays. When these two activities are formed together by bombarding Zr with deuterons the 67.8-day Zr^{95} is readily found to decay into the 3.75-day Cb^{95} which then decays into the 35-day Cb^{95} isomer. A series of x-ray spectrograms supporting the above conclusions is shown in Fig. 1.

Mo^{93}: It may be difficult to discern the presence of x-ray emission when one or more strong gamma-rays accompany the decay. For x-rays, Geiger tubes have a sensitivity which is low compared with that for gamma-rays. Compton- and photo-electrons make simple ionization chamber detection unsatisfactory. The rate at which the x-rays are absorbed by foils can well be about equal to the rate at which Compton- and photo-electrons reach a saturation intensity in the foils. However, when the radioactive sample and also the various absorbing foils are both placed in a strong magnetic field, distinct x-rays, if they are really present, can be readily found with the aid of an ionization chamber.

The above difficulties in the detection of x-rays is exemplified by Mo^{93} which decays with a half-life of 6.7 hours. Under usual ionization measuring technique no x-radiation is found. However, using the magnetic field method, x-rays are easily observed and measured to be those characteristic of Mo. In addition this nucleus emits a 0.30-MeV gamma-ray which is 90% internally converted, a 0.70 MeV gamma-ray which is about 0.5% internally converted, and a 1.7 Mev gamma-ray which is not converted. By means of coincident Geiger counter measurements the three gamma-rays are found to be in tandem. Since the x-rays are characteristic of Mo, a long lived Mo^{93}

ground state must be inferred which is isomeric with the 6.7-hour Mo^{93} excited state[7]).

Mo^{93} is unusual in another respect. It is not possible to produce this 6.75-hour activity by the common (d, p) or (n, γ) reactions. The assignment of the activity to Mo^{93} is not in question, however, since the activity can be produced by the reactions $Zr^{90}(\alpha, n)$, Zr^{91}

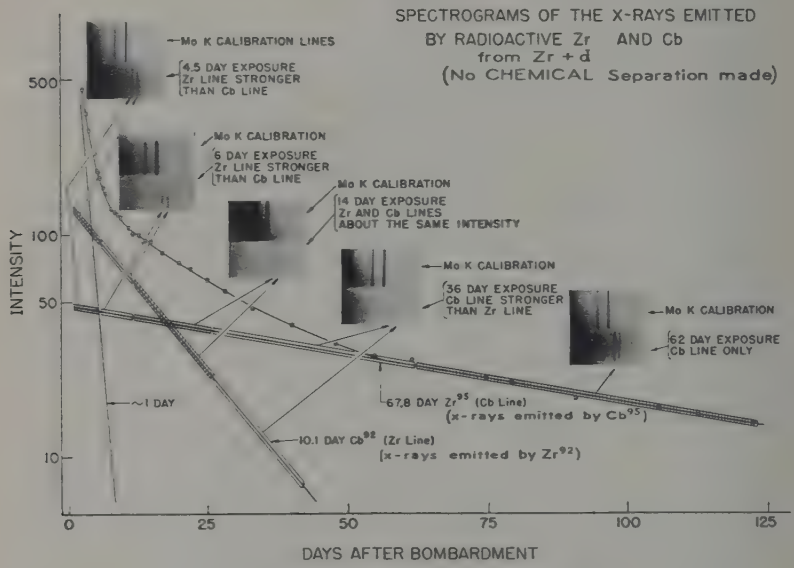

Fig. 1.

Cauchois spectograms taken at various times of a Zr sample subsequent to a bombardment with deuterons. The lengths of exposures are indicated on the resolved decay curve.

$(\alpha, 2n)$, Cb^{94} $(d, 2n)$, Cb^{94} (p, n) and Mo^{94} $(n, 2n)$*). It is to be noted that Mo^{92} is one of the magic number nuclei and probably has a very low neutron capture cross section. Mo^{92} (d, p) Mo^{93} is the only reaction of the (d, p) type that our cyclotron, furnishing 10 MeV deuterons, has failed to produce.

Cd^{107}: This 6.7-hour activity is useful as an x-ray source since it can be so easily produced by the Ag $(d, 2n)$ reation. The few positrons[8], which are present to only 0.3% and of energy of 0.32 Mev. can be removed with an aluminium foil.

*) Enriched isotopes were supplied by the Y-12 plant, Carbide and Carbon Chemicals Corporation through the Isotopes Division, U. S. Atomic Energy Commission, Oak Ridge, Tennessee.

These x-rays are of about the correct wavelength to render good detail in thin flesh and bone structures.

Cs^{131}: In order to see in an x-ray shadow photograph, details in the bone structure itself, a "harder" x-ray is required. Cs^{131} seems to be a very satisfactory source. The half-life is 10.2 days; no gamma- or beta-rays are emitted. The activity can be produced by the reaction Ba^{130} (d, p) or Ba^{130} (n, γ). The latter reaction is recommended since pile neutrons can be used. From the barium the caesium is

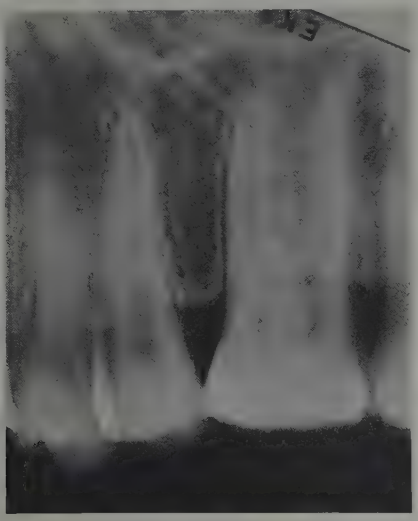

Fig. 2.
Dental picture obtained with a radioactive x-ray source placed in the back portion of the mouth. The view is from the inside outward.

easily extracted in sub-microchemical quantities. A point x-ray source can then be prepared. Since the decay is by K-capture, the x-rays are those of Xe.

Fig. 2 shows a dental picture obtained by putting the x-ray source in the back portion of the mouth. The view is therefore from the inside outward. There is shown in this figure the first and second premolars and first molar, a small portion of the floor of the maxillary sinus, and the contiguous bone structure[9]).

With the new availability of minute but strong monoergic x-ray sources the future surely holds in store many interesting anatomical views and perhaps many important new methods in x-ray therapy.

Table I.

List of radioactive x-ray emitters. μS, S, M, H, D, Y are respectively microseconds, seconds, minutes, hours, days, and years. Class A, B, etc., are same as those used by SEABORG and PERLMAN. Under column marked radiations, the characteristic x-rays emitted are listed together with accompanying beta- and gamma-ray emission, if any.

Element	Half-Life	Class	Radiations
Be 7	43 D	A	X(Li), γ
Cl 36	2×10^6 Y	A	X(S), β
A 37	34.1 D	A	X(Cl)
K 40	1.5×10^9 Y	A	X(A), β, γ
Sc 44	3.92 H	A	X(Ca), β, γ
Sc 44	2.44 D	A	X(Sc), γ
Sc 46	20 S	A	X(Sc), γ
Sc 46	85 D	A	X(Ca), β, γ
V 48	16.0 D	A	X(Ti), β, γ
V 49	1.65 Y	B	X(Ti)
Cr 51	26.5 D	A	X(V), γ
Mn 52	6.5 D	A	X(Cr), β, γ
Mn 54	310 D	A	X(Cr), γ
Fe 55	4 Y	A	X(Mn)
Co 56	72 D	A	X(Fe), β, γ
Co 57	270 D	A	X(Fe), β, γ
Co 58	72 D	A	X(Fe), β, γ
Co 60	10.7 M	A	X(Co), β, γ
Ni 59	5×10^4 Y	B	X(Co), β
Cu 61	3.4 H	B	X(Ni), β, γ
Cu 64	12.8 H	A	X(Ni), β, γ
Zn 62	9.5 H	A	X(Cu)
Zn 63	38.3 M	A	X(Cu), β, γ
Zn 65	250 D	A	X(Cu), β, γ
Zn 69	13.8 H	A	X(Zn), β, γ
Ga 65	15 M	A	X(Zn), γ
Ga 67	3.26 D	A	X(Zn), γ
Ga 70	19.8 M	A	X(Zn), β
Ge 68	250 D	A	X(Ga)
Ge 69	1.65 D	B	X(Ga), β, γ
Ge 71	11.4 D	A	X(Ga)
Ge 72	0.5 μS	A	X(Ge)
As 71	2.08 D	B	X(Ge), β
As 72	1.08 D	A	X(Ge), β, γ
As 73	76 D	A	X(Ge), γ
Se 72	9.5 D	A	X(As)
Se 73	7.1 H	A	X(As), β
Se 75	127 D	A	X(As), γ
Se 77	17.5 S	A	X(Se), γ
Se 81	57 M	B	X(Se), γ
Br 75	1.7 H	A	X(Se), β
Br 77	2.4 D	B	X(Se), β, γ
Br 80	4.54 H	A	X(Br), γ
Kr 77	1.1 H	A	X(Br), β, γ
Kr 79	1.44 D	A	X(Br), β, γ

Element	Half-Life	Class	Radiations
Kr 83	113 M	A	X(Kr)
Sr 85	66 D	A	X(Rb), γ
Sr 85	1.15 H	A	X(Sr), γ
Sr 87	2.75 H	A	X(Sr), γ
Y 87	3.3 D	B	X(Sr)
Y 87	14 H	B	X(Y), γ
Y 88	105 D	A	X(Sr), β, γ
Y 91	50 M	A	X(Y), γ
Zr 89	4.5 M	A	X(Zr), γ
Cb 91	62 D	A	X(Cb), γ
Cb 92	9.8 D	A	X(Zr), β, γ
Cb 93	42 D	F	X(Cb)
Cb 94	6.6 M	B	X(Cb), β, γ
Cb 95	3.75 D	A	X(Cb), β, γ
Mo 93	6.7 H	A	X(Mo), γ
Tc 92	47 M	B	X(Mo), γ
Tc 93	2.75 H	B	X(Mo), β, γ
Tc 94	50 M	B	X(Mo), β. γ
Tc 95	20 H	A	X(Mo), γ
Tc 95	52 D	A	X(Mo), γ
Tc 96	4.2 D	A	X(Mo), γ
Tc 97	91 D	A	X(Tc), γ
Ru 95	1.65 H	A	X(Tc), β, γ
Ru 97	2.8 D	A	X(Tc) γ
Rh 100	19.4 H	B	X(Ru), β, γ
Rh 101	4.3 D	B	X(Ru), γ
Rh 102	210 D	A	X(Ru), β, γ
Rh 103	52 M	A	X(Rh), γ
Rh 104	4.34 M	A	X(Rh), γ
Pd 100	4.0 D	B	X(Rh), γ
Pd 101	9 H	B	X(Rh), β, γ
Pd 103	17 D	A	X(Rh)
Pd 111	26 M	A	X(Rh), β
Ag 105	45 D	D	X(Pd), γ
Ag 106	8.2 D	A	X(Pd), γ
Ag 107	44.3 S	A	X(Ag), γ
Ag 109	39.2 S	A	X(Ag), γ
Ag 110	225 D	A	X(Pd), β, γ
Cd 107	6.7 H	A	X(Ag), β, γ
Cd 109	330 D	A	X(Ag), γ
Cd 111	48.7 M	A	X(Cd), γ
Cd 113	2.3 M	A	X(Cd)
In 109	5.2 H	A	X(Cd), γ
In 111	2.7 D	A	X(Cd), γ
In 112	9 M	B	X(Cd), β, γ
In 112	23 M	B	X(In), γ
In 113	1.74 H	A	X(In), γ
In 114	48.5 D	A	X(In), γ
In 115	4.5 H	A	X(In), γ
Sn 113	105 D	A	X(In), γ
Sb 117	2.8 H	B	X(Sn), γ
Sb 118	5.1 H	B	X(Sn), γ
Sb 119	1.63 D	A	X(Sn), γ

Element	Half-Life		Class	Radiations
Sb 120	6.0	D	A	X(Sn), γ
Sb 122	3.5	M	A	X(Sb), γ
Sb 124	21	M	A	X(Sb), β, γ
Te 118	6.0	D	D	X(Sb)
Te 119	4.5	D	B	X(Sb), γ
Te 121	17	D	A	X(Sb), γ
Te 121	0.05	μS	A	X(Te), γ
Te 121	143	D	A	X(Te), γ
Te 122	30	D	C	X(Te), γ
Te 125	60	D	B	X(Te), γ
Te 127	90	D	A	X(Te), γ
Te 129	35.5	D	A	X(Te), γ
Te 131	1.2	D	A	X(Te), γ
I 125	56	D	B	X(Te)
Xe 127	1.25	M	B	X(Xe), γ
Cs 131	10.2	D	B	X(Xe)
Cs 132	7.1	D	B	X(Xe), γ
Cs 134	3.15	H	A	X(Cs), β, γ
Ba 131	11.7	D	B	X(Cs), γ
Ba 133	20	Y	C	X(Cs), γ
Ba 133	1.67	D	A	X(Ba), γ
Ba 135	1.2	D	D	X(Ba), γ
Ba 137	2.64	M	A	X(Ba), γ
La 135	17.5	H	B	X(Ba), γ
Ce 137	1.5	D	A	X(La), γ
Ce 139	140	D	B	X(La), γ
Eu 152	9.2	H	A	X(Sm), β, γ
Eu 154	20	Y	A	X(Sm), β, γ
Gd 153	155	D	B	X(Eu), β, γ
Tb 152	4.5	H	D	X(Gd)
Tb 153	5.1	D	D	X(Gd)
Tb 154	17.2	H	D	X(Gd), β, γ
Tb 155	1	Y	D	X(Gd)
Dy 165	1.25	M	A	X(Gd)
Ho 161	4.5	H	C	X(Dy), $\beta. \gamma$
Ho 163	7.	D	B	X(Dy)
Tm 166	7.7	H	B	X(Er), β, γ
Tm 167	9	D	B	X(Er), γ
Tm 167	100	D	C	X(Er), γ
Tm 169	1	μS	B	X(Tm)
Yb 169	33	D	B	X(Tm), γ
Lu 170	2.15	D	B	X(Yb), β, γ
Lu 171	9	D	B	X(Yb), β
Lu 176	2.4×10^{10}	Y	A	X(Yb), β, γ
Lu 177	6.8	D	A	X(Yb), β, γ
Hf 177	19	S	C	X(Hf), γ
Ta 176	8	D	B	X(Hf), γ
Ta 177	2.66	D	B	X(Hf), γ
Ta 177	16	D	C	X(Hf), β
Ta 180	8.2	H	A	X(Hf)
Ta 181	20	μS	A	X(Ta), β, γ
Ta 182	16.2	M	B	X(Ta), β, γ
W 178	2.25	H	C	X(Ta), γ

Element	Half-Life	Class	Radiations
W 181	140 D	B	X(Ta), γ
Re 182	2.7 D	B	X(W), β, γ
Re 183	80 D	C	X(W), γ
Re 184	50 D	A	X(W), β, γ
Re 187	0.65 μS	A	X(Re)
Os 185	94.7 D	C	X(Re), γ
Ir 190	10.7 D	B	X(Os), γ
Ir 192	1.42 M	A	X(Ir), γ
Pt 191	3 D	D	X(Ir), γ
Pt 193	4.33 D	B	X(Ir), γ
Pt 195	1.3 H	D	X(Pt), γ
Au 192	4.7 H	D	X(Pt), γ
Au 193	15.8 H	B	X(Pt), γ
Au 194	165 D	D	X(Pt), γ
Au 195	195 D	D	X(Pt), γ
Au 196	14 H	B	X(Pt)
Au 196	5.55 D	B	X(Pt), γ
Au 197	7.4 S	A	X(Au), γ
Hg 197	23 H	A	X(Au), γ
Hg 197	2.66 D	A	X(Au), γ
Hg 198	0.3 μS	F	X(Hg), γ
Hg 199	44.4 M	C	X(Hg), γ
Tl 198	1.8 H	D	X(Hg), γ
Tl 199	7 H	D	X(Hg), γ
Tl 200	1.12 D	B	X(Hg), γ
Tl 202	11.8 D	B	X(Hg), γ
Pb 201	5 H	D	X(Tl), γ
Pb 203	2.16 D	A	X(Tl), β, γ
Pb 204	1.1 H	A	X(Pb), γ
Pb 207	1.6 M	D	X(Pb), γ
Bi 204	12 H	A	X(Pb), γ
Bi 206	6.4 D	A	X(Pb), γ
Po 206	9 D	A	X(Bi), α, γ
At 210	8.3 H	A	X(Po), γ
Ac 223	2.2 M	A	X(Ra), β
Ac 224	2.5 H	A	X(Ra), α
Pa 229	1.5 H	B	X(Th), α
Pa 230	17 D	A	X(Th), β, γ
Pa 234	1.14 M	A	X(Pa), β, γ
U 231	4.2 D	B	X(Pa)
Np 234	4.4 D	A	X(U), γ
Np 235	240 D	A	X(U), α, γ
Pu 234	8 H	A	X(Np), β
Pu 237	40 D	B	X(Np)
Am 239	12 H	B	X(Pu), α, γ
Am 240	2.1 D	B	X(Pu), γ
Cm 241	55 D	E	X(Am)

References.

[1]) J. Mattauch and A. Flammersfeld, Isotopenbericht, Verlag der Zeitschrift für Naturforschung, Tübingen, 1949.

[2]) Paul K. Weimer, J. D. Kurbatov and M. L. Pool, Phys. Rev. **60**, 469 (1941).

[3]) D. A. McCown, L. L. Woodward and M. L. Pool, Phys. Rev. **74**, 1311 (1948).

[4]) David E. Matthews and M. L. Pool, Phys. Rev. **72**, 163 (1947).

[5]) H. F. Gunlock and M. L. Pool, Phys. Rev. **74**, 1264 (1948).

[6]) J. E. Edwards, M. L. Pool and F. C. Blake, Phys. Rev. **67**, 150 (1945).

[7]) D. N. Kundu and M. L. Pool, Phys. Rev. **76**, 183 (1949); D. N. Kundu, John L. Hult and M. L. Pool, Phys. Rev. in press.

[8]) H. Bradt, P. C. Gugelot, O. Huber, H. Medicus, P. Preiswerk and P. Scherrer, Phys. Rev. **68**, 57 (1945).

[9]) Harry D. Spangenberg, Jr. Ohio State Univ. Engr. Experiment Station News, **20**, No. 5, 48 (1948).

Detection of alignment of nuclear spins.

O. J. Poppema, Groningen.

Nuclear magnetism is a subject that interests nuclear physicists as well as low-temperature-physicists. For instance F. Simon discussed the possibility of attaining temperatures as low as 10^{-6} °K by adiabatic demagnetization of nuclear spins. The first step in this process was the alignment of the nuclear spins. A method to do this has been suggested by C. J. Gorter[1]). Here we shall deal with the problem how to detect any alignment of a system of nuclear spins. We shall discuss two different ways which under certain circumstances are suitable to detect the alignment.

A. With the aid of neutron absorption.

The absorption of a neutron by a nucleus depends on the relative spin-orientation of neutron and nucleus. Suppose that a nucleus has a spin J in the groundstate and that there exists a resonance level for slow neutron capture. The compound nucleus corresponding with this level has a spin $J + {}^1/_2$ or $J - {}^1/_2$. In order to explain the principle of the method let us suppose the nuclear spins to be completely aligned and the neutron beam to be completely polarized with spins parallel to the nuclear spins.

Now if the spin of the compound nucleus is $J - {}^1/_2$ no neutrons will be absorbed at all. Of course this is a strongly idealized example. In practice one can only work with a partly polarized neutron beam and a partly polarized absorber.

The most promising way to demonstrate the alignment of the nuclei with the aid of neutronabsorption would be to measure the transmission of a polarized neutron beam through a polarized absorber by a detector which is polarized too. Neutronpolarizations up to 40% have been obtained[2]), but in practice it is impossible to get a high polarized beam of sufficient intensity if a strong neutron source is not available.

However, the system of nuclear spins the alignment of which has to be detected, will act as a polarizer itself. A non-polarized neutron beam is equivalent to two completely polarized beams of half intensity with opposite directions of polarization. These two polarized beams will have different absorption coefficients in the polarized

absorber. The deeper the neutrons penetrate into the absorber the larger the difference between the relative intensities of the polarized beams will be. A more detailed treatment gives that the total transmission is always greater for aligned nuclei than for random orientation.

The properties required for an element which can be used as polarizer-absorber are the following three:

1. The atom must have a paramagnetic moment. This is necessary for the alignment of the nuclei.
2. The nuclear spin must be non-zero.
3. There must be a strong resonance level for slow neutroncapture, preferably not far from thermal energy.

It appears then that Eu en Gd are the only suitable elements. Eu is hard to obtain, especially in a high grade of purity. So we are forced to use a Gd-absorber. This rare earth has a strong resonance level at thermal energy, so that a already small amount of it gives sufficient absorption.

As we have mentioned it is preferable to employ a polarized detector. Then the properties required for the detector element are the same three as for the absorber and moreover capture of slow neutrons should induce β-activity. Only Eu fulfills these four conditions but we have seen already that Eu cannot be obtained. So there is no possibility of using a polarized detector. Then the best element for the detector seems to be Rh.

The experiment has been carried out at the cryogenic Kamerlingh Onnes laboratory at Leiden. A 200 mc Ra – Be source was placed inside the cryostat. This source was surrounded by a 1.9 cm thick layer of paraffin. The absorber (Gadolinium-sulphate, mixed with chromalum) was contained in a vessel of German silver mounted around the paraffin cylinder.

The neutron detector, a Rh-foil, was placed at the outside of the cryostat. The cryostat was mounted between the pole-pieces of a strong electromagnet. The β-activity of the Rh-foil has been measured after five minutes of irradiation with and without cadmium and with and without alignment of the Gd-nuclei.

Two series indeed showed an increase of transmission when the nuclei were supposed to be aligned. A third measurement showed no change in transmission. It should be emphasized however, that there were troubles in maintaining the low temperatures.

B. Another method to detect alignment of nuclear spins is to investigate the distribution in space of the emitted radiation. As J. A. Spiers has pointed out[3]) there will be a certain non-isotropic

angular distribution of the radiation with the magnetic field as an axis of symmetry if the nuclear spins are aligned.

In the same laboratory at Leiden we have tried to demonstrate this phenomenon. A sample of γ-active iron was placed inside the cryostat and the ratio of the intensities of the γ-radiation in the direction of the magnetic field and perpendicular to it has been determined with aligned iron nuclei and with random orientation of the nuclei. The largest effect found was $2 \pm 1\%$. A higher accuracy could not be ontained because of the short time of counting (about 10 minutes) as the low temperature could not be maintained longer.

It should be noticed that these two measurements were of a preliminary character. We will continue these measurements in the near future with an improved arrangement.

Bibliography.

[1]) C. J. Gorter, Physica XIV, 504 (1948).

[2]) D. J. Hughes, J. R. Wallace, R. H. Holtzman, Phys. Rev. **73**, 1277 (1948).

[3]) J. A. Spiers, Nature **161**, 807 (1948).

Pouvoir d'arrêt des émulsions photographiques nucléaires pour les particules chargées d'énergie relativement faible

par **P. Cüer, J. P. Lonchamp, J. Combes** et **S. Gorodetzky**, Strasbourg.

L'objet de cette courte communication est d'attirer l'attention sur quelques points relatifs à la courbe parcours énergie dans le domaine des énergies assez faibles.

La courbe obtenue par Lattes, Fowler, Cüer est généralement utilisée. Elle a été établie avec un grand soin et son application donne des résultats très satisfaisants. Cependant dans le domaine des énergies faibles il est apparu il y a quelque temps déjà que le pouvoir d'arrêt donné par la courbe semblait un peu faible.

Le point d'énergie la plus basse est celui obtenu pour des tritons de 9,3 cm d'air (correspondant à des protons de même vitesse de 3,1 cm d'air), le parcours dans l'air étant obtenu à part du bilan d'énergie admis alors. On obtenait ainsi un pouvoir d'arrêt de 1606. Les tritons étaient obtenus par la réaction:

$$\mathrm{Be}_4^9 + \mathrm{H}_1^2 \longrightarrow \mathrm{H}_1^3 + \mathrm{Be}_4^8. \qquad \text{(I)}$$

Le bilan d'énergie Q admis alors étant de 4,32 MeV. Si l'on prend les valeurs des masses admises actuellement, on obtient pour Q une valeur un peu plus grande, soit 4,53 MeV. Ceci conduit pour le pouvoir d'arrêt à la valeur 1700, paraissant meilleure que la valeur 1606 utilisée précédemment.

Nous avons cherché à obtenir d'une manière précise un point correspondant à une énergie encore plus faible, soit pour des protons de parcours dans l'air de 2 cm.

Nous avons utilisé la réaction

$$\mathrm{Li}_3^6 + \mathrm{n}_0^1 \longrightarrow \mathrm{He}_2^4 + \mathrm{H}_1^3. \qquad \text{(II)}$$

Nous avons admis comme bilan d'énergie $Q = 4.69$ MeV, valeur donnée par Boggild et Minnhagen (Phys. Rev. 1949).

Nous avons utilisé des plaques à grain fin et à seuil de sensibilité élevé. L'énergie des tritons de cette réaction est 2,65 MeV (donnant un parcours dans l'air d'environ 6 cm).

Le parcours mesuré est 35,46 $\mu \pm 0{,}2\ \mu$. Cette mesure a été faite avec un grand soin.

Ceci correspond — à vitesse égale — à des protons de 0,883 MeV et 11,82 μ. Le parcours dans l'air des protons est voisin de 2 cm. Le pouvoir d'arrêt des protons est à cette énergie de 1690. Ceci confirme l'interprétation faite de la réaction (I).

Signalons aussi que nous avons mesuré, mais sans très grande précision cette fois-ci, le parcours des He_2^4 de la réaction (II). On trouve environ 6 μ, soit un pouvoir d'arrêt de l'ordre de 1650, voisin de celui des particules du Samarium, qui ont elles-mêmes un parcours de 6,9 μ. Ceci est une confirmation un peu moins précisée de l'interprétation précédente.

Signalons encore qu'un point de la courbe pour une énergie encore plus basse — en fait le point le plus bas — a été obtenu déjà par Cüer, Morand, etc. C. R. 1949, 228 p. 557.

La réaction utilisée était

$$N_7^{14} + n_0^1 \longrightarrow H_1^1 + C_6^{14}.$$

Les protons ont une énergie de 0,56 MeV (soit environ 1 cm d'air). Le parcours mesuré dans la plaque est 6,13 $\pm$ 0,08 μ.

Utilisation des émulsions photographiques pour l'étude des rayons alpha naturels

par **G. Ambrosino** et **H. Piatier.**

Les expériences décrites dans cette note ont été entreprises afin d'estimer la valeur des émulsions photographiques d'une part au point de vue de la détermination des énergies des particules alpha émises par les radioéléments naturels, d'autre part au point de vue de leur pouvoir de résolution.

Nos expériences ont été effectuées avec des émulsions Ilford des types *C*. 2 et *E*. 1. Les plaques sont plongées dans une solution radioactive diluée pendant toute la durée de l'impression, puis lavées et développées, la durée de l'impression étant grande devant la durée du traitement ultérieur. Les trajectoires sont mesurées au microscope à immersion muni d'un oculaire à vis micrométrique (une division du tambour = 0,1 μ).

La longueur la plus probable d'un groupe de particules alpha monocinétiques est donc mesurée avec une erreur n'excédant pas 0,1 μ, soit, pour le Polonium, avec une précision de l'ordre de 0,5%. L'erreur commise sur la valeur de l'énergie dépend en outre de la précision avec laquelle a été établie la courbe Energie-Parcours pour le type d'émulsion utilisé. L'énergie des particules alpha émises par l'Uranium I et par l'Uranium II est maintenant connue avec une précision de l'ordre de 0,4%[1]; la courbe Energie-Parcours publiée par Lattes, Fowler et Cuer[2]) est, d'après ses auteurs, établie à 2% près, les parcours étant donnés à 0,2 μ près. En fait, dans la région qui s'étend de 4 MeV à 5,5 MeV, l'erreur affectant cette courbe est, d'après nos résultats, inférieure à 1%, comme le montre le tableau suivant:

Radio-élément	Energie en MeV	Parcours en μ d'après Lattes	Parcours en μ dans nos essais	K
U I	4,180 ± 0,015	15,95	17,2 ± 0,1	1,078
U II	4,763 ± 0,015	19,15	20,6 ± 0,1	1,076
Ra F (Po)	5,298 ± 0,002	22,35	24,1 ± 0,1	1,078

K = Parcours moyen dans nos expériences / Parcours moyen d'après la courbe de Lattes, etc.

Nous trouvons que le coefficient de passage, K, est en moyenne égal à 1,077. Cette concordance se répète avec d'autres émulsions et montre que la courbe Energie-Parcours, indiquée par Lattess Fowler et Cuer, n'a pas lieu d'être modifiée dans cette région des énergies.

L'erreur sur l'énergie due à l'incertitude sur la valeur moyenne du parcours est d'environ 15 keV; à cette erreur s'ajoute celle qui provient de l'imprécision avec laquelle sont fixés les points de référence

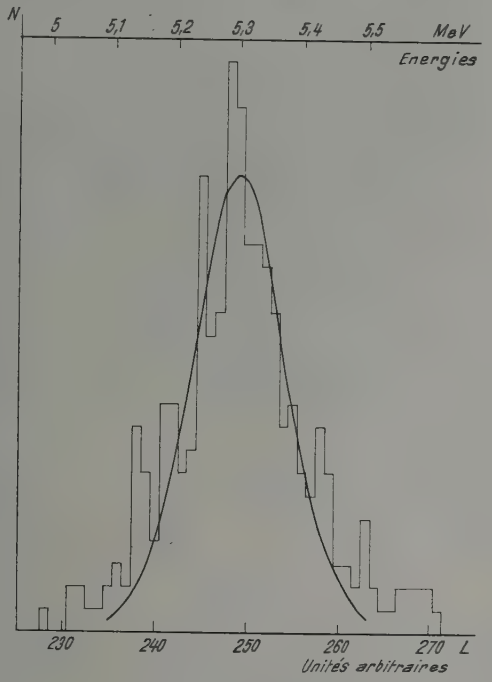

Fig. 1.
Rayons α du Polonium.

de la courbe Energie-Parcours, soit encore environ 15 keV. Les émulsions photographiques permettent donc d'apprécier les énergies des particules alpha, dans la région de 4 MeV à 5,5 MeV, à environ 30 keV près.

La courbe de distribution statistique des traces de particules alpha de même énergie en fonction de leur longueur est, aux fluctuations près, une courbe symétrique. Même en tenant compte de ces fluctuations, il ne semble pas qu'une courbe de Gauss puisse

être superposée à l'ensemble de la courbe expérimentale. Toutefois ce point demanderait à être confirmé par une statistique plus riche, bien qu'il ait été également signalé par Bogaardt et Bottema[3]). Dans tous les cas étudiés, la courbe décroît très rapidement de part et d'autre du maximum, puis s'étale assez largement au niveau de sa base. L'ensemble de la courbe de répartition des longueurs des traces présente un aspect effilé, favorable à la discrimination de deux groupes de particules alpha d'énergies voisines, mais désavantageux lorsqu'il s'agit d'évaluer leur nombre respectif.

Sur la figure représentant l'histogramme des particules alpha du Polonium, nous avons superposé une courbe de Gauss concordant avec la partie supérieure de la courbe expérimentale, ce qui revient à négliger environ 16% du nombre total des trajectoires mesurées, les trajectoires négligées se trouvant réparties à droite et à gauche sur les parties de l'histogramme les plus éloignées de la moyenne. Cette courbe de Gauss correspond à un paramètre relatif de distribution de 2,8%.

En résumé, la courbe expérimentale apparaît comme une courbe de Gauss se détachant d'un fond continu qui s'étend sur 4 μ environ. Dans ces conditions, il est difficile de définir exactement un pouvoir de résolution en énergie, mais en prenant la définition habituelle, à savoir la largeur de l'histogramme à mi-hauteur, on peut estimer que les émulsions photographiques ont un pouvoir de résolution de 150 à 200 keV dans la région d'énergie correspondant aux rayons alpha du Polonium.

La méthode discutée dans cette note est appliquée à l'étude du spectre de rayons alpha de l'Uranium qui fera l'objet d'une prochaine publication.

References.

[1]) Clark, Spencer-Palmer et Woodward, British Atomic Energy Report. BR 522 (1944).

[2]) C.M.G. Lattes, P. H. Fowler et P. Cuer, Proc. Phys. Soc. **59**, 883 (1947). Tsien San-Tsiang, R. Chastel, H. Faraggi et L. Vigneron, C. R. Acad. Sc. **223**, 571 (1946).

[3]) M. Bogaardt et M. Bottema, Physica, XV, 358 (1949).

IV.

Theorie der Atomkerne und ihre experimentellen Grundlagen

High energy scattering of Neutrons and Protons

by **Emilio Segrè**

Radiation Laboratory Department of Physics,
University of California, Berkeley, California.

Summary. A summary of the experiments on neutron-proton scattering at 280, 90 and 40 MeV and of proton-proton scattering at 340 and 32 MeV is presented. The measurements, obtained with various techniques, concern the total cross section and the angular distribution of the scattering.

Attempts to interpret the experiments by a nucleon-nucleon potential are described. These attempts are successfull only to a limited degree. The experimental data are incompatible with the hypothesis of the equality of $n-p$ and $p-p$ interaction.

Some of the most instructive experiments on atomic structure were the famous experiments on the scattering of alpha particles, which showed the existence of the nucleus and the coulomb repulsion between an alpha particle and the nucleus itself. By analogy it might be thought that experiments on n -p, p -p and n -n scattering might give us the clue on the law of force between nucleons, and for this reason they have always been in the minds of the physicists as some of the most interesting to perform. We think now that the scattering of neutrons and protons are more complicated phenomena than it was assumed a few years ago, and the hope that their experimental study will give easily interpretable answers is fading. Nevertheless they still remain as important facts that any future theory will have to explain.

It is also clear that as long as the DeBroglie wave length $\lambda/2\pi$ in the center of mass system

$$\left(\frac{9\times 10^{-13}}{\sqrt{E}},\ E \text{ in MeV in the laboratory system}\right)$$

is large compared to the nuclear dimensions the obtainable information can not reveal details of the short range nuclear forces: only the recent high energy accellerators bring us in the region of interest.

As soon as the new machines of the Radiation Laboratory in Berkeley started to operate, investigation of these scattering problems began and is being actively pursued. This is a report on this work, and more a progress report than a description of finished work.

The experiments concern mainly the measurement of the total scattering cross section σ, and the angular dependence or differential scattering cross section $\sigma(\vartheta)$. The energies and particles used for the experiments are determined by the accelerators available and the whole group of experiments is tabulated in Table 1.

Table 1.

Experiment	Energy (lab syst.) MeV	β (center of mass system)	Particles	Measurement	Technique	Reference
(1)	40	0.14	$n-p$	$\sigma, \sigma(\vartheta)$	Prop. counters	[1]
(2)	90	0.21	$n-p$	$\sigma, \sigma(\vartheta)$	Prop. counters cloud chamber	[1] [2]
(3)	260	0.35	$n-p$	$\sigma, \sigma(\vartheta)$	Prop. counters crystal counters	[3]
(4)	32	0.13	$p-p$	$\sigma, \sigma(\vartheta)$	Prop. counters phot. plate	[4] [5]
(5)	340	0.39	$p-p$	$\sigma, \sigma(\vartheta)$	Prop. counters crystal counters	[6]

References.

[1]) J. Hadley, E. Kelly, C. Leith, E. Segrè, C. Wiegand, H. York, Phys. Rev., **75**, 351 (1949).

[2]) K. Brückner, W. Hartsough, E. Hayward, W. M. Powell, Phys. Rev. **75**, 555 (1949).

[3]) E. Kelly, C. Leith, C. Wiegand, Phys. Rev. **75**, 589 (1949) and private communication.

[4]) B. Cork, L. Johnston, C. Richman, Phys. Rev. **75**, 1465 (1949) and private communication.

[5]) W. K. H. Panofsky and F. Fillmore, Phys. Rev. **75**, 1465 (1949) and private communication.

[6]) O. Chamberlain and C. Wiegand, private communication.

No direct experiment on $n - n$ scattering is contemplated, but it is hoped that a study of $d - p$ scattering and $n - d$ scattering (d deuteron) combined with the data of the direct $n - p$ and $p - p$ experiments may shed some light on the $n - n$ interaction.

The counter technique used in experiments one, two and three is illustrated in Fig. 1. The neutrons produced in the 184-inch cyclotron by stripping deuterons on beryllium or by collision of protons with beryllium, emerge from the thick concrete shielding of the cyclotron which acts also as a collimator. They are scattered by a polyethylene target and the scattered *protons* are detected by a system of counters in coincidence (counter telescope). The main

beam is monitored either by a bismuth fission chamber or by a secondary scatterer. The hydrogen effect is measured as the difference between the effect observed with a polyethylene and a graphite scatterer. With this apparatus one obtains a quantity proportional to $\sigma(\vartheta)$. The proportionality factor is determined by measuring the total cross section of hydrogen in an attenuation experiment and imposing the condition that $\sigma = \int \sigma(\vartheta)\, d\omega$. The absorber A of Fig. 1 limits the smallest energy detected in the telescope and hence since the energy of the protons E_p is approximately $E_n \cos^2 \Phi$, also the energy of the neutrons considered in the experiment.

In experiments one and two the thickness of absorber A is so small that the correction due to nuclear scattering and multiple

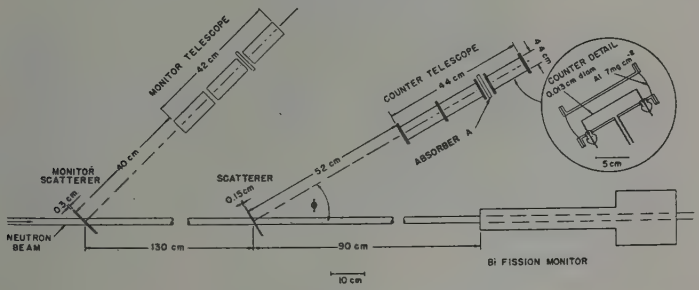

Fig. 1.

Schematic diagram of the scattering apparatus used in experiments (1), (2) and (3).

scattering in the absorber does not constitute a serious problem. At the higher energy of experiment three the thickness of absorber A reaches a maximum of 45 gr/cm^2 wolfram and introduces a large uncertainty in the result because the correction due to it is about a factor of 2 in the most unfavorable circumstances. It might be added that the neutrons used in experiment three are obtained by bombarding beryllium with 340 MeV protons. Their spectrum is much less known theoretically and experimentally than the spectrum of the stripped neutrons used in experiments one and two and the value of 260 MeV is a rather crude approximation for a broad distribution of which the upper limit is about 310 MeV. The total cross section for $n - p$ scattering at 260 MeV has been measured by an attenuation experiment using crystal counters.

The cloud chamber used for experiment three had a diameter of 16 in. It was filled with 110 cm of H_2 and saturated with a water alcohol mixture and was placed in a magnetic field of 14,000 gauss.

The stereoscopic pictures were reprojected and reconstructed in space and from the $H\varrho$ of the scattered protons and the angle of scattering one found the energy of the impinging neutrons. The results are in agreement with the ones of the counter experiment and cover approximately the same angular range.

The counter technique used in experiment four is illustrated in Fig. 2. The beam of the linear accelerator (32 MeV) is carefully collimated and enters a chamber full of hydrogen. The counters of a special annular design are closed by a thin window that lets the protons

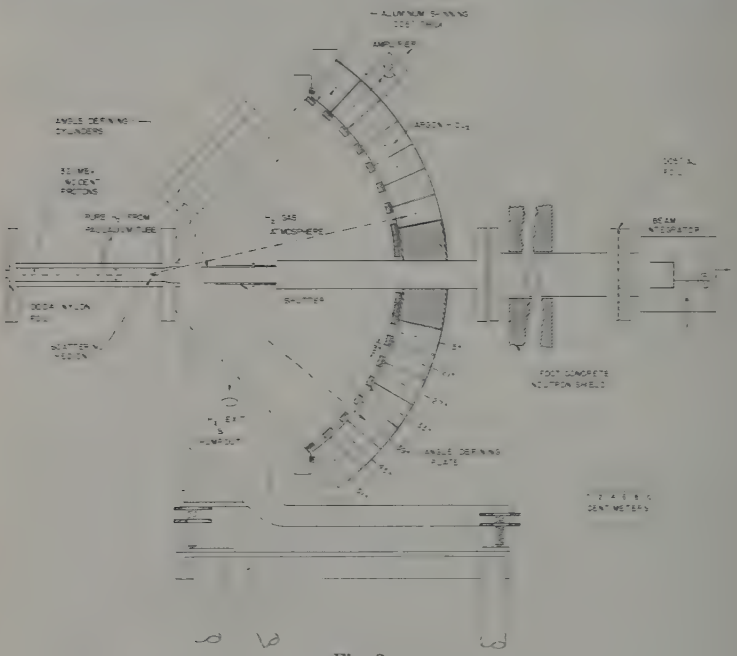

Fig. 2.
Proton—Proton Scattering Chamber
Schematic diagram of apparatus used in experiment (4).

through and absorbers suitable for each angle are used. $\sigma(\vartheta)$ is measured directly and absolutely from the counting rate, the density of the hydrogen in the apparatus, and the current carried by the beam which is integrated and measured in a Faraday cup. The effective volume of the scattering gas is calculated from the geometry and background effects are detected by introducing a shutter around the scattering volume.

In the same energy range $\sigma(\vartheta)$ for $p-p$ scattering has been investigated by the photographic plate technique as shown in Fig. 3. The scattering volume is here a cylinder and the angle of scattering is read from the angle of the proton track in the emulsion and the geometry of the apparatus. A check on the primary energy is given by the fact that from the range of the scattered particle its energy is determined and the scattering angle ϑ is known ($E_p - E_0 \cos^2 \Theta$). The study of the plates gives directly $\sigma(\vartheta)$. The normalization constant is obtained from the density of the gas, the geometry and the charge collected in a Faraday cup and hence the absolute values of $\sigma(\vartheta)$ in the two $p-p$ scattering experiments at 32 MeV are completely independent. The laboratory scattering angles cover the

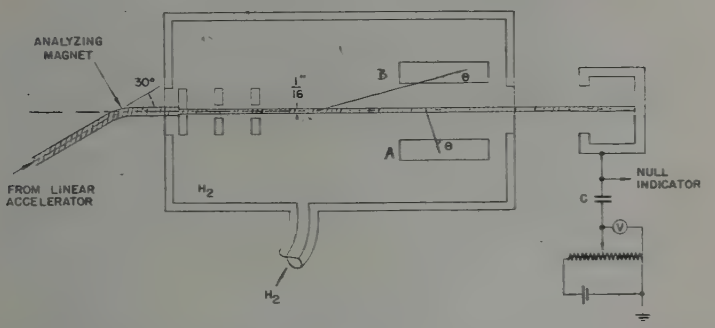

Fig. 3.

Schematic diagram of apparatus used in experiment (4). The planes of the photographic plates A and B are parallel and equidistant from the beam, and do not contain the beam.

range of $10^0 < \Theta < 80^0$ so that all data are duplicated about 45^0, serving as a check on gas purity, background and observer reliability.

The investigation of $p-p$ scattering at 340 MeV has been carried out by two methods. In the first the apparatus used is practically identical to the one of Fig. 1 except that the proton beam was measured with a Faraday cup. The absolute cross section has been determined by plotting the coincidence counting rate of the telescope as a function of the thickness of absorber A and extrapolating to zero thickness, but the procedure is rather inaccurate. Another line of approach is to use 90^0 coincidences between the two protons. In this experiment one telescope of two counters and a single counter at an angle of about 90^0 have been used. Incidentally the angular

resolution of the apparatus is about 2 degrees and the relativity effect ($\beta = 0.39$ in the center of mass system) that makes the angle between the 2 protons different from 90° is very well visible. The measurements obtained at 340 MeV up to now cover a limited range of angles and will be extended with a different technique using very fast distributed amplifiers and crystals counters.

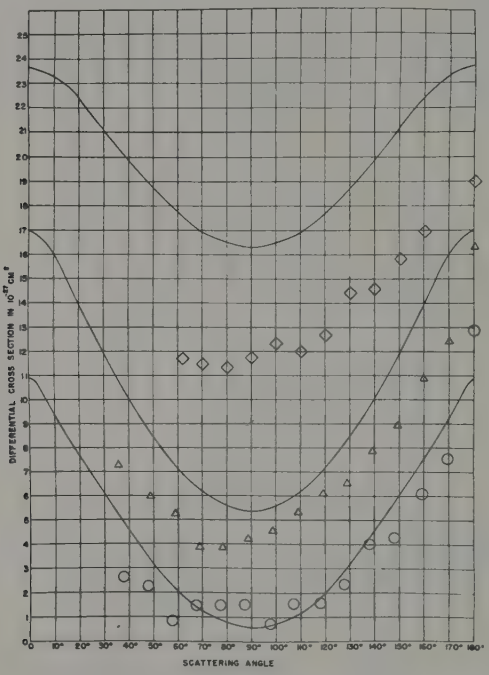

Fig. 4.

Differential neutron-proton scattering cross section in the center of mass system. Squares 40 MeV (lab. system), triangles 90 MeV, circles 260 MeV. In the same figure we have plotted a scattering curve calculated with a Yukawa potential and $R = 1.35 \cdot 10^{-13}$ as indicated in the text. The normalization of the experimental curves depends on measurements of the total cross section and errors of 20% are possible.

The results obtained in experiments one, two and three are summarized in Fig. 4. It must be remembered that there might still be considerable systematic errors in the curve at 260 MeV and the data reported for it are to be considered as provisional.

The results obtained in experiments four are summarized in Fig. 5.

The results on $p - p$ scattering at 340 MeV (experiment five) are given by the following values of $\sigma(\vartheta)$ (cm^2 per steradian in the cm system)*)

$\vartheta =$	41^0	43^0	49^0	60^0	62^0	85^0	90^0
$\sigma(\vartheta) \times 10^{27}$	5.5 ± 0.9	5.2 ± 1.1	5.1 ± 1.1	6.0 ± 0.9	5.3 ± 0.7	6.5 ± 0.9	5.1 ± 0.6

where ϑ is the scattering angle in the center of mass system.

The theoretical interpretation of these experiments is due to the theoretical group of the Radiation Laboratory, directed by Profes-

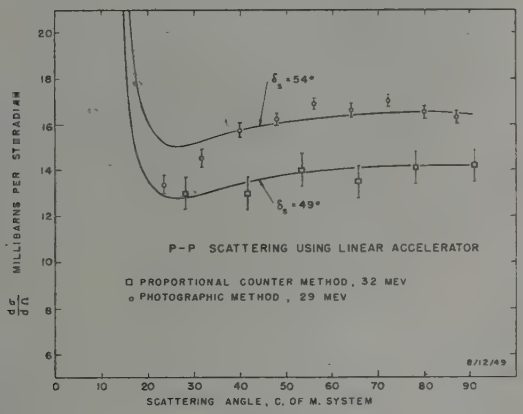

Fig. 5.

Differential proton-proton scattering cross section at 32 and 29 MeV. The theoretical curves are drawn considering the s-wave alone.

sor R. Serber. Prof. Chew, Mr. Hart, Mr. Christian and Mr. Noyes have been especially concerned with this work.

A phenomenological approach has been used throughout because it does not seem profitable at the present to try to deduce a potential from meson theory. Rather the attempt was made to fit all data known on the $n - p$ system into a consistent scheme and, if possible, find a potential which when introduced in the Schroedinger equation would fit the data. We shall see in the following to what extent this program has been successful.

We consider first the $n - p$ system. A particularly simple interaction potential was chosen, whereby all the forces had the same

*) This definition is normalized in the same way as in Mott and Massey. Theory of atomic Collisions, London (1933), page 73 and is valid also for Fig. 5.

radial dependence. The spin dependent interaction potential was written in the form

$$V(r,\sigma) = {}^1/_2\,(1+P_x)\,(\alpha+\beta\,\sigma_1\cdot\sigma_2+\gamma\,S_{12})\,J(r/R),$$

where P_x is an exchange operator acting on the coordinates alone, S_{12} is the tensor operator $3\,\frac{(\sigma_1\cdot r)\,(\sigma_2\cdot r)}{r^2} - \sigma_1\cdot\sigma_2$, and $J(r/R)$ gives the radial form of the potential. The depths α, β and γ as well as the range R are determined by means of the following low energy data: (1) binding energy of the deuteron, (2) singlet scattering length, (3) triplet scattering length and (4) the quadrupole moment of the deuteron. (The magnetic dipole moment was not fitted although the models considered do give reasonable values.)

The ${}^1/_2\,(1+P_x)$ factor was chosen to suppress all the waves of odd angular momentum and make $\sigma(\vartheta)$ symmetrical around 90^0. Although there is no theoretical foundation for this particular form, it has been adopted because (1) the asymmetry around 90^0 in the region thus far explored is relatively small and (2) this gives a minimum total cross section. With the more general exchange interaction $(1-a+a\,P_x)$ it was found that the limits on a are between 0.5 and 0.6.

Calculations were then made using various forms for the radial dependence $J(r/R)$. It was found that a potential with a long-tail was necessary to fit the 40 and 90 MeV scattering simultaneously. The most successful models have been the Yukawa, $[\exp(-r\,R)]/(r/R)$, and the exponential, $\exp(-r/R)$, with $R = 1.35\cdot10^{-13}$ cm and $R = 0.75\cdot10^{-13}$ cm, respectively. The fit of the angular distribution as predicted by the Yukawa well is fair, however the total cross section is 20 -30% too high. This latter defect can be removed by using the exponential well at the expense of a poorer fit to the angular distribution.

The general degree of agreement of these calculations with the experiments is shown in Fig. 4, where the predicted results for the Yukawa well at 40, 90 and 260 MeV are compared with the experimental data.

A detailed discussion of how the various parameters affect $\sigma(\vartheta)$ is found in a paper by R. Christian and E. W. Hart, to be published soon. It has been our privilege to have their manuscript available.

Considering next the $p-p$ scattering data we find that only the range and depth of the singlet interaction has been determined from the low energy scattering. The singlet $n-p$ potential can be chosen with the same range and depth (within 1%). This fact has formed

the experimental basis of the often assumed "charge independence of nuclear forces".

The 32 MeV $p - p$ experimental data is compatible with an s-wave interaction alone (having a phase shift slightly larger than that predicted by a Yukawa well, adjusted to fit the low energy data). However when a potential model is used a d-wave is automatically predicted that is incompatible with the experimental data. This argument speaks strongly against the "charge independence" hypothesis. The potential model can be made to give agreement by postulating a tensor interaction in the odd (triplet) states which just masks the d-wave effect.

The 340 MeV $p - p$ data shows an anomalously high and flat cross section, which can not be explained by means of s-wave scattering alone, since the cross-section is approximately twice $4\pi\lambda^2$. Again a tensor interaction may be invoked to obtain agreement when using the potential model.

In all the above calculation relativistic effects have been neglected. Our present ignorance of the whole subject precludes even a valid guess, other than that the corrections are proportional to β^2, and hence at the higher energies may not be inappreciable. It is believed, considering the agreement obtained in the $n - p$ system, that at least in this case, they are not of major importance.

Finally it should be mentioned that the near symmetry of the 90 MeV scattering has shown that the repulsive forces are small between unlike particles. This, coupled with the lack of any repulsive forces in the 32 MeV $p - p$ scattering, is one of the most striking features of the data, since models based on these experiments will not lead to nuclear saturation.

Die Photospaltung des Deutons mit der Lithium-Gammastrahlung

von **H. Wäffler** und **S. Younis** (Eidg. Techn. Hochschule, Zürich).

Eine experimentelle Untersuchung des Kernphotoeffektes am Deuton gestattet grundsätzlich, zwischen den verschiedenen Kraftansätzen der Mesontheorie zu entscheiden. Die Theorie dieses Kernprozesses erlaubt nämlich eine exakte Berechnung des Wirkungsquerschnittes σ und der Winkelverteilung $J(\Theta)$ der emittierten Photoprotonen (bzw. Photoneutronen). Beide Grössen hängen von dem der Rechnung zugrundegelegten Ansatz ab. Vor allem im Gebiet hoher Quantenenergien ($h\nu \gg 2{,}2$ MeV) sind Messungen von Nutzen, weil dort die verschiedenen Kraftansätze zum Teil stark voneinander abweichende Resultate ergeben.

Die im Prozess Li^7 (p, γ) Be^8 emittierte Gammastrahlung besteht aus zwei Linien mit den Quantenenergien $h\nu = 17{,}6$ bzw. $h\nu = 14{,}8$ MeV. Ihr Intensitätsverhältnis: J(17,6) J(14,8) beträgt sowohl in Richtung des einfallenden Protonenstrahls[1]), als auch senkrecht dazu[2]) etwa 2/1. Mit diesen Gammastrahlen wurden Kernphotoplatten (Ilford C_2, Kodak NT2a, Schichtdicke 200 μ), welche in die Emulsion eingelagertes Deuterium enthielten, in streifender Inzidenz bestrahlt. Die Einlagerung des Deuteriums in die Platten erfolgte durch Tränken in schwerem Wasser (D_2O). Mit jeder D_2O-Platte wurde gleichzeitig eine in gewöhnlichem Wasser getränkte Platte mitbestrahlt. Auf je 21 cm² Plattenfläche entfielen in den H_2O-Platten rund 600, in den D_2O-Platten 1200 Protonenspuren mit Energien zwischen 5,6 und 8,8 MeV. Die Energieverteilung der 600 Protonen, welche man als Überschuss erhält, zeigt zwei ausgeprägte Maxima bei 6,3 bzw. 7,7 MeV, entsprechend den beiden Linien der Lithiumgammastrahlung. Die Winkelverteilung dieser Photoprotonen stimmt gut mit der theoretischen Formel

$$J(\Theta) = A + \sin^2 \Theta \qquad (1)$$

(Θ = Winkel zwischen Gammastrahl und Photoproton im Schwerpunktsystem) überein (s. Fig. 1). Für die exakte Bestimmung der

[1]) R. L. Walker und B. D. McDaniel, Phys. Rev. **74**, 315 (1948).

[2]) Nach eigenen noch unveröffentlichten Messungen.

Konstanten A verwendet man zweckmässigerweise nur Spuren, welche (im Schwerpunktsystem) innerhalb eines Rotationskegels um die 0°- bzw. 90°-Richtung liegen. Man kann zeigen, dass unter Zugrundelegung der Winkelverteilung (1) für einen angenommenen Wert der Grösse A der Öffnungswinkel 2α des Rotationskegels sich unabhängig von der Zahl der ausgemessenen Spuren so bestimmen lässt, dass der statistische Fehler von A ein Minimum wird. So beträgt beispielsweise für $A = 0{,}12$ dieser optimale Öffnungswinkel

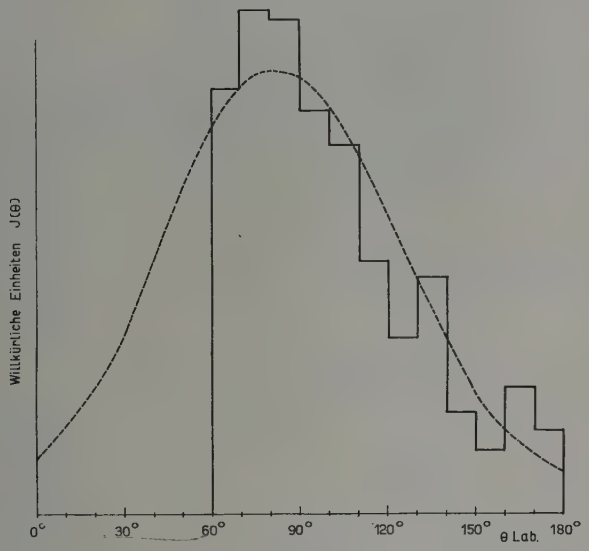

Fig. 1.

Winkelverteilung der Photoprotonen (ca. 600 Spuren).

——— Beobachtete Spurenzahl pro Raumwinkeleinheit (Laborsystem).

------- In das Laborsystem transformierte Verteilung: $J(\Theta) = 0{,}12 + \sin^2 \Theta$.

Die beiden Diagramme sind (im Winkelbereich $60^0 \leqslant \Theta_{\mathrm{Lab}} \leqslant 180^0$) *flächengleich* gezeichnet. Die experimentelle Verteilung wurde nur bis zu 60° aufgenommen, weil unter kleineren Winkeln nicht mehr eindeutig zwischen Photoprotonen und Rückstossprotonen unterschieden werden kann.

$2\alpha \sim 48^0$. Für die Auswertung können nur diejenigen in Richtung des Gammastrahls fallenden Photoprotonen, für welche $180^0 - \alpha \leqslant \Theta \leqslant 180^0$ ist, benützt werden. Infolge des natürlichen Deuteriumgehaltes des Protonenstrahls emittiert nämlich die Quelle ausser der Lithium-Gammastrahlung auch noch stets energiereiche, aus der Reaktion Li (D, n) stammende Neutronen. Diese Neutronen erzeugen in

der Emulsion Rückstossprotonen, welche die Ausmessung der Photoprotonen in der Vorwärtsrichtung ($0 \leqslant \Theta \leqslant \alpha$) verunmöglichen. Bei den vorliegenden Messungen wurde zur Berechnung der Konstanten A die Anzahl der Photoprotonen mit Energien zwischen 5,8 und 8 MeV, welche im *Schwerpunktsystem* innerhalb von Rotationskegeln mit 48° Öffnungswinkel und den Achsen

a) *senkrecht* zur Richtung des einfallenden Gammastrahls (2 Kegel, 250 Spuren); b) *in* Richtung des Gammastrahls (1 Kegel, $180^0 - \alpha \leqslant \Theta \leqslant 180^0$, 20 Spuren) bestimmt. Es ergibt sich für beide Linien zusammen

$$A\ 0{,}12 \pm 0{,}10 \text{ (mittlerer statistischer Fehler)} \qquad (2)$$

Der totale Wirkungsquerschnitt wurde aus der Zahl *aller* beobachteten Photoprotonen berechnet (600 Spuren). Sein Wert, für beide Linien zusammen, beträgt

$$\frac{2}{3}\sigma(17{,}6) + \frac{1}{3}\sigma(14{,}8) = (7{,}5 \pm 2{,}5) \cdot 10^{-28}\ \text{cm}^2 \text{ (Fehlergrenze)} \qquad (3)$$

Der Fehler in σ ist hauptsächlich durch die Unsicherheit in der absoluten Zahl der emittierten Gammaquanten bedingt. Diese

Tabelle I.

Theoretische Werte für σ (in 10^{-28} cm^2) und A
Quantenenergie $h\nu = 17{,}5$ MeV.

Art des Potentials	Reichweite der Kraft in 10^{-13} cm	Nichtzentrale Kräfte						Zentralkräfte		
		I.		II.		III.		I.	II.	III.
		σ	A	σ	A	σ	A	σ	σ	σ
Rarita & Schwinger:										
Kastenpotential . .	2,80	7,68	0,015	7,23	0,077	3,76	0,36			
Tsing-Ming Hu & Massey:										
Kastenpotential . .	2,62	7,23	0,019	6,87	0,119	4,27	0,436	7,53	7,42	5,71
Kastenpotential . .	3,05	8,09	0,013	7,86	0,037	3,99	0,341	8,20	8,26	4,00
Kastenpotential . .	3,49	8,96	0,010	9,00	0,017	2,80	0,292	9,29	8,77	1,72
Exponential-Potential	1,74	7,33	0,018	7,38	0,071	4,45	0,199			
Yukawa-Potential .	1,74	7,25	0,017	7,67	0,058	4,59	0,106			

wurde mit einem dickwandigen Aluminiumzähler, unter Benützung der von Fowler und Mitarbeitern[1]) gegebenen Kurven für die

[1]) W. A. Fowler, C. C. Lauritsen und T. Lauritsen, Rev. Mod. Phys. **20**, 236 (1948).

Quantenausbeute bestimmt. Der in (3) angegebene Fehler beruht auf der Annahme einer Unsicherheit von 20% in der absoluten Gammaintensität.

Die vorliegenden experimentellen Werte können mit der Theorie verglichen werden. In Tabelle 1 sind die Ergebnisse der Rechnungen von Rarita und Schwinger[1]) sowie von Tsing-Ming Hu und Massey[2]) zusammengestellt. DieseRechnungen wurden für die drei Krafttypen der sog. symmetrischen (I.,) geladenen (II.) und neutralen (III.) Theorie durchgeführt.

Ein Vergleich der experimentellen Werte mit den Grössen der Tabelle 1 ergibt eine ausserhalb des Fehlers liegende Abweichung gegenüber den Ergebnissen der neutralen Theorie. Dagegen sind die Messresultate sowohl mit der symmetrischen, als auch mit der geladenen Theorie verträglich.

---

[1]) W. Rarita & J. Schwinger, Phys. Rev. **59**, 556 (1941).

[2]) Tsing-Ming Hu & H. S. Massey, Proc. Roy. Soc. **196**, 135 135 (1949).

Binding energies and the energy surfaces in the Region of the heavy Natural radioactive isotopes

by **A. H. Wapstra**, Amsterdam.

The binding energies of these isotopes can be computed relative to the last members of their families by means of combinations of α and β decay energies. By the following method of interpolation we computed them relative to ^{206}Pb, the last member of the U-family. As is well-known the binding energies of the isotopes are lying on three surfaces in the n, A, E spaces; one for N and Z even, one for both odd, and one for N or Z even (n = neutron excess, A = mass number, N = number of neutrons, Z = number of protons). Sections of these surfaces with planes N, Z or A constant will nearly be parabolas in the region of maximum binding energies for isobars. We can therefore adjust the-family to the U-family by claiming, that the binding energies of the $e-e$ isotopes from these families with the same N or Z must fit to one parabola as accurately as possible. Then the $e-e$ and the $o-o$ surface are known respective to the binding energy of ^{206}Pb.

In order to adjust the odd mass families to the U-family we assume, that the $e-o$ surface lies in the mean halfway between the $e-e$ and the $o-o$ surface. The distance between the last two surfaces is found for some values of A by claiming, that the binding energies of isobars with even mass must lie on two parallel parabolas. The distance seems to increase from 1.8 MeV to 2,0 MeV for $A = 210$ to $A = 218$, and then to decrease to 1,2 MeV for A = 235.

In order to study the distance between the $e-o$ and the $e-e$ surface we consider an isotope with a value N or Z used in adjusting the Th- to the U-family. For this isotope we compute the height on the estimated parabolic section with the $e-e$ surface used. The difference with the binding energy of the isotope relative to the last member of its family will be a fair estimate of the distance between the $e-e$ and the $e-o$ surface, increased by the difference in binding energy of ^{206}Pb with ^{207}Pb or ^{209}Bi. The distances obtained in this way follow a course with A analogous to the distance between the $e-e$ and the $o-o$ surface, so it is possible to choose the differences in binding energy mentioned in such a way, that the $e-o$ surface is lying fairly well halfway the $e-e$ and the $e-o$ surface.

The result of our computations will be published in Physica.

Stationary states of light nuclei

by **L. Rosenfeld** (Manchester)

1. The interaction between two nucleons.

The present, very imperfect treatment of nuclear systems is based on the assumption that the total interaction between the constituent nucleons is primarily due to the interactions between pairs of nucleons, while many-body interactions would only contribute to higher approximations with respect to the nucleon velocities. Whether this assumption is quite justified remains open to question, since, as we shall see, theoretical calculations concerning systems of 3 or 4 nucleons, based on pair interactions only, exhibit large discrepancies from empirical results. A quantitative estimate of many-body interactions is at present precluded by the fundamental difficulties of field theory; we must therefore leave this question in a most unsatisfactory state, and base the following discussion on the assumption of pair interactions.

Our first task will then be to establish the most probable expression for the interaction operator between two nucleons; recent investigations make a renewed survey of this problem desirable. Let us start from the consideration of the interaction between neutron and proton, as revealed, on the one hand, by the experiments on scattering of very fast neutrons by protons, and on the other, by the properties of the ground state of the deuteron. The best theoretical approach to the first problem, in the present state of field theory, is the relativistic generalisation of Born's method, due to Moller. This method can readily be applied to the problem of proton-neutron scattering by assuming that the interaction between the particles results from a coupling of these particles to a meson field. It is then possible to derive in a consistent way the contributions to the scattering cross-section, not only from the static interaction usually considered, but also from the additional interaction terms of the first and second order in the nucleon velocities.

An expression for the total scattering cross-section has recently been obtained by Marty*), using Moller's method and assuming

*) Not yet published.

a coupling of the nucleons with a symmetrical mixture of pseudoscalar and vector meson fields, with arbitrary coupling constants. The vector field involves two constants g_1, g_2 corresponding to vector and tensor source densities, respectively; the pseudoscalar field is represented, owing to the elastic character of the scattering, by a single combination*)

$$f_3 \equiv f_2 + f_1 \frac{M_m}{2M}$$

of the two analogous constants f_1, f_2 (corresponding to pseudoscalar and pseudovector source densities), in conformity with Dyson's transformation. The dependence of the total cross-section on the coupling constants can be described as follows: There appears, in the first place, the expression which one would have obtained on Born's approximation, i. e. from the static interaction only, multiplied by the factor $[1 - (p/M)^2]$ (p denoting the momentum of the particles in the barycentric system of reference); to this term only the vector meson interaction contributes, and the combination of the coupling constants g_1, g_2 occurring in it are simple polynomials of the 4th degree. Besides this term, there is a further contribution in (p^2/M^2) whose coefficients are similar polynomials, but involving also the constants g_2 and f_3 multiplied by the large parameter (M/M_m). For an estimation of the relative importance of the two parts of the expression for the scattering cross-section, it is natural to take for the coupling constants g_1, g_2, f_3 values of the order of magnitude indicated by an analysis of the ground state of the deuteron based on the assumption of static interaction only. It then appears that for a value of the momentum p corresponding to incident neutrons of 90 MeV energy, the second part (in spite of the occurrence of the large coefficients M/M_m) contributes a correction of the order of a few percent of the first, which tends to increase the value of the cross-section corresponding to the assumption of static interaction, and thus to bring it farther from the experimental result. The discussion of the differential cross-section has not yet been completed: it remains to be seen whether, within the scope of symmetrical meson theory, there is still sufficient latitude in the choice of the precise values of the coupling constants to achieve agreement with the observed angular distribution of the scattering particles, without coming in conflict with the properties of the deuteron.

This leads us to a revision of the deuteron problem: does the usual treatment based on the assumption of a static interaction form an

*) The masses of a nucleon and a π-meson are denoted by M and M_m, respectively.

adequate approximation, or are velocity-dependent couplings, hitherto not properly considered, in fact of paramount importance? As is well known, the issue is obscured by the strongly singular character of the static interaction, which forces us, so long as we treat it separately, to introduce into the problem an arbitrary element in the form, e. g., of a cut-off of the static potential at small distances. One may expect that a further step in the approximation, similar to that which led to the relativistic expression for the scattering cross-section, discussed above, will give a simple answer to the question. The investigation of the ground state of the deuteron from this point of view has only recently been taken up, however, and its result will be awaited with great interest.

In the meantime, we may perhaps derive some guidance from a discussion of the problem in the static approximation, the arbitrary cut-off involved in this treatment being regarded as a rough way of accounting for the effect of the higher approximations. For the most general combination of meson fields, the effective static potential, for the ground state of the deuteron, has the form

$$-\mathfrak{J}\left[1+\alpha\mathfrak{D}^{(12)}\left(1+\frac{3}{\varkappa r}+\frac{3}{\varkappa^2 r^2}\right)\right]\frac{e^{-\varkappa r}}{r},$$

where $\mathfrak{J}$ and α are certain combinations of the coupling constants of the meson fields to the nucleons, while $\varkappa \equiv M_m c/\hbar$ and

$$\mathfrak{D}^{(12)} \equiv (\vec{\sigma}^{(1)}\vec{x}_0)(\vec{\sigma}^{(2)}\vec{x}_0) - \frac{1}{3}(\vec{\sigma}^{(1)}\vec{\sigma}^{(2)})$$

is the well-known operator of "axial dipole coupling" between the spins $\vec{\sigma}^{(i)}$ of the nucleons, depending on their orientation with respect to the line joining them (represented by the unit vector $\vec{x}_0$). For a given value of $\varkappa$, the wave-equations corresponding to the above potential, cut-off in a definite way for distances smaller than some critical value r_c, can be solved numerically for various sets of values of the parameters, $\mathfrak{J}$, α, r_c. Each solution corresponds to definite values for the binding energy, the quadrupole moment and the admixture of ^3D-state (derived from the magnetic moment): the adjustment to the empirical values of these quantities yields, in principle, the values of the parameters defining the effective potential. Extensive calculations of this type have been carried out by Grosjean*), first for a meson mass of 225 m, and recently also for the higher value M_m = 285 m of the mass of the π-meson res-

*) Not yet published.

ponsible for the nuclear field. His results present in both cases the same general features. In the first place, the value of $\varkappa$ must be about $^1/_2$; this does not correspond to any single type of meson field and would thus point to the necesssity of assuming some mixture of such fields: we shall adopt, as the simplest one, a mixture of pseudoscalar and vector fields. For values of $\varkappa$ in the neighbourhood of $^1/_2$, it then appears that the quadrupole moment is quite insensitive to the value of the cut-off radius, but that the admixture of D-state and the strength $\mathfrak{J}$ of the central part of the potential both vary almost linearly with r_c. Since the admixture of D-state is fixed only with poor accuracy (owing to uncertain relativistic corrections to the magnetic moment), neither $\mathfrak{J}$ nor r_c are accurately determined by this method. However, the possible $\mathfrak{J}$-values are of the same order of magnitude as the strength of the effective potential for the ^1S state, as estimated from the cross-section for scattering of very slow neutrons by protons. This means that the coupling constants $g_2^2\ hc$, $f_3^2\ hc$ are of the order of magnitude 10^{-1}, and that their difference, as indicated by the rather large value of $\varkappa$, is of the same order. The constant $g^2\ hc$, on the other hand, is still allowed a wide range of variation from zero to values only somewhat smaller than those of the other constants. It must be stressed that the high value of the cut-off radius, which is given by $\varkappa r_c \approx 0.7$, rather weakens the reliability of these results. Nevertheless, one might perhaps conclude that *the interaction between neutron and proton can be accounted for by a mixture of pseudoscalar and vector meson fields, in such proportions that the binding of the deuteron is largely due to the resulting axial dipole potential*. For the treatment of effects involving only small energies (up to 20 MeV, say), the model of nuclear potential proposed by Rarita and Schwinger (in which both the central and the dipole forces are represented by potential wells of the same width and appropriate depths) provides a convenient schematization. But it cannot, of course, account for the proper field effects already prominent in the domain of energies about 100 MeV.

In the preceding discussion, only one meson mass has been assumed. Attempts at introducing mesons of different masses in the nuclear field, according to Schwinger's proposal, have not proved successful. Empirical data on slow neutron diffraction, on the other hand, when analysed by means of the schematic potential well model, show that different widths must be assumed for the wells corresponding to the effective potentials for the ^3S and ^1S states. This conclusion, however, depends sensitively on the form of potential

adopted: it appears*) that the empirical results can be explained on the basis of meson potentials of single range for both types of states (as was assumed in the above discussion). In this connexion, it must be pointed out that the range value derived from the slow neutron diffraction and scattering data for the ^1S potential, in contrast to previous statements to the contrary, appears to be quite compatible with the range of the ^1S potential between two protons derived from proton-proton scattering experiments. There is thus no reason so far to doubt the (approximative) "charge independence" property of the nuclear potential, at any rate for ^1S states. Moreover, the scanty indications on the effective potential for ^3P states derived from proton-proton scattering data at higher energies (10... 14 MeV) are not incompatible with the extension of the charge independence property to all types of stationary states. The general conclusion of the preceding discussion of the evidence from two-nucleon systems may be condensed in the following expression for the interaction potential between two nucleons *of low velocity*:

$$-\frac{1}{3}\,\underline{\tau}^{(1)}\,\underline{\tau}^{(2)}\,\mathfrak{J}\left[\gamma+(1-\gamma)\,\tilde{\sigma}^{(1)}\,\tilde{\sigma}^{(2)}+\alpha\,\mathfrak{D}^{(12)}\left(1+\frac{3}{\varkappa r}+\frac{3}{\varkappa^2 r^2}\right)\right]\frac{e^{-\varkappa r}}{r},$$

with due emphasis on the many uncertainties which still beset the argument.

This formula, however, is still incomplete in one respect, about which two-nucleon systems cannot yield any evidence. Besides the axial dipole coupling, another type of non-central coupling is possible on general invariance grounds, namely, a spin-orbit coupling of the type

$$\mathfrak{M}^{(12)}\equiv(\tilde{\sigma}^{(1)}+\tilde{\sigma}^{(2)})\cdot(\tilde{l}/h),$$

where $\tilde{l}$ denotes the orbital angular momentum with respect to the centre of gravity of the nucleon pair. Such a coupling does not give any contribution to S-states of a two-nucleon system, but it might play a part in the stationary states of more complex systems. A spin-orbit coupling of relativistic origin (of the second order in nucleon velocities) must be present in any case; roughly, it will have the form, on meson theory,

$$\sim\ \frac{1}{3}\,\underline{\tau}^{(1)}\,\underline{\tau}^{(2)}\,\mathfrak{J}\left(\frac{M_m}{M}\right)^2\mathfrak{M}^{(12)}\left(\frac{1}{\varkappa r}+\frac{1}{\varkappa^2 r^2}\right)\frac{e^{-\varkappa r}}{r}.$$

A vector meson field will in general also give rise to a coupling of

*) See J. Blatt and J. Jackson, Phys. Rev. **76**, 18, (1949); H. Bethe, Phys. Rev. **76**, 38 (1949).

the same form, but with a factor $g_1\, g_2\, (M_m/M)$ instead of the factor $^1/_3\, \mathfrak{J}\, (M_m/M)^2$: if the constants g_1, g_2 are of the same order of magnitude, this effect is of the first order in the nucleon velocities. In view of the evidence, discussed in the following, which more or less directly points to the existence of considerable spin-orbit couplings in nuclei, this theoretical possibility should certainly be kept in mind.

2. The ground state of ^3H.

In the deuteron, the non-central interaction of the axial dipole type brings about a breakdown of the conservation of orbital angular momentum, with the result that the ground state, which belongs to the triplet system, is a mixture of S and D state. If the system contains more than two nucleons, there is even no conservation of spin; in the case of ^3H, the doublet and quartet systems are also combined. The ground state of ^3H, whose total angular momentum is $^1/_2$, will therefore be a combination of the form $^2S_{\frac{1}{2}} + {}^2P_{\frac{1}{2}} + {}^4P_{\frac{1}{2}} + {}^4D_{\frac{1}{2}}$. Moreover, in this mixture there are two types of doublet (S and P) states, according as the wave-function is symmetrical ($\bar{S}$, $\bar{P}$) or antisymmetrical ($\tilde{S}$, $\tilde{P}$) in the spins of the neutrons; likewise, there are two types of ^4D states (D_s, D_a), distinguished by the symmetrical or antisymmetrical character of the dependence of the wave-function on the variables $\vec{x}$ (radius vector joining the neutrons) and $\vec{X}$ (radius vector joining the proton to the centre of gravity of the neutrons). To a first approximation, one may assume that the two neutrons will be "paired" in a configuration with saturated spins, corresponding to a $^2\bar{S}_{\frac{1}{2}}$ state. By axial dipole interaction, this state will be directly coupled only to the $^4D_{\frac{1}{2}}$ state; any admixture of other states in appreciable amount will be an indication of the occurrence of other couplings, either of the spin-orbit or of the 3-body type.

Definite indications of this kind can in fact be inferred from two fundamental properties of the triton: its binding energy and its magnetic moment. A calculation of the binding energy on the assumption of a Rarita-Schwinger interaction between the pairs of nucleons (i. e. involving only axial dipole coupling) yields a much smaller absolute value than the empirical one: it appears that the axial dipole coupling, so efficient in bringing about the deuteron binding, has a much smaller total effect in the 3-nucleon case. The fact that the magnetic moment is *larger* than the proton moment likewise cannot be understood on the basis of axial dipole coupling:

for a magnetic moment equal to the proton moment (as would correspond to a pure $^2\tilde{S}_{\frac{1}{2}}$ state) could only be lowered by an admixture of ^4D_s state. It is true that a nuclear field effect, the "exchange moment", might give an additional contribution in the right direction, but this could hardly be sufficient to bring the needed overcompensation of the ^4D_s term. On the other hand, a more complicated mixture of states would lead to an additional magnetic moment which may be of either sign. Whether agreement with experiment in both cases could actually be reached by taking into account spin-orbit or 3-body interactions has, however, not yet been investigated.

3. The quasi-atomic model.

Experimental data concerning the stationary states of light nuclei are rapidly accumulating. The *energies and widths of excited levels* can be inferred from the occurrence of resonances in the yield of nuclear reactions induced by impact of particles or γ-rays, or from the study of β-decay processes, especially when such processes are accompanied by the emission of γ-rays or electron pairs. Methods of high precision have been developed to measure the *total angular momenta, magnetic moments and quadrupole moments of the ground states* of stable and even some unstable nuclei. In favourable cases, the application of selection rules also allows inferences to be made concerning the *quantum numbers and parity of excited states*. Another source of information bearing more especially on the *orbital quantum numbers* entering into the composition of excited states is provided by the study of the angular distribution of particles ejected in the final stage of the nuclear reaction studied.

The theoretical approach to the problem of the stationary states of nuclear systems, on the other hand, is hampered by the lack of adequate methods of approximation for treating assemblies of closely coupled particles. The general view-points of group theory offer only a rather loose frame: the classification of nuclear states into *supermultiplets*, characterized, for a given mass number A, by 3 quantum numbers (P, P', P'') with the following interpretation. Consider the operators

$$T_{\underline{x}} = \frac{1}{2}\sum_i \tau_{\underline{x}}^{(i)}, \qquad S_z = \frac{1}{2}\sum_i \sigma_z^{(i)}, \qquad \underline{Y}_z = \frac{1}{2}\sum_i \tau_{\underline{x}}^{(i)}\sigma_z^{(i)},$$

which represent, respectively, half the neutron excess, the component of the total spin in an arbitrary direction, and the component of the difference between total neutron and proton spin in this direc-

tion. Then P is the largest eigenvalue that any of these operators can take in the supermultiplet, P' is the largest eigenvalue of a second one among these operators which is compatible with the value P of the first, P'' is the largest eigenvalue of the third compatible with the values P, P' of the other two.

Pure supermultiplet states (characterized by eigenvalues of T_3, S_z, $\underline{Y}_z$) could only occur if the nuclear interactions were central forces independent of the spin and isotopic variables of the constituent nucleons; in general, they would be degenerate, being superpositions of states belonging to different spin or charge multiplicities. Central forces depending on spin and isotopic variables will split up the supermultiplet states into different spin and charge multiplets, but in this splitting, supermultiplet states with different values of $\underline{Y}_z$ will in general combine, so that $\underline{Y}_z$ ceases to furnish a quantum number. Non-central couplings will further mix the multiplet substates; the resulting energy spectrum could only be obtained by the consideration of a more specific nuclear model. The Coulomb repulsion between the protons has the effect of decreasing the (absolute) binding energy values of supermultiplet states with decreasing neutron excess; for light nuclei, however, this is a rather unimportant feature.

The supermultiplet scheme is useful for the establishment of general regularities of a semi-qualitative nature (such as selection rules for β-decay, peculiarities of the mass-defect curve, distribution of magnetic moments), but, of course, it hardly provides an adequate starting point for actual calculations of energy levels in specific cases. For this purpose, recourse must be had to some model to which the methods of quantum mechanics can be applied. The *quasi-atomic model* consists in assuming that in first approximation each constituent nucleon occupies an individual state independently of the others, and in applying to the interaction between the nucleons the usual methods of approximation developed for the treatment of atomic systems. In the latter case, this procedure is justified by the predominance of the electrostatic field of the atomic nucleus; in the case of nuclear systems, however, one has to introduce for the definition of the individual states of the nucleons some fictitious "average nuclear field" which, on account of the saturation properties and above all of the non-additive character of the nuclear forces resulting from the existence of considerable many-body interactions, does not correspond even roughly to any physical reality. The greatest shortcoming of the calculations hitherto carried out by this method, however, is that they use only central

interactions. It is above all the neglect of non-central forces which makes the results of such calculations quite unreliable: even the order of succession of the multiplet levels cannot be predicted with any certainty.

On the quasi-atomic model, the individual nucleon states may be ascribed orbital quantum numbers, and the building up of the ground states of nuclei of increasing mass number may accordingly be pictured as a gradual filling up of the "shells" corresponding to the successive individual nucleon states. Any nuclear potential accounting for the properties of two-nucleon systems will favour a configuration of any pair of constituent nucleons of the same shell with an *even* value of the total orbital momentum: for it will lead to an attraction between the two nucleons in such a configuration, while (on the charge independence hypothesis) we shall expect a repulsive interaction in all configurations of odd total orbital momentum. More specifically, in an even configuration, the attraction between two nucleons with opposite spins will in any case be purely central, while the interaction between a proton and a neutron with parallel spins will be a stronger attraction, which might be central or non-central. These forces will in the first place tend to the formation, within each shell, of groups consisting of a neutron pair and a proton pair, both with saturated spins ("α-clusters"). Any two additional like nucleons, in the shell, will tend to "pair" themselves in an even singlet configuration: this general conclusion, however, does not suffice to give an interpretation of the fact that even nuclei have zero angular momentum and no magnetic moment, corresponding to a ^1S ground state.

When we try to apply the model to light odd nuclei, in which non-central forces become prominent, we run at once into still greater difficulties. An example of typical interest is that of the nucleus ^{10}B, whose ground state has recently been found to have a total angular momentum $J = 3$, quite at variance with expectation from the quasi-atomic model with central interactions only. In fact, on this model, the configurations of lowest energy of the nucleus ^{10}B consist of a filled s-shell (α-cluster) and a p-shell containing an α-cluster and a proton-neutron pair with parallel spins. On the assumption of central interactions, such configurations would give rise, in first approximation, to the states ^3S, ^3D, ^3D, ^3F, ^3G in order of decreasing binding: the ground state would thus be expected to have the angular momentum $J = 1$. Higher approximations will produce some displacement of these levels by mixture with higher levels of the same type: but this effect has been found

by VAN WIERINGEN*) to be negligible. It is clear that in order to explain the presence of any level of higher orbital momentum below the ^3S state, non-central (and possibly many-body) forces must be assumed not merely to give rise to perturbations of levels corresponding to central interactions, but even to play a prominent part in the binding of the nucleus.

A more precise indication of the nature of the ground state of ^{10}B may be derived from the knowledge of its magnetic moment. In fact, the ground state of angular momentum $J = 3$ may be a mixture of the states ^3D, ^3F, ^3G mentioned above, with in addition the state ^1F from the singlet system belonging to the same supermultiplet. If the proportions of these states in the mixture are denoted by the symbols of the states between brackets, the magnetic moment may be written in the form

$$\mu = \mu_p + \mu_n + 1 - \left(\mu_p + \mu_n - \frac{1}{2}\right)\left[(^1F) + \frac{3}{4}(^3F) + \frac{7}{4}(^3G)\right];$$

in this easily derived formula, μ_p and μ_n denote the proton and the neutron moment, respectively, and (^3D) has been replaced by $1 - [(^1F) + (^3F) + (^3G)]$. From the experimental value $\mu = 1.794$ one therefore concludes that the ground state is mainly a ^3D state, but with an admixture of at least 22% of other states.

The discovery of the high angular momentum of ^{10}B has provided the solution of the riddle presented by the highly forbidden character of the β-transition $^{10}\text{Be} \rightarrow {}^{10}\text{B}$, in which the even isobar ^{10}Be must be expected to have zero angular momentum. Moreover, it has recently been found that the β-decay of the conjugated**) isobar ^{10}C into ^{10}B, which is an allowed transition, is accompanied by a γ-ray, so that it involves an excited state of ^{10}B which may well have an angular momentum 1. The quantitative relations between the isobars of mass 10, shown on the accompanying diagram, allow an interesting comparison of the nuclear structures involved***). The configuration of the conjugated even isobars ^{10}Be and ^{10}C can be pictured as one in which all pairs of like nuclei have saturated spins. Compare with these the configuration ^{10}B* of the odd isobar ^{10}B in which the proton and the neutron in excess of α-clusters have opposite spins: this will, of course, correspond to some excited state of the ^1S type. The differences of Coulomb energies between these

*) Not yet published.

**) Two nuclei are called *conjugated* if the one goes over into the other by changing protons into neutrons and vice-versa.

***) R. SHERR, H. MUETHER, M. WHITE, Phys. Rev. **75**, 282 (1949).

configurations (assuming the nuclear radii to be the same) are easily estimated at

$$^{10}\mathrm{C} - {}^{10}\mathrm{B}^* = 2{,}04\ \mathrm{MeV}, \quad {}^{10}\mathrm{B}^* - {}^{10}\mathrm{Be} = 1{,}48\ \mathrm{MeV},$$

whence

$$^{10}\mathrm{C} - {}^{10}\mathrm{Be} = 3{,}52\ \mathrm{MeV},$$

in remarkable agreement with the empirical result. We are therefore entitled to conclude that in the three isobaric configurations considered, the proper nuclear energy is the same: this entails not

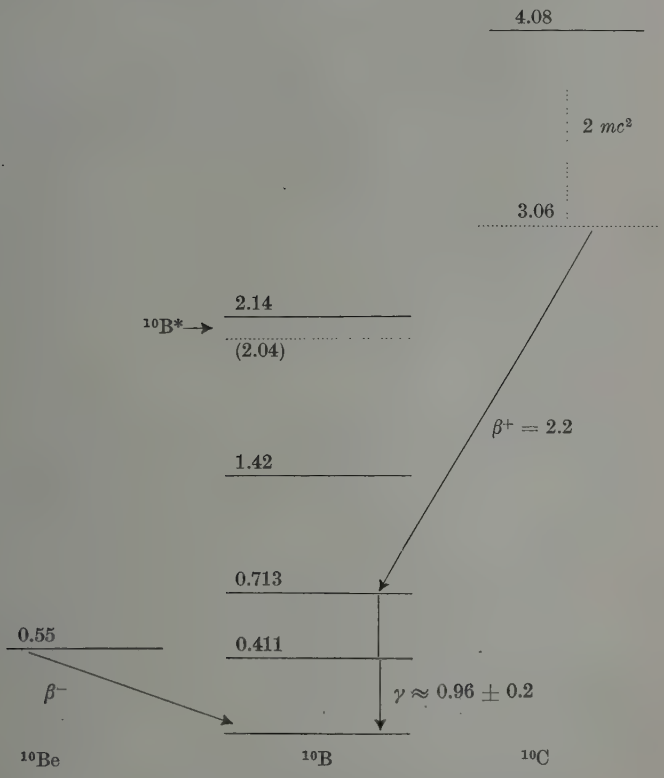

The isobars of mass 10. (Energies in MeV)

only symmetry of nuclear interactions with respect to charge, but also charge independence of these interactions in configurations of the ^1S type.

4. The α-particle model.

At first sight, it would seem that a much better approach to the problem of nuclear states would be provided by the *α-particle model*, in which the nucleus is assumed to consist of α-clusters with the necessary number of additional nucleons. In the first place, a tendency to the formation of such α-clusters is, as we have seen, an obvious consequence of the properties of nuclear interactions. In fact, the binding energy of an α-particle is so large that if this energy is, on the average, assigned to each of the constituent α-clusters, the greatest part of the total binding energy of the nucleus is accounted for; the mutual binding of the α-clusters and additional nucleons is comparatively small. It would seem, therefore, that a model in which this large contribution to the binding energy is included from the start represents a considerable improvement on the quasi-atomic model, which is quite inadequate in this respect.

Unfortunately, on closer examination, the picture loses its treacherous simplicity. It cannot be supposed, of course, that the α-clusters retain their identity within the nucleus. One has rather to imagine that they form and dissolve continually in the course of chance encounters of nucleons in their chaotic motion. By studying some simple system, like ^{8}Be, and trying to represent it as a superposition of an 8-nucleon quasi-atomic system and a system of two α-particles, it is possible to obtain a rough estimate of the "degree of dissociation" of the α-clusters with respect to the "gas" of nucleons. The result is that this degree of dissociation is rather high, and this at once forces us to question seriously the accuracy of any "geometrical" model in which the assembly of α-clusters is compared to a close packing of rigid spheres held together by a certain number of "bonds" (determined by the number of points of contact of the spheres in the given configuration). Such doubts increase on closer inquiry into the nature of the "bond" between two α-particles: it appears that this bond is not primarily an ordinary interaction similar to the van der Waals intermolecular forces, but rather an interaction of the "exchange" type, conditioned by the exchange of nucleons between the clusters, and more nearly comparable to the chemical binding forces. In particular, the non-additive character of exchange interactions precludes any simple interpretation of the remarkable empirical fact that the binding energies of the light "α-nuclei" (i. e. nuclei consisting only of α-clusters) are proportional to the numbers of bonds of the corresponding geometrical models.

We must therefore abandon the hope of finding in the α-particle model a suitable starting point for the computation of nuclear bind-

ing energies. For more qualitative purposes, however, the model has many advantages over the quasi-atomic picture. It can be shown, for instance, that in spite of their transient character, the α-clusters may be expected to retain their cohesion during times long compared with the periods of vibration and rotation of the configurations in which they arrange themselves in the lightest α-nuclei. On this basis, it is possible to give a qualitative and even semi-quantitative description of the excited levels of these nuclei in analogy with the treatment of vibration and rotation levels of polyatomic molecules. An interesting feature of this treatment arises from the identity of the constituent α-clusters, which has the effect of pushing upwards a certain number of rotation levels according to the symmetry or quasi-symmetry of the configuration, thus explaining the absence of any rotational fine structure of low excitation energy, especially in heavier nuclei. A simple case of this kind is that of ^{8}Be, in which only the even values of the angular momentum are allowed by symmetry.

Some general regularities of magnetic moments and electric quadrupole moments of nuclei can be better understood, at least qualitatively, on the α-particle model than on any model in which the nucleons are considered individually. On the one hand, the values of the magnetic moments of odd mass nuclei can be roughly accounted for as if they were due to the individual motion of the odd nucleon in the field of the residual nuclear structure; on the other hand, the positive values of many quadrupole moments likewise point to the existence of a structure of some "rigidity" within the nucleus; closer examination shows that the picture offered by the α-particle model would just provide such a structure with suitable properties.

The α-particle model affords also a convenient starting point for a semi-quantitative treatment of the ground states of light nuclei differing from α-nuclei by an additional or a "missing" neutron. The extra particle or "hole" can be considered as moving in the field of the α-cluster configuration representing the α-nucleus, and the energy of its binding to this nucleus can readily be expressed in terms of the interaction energy operator between neutron and α-particle and the corresponding eigenfunctions of a neutron in the field of an α-particle. As an illustration of the method, let us consider the ^{8}Be configuration and the two neighbouring nuclei ^{7}Be and ^{9}Be. If ψ_1, ψ_2 represent the p-state eigenfunction of lowest energy of a neutron in the field of the α-particle 1 or 2, respectively, and if we assume this eigenfunction to be very concentrated around the centre of the α-particle, with a node at the centre, the eigen-

function ψ of a neutron or hole in the field of the two α-particles has either of the approximative forms

$$\frac{1}{\sqrt{2}}(\psi_1 + \psi_2) \quad \text{or} \quad \frac{1}{\sqrt{2}}(\psi_1 - \psi_2).$$

In order to obtain the lowest energy state of the corresponding nucleus, we must choose the eigenfunction of lowest energy in the case of an additional neutron, of highest energy in the case of a hole. These two cases correspond to the first and second of the above eigenfunctions, respectively, as appears from a consideration of the numbers of nodes of these functions. Now, let V_1, V_2 be the interaction energy operators of the α-particles 1,2 with the neutron, K the kinetic energy operator of the neutron. $H = V_1 + V_2 + K$ its Hamiltonian. Define the energy of the neutron in the field of an α-particle

$$B \equiv \int \psi_1^* (V_1 + K) \psi_1,$$

the average interaction energy of a neutron bound to one of the α-particles with the other

$$R \equiv \int \psi_1^* V_2 \psi_1,$$

and the exchange interaction energy

$$Q \equiv \Re \int \psi_1^* H \psi_2.$$

Then the energy of the additional neutron, i. e. the difference between the energies of ^{9}Be and ^{8}Be $- n$, is approximately given by $B - R - Q$: and the difference between the energies of ^{7}Be and ^{8}Be $- n$ is given by $B - R - Q$. A complete discussion of this method, including a comparison with the empirical data, will be found in Hafstad and Teller's fundamental paper on the α-particle model*). An extension of the same procedure to the case of two additional nucleons, and in particular to the nucleus ^{10}B, might perhaps reduce to manageable proportions the problem of the interaction between the two additional particles in this nucleus, on which the explanation of the observed value of the angular momentum ultimately depends.

*) L. Hafstad and E. Teller, Phys. Rev. **54**, 681 (1938).

Diskussion zum Vortrage von Prof. L. Rosenfeld

Following his lecture, Prof. Rosenfeld has given a brief account of some recent considerations of Prof. N. Bohr on the adequacy of the quasi-atomic model in accounting for the properties of the heavier nuclei. Bohr points out that the justification for assuming the single nucleons to occupy individual states in an average field of force must be sought in a comparison of the orbital periods of those states with the periods of the exchange effects in which nucleons interchange their states. The latter periods are difficult to estimate but if, as seems probable, they are much longer than the orbital periods, the quasi-atomic model should be expected to provide an adequate description of the stationary states of nuclei.

Prof. Heisenberg: Hinsichtlich der Frage, ob das Potentialtopfmodell oder das α-Teilchenmodell die Atomkurve besser beschreibt, möchte ich darauf hinweisen, dass diese Frage wohl durch die neuen Untersuchungen von Haxel-Jensen-Süss einerseits, Maria Goeppert-Mayer andererseits für die tiefsten Zustände der Kerne zugunsten des Potentialtopfmodells entschieden ist. Es hat sich herausgestellt, dass man den empirischen Schalenaufbau der Atomkerne erklären kann, wenn man von einzelnen Teilchen in den stationären Zuständen eines Potentialtopfes ausgeht und ausserdem eine starke Spin-Bahnkopplung annimmt. Diese Entdeckung scheint mir ein wichtiger Fortschritt der Kernphysik und es entsteht jetzt die Aufgabe, zu erklären, woher die grosse Spin-Bahnkopplung kommt und warum die individuelle Wechselwirkung einzelner Nukleonen relativ wenig ausmacht. Teller hat den Gedanken ausgesprochen, dass das Mesonenfeld im Kern vielleicht einer nicht linearen Wellengleichung genügt, bei der die Nichtlinearität verhindert, dass die Feldstärke einen gewissen Wert übersteigt. Eine solche Annahme würde einerseits die scheinbare Absättigung der Kernkräfte erklären, die nach den neuesten Versuchen in Berkeley über Neutron-Proton-Streuung nicht auf die früher übliche Weise gedeutet werden kann; andererseits würde sie das Mesonfeld im Kern glätten, da es innerhalb des Kerns überall dem Maximalwert nahe wäre. Die individuelle Wechselwirkung einzelner Teilchen würde also wenig zur Geltung kommen. Für die grosse Spin-Bahnkopplung fehlt jedoch bisher jede Deutung.

Die Brauchbarkeit des Potentialtopfmodells würde natürlich nicht verhindern, dass es im Atomkern auch α-Teilchenartige Gruppierungen von Nukleonen gibt, und ist auch vereinbar mit der Annahme, dass für Stossprozesse das „Sandsack-Modell" eine gute Approximation darstellt.

Prof. Rosenfeld in reply to a question of Prof. Heisenberg: The problem of the saturation of nuclear forces is at present very obscure in view of the importance of the non-central interactions which has been disclosed by recent evidence. The treatment of this problem in fact has hitherto been almost entirely confined to the case of central interactions. Axial dipole couplings, however, will have the tendency to favour those nuclear configurations in which the spins of the nucleons are parallel, and whose shapes strongly deviate from spherical symmetry. This tendency will be counteracted by the kinetic energy of the nucleons, but the question whether the balance of these antagonistic tendencies results in saturation effects in agreement with the empirical evidence is by no means decided.

Prof. Süss: Man hat zwei Sorten „magic numbers" zu unterscheiden:

	2		8		20		(40)		(70)		...	
und		(6)		(14)		28		50		82		126 ...

Von den Zahlen der 2. Zeile, insbesondere von 50 und 82 ist schon längere Zeit bekannt, dass sie für die Kernstruktur von Wichtigkeit sind; z. B. haben Elsasser 1932 oder Goldschmidt in einer Diskussion über die kosmischen Häufigkeiten der verschiedenen Kernarten hierauf verwiesen. Die Zahlen der 1. Zeile zeigen sich deutlich in den Eigenschaften leichter Kerne bis zu einer Massenzahl 40. Dagegen kann man die Zahlen 40 und 70 nur erkennen, wenn man die kosmischen Kernhäufigkeiten genau untersucht. Ihre Existenz lässt sich jedoch weiter durch die Tatsache begründen, dass die metastabilen Zustände vor allem bei solchen Kernen auftreten, deren Protonen- oder Neutronenzahl in der Nähe von 40 oder 70 liegt. Die Zahlen der 1. Zeile lassen sich ganz einfach deuten, während zur Deutung derjenigen der 2. Zeile unserer Meinung nach die Annahme einer starken Spin-Bahnkopplung notwendig ist. Die Modelle Feenbergs oder Nordheims geben ebenfalls eine Erklärung für die Zahlen der 2. Zeile, dagegen ist ihre Erklärung der Zahlen der 1. Zeile komplizierter.

Prof. Racah remarks that the papers of Maria Goeppert-Mayer and of the people of Goettingen do not constitute a sufficient proof

for a strong spin-orbit coupling, as FEENBERG and HAMMACK and NORDHEIM were able to explain the magic numbers also without assuming spin-orbit coupling.

Prof. HALBAN: Mrs. GOEPPERT-MAYER told me in a letter that her shell model predicts that dipole transitions of low energy do not exist. I believe this not to be the case for the models of FEENBERG and NORDHEIM. Recently a certain number of results concerning the character of the lowest transitions in certain nuclei have been obtained by the method of angular correlation. More results of this kind will soon be available and they might help to distinguish between the different models.

Prof. ROSENFELD: Does the existence of the "magic numbers" really provide overwhelming evidence in favour of the quasi-atomic model, to the extent of excluding any other possibility? One should not lose sight of the fact that the quasi-atomic model itself implies the existence of a tendency to "α-clustering" and that there are numerous nuclear properties, such as the regularities of magnetic moments and the predominantly positive sign of the electric quadrupole moments, which seem to require for their explanation some kind of relatively rigid structure, such as would result from the α-particle model. It seems to me that the magic numbers might also be accounted for by a model which is less extreme than the quasi-atomic one, and which allows for the structural properties just mentioned.

H. KOPFERMANN: Ich möchte in diesem Zusammenhang darauf hinweisen, dass sich auch die elektrischen Quadrupolmomente in Nachbarschaft der Kernladungszahlen $Z = 28$, 50, 82 im Sinne des "quasiatomic" Kernmodells verhalten. Sie haben bei $Z = 29$, 51, 83 negatives, bei $Z = 27$, 49, 81 positives Vorzeichen.

Prof. RABI: I have talked to Dr. GOEPPERT-MAYER about her nuclear model and she told me that she finds no way of reconciling the large nuclear quadrupole moments with her single particle model. I have reason to believe that our accepted values of nuclear quadrupole moments are too low.

Prof. FERMI: The nuclear quadrupole moments are in many cases so large that it seems hopeless to attempt to explain them in terms of the contribution of a single nucleon. The more so that in most instances the quadrupole moments are positive so that a single nucleon description would give not only the wrong magnitude but even the wrong sign. It appears more likely that in a nucleus con-

taining an odd nucleon the quadrupole moment is better described as a property of the residual nucleus left over by removing the odd nucleon. The main effect of the odd nucleon would then be merely to orient the axis of the residual nucleons.

A mechanism that would yield an adequately large quadrupole moment of the residual nucleus is the zero point oscillation of the fission degrees of freedom. One can estimate by a naive calculation based on the drop model that due to the anharmonicity of this oscillation the drop behaves in the average like an elongated ellipsoid of such axis ratio as to give a quadrupole moment which is a function of Z and which is in magnitude as large as the largest observed quadrupole moments.

Unfortunately I am not in a position to make a definite statement as to what mechanism may be responsible for orienting this quadrupole moment along the spin axis of the odd nucleon.

If the present view of the origin of quadrupole moments is at all correct one would expect this mechanism to be most efficient for nuclei where a shell is about half filled.

On the Calculation of Nuclear Levels

by **Giulio Racah**
The Hebrew University, Jerusalem, Israel.

We shall not discuss in this paper if the nuclear forces are charge-symmetrical, nor if the nuclear-shell model is correct; but, assuming that the forces are charge-symmetrical and that the nuclear-shell model has some significance, we consider the problem of calculating the nuclear levels in this approximation.

This problem does not involve fundamental difficulties, but only technical difficulties connected with the great number of terms which appear in a nuclear configuration. It suffices to remember that the configuration p^6 has 12 supermultiplets with 40 terms, d^5 has 77 supermultiplets with 244 terms, d^{10} has 472 supermultiplets with 2420 terms.

The calculation of the term energies and the tabulation of the results may be simplified very much by using the group-theoretical methods developed by the author for the calculation of the spectra of the atomic configurations f^n [1].

The configurations p^n.

For spin-independent forces (Wigner and Majorana interactions) the term-values of p^n were calculated by Hund[2]; he represented his results with two empirical formulas, which were later demonstrated by the author[3]:

$$V_W = \frac{n(n-1)}{2} F_0 + \left[6M - \frac{3}{2} L(L+1) - n(n+4)\right] F_2, \qquad (1)$$

$$V_M = M(F_0 + F_2) + \frac{3}{2}[n(n+1) - L(L+1)] F_2; \qquad (2)$$

here F_0 and F_2 are the well known parameters of Slater[4], and M is the eigenvalue of the Majorana operator, which depends only on the partition Σ characterizing the supermultiplet to which the term belongs.

For spin-dependent forces (Bartlett and Heisenberg interactions) some term values were calculated by Feenberg and

PHILLIPS[5]): using their equations (6), (7) and (8) we may obtain the general formula

$$V_B - V_H = \left[R(R+1) + S(S+1) + \frac{n(n-4)}{2}\right](F_0 - 5F_2), \qquad (3)$$

and we may give to $V_B + V_H$ the more convenient form

$$V_B + V_H = [S(S+1) - R(R+1)]\left(F_0 + \frac{5}{2}F_2\right) + 6XF_2, \qquad (4)$$

where X is a matrix which is diagonal with respect to R, S and L, but not with respect to Σ.

The whole problem is now reduced to the calculation of the matrix X, and the main result of the group-theoretical methods is that its elements are the product of two independent functions:

$$X = (\Sigma|X(R,S,L)|\Sigma') = (\Sigma|\Phi(R,S)|\Sigma')(\Sigma|\Psi(L)|\Sigma'). \qquad (5)$$

The functions Φ and Ψ may be calculated separately, and their non-vanishing elements are given in Tables I—III.

Table I.

$\Phi(R, S)$ and $\Psi(L)$ for p^2 and p^4.

Conf.	Σ—Σ'	$\Phi(R,S)$ (11)	(31)	(13)	(33)	(51)	(15)	$\Psi(L)$ S	P	D	F
p^2	200—200		1	−1				−5/2		1/2	
	211—310		$\sqrt{3}$	$\sqrt{3}$	2				$\sqrt{5/2}$		
	220—220	0			0	1	−1	−5/2		1/2	
p^4	220—310				1					−$\sqrt{3}$	
	220—400	1						2$\sqrt{10}$		−$\sqrt{7}$	
	310—310		1	−1	0				3	−5 2 1 2	

Table II.

$\Phi(R, S)$ and $\Psi(L)$ for p^3 and p^5.

Conf.	Σ—Σ'	$\Phi(R,S)$ (22)	(42)	(24)	44)	$\Psi(L)$ S	P	D	F
p^3	210—210	0	1/2	−1/2			−5/2	3/2	
	210—300	1					$\sqrt{10}$		
	221—320	0	1	−1			5$\sqrt{3}$/4		
	221—410	1					$\sqrt{15}$		
p^5	311—311	0	3 2	−3 2	0	5 2		−1 2	
	311—320	4	$\sqrt{5}$	$\sqrt{5}$				3 2$\sqrt{5}$	
	320—320	0	1/2	−1/2			−3	5/2	−1/2
	320—410	1					−3	−$\sqrt{14/5}$	2

Table III.

$\Phi(R, S)$ and $\Psi(L)$ for p^6.

Σ—Σ'	$\Phi(R,S)$							$\Psi(L)$					
	(11)	(31)	(13)	(33)	(33)′	(51)	(15)	S	P	D	D'	F	G
222—420		1	1					$5\sqrt{3}/2$					
321—321		3/5	−3/5	−2/3	2/3	1	−1		5/2	−3/2			
321—A				1					$4\sqrt{5}/3$				
321—B					1				$4\sqrt{5}/3$				
321—420		1	1							$4\sqrt{21}/5$			
A—A	1			−1/3					−2			3	
B—B	−1				1/3				−2			3	
420—420		1	−1					−3		9/10	−3/2	3/2	−1/2

$\psi(\mathrm{A}) = [\psi(411) + \psi(330)]/\sqrt{2}$, $\psi(\mathrm{B}) = [\psi(411) - \psi(330)]/\sqrt{2}$.

The configurations d^n.

The first problem which arises for the configurations d^n is a convenient classification of the different states with the same L which belong to the same partition. As the partition numbers classify the terms according to the representations of the five-dimensional linear group, and the quantum number L according to the representations of the three-dimensional rotation group, a couple of quantum numbers $W \equiv (w_1\, w_2)$ may be introduced, which classifies the terms according to the representations of the five-dimensional rotation group. The quantum numbers W do not solve completely our problem, but are sufficient for our purpose: no more than three terms with the same L may belong to the same representation W, when also 18 may belong to the same partition.

The term values for $n \leqslant 4$ were obtained by JAHN[6]) by very long calculations based on a previous method of the author[7]). With the new group-theoretical methods we obtained for d^n the following formulas, which correspond to Eqs. (1) to (4):

$$V_W = \frac{n(n-1)}{2} F_0 + \left[5M - \frac{n(n-11)}{2} - \frac{5}{4}\gamma(W)\right](F_2 + 9F_4) + [2X^{(1)} - \omega(L,W)](F_2 - 5F_4) \tag{6}$$

$$V_M = MF_0 + \left[\frac{3}{2}M + \frac{5n(n+3)}{4} - \frac{5}{4}\gamma(W)\right](F_2 + 9F_4) + [2\omega(L,W) - X^{(1)}](F_2 - 5F_4) \tag{7}$$

$$V_B - V_H = \left[R(R+1) + S(S+1) + \frac{n(n-4)}{2}\right]\left[F_0 - \frac{7}{2}(F_2 + 9F_4)\right] + X^{(2)}(F_2 - 5F_4) \quad (8)$$

$$V_B + V_H = [S(S+1) - R(R+1)]\left[F_0 + \frac{7}{3}(F_2 + 9F_4)\right] + X^{(3)}(F_2 - 5F_4) + X^{(4)}(F_2 + 9F_4) \quad (9)$$

with

$$\gamma(W) = w_1(w_1+3) + w_2(w_2+1)$$

and

$$\omega(L,W) = \frac{1}{2}L(L+1) - \frac{3}{4}\gamma(W);$$

and the problem is reduced to the calculation of the four matrices $X^{(r)}$. The elements of these matrices have now the general expression

$$(\Sigma W | X^{(r)}(R,S,L) | \Sigma' W') = \sum_1^a{}_\alpha \sum_1^b{}_\beta (\Sigma W | A^{(r)}_{\alpha\beta} | \Sigma' W') (\Sigma | \Phi^{(r)}_\alpha(R,S) | \Sigma') (W | \Psi^{(r)}_\beta(L) | W') \quad (10)$$

with $a, b \leqslant 3$; and it may also be shown that

$$\Phi^{(1)}_1 = \delta(\Sigma,\Sigma'), \quad \Phi^{(1)}_2 = \Phi^{(1)}_3 = 0, \quad \Phi^{(3)}_\alpha = \Phi^{(4)}_\alpha,$$
$$\Psi^{(4)}_1 = \delta(W,W'), \quad \Psi^{(4)}_2 = \Psi^{(4)}_3 = 0, \quad \Psi^{(1)}_\beta = \Psi^{(2)}_\beta = \Psi^{(3)}_\beta \quad (11)$$

Tables of these functions for the configurations d^n with $n \leqslant 5$ were calculated, and will be published elsewhere.

References.

[1]) G. Racah, Phys. **76**, 1352 (1949).
[2]) F. Hund, Zeits. f. Physik **105**, 202 (1937).
[3]) G. Racah, Phys. Rev. **61**, 190 (1942).
[4]) E. U. Condon and G. H. Shortley, Theory of Atomic Spectra (Cambridge 1935) p. 177.
[5]) E. Feenberg and M. Phillips, Phys. Rev. **51**, 597 (1937).
[6]) H. A. Jahn, Communication at the Conference on Nuclear Physics, Birmingham, 1948.
[7]) G. Racah, Phys. Rev. **62**, 438 (1942) and **63**, 367 (1943).

V.

Quantenelektrodynamik

Zur anomalen Feinstruktur der He^+-Linie $\gamma = 4686$ Å

von **H. Kopfermann**

(nach gemeinsamer Untersuchung mit **H. Krüger** und **H. Öhlmann**).

Aus der Frequenzverschiebung der Feinstrukturkomponenten $4\,P_{1/2} - 3\,S_{1/2}$ und $4\,S_{1/2} - 3\,P_{1/2}$ gegen den aus der Sommerfeld-Dirac'schen Feinstrukturformel folgenden gemeinsamen Wert wurde in der Feinstruktur der He^+-Linie $\nu = 4686$ Å aus 20 Fabry-Perot-Aufnahmen mit 2 mm und 2,4 mm Etalon die quantenelektrodynamische Verschiebung des 3 S-Terms bestimmt zu: $\Delta\nu_{3S} = (0{,}118 \pm 0{,}003)\ \mathrm{cm}^{-1}$ und die des 4 S-Terms abgeschätzt zu: $\Delta\nu_{4S} = 0{,}06\ \mathrm{cm}^{-1}$. Obwohl die als Lichtquelle dienende Hohlkathode mit flüssiger Luft gekühlt wurde, betrug die Halbwertsbreite der einzelnen Feinstrukturkomponenten 0,22 cm^{-1}, die sich in fast gleichem Mass aus Dopplerbreite und Apparatebreite zusammensetzte. Daher war zwar das Maximum der intensiveren Komponente $4\,S_{1_2} - 3\,S_{1_2}$ gut vermessbar, aber die sichere Lagebestimmung der schwächeren Komponente $4\,S_{1_2} - 3\,P_{1_2}$, die nur $^1/_{250}$ der Gesamtlinienintensität besitzt, war nicht möglich. Die nicht völlig aufgelöste Struktur bedingte kleine Anziehungskorrekturen, die auf Grund eines numerischen Verfahrens, welches die Intensitätsverteilung aller Komponenten berücksichtigt, angebracht werden konnten. Die von Bethe errechnete 3 S-Termverschiebung $\Delta\nu_{3S} = 0{,}130\ \mathrm{cm}^{-1}$ liegt ausserhalb der Fehlergrenze.

A propos des divergences en théorie des champs quantifiés

par **E. C. G. Stueckelberg** et **D. Rivier**, Genève.

Comme nous le montrons ailleurs[1]), la causalité impose à la matrice S qui décrit l'évolution d'un système une structure bien déterminée: lorsqu'on développe celle-ci suivant les opérateurs de translation dans l'espace des quanta, les coefficients $S^{(i)}[\tau''; u''\cdots/\tau'; u'\cdots]$ sont des intégrales multiples où n'apparaissent, à côté des champs liés à un seul point de l'espace temps, que les fonctions*):

$$D^c(x/y) = D^s(x/y) + \frac{i}{2} D^1(x/y) \quad x \neq y \tag{1}$$

Formellement, cette structure est aussi celle que l'on obtient par intégration invariante de l'équation différentielle[2]) d'évolution du système à la différence suivante près: tandis que l'intégration conduit à une expression à première vue déterminée pour la matrice S, la construction causale de S laisse une certaine indétermination pour le noyau intégral formé des fonctions $D^c(x/y)$: en effet, de la manière dont ces fonctions sont introduites, il n'est pas possible de leur fixer a priori une valeur au point $x = y$. Cela est essentiel: en effet, si l'on défini aussi en $x = y$ la fonction $D^c(x/y)$ par (1) comme *doit* le faire l'intégration de l'équation différentielle, on est alors conduit à des coefficients $S^{(i)}[\ldots$ qui divergent en général. Par contre, l'indétermination de la fonction $D^c(x/y)$ au point $x = y$ permet une détermination a posteriori des noyaux intégraux qui conduisaient dans la théorie différentielle à des divergences; cette définition est univoque et donne une valeur finie aux coefficients $S[\ldots$. Comme nous allons le montrer, il subsiste après cela dans ces coefficients un certain arbitraire; mais celui-ci peut être partiellement éliminé par des considérations physiques.

Le procédé de définition des noyaux intégraux $\Delta^c(x/y)$ est appuyé sur le fait que les divergences proviennent essentiellement des singularités non intégrables des produits de fonctions $D^c(x/y)$, situées aux points $x = y$. Il est alors indiqué de définir les noyaux «vrais» à partir de ceux que donne l'intégration en leur ôtant leurs singularités non intégrables. On y parvient d'abord par l'utilisation

*) Pour les notations, voyez le second travail cité sous [2]).

d'un opérateur ϑ tel que $\vartheta\, \Delta^c(x/y)$ soit intégrable. Il suffit de prendre pour ϑ la multiplication par la fonction:

$$\vartheta^{(n)}(iz) = a_{\alpha_1 \ldots \alpha_n}\,(iz^{\alpha_1}) \cdots (iz^{\alpha_n}) \tag{2}$$

où $z^{\alpha i} = x^{\alpha i} - y^{\alpha i}$, avec sommation de 1 à 4 sur les indices vectoriels $\alpha_1 \ldots \alpha_n$, et où n dépend de l'acuité de la singularité. Puis, pour conserver au résultat sa signification, il est nécessaire de multiplier la valeur de l'intégrale par un opérateur ϑ_s qui doit se réduire, dans le domaine où $\Delta^s(x/y)$ est intégrable, à l'inverse de ϑ.

La réalisation de ces opérations est simple dans l'espace de Fourier; si nous écrivons (en prenant pour fixer les idées un terme du deuxième ordre):

$$S^{(2)}(\varphi''/\varphi') = \int (dx'')^4\, \varphi''(x'')\, \boldsymbol{\Delta}^c \varphi'(x'') \tag{3}$$

où:

$$\boldsymbol{\Delta}^c\, \varphi'(x) = \frac{1}{2} \int (dx)^4 \left(D^c(x/y)\right)^2 \varphi'(y)$$

il suffit d'étudier*):

$$\boldsymbol{\Delta}^s\, \varphi(x) = \int (dy)^4\, \Delta^s(x/y)\, \varphi(y) \tag{4}$$

où:

$$\Delta^s(x/y) = \frac{i}{4}\,(D^1 D^s + D^s D^1)\,(x-y)$$

qui s'écrit dans l'espace de Fourier:

$$\boldsymbol{\Delta}^s \varphi(x) = (2\pi)^{-3/2} \int dV(\tilde{k})\, \Delta^s(k)\, e^{ikx}\, \psi(\tilde{k}) \tag{5}**)$$

avec:

$$\Delta^s(k) \sim \frac{i}{4}\,(2\pi)^{-3} \int (dp)^4 \left[\frac{\delta(p^2 + \varkappa^2{}_u)}{(k^2 - p)^2 + \varkappa^2{}_u} + \frac{\delta((k-p)^2 + \varkappa^2{}_u)}{p^2 + \varkappa^2{}_u} \right] \tag{6}$$

ou encore, en utilisant un algorithme dû à M. Schwinger[3]) et en effectuant la translation[4]) $p^\alpha \to p^\alpha + uk^\alpha$

$$\Delta^s(k) \sim \int (dp)^4\, \Delta^s(k^2, p^2) \tag{6a}$$

avec:

$$\Delta^s(k^2, p^2) \sim -\frac{i}{4}\,(2\pi)^{-3} \int_0^1 du\; \delta'[p^2 + (\varkappa^2 + (u - u^2)\, k^2)] \tag{7}$$

*) Nous nous limitons au cas où τ'' et τ' dans $S^2[\tau''\, \varphi''/\tau'\, \varphi']$ sont des surfaces à l'infini: $\tau'' - \tau' - x^{4\prime\prime} \to \infty$.

**) $\psi(\tilde{k})$ est la composante de Fourier du paquet d'ondes $\varphi(x)$.

En lieu et place de l'intégrale (6a) qui *diverge* en général, comme c'est le cas ici, nous écrivons alors:

$$\Delta^s(k^2) = \underbrace{\int_0^{(k^2)} d(k^2) \ldots \int_0^{k^2} d(k^2)}_{(n)} \int (dp)^4 \cdot \left(\frac{\partial}{\partial (k^2)}\right)^n \Delta^s(k^2, p^2) \qquad (8)$$

où $n \geqslant 0$ est le plus petit entier tel que:

$$\int (dp)^4 \left(\frac{\partial}{\partial (k^2)}\right)^n \Delta^s(k^2, p^2) \qquad (9)$$

ait un sens.

La vraie valeur du noyau $\Delta^s(k^2)$ est donc:

$$\Delta^s(k^2) = \Delta^s_{\text{déf}}(k^2) + b_0 + b_1 k^2 + \cdots b_{n-1} k^{2(n-1)} \qquad (10)$$

où $\Delta^s_{\text{déf}}(k^2)$ est une fonction parfaitement définie de k^2. Il s'introduit donc n constantes arbitraires b_i et dans l'espace x, $\Delta^s(x/y)$ n'est définie qu'à la série:

$$b_0 \delta(x-y) + b_1 \Box \delta(x-y) + \cdots b_{n-1} \Box^{(n-1)} \delta(x-y) \qquad (11)$$

près, faisant apparaître des singularités intégrables à l'origine $x - y = 0$. Dans l'exemple choisi (6), on a $n = 1$ et:

$$\Delta^s_{\text{déf}}(k^2) = \frac{1}{32\, i\, \pi^2} \left[\text{Log}\, \varkappa^2 \left(\frac{\alpha+1}{\alpha-1}\right)^\alpha - 2\right] \qquad \alpha^2 = 1 + \frac{4\varkappa^2}{k^2}$$

Nous avons étudié avec cette méthode les termes de seconde approximation et en partie ceux de la troisième. On peut brièvement résumer les résultats de la manière suivante:

Toutes les divergences dues à la limite supérieure infinie de k (catastrophe ultraviolette) disparaissent. Grâce aux constantes arbitraires b_i, dans l'approximation du *deuxième* ordre le terme appelé énergie propre ou masse propre du photon (ou du méson) peut être annulé (dans le cas du photon, il suffit pour cela de poser nulle une des constantes). Dans la même approximation, il est possible d'éviter une renormalisation de la charge: la charge induite *le* peut être annullée. Notons encore à propos de la deuxième approximation que le courant induit satisfait à l'équation de continuité, à moins que le potentiel inducteur soit lui-même induit par un courant ne satisfaisant pas à l'équation de continuité, cas offrant, semble-t-il, peu d'intérêt.

En *troisième* approximation et dans le cas de l'électrodynamique, l'étude du rapport des coefficients des opérateurs de mo-

ment intrinsèque $S^{\alpha\beta}$ et de moment orbital $L^{\alpha\beta}$ dans la matrice S montre que ce rapport, qui vaut $g_0 = 2$ en première approximation, s'écrit*):

$$g = g_0 + 2\,\varkappa_u\,\frac{\mu}{e}$$

où:

$e = \varepsilon\,(1 + a\,\varepsilon^2)$ charge de l'électron «renormalisée»

$\varkappa_u$ = masse de l'électron

$\mu - \frac{1}{2\pi\,\varkappa_u}\,\varepsilon^3$

a est arbitraire; on obtient donc:

$$g = 2 + \frac{\varepsilon^2}{\pi}\,[1 - \varepsilon^2\,(a + \cdots)] \tag{13}$$

$\varepsilon^2\,a \ll 1$ est nécessaire pour conserver un sens à un développement en ε. Donc, limité à ε^2, notre résultat, qui coïncide avec celui de M. Schwinger[5]), est indépendant d'une renormalisation de la charge.

Références.

[1]) E. C. G. Stueckelberg et D. Rivier, H. P. A. **23**, 215 (1950).

[2]) Par exemple A. Houriet et A. Kind, H. P. A. **22**, 319 (1949); D. Rivier, H. P. A. **22**, 265 (1949).

[3]) J. Schwinger, Phys. Rev. **75**, 651 (1949).

[4]) Due aussi à M. Schwinger.

[5]) J. Schwinger, Phys. Rev. **76**, 790 (1949).

*) Nous remercions M. T. Green qui nous a aidé dans l'évaluation du facteur μ.

The radiation Theory of Feynman

by **F. J. Dyson** (Birmingham).

There are two points of view from which to consider this theory. First, one may consider it[1]) as a supplement to the Tomonaga-Schwinger theory, not differing from the latter in any of its basic assumptions but only in its method of handling problems. The theory then appears as a set of rules for the calculation of the element of the HEISENBERG S-matrix corresponding to any prescribed scattering process involving electrons, positrons and photons. These rules may be derived in a direct way from the SCHWINGER theory. From this viewpoint, the contribution of the FEYNMAN theory lies only in the following; by concentrating attention on the overall behaviour of a physical system as HEISENBERG has done in his S-matrix program, and ceasing to ask questions about the instantaneous state of the system at intermediate times, one finds quick and general ways to derive results which are otherwise obtained only by more laborious and special considerations.

The second point of view from which to consider the theory is the one followed by FEYNMAN himself. This point of view I wish to discuss to-day. Unfortunately there is as yet no published exposition of these ideas. I can refer only to one published paper[2]) and to two unpublished papers of FEYNMAN ("The Theory of Positrons" and "Space-time Approach to Quantum Electrodynamics") which are due to appear shortly. At least one paper in addition to these has still to be written before the foundations of the theory can be considered complete.

From the second viewpoint, it is not the similarity of the conclusions reached by SCHWINGER and FEYNMAN, but the dissimilarity of their starting-points, which is important. SCHWINGER's program has been to start from the HEISENBERG-PAULI electrodynamics and to reformulate it with the minimum modifications that are necessary to make it into a useable theory. FEYNMAN's program has been a critical re-examination of the basic principles of electrodynamics, taking nothing of the earlier theories for granted, building the whole theory up from postulates which are less mathematical and more physically intuitive than those to which we are accustomed. SCHWINGER has been constructing a single theory. FEYNMAN has

been constructing a framework into which many different theories can be made to fit; the fact that the framework is loose, allowing a wide freedom of choice to the future, is regarded by FEYNMAN as one of its merits.

The first departure of FEYNMAN from orthodox quantum theory is his use of the Lagrangian instead of the Hamiltonian as the basic function characterizing a system. Already in his non-relativistic theory[2]) the Lagrangian method is used. And because the Lagrangian is relativistically invariant while the Hamiltonian is not, this theory can be made relativistic with much greater ease than the usual SCHRÖDINGER theory. The Lagrangian method is based on the following two postulates.

I. Suppose a system to be given in a state A at one time, then the probability that it will be in a state B at a later time is $|\Sigma_H c(H)|^2$. Here the variable of summation H denotes any conceivable history or route which the system might follow in passing from A to B, and $c(H)$ is a complex number depending on H, called the "probability amplitude for the history H".

II. The value of $c(H)$ is $N \exp(iS/h)$, where N is a normalizing factor independent of H, and S is the classical action-integral of the system computed for the history H. In the case of a system of particles, S will be a sum of time-integrals of the particle Lagrangians taken along the world-lines of the particles. In the case of a system of fields specified by a classical Lagrangian-density defined at each point of space and time, S is the integral of the Lagrangian-density, integrated over the whole space and over the duration of H.

Starting from these two postulates and using various types of Lagrangian, a variety of relativistic quantum-mechanical systems can be described. In particular, it is not difficult to include systems with retarded interactions which cannot be quantized by the Hamiltonian method.

A second departure of FEYNMAN from orthodox methods is his treatment of the positron. Here he uses an old idea of WHEELER[3]) and STUECKELBERG[4]) that a positron can be regarded as an electron travelling backwards in time. The hole theory of Dirac is reconstructed in terms of this idea. In resolving the paradoxes presented by particles travelling backwards in time, FEYNMAN has made an analysis of the conditions that have to be satisfied by a quantum-mechanical system in order that physical requirements of causality be preserved. This has led him to duplicate in his theory several ideas discovered earlier by STUECKELBERG.

In conclusion, I wish to stress that the FEYNMAN theory is not to be regarded as a theory in competition with the SCHWINGER theory. It is rather a collection of ideas, of a somewhat intuitive character, which create a deeper understanding, on the one hand of the physical assumptions underlying existing electrodynamics, and on the other hand of the possibilities which exist for new theoretical developments.

References.

[1]) F. J. DYSON, Phys. Rev. **75**, 486 and 1736 (1949).

[2]) R. P. FEYNMAN, "Space-time Approach to Non-relativistic Quantum Mechanics", Rev. Mod. Phys. **20**, 367 (1948).

[3]) R. P. FEYNMAN, Phys. Rev. **74**, 939 (1948).

[4]) E.C.G. STUECKELBERG, Helv. Phys. Acta **15**, 23 (1942).

Relativistic Heisenberg picture

by **Bruno Zumino.**
Centro di Studio per la Fisica Nucleare del Consiglio Nazionale delle Ricerche, Roma.

Greek indices μ, ν, λ run from 0 to 3, small italic indices r, s from 1 to 3; $\hbar = c = 1$; the metric tensor is $g_{\mu\nu} = 0$ for $\mu \neq \nu$, $g_{00} = 1$ $g_{11} = g_{22} = g_{33} = -1$.

We start from the simpler case of a single electron in a given electromagnetic field, the wave equation of which is Dirac's equation. The corresponding Heisenberg picture, as usually expressed, is not in relativistic form owing to the fact that the time is treated in a different way then the space coordinates. This inconvenience can be avoided by the introduction of an independent space-like surface S, from which all dynamical variables, including the time, depend (see also DIRAC[3]).

In the following x_μ, x'_μ, x''_μ will denote coordinates of a free world point, and z'_μ, z''_μ of a world point lying on S. To write the equations of the theory we define for each $\zeta[S]$ functional of S, the operation

$$D_\mu \xi = \int_S \frac{\delta \zeta[S]}{\delta S(z')} dS'_\mu ; \text{ here } \frac{\delta \zeta[S]}{\delta S(z')} = \lim_{\delta\omega \to 0} \frac{\zeta[S_1] - \zeta[S]}{\delta \omega}$$

is the functional derivative with respect to S in the point z' of S (see SCHWINGER[4]); S_1 is a space-like surface different from S only in the neighborhood of the point z' and $\delta\omega$ the four-dimensional volume enclosed between the two surfaces; dS'_μ are the components of a vector of length dS, normal to S at the point z'; the formula

$$\frac{\delta}{\delta S(z'')} \int_S f(z') dS'_\mu = \frac{\partial f(z'')}{\partial z''^\mu} \tag{1}$$

and Schwinger's lemma, holding for closed systems,

$$\int_S \frac{\partial}{\partial z'^\mu} f(z') dS'_\nu = \int_S \frac{\partial}{\partial z'^\nu} f(z') dS'_\mu \tag{2}$$

are often useful; it can also be demonstrated that $D_\mu D_\nu \zeta - D_\nu D_\mu \zeta$).

Dirac's equation can be written in the form

$$\left\{\gamma_\mu\left[\frac{\partial}{\partial x_\mu}+i\,e\,A^\mu(x)\right]+m\right\}\langle x\,|=0; \tag{3}$$

the basic vector (see DIRAC[2]). $\langle x\,|$ has four components and γ_μ are four-rowed matrices; γ_0 is anti-Hermitian, γ_r Hermitian and they satisfy $\gamma_\mu\gamma_\nu+\gamma_\nu\gamma_\mu=-2\,g_{\mu\nu}$.

Defining $|\,x\rangle^+=-i\,|\,x\rangle\,\gamma_0$, the adjoint equation is

$$|\,x\rangle^+\left\{\gamma_\mu\left[\frac{\overleftarrow{\partial}}{\partial x_\mu}-i\,e\,A^\mu(x)\right]-m\right\}=0;$$

it follows $\frac{\partial}{\partial x_\mu}\{-i\,|\,x\rangle^+\gamma_\mu\langle x\,|\,\}=0$ so that

$$1=-i\int_S|\,z'\rangle^+\gamma_\lambda\langle z'\,|\,dS'^\lambda \tag{4}$$

is independent from S.

In the case in which an electromagnetic field is present, no simple expression can be given for $\langle x'\,|\,x''\rangle^+$; but we can always assert that

$$f(z'')=-i\int_S f(z')\,\gamma_\mu\langle z'\,|\,z''\rangle^+\,dS'^\mu=-i\int_S\langle z''\,|\,z'\rangle^+\gamma_\mu f(z')\,dS'^\mu \tag{5}$$

provided z' and z'' are both on S; here $f(x)$ needs not to satisfy Dirac's equation.

As a relativistic generalization of the coordinates and momenta of the electron at a given time, we define

$$z_\mu[S]=-i\int_S|\,z'\rangle^+\gamma_\lambda z'_\mu\,\langle z'\,|\,dS'^\lambda$$

and

$$p_\mu[S]=\int_S|\,z'\rangle^+\gamma_\lambda\frac{\partial}{\partial z'^\mu}\langle z'\,|\,dS'^\lambda=-\int_S\left(\frac{\partial}{\partial z'^\mu}\,|\,z'\rangle^+\right)\gamma_\lambda\langle z'\,|\,dS'^\lambda;$$

in force of (5) they satisfy

$$\langle z'\,|\,z_\mu[S]=z'_\mu\langle z'\,|\,,\ z_\mu[S]\,|\,z'\rangle^+=|\,z'\rangle^+z'_\mu$$

and

$$\langle z'\,|\,p_\mu[S]=i\frac{\partial}{\partial z'^\mu}\langle z'\,|\,,\ p_\mu[S]\,|\,z'\rangle^+=-i\frac{\partial}{\partial z'^\mu}\,|\,z'\rangle$$

(z' always on S). In a similar way

$$\gamma_\mu[S]=-i\int_S|\,z'\rangle^+\gamma_\lambda\gamma_\mu\langle z'\,|\,dS'^\lambda,\ \langle z'\,|\,\gamma_\mu[S]=\gamma_\mu\langle z'\,|,$$

whereas $\gamma_\mu[S]\,|\,z'\rangle^+$

is not even independent from the particular surface S through z'; we have instead, for

$$\bar{\gamma}_\mu[S] = i\int_S |\, z'\rangle^+ \gamma_\mu \gamma_\lambda \langle z'\,| \, dS'^\lambda, \text{ the relation } \bar{\gamma}_\mu[S]\,|\, z'\rangle^+ = -\,|\, z'\rangle^+ \gamma_\mu.$$

Using the definitions of the dynamical variables and their properties just exposed, it is easy to find their Poisson brackets. For instance, remembering also (1) (2) and (4),

$$[p_\mu, z_\nu] = \frac{p_\mu z_\nu - z_\nu p_\mu}{i} = -\int_S \left(-i\frac{\partial}{\partial z'^\mu}\,|\, z'\rangle^+\right) \gamma_\lambda z'_\nu \langle z'\,|\, dS'^\lambda +$$

$$+\int_S |\, z'\rangle^+ z'_\nu \gamma_\lambda\, i\frac{\partial}{\partial z'^\mu}\langle z'\,|\, dS'^\lambda = i\int_S \frac{\partial}{\partial z'^\mu}\{|\, z'\rangle^+ \gamma_\lambda z'_\nu \langle z'\,|\}\, dS'^\lambda -$$

$$-i\int_S |\, z'\rangle^+ \gamma_\lambda \langle z'\,|\, \frac{\partial z'_\nu}{dz'^\mu}\, dS'^\lambda = i\int_S \frac{\partial}{\partial z'_\lambda}\{|\, z'\rangle^+ \gamma_\lambda z'_\nu \langle z'\,|\}\, dS'_\mu +$$

$$+ g_{\mu\nu} = -D_\mu z_\nu + g_{\mu\nu}.$$

The complete scheme is

$$[z_\mu, z_\nu] = 0\,, \qquad [z_\mu, \gamma_\nu] = 0\,, \qquad \gamma_\mu\gamma_\nu + \gamma_\nu\gamma_\mu = -2\,g_{\mu\nu}\,, \tag{6}$$

$$p_\mu, z_\nu] = g_{\mu\nu} - D_\mu z_\nu, \quad [p_\mu, \gamma_\nu] = -D_\mu \gamma_\nu, \quad [p_\mu, p_\nu] = D_\nu p_\mu - D_\mu p_\nu. \tag{7}$$

Attention must be paid to formulas such as (7). The first of it, for instance, specializing S to have the equation $x_0 = z'_0$, becomes

$$[p_r, z_s] = -\,\delta_{rs}\,, \quad [p_0, z_s] = -\frac{dz_s}{dz'_0}\,, \quad [p_0, z_0] = 0\,,$$

so that it can be considered a relativistic expression for both the Poisson bracket relations between coordinates and momenta and the Hamiltonian law of dependence of the coordinates from the time.

(6) and (7) can be taken as the starting point of the theory and it becomes of interest to check their consistency. This can be done showing that they have as a consequence the relations

$$D_\lambda[z_\mu, z_\nu] = 0 \qquad D_\lambda[z_\mu, \gamma_\nu] = 0 \qquad D_\lambda(\gamma_\mu\gamma_\nu + \gamma_\nu\gamma_\mu) = 0$$

$$D_\lambda[p_\mu, z_\nu] = D_\mu[p_\lambda, z_\nu] \qquad D_\lambda[p_\mu, \gamma_\nu] = D_\mu[p_\lambda, \gamma_\nu]$$

$$D_\lambda[p_\mu, p_\nu] + D_\mu[p_\nu, p_\lambda] + D_\nu[p_\lambda, p_\mu] = 0$$

which correspond to properties of the second members of (6) and (7) themselves (remember $D_\mu D_\nu = D_\nu D_\mu$). For instance

$$D_\lambda[p_\mu, z_\nu] - D_\mu[p_\lambda, z_\nu] = [D_\lambda p_\mu - D_\mu p_\lambda, z_\nu] + [p_\mu, D_\lambda z_\nu] - [p_\lambda, D_\mu z_\nu] =$$

$$= [[p_\mu, p_\lambda], z_\nu] + [p_\mu, [z_\nu, p_\lambda]] - [p_\lambda [z_\nu, p_\mu]] = 0$$

in force of the identity of Poisson Jacoby.

The relations (6) and (7) make no reference to the particular kind of forces to which the particle is subjected; they are the relativistic generalization of the non relativistic Hamiltonian formulation of the one-particle theory if the form of the Hamiltonian function is not yet specified. We can specialize the problem adding the statement that

$$F = \gamma_\mu [p^\lambda - e A^\lambda(z)] + i m = 0 \tag{8}$$

be valid for every space-like surface S. (This follows from (3) by multiplication on the left with $|\, x\rangle^+ \gamma_\varrho\, dS^\varrho$ and integration.)

We have as a consequence, using (6), (7) and the properties of the Poisson brackets,

$$0 = [F, z_\mu] = \gamma_\mu - \gamma_\lambda D^\lambda z_\mu; \tag{9}$$

$$0 = [F, p_\mu] = D_\mu \gamma_\lambda (p^\lambda - e A^\lambda) + \gamma_\lambda (D_\mu p^\lambda - D^\lambda p_\mu) -$$

$$- e \gamma_\lambda \frac{\partial A^\lambda}{\partial z^\varrho} (D_\mu z^\varrho - \delta^\varrho_\mu)$$

but

$$0 = D_\mu F = D_\mu \gamma_\lambda (p^\lambda - e A^\lambda) + \gamma_\lambda D_\mu p^\lambda - e \gamma_\lambda \frac{\partial A^\lambda}{\partial z^\varrho} D_\mu z^\varrho$$

so that

$$\gamma_\lambda D^\lambda p_\mu = e \gamma_\lambda \frac{\partial A^\lambda}{\partial z^\mu}; \tag{10}$$

$$0 = [F, \gamma_\mu] = -i (\gamma_\lambda \gamma_\mu - \gamma_\mu \gamma_\lambda)(p^\lambda - e A^\lambda) - \gamma_\lambda D^\lambda \gamma_\mu$$

but

$$-i (\gamma_\lambda \gamma_\mu - \gamma_\mu \gamma_\lambda) = 2 i (\gamma_\mu \gamma_\lambda + g_{\mu\lambda})$$

so that, using (8) again,

$$\gamma_\lambda D^\lambda \gamma_\mu = 2 i \{- i m \gamma_\mu + p_\mu - e A_\mu(z)\}. \tag{11}$$

(9), (10) and (11) are the relativistic generalization of the equation of motion for our dynamical variables.

The foregoing theory can be easily generalized to give the relativistic Heisenberg picture corresponding to Dirac's many times theory usually expressed correctly only by means of wave equations (see DIRAC, FOCK and PODOLSKY[1]).

References.

[1]) DIRAC, FOCK and PODOLSKY, Phys. ZS. d. Sowjetunion **2**, 468 (1932).
[2]) DIRAC, Proc. Camb. Philos. Soc. **35**, 416 (1939).
[3]) DIRAC, Phys. Rev. **73**, 1092 (1948).
[4]) SCHWINGER, Phys. Rev.,, **74**, 1439 (1948).